Institute of Condensed Matter and Nanosciences
Molecular Chemistry, Materials and Catalysis division

Conversion of Borohydrides in Reactions with BH_3 and CO_2

Jian Wang

Supervisor: **Professor Yaroslav Filinchuk**

Thesis submitted in fulfilment of
the degree of Doctor in Sciences

Louvain-la-Neuve 2024

Institute of Condensed Matter and Nanosciences
Molecular Chemistry, Materials and Catalysis division

Conversion of Borohydrides in Reactions with BH_3 and CO_2

Jian Wang

Members of Jury:

Prof. Yaroslav Filinchuk (UCLouvain), supervisor
Prof. Eric Gaigneaux (UCLouvain), president
Prof. Michael Singleton (UCLouvain)
Prof. Tom Leyssens (UCLouvain)
Prof. Hai-Wen Li (HGMRI, China)
Prof. Torben René Jensen (AU, Denmark)

Thesis submitted in fulfilment of
the degree of Doctor in Sciences

Louvain-la-Neuve 2024

Abstract and Structure of the Thesis

In terms of energy-related applications, boron-hydrogen based compounds have received considerable interest. Borohydrides, such as $LiBH_4$, $Ca(BH_4)_2$, and $Mg(BH_4)_2$, with high volumetric and gravimetric content of hydrogen, are considered attractive candidates for closing hydrogen cycles. The *closo* borate anion, such as $B_{10}H_{10}^{2-}$ and $B_{12}H_{12}^{2-}$, with remarkable chemical and thermal stability, salt-like behavior, and weak coordinating ability towards alkali metal cations, has gained growing significance in the development of solid-state ionic conductors. Notably, there is a close relation between metal borohydrides and *closo* borate anions. The major obstacle to the reversibility of borohydrides as hydrogen stores is the formation of very stable *closo* borate intermediates, which act as thermodynamic and kinetic sinks, whereas the synthesis of *closo* borates often uses borohydrides as precursors. Experimental understanding of the formation mechanism of *closo* borate intermediates can not only allow for developing hydrogen storage materials with better re-hydrogenation properties but also contribute to wider their application, such as the development of all solid-state batteries.

The $B_{12}H_{12}^{2-}$ anion is generally synthesized from borohydrides and toxic boranes (B_2H_6, B_5H_9, $B_{10}H_{14}$) in ethereal solvents, followed by careful cation exchange with large monovalent cations such as triethylammonium, yielding water-insoluble products ($[(CH_3)_3NH]_2B_{12}H_{12}$) with no coordinating diglyme. Hydrated metal-$B_{12}H_{12}$ can then be obtained by cation exchange between

$[(CH_3)_3NH]_2B_{12}H_{12}$ and corresponding metal hydroxide salts in water, anhydrous metal-$B_{12}H_{12}$ can be obtained by dehydration of the hydrated metal-$B_{12}H_{12}$. Herein, we report our efforts on developing a novel synthesis route for $B_{12}H_{12}^{2-}$ based on using metal hydrides or borohydrides and borane dimethyl sulfide complex ($DMS{\cdot}BH_3$), which presents fewer handling issues. The procedure results in high purity and high yield material compared to any of the methods described in the literature. Furthermore, the mechanism for the formation of $B_{12}H_{12}^{2-}$ from BH_4^- between borohydrides and boranes has been established, revealing a stepwise formation of $B_2H_7^-$, $B_3H_8^-$, $B_9H_{14}^-$, $B_{11}H_{14}^-$, and $B_{11}H_{13}^{2-}$ intermediates. Although the initial step reaction in the autoclave and Schlenk setup produces ethers-solvated metal-$B_{12}H_{12}$ salts, we also demonstrate here that these ethers can be removed through simple exchange with weaker coordinating solvents like DMSO or H_2O, instead of using complicated cation exchange, to obtain anhydrous metal-$B_{12}H_{12}$ salts. Thus, we have developed a new approach to obtain a series of high-purity unsolvated $B_{12}H_{12}^{2-}$ salts ($Li_2B_{12}H_{12}$, $Na_2B_{12}H_{12}$, $K_2B_{12}H_{12}$, $CaB_{12}H_{12}$, and tetraalkylammonium $B_{12}H_{12}$) in this thesis work. Furthermore, as the first open porous hydridic metal borohydrides (γ-$Mg(BH_4)_2$) containing tubular-shaped microporous channels and the preliminary observation of the first porous hydridic *closo*-borate $[(CH_3)_3N)]_2B_{12}H_{12}$ with isolated pores without interconnecting channels in the structure, their application in the conversion and physical adsorption of CO_2 under ambient conditions is also presented in the thesis.

In Chapter 1, we introduce the boron-hydrogen based materials and their applications, especially in the context of hydrogen and CO_2

cycles. We are first discussing the properties of borohydrides and its role in hydrogen cycle and carbon cycle. After that, the known methods for synthesis of boranes, *closo* borates and their properties and applications will be described in detail, with special focus on the synthesis of $B_{12}H_{12}^{2-}$.

Chapter 2 of the thesis provides an overview of the methodologies used in the research, including experimental details and characterization methods, especially NMR and X-ray diffraction, as well as vibration and thermal analysis used in this work to analyze desolvation of borates, the detailed descriptions of these methodologies and their results are presented in subsequent chapters 3-7.

Chapter 3 of the thesis describes the one-pot autoclave synthesis of high purity $Na_2B_{12}H_{12}$ and $K_2B_{12}H_{12}$. We started the work with the cheapest borohydride ($NaBH_4$) and $DMS{\cdot}BH_3$. Our results show that temperature is a crucial factor for the outcome of the synthesis. High-purity $Na_2B_{12}H_{12}$ solvate, obtained *via* an intermediate formation of $B_3H_8^-$, $B_9H_{14}^-$, and $B_{11}H_{14}^-$, all of which are soluble in diglyme, allows the effective isolation of the target product. The coordinated diglyme can be removed by applying vacuum high temperatures. The synthetic method was further applied to $K_2B_{12}H_{12}$ synthesis, where ball milling KBH_4 prior to the synthesis enabled us to significantly improve the final yield. The work on $Na_2B_{12}H_{12}$ and $K_2B_{12}H_{12}$ was put in the context of the synthesis of other metal-$B_{12}H_{12}$ salts.

Chapter 4 of the thesis describes the solvothermal synthesis of lithium dodecaborate ($Li_2B_{12}H_{12}$). The reaction can conveniently be

performed either in a Schlenk flask with or without reflux, or in an autoclave. The enclosed system provided by an autoclave is shown to be more favorable for the synthesis of the $B_{12}H_{12}^{2-}$ anion and enables reaching the highest yields. The reaction mechanism has been investigated by ^{11}B NMR spectroscopy, revealing a stepwise formation of $B_2H_7^-$, $B_3H_8^-$, $B_9H_{14}^-$, $B_{11}H_{14}^-$ and $B_{11}H_{13}^{2-}$ intermediates. The formation of critical intermediates $B_{11}H_{14}^-$ and $B_{11}H_{13}^{2-}$ is discussed. The coordinated environment of $B_{12}H_{12}^{2-}$ salts of alkali metal (Li, Na, K) with glymes is evidenced by single crystal X-ray structural analysis, we show here that these coordinated glymes can be removed through simple exchange with weaker coordinating solvents like DMSO or H_2O.

Chapter 5 of the thesis describes the strategy optimized for obtaining $CaB_{12}H_{12}$. High-purity $CaB_{12}H_{12}$ was obtained from cheap CaH_2 and $DMS{\cdot}BH_3$, using a combination of tetrahydrofuran (THF) and monoglyme (DME) as solvents: The use of DME helps to avoid formation of $B_{12}H_{12-x}^{2-}$ anion during reaction, whereas THF allows for a higher solubility of Ca^{2+} salts, this helps reaching higher purity of the product. In attempt to obtain $MgB_{12}H_{12}$, the use of non-coordinating solvents such as toluene led to insolubility of the borohydride and promoted the self-condensation of $DMS{\cdot}BH_3$, leading to the formation of $B_{12}H_{11}S(CH_3)_2^-$, as demonstrated by the isolation of $(CH_3)_3SB_{12}H_{11}S(CH_3)_2$ single crystals.

Chapter 6 of the thesis, we address the adsorption and conversion of CO_2 in porous magnesium borohydride (γ-$Mg(BH_4)_2$). The distribution of CO_2 molecules along the channels of the porous polymorph of magnesium borohydride was determined by X-ray and

neutron diffraction techniques. The reaction pathway and intermediate products in the solid and gas phases were systematically analyzed through the combination of TG-MS and solid state NMR analysis. We observed the formation of methoxy and formate groups in the amorphous solid, with a carbon content higher than 20 wt.%.

Chapter 7 of the thesis focuses on the one-pot synthesis of tetraalkylammonium-$B_{12}H_{12}$ and tetraalkylammonium-B_3H_8. Particular attention is given to $[(CH_3)_3N)]_2B_{12}H_{12}$, the first observed porous $B_{12}H_{12}^{2-}$ containing material, showing potential for gas adsorption.

Chapters 3-7 present research findings and thorough discussions. Chapter 8 intends to provide a concise summary of the key findings and articulate a perspective for future research.

Authors' Contributions

The author and his supervisor, Professor Filinchuk Yaroslav, discussed and designed this thesis.

The author conducted the experiments, recorded and analyzed the data, and interpreted the results presented in this thesis with the following exceptions:

Anne Iserentant measured the ICP-OES data in Chapter 3.

Thermogravimetric analyses were conducted by Dr. Timothy Steenhaut (UCLouvain) and Jean-François Statsyns (UCLouvain).

All single crystal measurements and structures in this work were determined by Dr. Koen Robeyns (UCLouvain).

Initial work on interaction between CO_2 and the porous $Mg(BH_4)_2$ was done by the supervisor, together with past members of the lab, namely Nikolay Tumanov and Antoine Railliet.

Jakob Grinderslev and Prof. Torben R. Jensen (Interdisciplinary Nanoscience Center (iNANO) and Department of Chemistry, University of Aarhus, Denmark) provided help with the solid-state NMR in Chapter 6.

Acknowledgements

It would not be possible to finish this thesis without the help of many kind people surrounding me. I would like to gratefully acknowledge those who have contributed to this thesis and supported me during my PhD study, heartfully!

First and foremost, I would like to express my deepest gratitude to my supervisor, Professor Yaroslav Filinchuk, for granting me the privilege to work in his research group and for providing constant encouragement and patient guidance throughout my studies. I am particularly thankful for the tremendous assistance he offered in my Ph.D., helping me to settle down and providing support after the Covid lockdown. I am not a 'worry-free' student, his wisdom, optimism, and open-mindedness have always guided me to become a better person. I consider myself immensely fortunate to have had the opportunity to work under his supervision.

A special thanks to Dr. Timothy Steenhaut for his invaluable assistance in correcting and improving the writing of my thesis. He has consistently offered his support whenever there were issues with equipment or instrumentation, generously sharing his expertise and insights. I am grateful to Dr. Koen Robeyns for his extensive assistance with single crystal measurements, as well as for his meaningful discussions and valuable suggestions regarding both work and life. His contributions to correcting the writing of the thesis is also greatly appreciated. I am also thankful to my colleagues in the research group, as well as Prof. Tom Leyssens and his group members who share the B1 floor. People on the B1 floor are incredibly kind, and I thank you all for making my PhD a colorful experience. Lastly, I extend my heartfelt thanks to all the jury members for their time and expertise dedicated to evaluating this work, as well as for their support and encouragement.

I would like to extend my thanks to Prof. Hai-Wen Li for providing me with opportunities to participate in Energy Week in Japan. It was pity that I was unable to attend it due to the Covid lockdown. Additionally, my thesis works greatly relied on the autoclave he provided. He is a humorous and meticulous person, and I am grateful for his help and guidance. I would also like to extend my

thanks to Prof. Torben René Jensen and his group members, including Dr. Jakob Grinderslev, Jørgen Skibsted, and Lasse Gammelgaard Kristensen, for their kind assistance with solid-state NMR measurements. My gratitude to Dr. Dmitry Chernyshov, and all other staff from the Swiss Norwegian Beam Lines at the ESRF for their help and training with synchrotron radiation measurements. I would like to thank Prof. Hans Hagemann, Dr. Igor E. Golub, and Dr. Xiaodong Lin for their meaningful discussions.

Special thanks to Jean-François Statsyns for his assistance with TGA measurements and timely help when we had questions while working in the B3 lab. My appreciation to our technicians Jean-Charles Godefroid and Pascal Valvassori for their great help with the installation of the autoclave in the Bunker, as well as to François Billard for training.

I have been through a process of being ‘lost’ during the preparation of thesis, I appreciate the friends who help me out. My appreciation to all the friends I met in Belgium, friends who shared happiness together, friends who offer hands when there are difficulties. I cannot list all your names here, but it is my pleasure to have met all of you. I hope our friendship lasts forever, lifelong.

I feel lucky to have met my girlfriend, Yujie. We went through university in the same place, pursued our master's degrees together, and also complete our doctoral studies in European countries together. It has been a decade-long in relationship, I am grateful for her companionship as I continuously strive to become a better one of myself. I feel honored that she is willing to be my wife.

Finally, I would like to express my heartfelt thanks to my parents, Gui-Yuan Wang and Jin-Man Dong, for bringing me into this world and supporting me into adulthood. And also, to my sisters, being as the youngest in the family, they gave me all the care they could.

Last but not least I’m grateful to FNRS and the Communauté Française de Belgique (ARC Grant) for the financial support with the thesis work. I appreciate the financial support from the China Scholarship Council (CSC) for my life and stay in Belgium.

Table of Contents

List of Abbreviations

ATR	**A**ttenuated **T**otal **R**eflectance
Å	**å**ngström
a. u.	**A**rbitrary **u**nit(s)
BMS	**B**orane **D**imethyl **S**ulfide complex
CCDC	**C**ambridge **C**rystallographic **D**ata **C**entre
˚C	**C**elsius degree
CIF	**C**rystallographic **I**nformation **F**ile
COD	**C**rystallography **O**pen **D**atabase
CSD	**C**ambridge **S**tructural **D**atabase
δ	Chemical Shift (NMR spectroscopy)
d	**D**oublet
°	**D**egree
Diglyme	**D**iethylene glycol dimethyl ether
DME	**D**imethoxymethane
DMS	**D**imethyl **S**ulfide
DSC	**D**ifferential **S**canning **C**alorimetry
e^-	**E**lectron
ESRF	**E**uropean **S**ynchrotron **R**adiation **F**acility
FTIR	**F**ourier **T**ransform **I**nfrared **S**pectroscopy
h	**H**our (s)
HCl	**H**ydrogen **C**h**l**oride
HT	**H**igh **T**emperature
ICSD	**I**norganic **C**rystal **S**tructure **D**atabase
ICP-OES	**I**nductively **C**oupled **P**lasma – **O**ptical **E**mission **S**pectroscopy
LT	**L**ow **T**emperature

J	Coupling constant
λ	Wavelength
mL	Milliliter
MS	**M**ass **S**pectrometer
N/A	**N**ot **A**vailable
N/D	**N**ot **D**etermined
NMR	**N**uclear **M**agnetic **R**esonance
$Mg(n\text{-}Bu)_2$	Butylmagnesium
M(BH4)n	Metal borohydrides
$M_nB_{12}H_{12}$	Metal dodecaborate
MS	**M**ass **S**pectrometry
MOFs	**M**etal **O**rganic **F**rameworks
PXRD	**P**owder **X**-**R**ay **D**iffraction
ppm	**P**arts **p**er **m**illion
SNBL	**S**wiss-**N**orwegian **B**eam**l**ine
SCXRD	**S**ingle **C**rystal **X**-**R**ay **D**iffraction
SNBL	**S**wiss-**N**orwegian **B**eam**l**ines
sol	**Sol**ution
s	**S**olid state
S-PXRD	**S**ynchrotron **P**owder **X**-**R**ay **D**iffraction
SI	**S**upporting **I**nformation
Θ	Theta
3D	**T**hree-dimensional
t	**T**ime
TGA	**T**hermal **G**ravimetric **A**nalysis
THF	**T**etra**h**ydro**f**uran
wt.%	Weight percent

Scientific Contributions

Publications within the scope of This Thesis

Wang, J.; Steenhaut, T.; Li, H.-W.; Filinchuk, Y., High Yield Autoclave Synthesis of pure $M_2B_{12}H_{12}$ (M = Na, K). *Inorg. Chem.* **2023,** *62* (5), 2153–2160.

Golub, I. E.; Heere, M.; Gounaris, V.; Li, X.; Steenhaut, T.; **Wang, J.**; Robeyns, K.; Li, H.-W.; Dovgaliuk, I.; Ikeda, K.; Hautier, G.; Filinchuk, Y. Structural Insight into the Magnesium Borohydride – Ethylenediamine Solid-State Mg-Ion Electrolyte System. *Dalton Transactions* **2023**, *52* (8), 2404–2411.

Wang, J., et al. A Simple and Efficient Preparation of High-Purity and High-Yield Unsolvated Lithium Dodecaborate. Submitted. 10.26434/chemrxiv-2024-7vf8d

Wang, J., et al. Autoclave-Mediated Synthesis of Calcium Dedecaborate in a Mixture of Complex Ethers. To be submitted.

Conference participations

Poster, ***Energy Week 2020***, Fukuoka, Japan;

Poster, ***Belgian Crystallography Symposium 11***, Brussels, Belgium, 17/03/2021;

Poster, ***Energy Week 2021***, Fukuoka, Japan, 22/01/2021-29/01/2021;

Poster, ***HydEM 2022***, Louvain-la-Neuve, Belgium, 18/05/2022-20/05/2022;

Three Minutes Thesis, ***Ph.D. Students' Day 2021,*** Louvain-la-Neuve, Belgium, 21/05/2021.

Poster, ***MH 2024***, Saint-Malo, France, 26/05/2024-31/05/2024

Chapter 1. Introduction

In this chapter, our focus is on the synthesis, properties, and applications of boron-hydrogen-based compounds, specifically dodecaborates ($B_{12}H_{12}^{2-}$). The formation of $B_{12}H_{12}^{2-}$ typically involves a condensation reaction between borohydrides and boranes. Therefore, we will start this chapter with a brief description of borohydrides and their potential roles in the hydrogen and carbon cycles. Following this, we will delve into the properties of diborane (B_2H_6) and other chemicals that can serve as alternatives of B_2H_6 for condensation reactions. After that, we will provide a detailed description of the synthesis of $B_{12}H_{12}^{2-}$. Finally, we will outline the objectives of the thesis, and detail the specific research goals and outcomes we aim to achieve.

Chapter 1

1.1. Hydrogen cycle and carbon cycle

Energy is a fundamental requirement for human survival and progress: the limited fossil fuel resources and the environmental impact of their use require a shift to renewable energy sources in the 21st century.[1–3] Renewable energy sources such as solar, wind, and wave power are clean and sustainable alternatives to fossil fuels.[2] However, the sun does not always shine, wind does not always blow, the intermittency of these sources of energy makes them incapable of fulfilling the demands of base-load energy usage. Therefore, developing efficient, low-cost and scalable energy carrier coupled with the renewable energy as it is produced, and used later or when needed, is the key factor for ensure the continuous energy supply. In the context of mobile applications, an efficient energy carrier that can be produced and utilized in a closed cycle is required.[4–6]

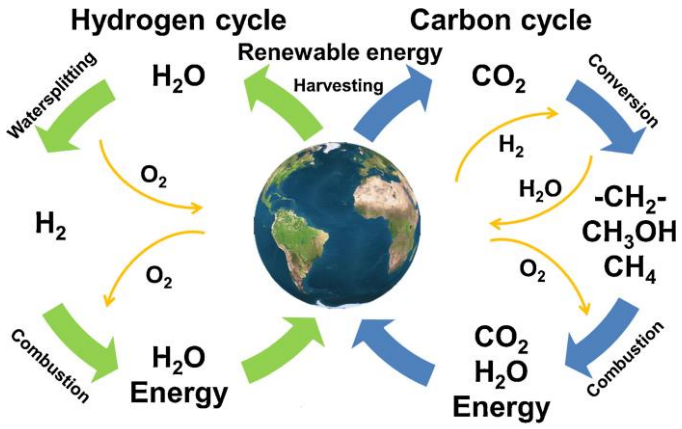

Figure 1. The hydrogen cycle and carbon cycle.[6]

Hydrogen, the most abundant element in the universe, has long been seen as a potential energy carrier for the storage of renewable

energy. In recent years, hydrogen has emerged as the most practical and scalable energy carrier, capable of large-scale production within realistic timelines. The production of hydrogen in the hydrogen cycle, as indicated by the green arrows in Figure 1, can typically be achieved through water splitting or by cracking hydrogen-containing carriers such as ammonia or methanol, harnessing energy from renewable sources. When hydrogen is used, whether in fuel cells, combustion engines, or turbines, it generates only water as a byproduct, essentially forming a self-sustaining closed-loop system.[6,7] However, there are a few obstacles that must be overcome before the hydrogen cycle can be fully utilized as a sustainable and clean energy source. A major challenge is the cost and efficiency of hydrogen production, particularly in electrolytic hydrogen production processes, which currently require significant energy inputs and expensive components.[8,9] Following hydrogen production, the storage and transportation of hydrogen present additional technical and safety complexities due to its inherent properties, including low density, low boiling point, and high reactivity.[10] The widespread acceptance of hydrogen as a practical and ecologically friendly fuel source greatly depends on the development of safe and effective hydrogen storage materials. Addressing these obstacles can not only improve developing hydrogen as an energy carrier, but also helps to create a greener and more sustainable energy landscape, paving the way for a cleaner and efficient energy future.[2,11]

Hydrogen can be securely stored in the form of atoms or molecules, particularly within hydrides. In the context of on-board hydrogen storage for mobile applications, there is a wide array of technologies currently under exploration.[12,13] Which include storing compressed hydrogen gas in high-pressure tanks or maintaining liquid hydrogen at cryogenic temperatures to capitalize on its enhanced

energy density.[14] Metal hydrides and complex hydrides have emerged as promising candidates for storing and releasing hydrogen under regulated conditions.[15–18] Chemical storage technologies, such as using ammonia and liquid organic hydrogen carriers, provide additional options.[19] Adsorption onto porous materials such as activated carbon or metal-organic frameworks (MOFs) is a unique technique.[20] These methods come with their own advantages and challenges, demanding constant study to improve efficiency, strengthen safety standards, and reduce costs. Notably, the investigation of metal hydrides, compounds formed through the interaction of hydrogen with metals, stands out for their commendable volumetric energy density and reversible hydrogen absorption and release characteristics. As indicated by their wide use, metal hydrides play a crucial role in the continuous pursuit of advanced on-board hydrogen storage solutions.

Among the current hydrides, complex hydrides containing lightweight elements are emerging as viable materials for hydrogen solid-state storage.[21–23] The reversibility of hydrogen absorption and desorption in borohydrides are a key focus of research on solid-state hydrogen storage materials.[1,10,24–32]

On the other hand, our current energy system is highly dependent on carbon-based materials, such as fossil fuels and coal, Unfortunately, this energy system is not a “closed materials cycle”. Fuels are consumed much faster than they produced, the unsustainable situation leading to an increasing concentration of CO_2 in the atmosphere, keep contributing mainly for global warming and climate change.[33,34]

To achieve a closed carbon cycle (blue arrow in Figure 1b), the key is to develop methods for converting the produced CO_2 into useful fuel. The catalytic reduction of carbon dioxide to fuels and value-

added chemicals is of significance for the development of carbon recycling technologies.[35] The main challenges associated with catalytic CO_2 reduction is product selectivity: the formation of carbon monoxide, molecular hydrogen, formate, methanol, and other products occurs with similar thermodynamic driving forces, making it difficult to selectively reduce CO_2 to one target product.[36] One promising approach involves using metal borohydrides, which have been recently explored for their potential in CO_2 capture and recycling without using catalyst. The CO_2 enhanced hydrolysis of KBH_4 has been proposed to generate hydrogen, which can be used for fuel cells, using the waste products of fossil fuel combustion.[37] More recently, tetraalkylammonium borohydrides were found efficiently capture and reduce CO_2 to formate even at low concentrations and room temperature, with BH_4^- anions reacting with three CO_2 molecules to create triformatoborohydride. The kinetics and thermodynamics of the reaction depend on the alkyl chain length, and the addition of HCl allows for recycling through the formation of formic acid and the corresponding chloride ammonium salt, enabling the transfer of formate for N-formylation of an amine.[19] which is very promising to create a closed loop, where the waste products of one process become the starting materials for another process.

Hydrides based materials hold great promise for closing the hydrogen cycle and carbon cycle. The unique chemical and physical properties make hydrides and complex hydrides excellent materials for developing new and innovative approaches for sustainable energy storage and conversion.

1.2. Borohydrides for H_2 cycle and carbon cycle

1.2.1. Borohydrides

Borohydride refers to the anion BH_4^-, which is also called tetrahydridoborate, and its salts. This anion consists of a boron atom surrounded by four hydrogen atoms in a tetrahedral arrangement, the geometries and sizes of BH_4^- is shown in Figure 2.[38]

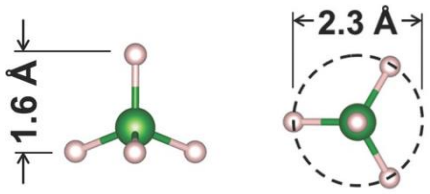

Figure 2. The geometries and sizes of BH_4^- shown from both top and side views.

Color code: **B** green; **H** white spheres.[39]

The first borohydride compound, lithium borohydride ($LiBH_4$), was made by Schlesinger and Brown in 1940 through a reaction between ethyl-lithium (CH_3CH_2Li) and diborane (B_2H_6).[40] Later, sodium borohydride ($NaBH_4$) was synthesized.[41] Today, $NaBH_4$ is the most commonly produced and used borohydride, and is often used as precursors for the synthesis of other metal borohydrides. Along with the discovery of $NaBH_4$, the synthesis and structures of other borohydrides, such as potassium borohydride (KBH_4) and magnesium borohydride ($Mg(BH_4)_2$), have been explored and synthesized. Borohydrides have gained much attention and have developed into a large family of chemicals with many derivatives.[42]

The hydrogen atoms in borohydrides are bonded to the metal ions either ionically or covalently through different coordination types, as

shown in Figure 3. A unique property of borohydrides is their ability to form both ionic compounds with alkali and alkaline-earth metals and covalent complexes with transition metals. The coordination mode and the physicochemical properties of borohydrides are significantly influenced by the type of metal and its oxidation state, which in turn impact the thermodynamic stability of the borohydride compounds.[43]

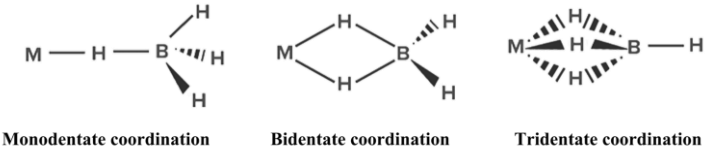

Figure 3. Covalent bonding modes in borohydrides, image from Aakash.ac.in.

1.2.2. Borohydrides for H_2 cycle

Borohydrides are emerging as promising on-board hydrogen storage materials due to their high hydrogen content. These compounds are capable of adsorbing hydrogen and storing it in solid form, subsequently releasing it through thermal decomposition or hydrolysis. This makes borohydrides particularly promising for renewable energy applications and hydrogen fuel cells, providing a promising solution for clean energy storage and transportation.

Table 1. Properties of several representative metal-borohydrides.[4]

$M(BH_4)_n$	**Density (g/mol)**	**Hydrogen (wt.%)**	**Desorption temperature (°C) /Emission gas under pyrolysis**	**T_{dec} (°C)**
$LiBH_4$	21.78	18.36	390 / H_2	265
$NaBH_4$	37.83	10.57	400 / H_2	505
KBH_4	53.94	7.42	40 sublimation /B_2H_6+H_2	585
$Mg(BH_4)_2$	53.99	14.82	230 / H_2	320
$Ca(BH_4)_2$	69.76	11.47	300 / H_2	260
$Al(BH_4)_3$	71.51	16.78	61 / B_2H_6+H_2	/

In particular, most of the $M(BH_4)_n$ compounds boast exceptional

hydrogen storage densities exceeding 10 wt.% as outlined in Table 1.

The ability of a hydrogen carrier to undergo complete dehydrogenation and rehydrogenation cycles is crucial for the utility of a storage material. Metal borohydrides can release hydrogen through hydrolysis or thermolysis processes, as mentioned above.[44] The reactions for hydrogen release can be expressed as follows:

$$M(BH_4)_n \rightarrow MH_m + n\,B + (4\,n\text{-}m)/2\,H_2 \quad (1)$$

$$M(BH_4)_n + (2\,n + m)\,H_2O \rightarrow M(BO_2)_n \cdot mH_2O + 4n\,H_2 \quad (2)$$

The pyrolysis of borohydrides for hydrogen production is promising for a closed-loop chemical recycling process. Significant efforts are being devoted to investigating the decomposition pathways and resultant products of thermolysis, along with their impact on the reversibility of borohydrides.[45–49] The decomposition of borohydrides can occur at moderate temperatures, proceeding through multiple steps. For example, the desorption process for $LiBH_4$ has a dehydrogenation enthalpy about 75 kJ mol^{-1}.[50,51] The dehydrogenation process can be summarized as following:

$$LiBH_4 \rightarrow LiH + B + {}^3/_2\,H_2 \quad (3)$$

However, the strong covalent bonds between B and H, and ionic bonds between metal ions and BH_4^- lead to a high thermal stability, resulting in elevated dehydrogenation temperatures, generally above 200 °C for classical borohydrides, as summarized in Table 1.[31,43,52] Furthermore, the low reactivity of B towards H induces high kinetic barriers for the reformation of rehydrogenation products. Thus, these borohydrides suffer from high desorption temperatures and poor hydrogen reversibility, involving the formation of aromatic intermediates such as $B_{10}H_{10}^{2-}$ and $B_{12}H_{12}^{2-}$ during the hydrogen cycle. The robust B−B bonds in these dehydrogenated intermediates further

challenge rehydrogenation ability, compromising reversibility.[53,54] Recent research focus mainly on thermodynamic adjustments and kinetic enhancements.[52,55,56]

1.2.3. Role of B_2H_6 formation in H_2 cycling by borohydrides

The experimental investigation of decomposition products of borohydrides often requires the use of nonconventional methods, such as solid-state NMR (SSNMR), particularly for the observation of formation of stable aromatic intermediate molecules, such as $B_{10}H_{10}^{2-}$ and $B_{12}H_{12}^{2-}$ as mentioned earlier. In the context of using borohydrides for on-board hydrogen storage, the high decomposition temperature and reduced reversibility of borohydrides have been identified as a key barrier to the use of borohydrides as effective hydrogen storage materials.

The release of B_2H_6 at low temperatures (below 100 °C) is also observed during the decomposition of borohydrides. The formation of B_2H_6 under these conditions can lead to condensation reactions, resulting in the formation of intermediates with stable B-B bonds.[57]

The formation mechanism of B_2H_6 during dehydrogenation has been proposed as B-H bonds break, forming BH_2^+ and BH_4^- intermediate species that recombine to produce B_2H_6, the mechanism proposed is proposed as follows [58]:

$$2\ M^+ + 2\ BH_4^- \rightarrow 2\ M^+ + (H^-)_2 + BH_2^+BH_4^- \rightarrow 2\ M + H_2 + B_2H_6 \quad (4)$$

Another study shows that the thermal decomposition of $LiBH_4$ has led to $Li_2B_{12}H_{12}$ as the stable intermediate in the system. The proposed reaction scheme for $LiBH_4$ is complete decomposition, including the

intermediate $Li_2B_{12}H_{12}$ phase, as provided below [59]:

$$\begin{aligned} LiBH_4 &\rightarrow {}^{1}/_{12}\ Li_2B_{12}H_{12} + {}^{5}/_{6}\ LiH + {}^{13}/_{12}\ H_2 \\ &\rightarrow LiH + B + {}^{3}/_{2}\ H_2 \end{aligned} \qquad (5)$$

The formation of B_2H_6 during dehydrogenation of borohydrides is typically seen as undesirable due to its impact on hydrogen purity and storage capacity reduction with each rehydrogenation and dehydrogenation cycle.[60] However, the evolution of diborane also contributes to the formation of $Li_2B_{12}H_{12}$, which is not just as an intermediate, but rather as a reaction by-product resulting from the *in situ* reaction of $LiBH_4$ and B_2H_6, a proposed equation is given below[61]:

$$2\ LiBH_4 + 5\ B_2H_6 \rightarrow Li_2B_{12}H_{12} + 13\ H_2 \qquad (6)$$

The similar observation of $MgB_{12}H_{12}$ intermediate formation during the decomposition of $Mg(BH_4)_2$ to MgH_2 was also proposed in a later work[62]:

$$\begin{aligned} Mg(BH_4)_2 &\leftrightarrow {}^{1}/_{6}\ MgB_{12}H_{12} + {}^{5}/_{6}\ MgH_2 + {}^{13}/_{6}\ H_2 \\ &\leftrightarrow MgH_2 + 2\ B + 3\ H_2 \\ &\leftrightarrow Mg + 2\ B + 4\ H_2 \end{aligned} \qquad (7)$$

Experimental investigation on thermal dehydrogenation of $Ca(BH_4)_2$ suggests a different mechanism, with the formation of the CaB_6 or $CaB_{12}H_{12}$, which is highly depending on temperature [26]:

$$\begin{aligned} &Ca(BH_4)_2 \leftrightarrow \text{amorphous intermediates} \\ &\leftrightarrow CaB_2H_x + (4 - {}^{x}/_{2})\ H_2 \\ &\leftrightarrow {}^{1}/_{3}\ CaB_6 + {}^{2}/_{3}\ CaH_2 + ({}^{x}/_{2} - {}^{2}/_{3})\ H_2 \end{aligned} \qquad (8)$$

$$\begin{aligned} &Ca(BH_4)_2 \leftrightarrow \text{amorphous intermediates} \\ &\leftrightarrow {}^{1}/_{6}\ CaB_{12}H_{12} + {}^{5}/_{6}\ CaH_2 + {}^{13}/_{6}\ H_2 \end{aligned} \qquad (9)$$

Based on the known mechanism, the preservation of dodecaborates within the system after a dehydrogenation process can substantially impact the cycling efficiency of the storage material and

the overall reversibility of the dehydrogenation process, as illustrated in Figure 4.

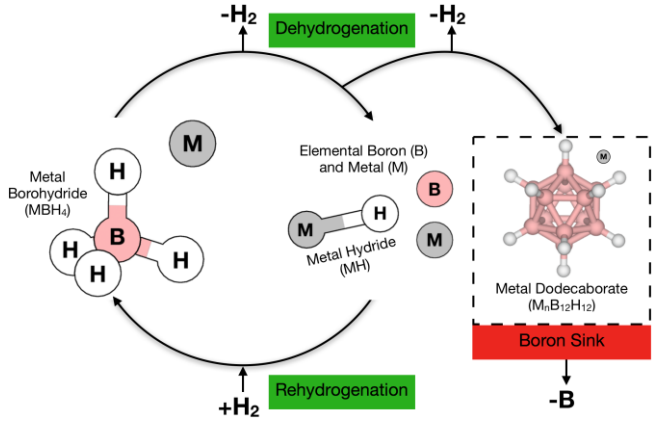

Figure 4. Schematic illustration of dodecaborates in the borohydride hydrogenation cycle.[53]

The formation of B_2H_6 in the system results in the 'sinking' of boron along with the release of hydrogen, whereas the formation of stable dodecaborate intermediates traps boron into an unwanted product. As a result, the formation of dodecaborates during the dehydrogenation of borohydrides significantly hindered the reversibility and storage capacity of the materials. To enhance the dehydrogenation ability, various strategies have been undertaken for the purpose to reduce the emission of B_2H_6. These strategies typically include increasing the hydrogen partial pressure, nanoconfinement, nanocomposites, or utilizing catalysts.[24,62,63]

1.2.4. Borohydrides for carbon cycle: CO_2 reduction

Transforming CO_2 into useful fuels like methanol (CH_3OH) is another promising approach for energy issue. CH_3OH can be used directly as a cleaner fuel or as a building block for making other important chemicals like acetic acid. However, CO_2 is a very stable

molecule, making it difficult to be activated under mild conditions. Usually, catalysts and additional hydrogen sources are needed to achieve this. An alternative method uses highly reactive compounds called borohydrides, which can convert CO_2 at room temperature without needing a catalyst.[64]

The pioneering studies on the reactivity of metal borohydrides with CO_2 can be traced back to as early as the 1950s. Heller et al. investigated the interaction between $LiBH_4$ and CO_2 in an ether solution.[65] Their findings revealed the formation of formate and diborane as the main products, along with a small amount of methanol. Later, Wartik and Pearson described the reduction of CO_2 using $NaBH_4$.[66] They observed that two equivalents of CO_2 react with one $NaBH_4$. Interestingly, increasing the CO_2 concentration in dimethyl ether led to the formation of triformatoborohydride ($[HB(OCHO)_3]^-$), subsequent treatment with dilute sulfuric acid yielded formic acid. However, these early findings focused mainly on product outcomes without detailed mechanistic investigations.

A significant step towards understanding the complexities of borohydride and CO_2 interactions without applying a solvent was taken in more recent years. The thermally induced reaction revealed a complex interplay of reactions, including $NaBH_4$ decomposition, during CO_2 capture. The identification of formate and methoxy groups in the solid products indicates the multi-faceted nature of these reactions.[67] Further insights into the reaction, mechanochemical and thermally induced solid-gas borohydride and CO_2 interactions emerged from the earlier work in our lab. The proposed mechanism for the formation of potassium formylhydroborates, $K[H_xB(OCHO)_{4-x}]$ ($x=1-3$), as main products, the stepwise formation of formylhydroborates proposed in Figure 5 as follows[68]:

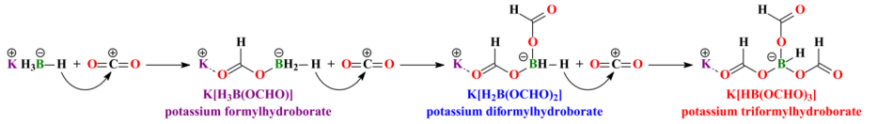

Figure 5. Schematic illustration of formation of formylhydroborates in the reaction between KBH_4 and CO_2.[68]

However, bulk $NaBH_4$ and KBH_4 lack reactivity, often requiring additional energy to induce the solid gas reactions. Current research is increasingly focused on CO_2 reduction under ambient conditions. Tetraalkylammonium borohydrides have been found to efficiently capture and reduce CO_2 to formate even at low concentrations and ambient conditions. In these reactions, BH_4^- anions interact with three CO_2 molecules to produce triformatoborohydride. The kinetics and thermodynamics of the reaction are influenced by the alkyl chain length.[69] In addition, porous $Mg(BH_4)_2$ has shown potential for efficient CO_2 conversion at room temperature. Importantly, research highlights the capability of $Mg(BH_4)_2$ as a recyclable catalyst, which is essential for sustainable CO_2 utilization and maintaining a closed cycle.[70,71]

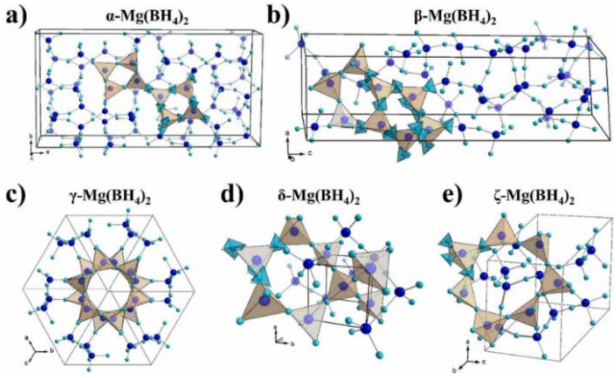

Figure 6. Reported crystal structures of the α, β, γ, δ and ζ phases of $Mg(BH_4)_2$. Mg blue; BH_4^- groups as tetrahedra.[72]

Notably, $Mg(BH_4)_2$ is a staple material in our laboratory, distinguished by its extensive range of experimentally observed and theoretically predicted crystal structures. This diversity surpasses that of any other known borohydride. Figure 6 represents the experimentally determined crystal structures of $Mg(BH_4)_2$, noting its structural diversity.

Among which, the gamma-phase of magnesium borohydride, γ-$Mg(BH_4)_2$, known as the first hydride with functional porosity, features interconnected channels with pore sizes ranging from 5.8 to 8.8 Å. Despite the absence of open metal sites for gas molecule coordination, the pores expose partially hydridic hydrogen atoms. These one-dimensional channels are capable of hosting small guest molecules. Moreover, it stands as the first complex metal hydride with the ability to reversibly adsorb hydrogen, nitrogen and hydrocarbons.[73–76] In this thesis work, we are also presenting the capture and reduction of CO_2 by γ-$Mg(BH_4)_2$.

1.3. Diborane and its derivatives

1.3.1. Diborane

Diborane is a colorless, sweet-smelling gas at room temperature, has been widely recognized for its electron deficiency, and as reducing reagent in various chemical reactions. For synthesis, it serves as a key precursor to a wide array of borane compounds. However, despite its utility, diborane requires careful handling due to its high flammability, particularly in moist conditions, and significant toxicity concerns.[77]

Diborane has a unique structure with an electron-deficient D_{2h}

symmetry, distinct from typical bonding models. As shown in Figure 7, the boron atoms in diborane structure are sp^3 hybridized, each of the boron forming two normal two centered two electron (2c-2e) bonds with terminal hydrogens. The remaining unpaired electron and the empty orbital on each boron form bridge three centered two electron (3c-2e) bonds with the bridged hydrogen atoms, resulting in what is known as a "banana bond".[78]

The lengths of the bridged B–H bonds in diborane are 1.33 Å, while the terminal B–H bonds are 1.19 Å. This difference in bond lengths indicates varying strengths, with the bridge bonds being weaker. This unique bonding configuration notably impacts its reactivity.

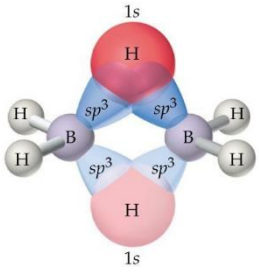

Figure 7. The structure of diborane, image from wps.prenhall.com

The reactivity of diborane is central to its significance in the synthesis of borohydrides, particularly in the formation of higher boranes.[77] At moderate temperatures and pressures, B_2H_6 readily undergoes homogeneous dissociation, yielding reactive BH_3 units that participate in a self-condensation reaction. This process leads to the formation of a variety of open-cage boranes like B_4H_{10}, B_5H_9 and $B_{10}H_{14}$, often forming through unstable intermediates. Additionally, diborane undergoes slow decomposition at room temperature, contributing to the formation of polymeric $(BH)_n$ species.[79] These reactions highlight the key role of diborane can be served as a

fundamental building block for higher boranes in boron chemistry.

1.3.2. Role of B_2H_6 in borohydride synthesis

Borohydride materials can be synthesized using two primary techniques: solvent-mediated synthesis and solvent-free synthesis. Solvent-free methods often use inexpensive borohydrides (e.g., $NaBH_4$) and halide salts of the desired metal borohydrides for metathesis. Solvent-free methods, such as ball milling is convenient, widely used, and sometimes essential for obtaining specific products. However, ball milling commonly produces significant amounts of halide salts as by-products. In contrast, solvent-mediated methods generally enable the production of high-purity materials by separating halides from the product through treatments such as filtration.[80]

In the solvent-mediated synthesis of borohydrides, diborane plays a crucial role in multiple aspects. First and foremost, it serves as a reducing agent, effectively converting various compounds into the corresponding borohydrides, e.g. $NaBH_4$, $LiBH_4$ and $Mg(BH_4)_2$, by reacting diborane with corresponding metal hydrides and alkoxide in a solvent, as evidenced by earlier studies[6]:

$$2\ MH + B_2H_6 \rightarrow 2\ MBH_4\ (M = Li, Na, K) \qquad (10)$$

Metal borohydrides then obtained from the solution as solvates with one or more solvent molecules, followed by a desolvation step to get the anhydrous ones. However, in some cases, thermal desolvation under vacuum can lead to the decomposition of $M(BH_4)_n$ with the release of H_2 before the desolvation point.[80] A detailed study of the synthesis mechanism involving the reaction between LiH and B_2D_6 was conducted by researchers who prepared H/D isotope-labeled samples. By tracking the H or D atoms in the borane or borohydride products using vibrational spectroscopy, it was determined that the

BH_4^- anions originated from the heterolytic splitting of diborane.[81] This process substitutes H ions from LiH to form $LiBH_4$ on the surface. For the synthesis of borohydrides, the presence of H^- defects may play a crucial role in the incorporation of BH_4^- into the bulk material.[82]

In addition to the synthesis of BH_{4-}, B_2H_6 is also widely used as a precursor for synthesizing a series of borate anions, based on recent studies. These include octahydrotriborate anion ($B_3H_8^-$), *nido* undecaborate anion ($B_{11}H_{14}^-$), and $B_{12}H_{12}^{2-}$. The formation of the desired borate anions is highly dependent on the borohydride and B_2H_6 ratio and reaction temperatures, as shown below[83–85]:

$$BH_4^- + B_2H_6 \rightarrow B_3H_8^- + H_2 \quad (11)$$

$$B_3H_8^- + 4\ B_2H_6 \rightarrow B_{11}H_{14}^- + 9\ H_2 \quad (12)$$

$$2\ BH_4^- + 5\ B_2H_6 \rightarrow B_{12}H_{12}^{2-} + 12\ H_2 \quad (13)$$

The role of diborane mainly work by attacks on electron-deficient centers, which makes them very effective for various reduction reactions. Since B_2H_6 is electron-deficient, it attacks electron-rich areas in functional groups. This unique way makes diborane an acidic-type reducing agent, which is very different from the basic-type reducing agents like hydrides and borohydrides. It is especially useful in reducing multiple bonds in conjugated systems and in reducing certain unsaturated compounds where it targets electron-rich sites.[86]

1.3.3. Replacing B_2H_6 with manageable chemicals

Considering that B_2H_6 is highly toxic, flammable, and corrosive substance, and commercially unavailable in some countries.

Chapter 1

Incremental improvements in synthetic approaches towards borate anions have mainly focused on replacing diborane with reducing agents that present fewer handling issues. Most preparations involve reactions of hydride donors with boron halides or alkoxides, or directly using borane Lewis base complexes. The specific research directions can be broadly categorized into the following areas:

1. Replace B_2H_6 with borane Lewis base complexes

Borane Lewis base complexes ($L{\cdot}BH_3$) are a class of chemical compounds consisting of a borane (BH_3) molecule bonded to a Lewis base (L). In these complexes, the borane acts as a Lewis acid, accepting electron pairs from the Lewis base. The general formula for these complexes is $L{\cdot}BH_3$, where L represents the Lewis base, which is commonly available as liquid reagents. These complexes can generate "free borane" (BH_3) during the reaction. Such complexes offer a convenient source of borane for use as a reducing agent. In solution, $L{\cdot}BH_3$ have proven exceedingly useful for hydroboration reactions, providing similar reactivity to B_2H_6 but with fewer storage and handling issues.

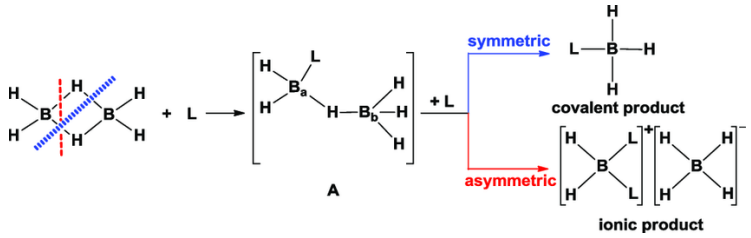

Figure 8. Symmetric and asymmetric cleavage of diborane, L representing Lewis base.[87]

The preparation of $L{\cdot}\ BH_3$ involved using diborane as precursor. Diborane can undergo cleavage through different pathways, namely symmetric or asymmetric cleavage (Figure 8). Symmetric cleavage

leads to a covalent product, such as $Et_3N{\cdot}BH_3$ and $DMS{\cdot}BH_3$, while asymmetric cleavage (red) produces the ionic species $[H_2B(NH_3)_2][BH_4]$, when ammonium (NH_3) used as the Lewis base.[87]

Among the available complexes, the borane-tetrahydrofuran complex ($THF{\cdot}BH_3$), borane-triethylamine complex ($Et_3N{\cdot}BH_3$), and $DMS{\cdot}BH_3$ are the most popular agents. These solutions offer less handling due to their relative stability, the reactivity of BH_3 is highly relevant with the Lewis basicity of the Lewis base in adduct. Although $THF{\cdot}BH_3$ is more reactive than $DMS{\cdot}BH_3$ and $Et_3N{\cdot}BH_3$, it is only commercially available as a solution (1 M) in THF and stabilized by 0.005 M $NaBH_4$. In contrast, $DMS{\cdot}BH_3$ and $Et_3N{\cdot}BH_3$ are more stable and are readily available as pure reagents. However, it is important to note that decomplexation of amine boranes is more difficult than $DMS{\cdot}BH_3$, possibly due to greater basicity of the alkylated nitrogen center that leads to a stronger boron-nitrogen bond. Based on the nucleophilicity substitution between B−H pair of electrons in the BH_4^- and $DMS{\cdot}BH_3$, recent research has been developed efficient synthetic methods towards lower-molecular-mass borates anions such as the $B_2H_7^-$ and $B_3H_8^-$.[88–90]

The Lewis base in borane complex must be chemically inert toward diborane. However, this is not the case. The formation of borane-ether complexes is known to occur, but more crucially, reductive cleavage of ether linkages by diborane is also known. Fortunately, reductive cleavage is a relatively slow reaction under normal conditions. With $THF{\cdot}\ BH_3$, heating for an extended period of time in a sealed tube is necessary to obtain a reasonable yield of tri-n-butyl borate.[77] Similarity, with $DMS{\cdot}\ BH_3$, the reductive cleavage in a sealed tube giving the formation of dimethyl sulfide substituted icosahedral boranes, mainly $B_{12}H_{11}(SMe_3)^-$, in combined with

trimethylsulfonium (SMe_3^+).[91]

2. *In situ* generation of BH_3 via the reaction of BH_4^- with organic halides

Another way to get diborane is through oxidative of BH_4^-. Alkyl fluorides, chlorides, bromides, and iodides are all inert toward diborane and the various borane-Lewis base complexes. Also, no reaction occurs between borane and aryl fluorides, chlorides, bromides, or iodides. However, under solvolysis conditions, sodium borohydride reacts with readily ionizable secondary and tertiary organic halides to give the corresponding hydrocarbon and BH_3. These organic halides can be used to oxidize excess borohydrides and forming BH_3 in situ, which subsequently react with borohydrides, the overall process can be illustrated as equations below[92]:

$$RX \rightarrow R^+ + X^- \quad (14)$$

$$R^+ + BH_4^- \rightarrow RH + BH_3 \quad (15)$$

The approach to the synthesis of $B_3H_8^-$ and $B_{11}H_{14}^-$ using alkyl halides to oxidize BH_4^- was considerably elaborated, the mechanism proposed as below: [92,93]

$$2\ \text{R-Hal} + 3\ NaBH_4 \rightarrow NaB_3H_8 + 2\ \text{NaHal} + H_2 + 2\ \text{RH} \quad (16)$$

$$10\ \text{R-Hal} + 11\ NaBH_4 \rightarrow NaB_{11}H_{14} + 10\ \text{NaHal} + 10\ H_2 + 10\ \text{RH} \quad (17)$$

Currently, the range of suitable organic halides for the oxidation of BH_4^- for condensation reactions was markedly extended ($C_5H_{11}Br$, $C_6H_5CH_2Cl$, n-C_4H_9Br, $C_2H_4Cl_2$, CH_2I_2, C_2HCl_3, etc.).

3. *in situ* generation of BH_3 *via* the reaction of BH_4^- with iodine

It is noteworthy that the use of the above listed approaches to the

synthesis of borohydride anions is complicated by the toxicity or explosiveness and poor accessibility of the starting compounds. A more convenient synthesis is based on the reaction of $NaBH_4$ with I_2 as a mild oxidant as shown in equations below[92]:

$$2\ NaBH_4 + I_2 \rightarrow B_2H_6 + H_2 + 2\ NaI \qquad (18)$$

$$3\ NaBH_4 + I_2 + \rightarrow NaB_3H_8 + 2\ H_2 + 2\ NaI \qquad (19)$$

Similarity to the reaction between organic halides and borohydrides, diborane is also formed in this reaction *in situ*, and then reacts with excess $NaBH_4$ to give $B_3H_8^-$ anion. Noteworthy, the decomposition of NaB_3H_8 giving $Na_2B_{12}H_{12}$ and $NaBH_4$ as products, the use of I_2 oxidation of $NaBH_4$ for the synthesis of borates has been regarded as a green "borane-free" method.

1.4. *Closo* borate anions and its properties

1.4.1. Structure and coordination in *closo* borates

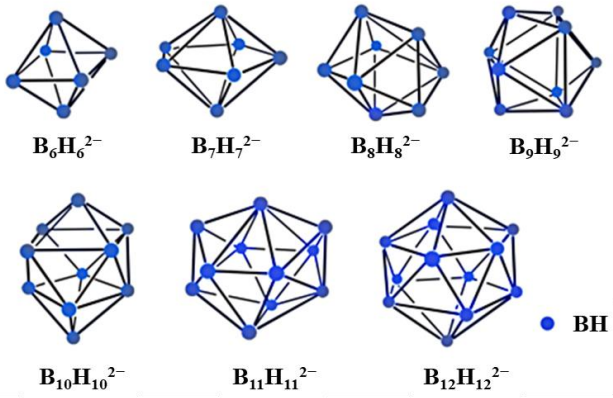

Figure 9. Illustration the polyhedral structures of $B_nH_n^{2-}$ (n = 6−12) dianions.[97]

Closo borates are defined as a class of anions with the formula $B_nH_n^{2-}$ (n = 6−12), featuring closed polyhedral clusters with a number of n boron atoms and n terminal hydrogen atoms, the structures of these borate anions are shown in Figure 9. These compounds exhibit exceptional stability due to delocalized bonding within the boron cage, resulting in symmetrical geometric shapes such as icosahedrons. Notable examples include the decaborate anion ($B_{10}H_{10}^{2-}$) and the dodecaborate anion ($B_{12}H_{12}^{2-}$). *Closo* borates have great potential in various fields, including medical treatments like boron neutron capture therapy (BNCT), materials science, and solid ionic conductors.

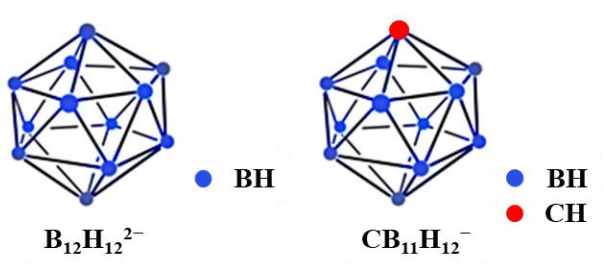

Figure 10. Illustration of the icosahedral structures of $B_{12}H_{12}^{2-}$ and $CB_{11}H_{12}^{-}$.

The structures of *closo* borates can be explained using Wade's rules for polyhedral (or “cluster”) materials. According to these rules, a polyhedral species with n vertices forms a *closo* structure (a closed, cage-like structure such as icosahedron) if there are n+1 electron pairs involved in the bonding within the polyhedron, with the cluster building atoms occupying all corners of the polyhedron. As an example in Figure 10, in the dianion $B_{12}H_{12}^{2-}$ contains a total of 50 valence electrons (36 from boron atoms, 12 from hydrogen atoms and 2 from charged cation). Of these, 24 electrons are available for boron-hydrogen (BH) vertices. Thus leaving 26 electrons (13 electron pairs) contributed for cage (cluster) bonding. Since n + 1 = 13, the structure

of the species is 12 vertexes polyhedral, specifically an icosahedron. When a boron-hydrogen (BH) vertex is substituted with a carbon-hydrogen (CH) vertex, the resulting structure is $CB_{11}H_{12}^{-}$. Although the total number of cage electrons remains at 26, the charge of the anion changes. This is because a carbon atom, with its six positive nuclear charges, replaces a boron atom, which has only five positive nuclear charges.

1.4.2. Localized bonds

In polyhedral boranes, electron delocalization leads to multi-center bonding, where electrons are shared among several atoms rather than localized between two. A unique feature is the formation of 3c-2e bonds, where two electrons are shared among three atoms. This creates a bonding situation stronger and more stable than typical 3c-2e bonds, contributing significantly to the robustness of B−B bonds. For example, the boron bonds in $B_{12}H_{12}^{2-}$ consist of ten B−B−B 3c-2e bonds and three normal B−B 2c-2e bonds. The geometric arrangement in these cage structures evenly distributes strain and minimizes repulsive interactions between atoms, further enhancing the robustness of B−B bonds.[99,100] Which enhances the stability of the structure by allowing for a more efficient distribution of electron density and lowering the overall energy of the molecule.[101,102]

Additionally, in open clusters borates (*nido* borates for instance), three centered B−H−B bridges are considered part of the cage framework while terminal B−H bonds are not included in this framework. Although the electrons involved in the cage construction of clusters are highly delocalized, the localized 3c-2e and 2c-2e orbital approaches can still explain the main features of boranes. Each B atom uses one electron to form a normal 2c-2e terminal B−H bond, and the

remaining two electrons are used in the framework.[102,103]

1.4.3. Aromaticity

The concept of aromaticity was initially introduced to explain the unusual structural and chemical properties of benzene. Aromatic molecules often exhibit resonance, where the π-electrons are delocalized over the entire ring structure, leading to increased stability. This concept extends beyond simple organic molecules to polycyclic aromatic hydrocarbons, and even some inorganic compounds, such as *closo* borates, which exhibit three-dimensional (3D) aromaticity due to similar delocalization of electrons. The polyhedral surfaces of boron cages are constructed with three centered boron atoms forming triangular units. The localized orbitals of these three-centered B-B-B bonds interact with each other, and the linear combinations of these interactions result in a aromatic character.[104] It was also shown that not only the closed clusters but also the open cage clusters such as *nido* and *arachno* boranes exhibit aromatic character. However, the aromaticity of the *closo* borates is significantly higher than that of the open structures due to the extensive electron delocalization. Among these, $B_{12}H_{12}^{2-}$ is the most aromatic borates, attributable to its highly symmetric structure. This intrinsic symmetry facilitates a greater extent of electron delocalization, thereby enhancing its aromatic character.[104,105]

1.4.4. Weak coordinating ability

An anion is weakly coordinating when its charge is delocalized over the entire surface of the anion rather than localized at a specific atom. Ideal weakly coordinating anions have a high degree of charge delocalization over the entire anion, a low charge, large sizes, and

properties typical of *colso* borates. Their properties as weakly coordinating ability of *colso* borates can be significantly improved by halogenation. These halogenated borate anions are extremely chemically and electrochemically robust, which can be attributed to the strength of the boron-halogen bond and their 3D aromatic electronic structure. In electrochemical applications, weakly coordinating anions contribute to higher ionic conductivity in electrolyte due to their dissociate completely without forming strong ion pairs.[106–108]

1.5. Synthesis and applications of $B_{12}H_{12}^{2-}$

1.5.1. Synthesis of $B_{12}H_{12}^{2-}$

At present, a large variety of synthesis methods has been developed to synthesize closo-$B_nH_n^{2-}$ (n = 6−12), among which, the convenient synthetic methods have been well developed for the synthesis of more stable borates anions such as $B_6H_6^{2-}$, $B_{10}H_{10}^{2-}$ and $B_{12}H_{12}^{2-}$, whereas the synthesis of lower symmetric borate anions such as $B_7H_7^{2-}$, $B_8H_8^{2-}$, $B_9H_9^{2-}$, $B_{11}H_{11}^{2-}$ require further improvement.[97,98] Among *closo* borate anion family, $B_{12}H_{12}^{2-}$ is the most stable member and known relatively easily to be synthesized. The $B_{12}H_{12}^{2-}$ anion, characterized by an icosahedral boron cluster with 12 identical B−H vertices, possesses unique properties, such as spherical electron delocalization. Its derivatives are known as weak coordinating anions and show promise for use as solid ionic conductor materials as mentioned above.[109–111] However, up to now, the high commercial cost of metal-salt derivatives of $B_{12}H_{12}^{2-}$ remains as an obstacle for its broader application.

The chemistry of $B_{12}H_{12}^{2-}$ developed after 1955 when Longuet Higgins and Roberts reported its electronic structure based on calculations. They proposed that icosahedral borane would be stable only as dianion $B_{12}H_{12}^{2-}$.[112] Later in 1960, Hawthorne and Pitochelli isolated the $B_{12}H_{12}^{2-}$ anion for the first time as a side product of the reaction of 2-iododecaborane and triethylamine in refluxing benzene.[69] Till now, several methods for its synthesis have been developed. The main synthesis routes based on the borane precursors are summarized in Figure 11.

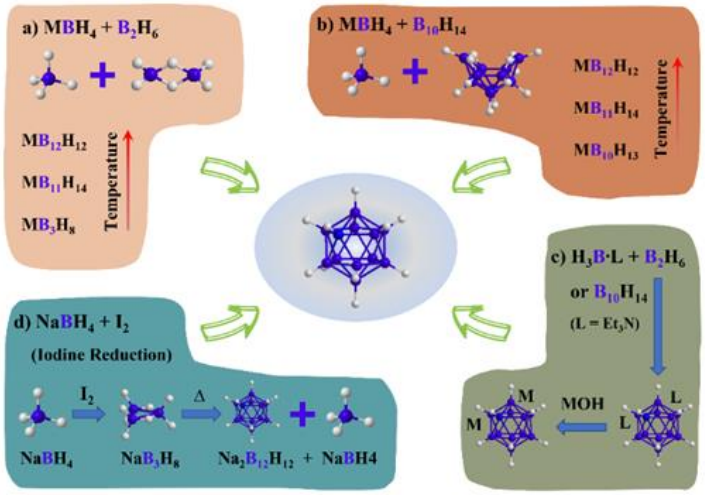

Figure 11. Schematic of known popular synthesis routes for the metal dodecaborates, classified by oxidants used.

The first method is the reaction of borohydrides with B_2H_6, which produces a series of boron rich anions (Figure 11a). The composition is temperature-dependent, the anions are tending to become larger and more stable at higher temperatures.[113] For example, the reaction between B_2H_6 and $NaBH_4$ resulted in $Na_2B_{12}H_{12}$ when carried out in triethylamine at 100−180 °C. Alternatively, at 25 °C in dimethoxyethane, the same reaction produced NaB_3H_8, but raising the

temperature above 50 °C led to a mixture of $NaB_{11}H_{14}$ and $Na_2B_{12}H_{12}$. More recently, solvent-free methods have been adopted, involving direct solid-gas reactions between borohydrides and diborane. However, significant yields of $M_xB_{12}H_{12}$ are achieved when reactions between MBH_4 and B_2H_6 are conducted in a mechanical mill to enhance diborane permeability through the newly formed $MB_{12}H_{12}$ layer, milling at elevated temperatures can also facilitate the formation of $MB_{12}H_{12}$.[114]

The second method relies on the use of $B_{10}H_{14}$, the solvent mediated reaction between $B_{10}H_{14}$ and borohydride in diglyme was firstly described in 1964.[115] In diglyme, the reaction be BH_4^- and $B_{10}H_{14}$ occurring at room temperature generates $B_{10}H_{13}^-$ at the first stage (eq. 20), $B_{11}H_{14}^-$ forms when the temperature is at about 90 °C, second equivalent of borohydride in this system undergoes further reaction at higher temperatures to form the $B_{12}H_{12}^{2-}$ ion. Similar work was conducted later by reacting BH_4^- and $B_{10}H_{14}$ in diglyme at 140 °C with a yield of $B_{12}H_{12}^{2-}$ of about 91%.[116] More recently, solvent-free reaction was reported involving by annealing alkali and alkali earth borohydrides with $B_{10}H_{14}$ in a sealed vessel at 200−450 °C and producing solvent-free $M_2B_{12}H_{12}$ (M = Li, Na, K) and $MB_{12}H_{12}$ (M = Mg, Ca).[117–119]

$$\begin{aligned} B_{10}H_{14} + BH_4^- + R_2O &\rightarrow B_{10}H_{13}^- + R_2O{\cdot}BH_3 + H_2 \\ &\rightarrow B_{11}H_{14}^- + R_2O + H_2 \\ BH_4^- + B_{11}H_{14}^- &\rightarrow B_{12}H_{12}^{2-} + 3\,H_2 \end{aligned} \qquad (20)$$

The reaction involving the borane Lewis base complex ($L{\cdot}BH_3$, with L = Et_3N) and boranes (B_2H_6, $B_{10}H_{14}$) results in a high yield of $B_{12}H_{12}^{2-}$, as illustrated in Figure 11c, up to an impressive yield of approximately 92 %.

The I_2 reduction is known as ‘‘borane free’’ method is a two-step

synthesis that relies on the oxidation of borohydrides by iodine (Figure 11d). During the first step, $NaBH_4$ reacts with I_2 in diglyme, giving NaB_3H_8 as the main intermediate. $Na_2B_{12}H_{12}$ can then be obtained as one of the pyrolysis products of NaB_3H_8, at 150 °C (eq. 21 and 22). While this procedure is cost-effective and specific for large scale production, it often produces $B_{12}H_{12}^{2-}$ in low yield, ranging from 50% to 60%. The reduced yield is mostly due to the restricted conversion of $NaBH_4$ and difficulties encountered during the purifying process.[84,120,121]

$$3\ NaBH_4 + I_2 \rightarrow NaB_3H_8 + 2\ NaI + 2\ H_2 \qquad (21)$$

$$5\ NaB_3H_8 \rightarrow Na_2B_{12}H_{12} + 3\ NaBH_4 + 8\ H_2 \qquad (22)$$

Looking at the starting materials summarized in Table 2 below, we conclude that synthetic approaches to the $B_{12}H_{12}^{2-}$ anion can be divided into three major groups:

A: Borohydrides, for example, MBH_4, MB_3H_8 and $MB_{11}H_{14}$, these borohydrides with the number of boron atoms in the cluster of less than 12.

B: Neutral boranes (or Lewis's acid reacting with borohydride generating boranes *in situ*, such as I_2, R-Hal), for example, B_2H_6, B_5H_9, $B_{10}H_{14}$.

C: Borane Lewis base complexes ($L{\cdot}BH_3$), for example, $Et_3N{\cdot}BH_3$, $DMS{\cdot}BH_3$

A variety of experimental parameters matters while synthesizing $B_{12}H_{12}^{2-}$, including the manipulation of specific conditions such as temperature, solvent of choice, reaction duration, and the effective removal of by-products formed throughout the process. Any combinations of groups A, B, and C, and any compounds belongs to A and C can contribute to synthesizing $B_{12}H_{12}^{2-}$.

Table 2. Known synthetic methods to access $B_{12}H_{12}^{2-}$.

Code	Reaction	Condition	Purity	Yields
1[95]	2-Iododecaborane+$N(C_2H_5)_3$	Refluxing benzene, 5 h	n/a	4 %
2[113]	2 $NaBH_4$ + 5 B_2H_6 → $Na_2B_{12}H_{12}$ + 13H_2 2 $(C_2H_5)_3N{\cdot}BH_3$ + 5 B_2H_6 → $[(C_2H_5)_3NH]_2B_{12}H_{12}$ + 13 H_2	Ethers, 100−180°C	n/a	90 %
3[124]	Mg $(BH_4)_2$ + 5 B_2H_6 → $MgB_{12}H_{12}$ + 13 H_2	150°C, 24 h	22.3 mol %	n/a
4[125]	2 $LiBH_4$ + 5 B_2H_6 → $Li_2B_{12}H_{12}$ + 13 H_2	150 °C, 10 bar H_2/B_2H_6	94 %	n/a
5[113]	$B_{10}H_{14}$ + Et_3NBH_3 → $B_{12}H_{12}^{2-}$	190 °C	n/a	92 %
6[116]	$B_{10}H_{14}$ + $NaBH_4$ → $Na_2B_{12}H_{12}$ + 3 H_2	Diglyme, 160 °C	n/a	91 %
7[118]	2 MH+1.2 $B_{10}H_{14}$ → $M_2B_{12}H_{12}$+ 3.4 H_2 (M=Li, Na) 2 MBH_4 + $B_{10}H_{14}$ → $M_2B_{12}H_{12}$ + 5 H_2 (M=Li, Na, K)	Annealing 200−450 °C, 10−20 h	n/a	n/a
8[126]	$M(BH_4)_2$ + $B_{10}H_{14}$ → $MB_{12}H_{12}$ + 5H_2 (M = Mg, Ca)	Annealing, 300°C Annealing, 380°C	n/a n/a	n/a
9[119]	2$LiBH_4$ + $B_{10}H_{14}$ → $Li_2B_{12}H_{12}$ + 5H_2	135°C +180 °C 200°C, 15 h	93 % 62 %	n/a n/a
10[121]	2 C_7H_7Cl + 3$NaBH_4$ → NaB_3H_8 + 2 NaCl + H_2 + 2 C_7H_8 5 NaB_3H_8 → $Na_2B_{12}H_{12}$ + 3 $NaBH_4$ + 8 H_2	Diglyme, 165°C	n/a	44 %
11[127]	8 $(C_2H_5)_4N{\cdot}B_3H_8$ → $[(C_2H_5)_4N]_2B_{12}H_{12}$ + $[(C_2H_5)_4N]_2B_{10}H_{10}$ + 4 C_2H_6 + 16 H_2 + 2 $(C_2H_5)_3N$ + 2 $(C_2H_5)_3NBH_3$	Toluene, 185°C	n/a	n/a
12[107]	3 $NaBH_4$ + I_2 → NaB_3H_8 + 2 NaI + 2 H_2 5 NaB_3H_8 → $Na_2B_{12}H_{12}$ + 3 $NaBH_4$ + 8 H_2	Diglyme, 100°C	n/a	51%
13[128]	NaB_3H_8 → $Na_2B_{10}H_{10}$ + $Na_2B_{12}H_{12}$	Ar, 150°C, 48 h	n/a	n/a
14[129]	12 $NaBH_4$+10 R-Hal→ $Na_2B_{12}H_{12}$ + 10 R−H+ 10 NaCl + 13 H_2	Ether	n/a	84%
15[130]	2 MBH_4 + 10 $(CH_3)_2S{\cdot}BH_3$ → $M_2B_{12}H_{12}$ + 10 $(CH_3)_2S$ + 13 H_2 (M=Na, K)	Autoclave, diglyme	pure	85 % 84 %
16[131]	KB_3H_8 + KB_9H_{14}	Diglyme, 120 °C, 36 h		82%
	KB_3H_8 + KB_9H_{14}	1,4−dioxane, 90 °C	n/a	0
	$NaB_{11}H_{14}$ + NaB_3H_8	Diglyme, 140 °C, 40 h		80%

In an alternative approach, the pyrolysis (dehydrogenation) of BH_4^- can also leads to the formation of a diverse range of *closo* borate compounds. For instance, Pyrolysis Et_4NBH_4 by refluxing

decanedodecane at temperatures between 175 and 190 °C results in the mixtures of $B_{12}H_{12}^{2-}$, $B_{10}H_{10}^{2-}$, $B_9H_9^{2-}$ and $B_{11}H_{14}^{-}$.[122] The thermolysis of $Mg(BH_4)_2$ in various glymes at 160−200 °C for 8 hours yields of $Mg(B_{10}H_{10})$ and $Mg(B_{12}H_{12})$ in different ratios.[123]

In comparison to the pyrolysis of BH_4^-, the pyrolysis of $B_3H_8^-$ is capable to yield higher purity $B_{12}H_{12}^{2-}$ salts. Direct pyrolysis of $B_3H_8^-$ in the presence of metal ions as counter cations yields various final products depending on the metal counter cation and the temperature used. For instance, direct pyrolysis of NaB_3H_8 at 160 °C gives a 90% yield of $Na_2B_{12}H_{12}$ in high purity but with BH_4^- formation, while the pyrolysis of KB_3H_8 at 180 °C yields a mixture of $B_{12}H_{12}^{2-}$, $B_{10}H_{10}^{2-}$, and $B_{11}H_{14}^{-}$.[88] And the pyrolysis of CsB_3H_8 at 185 °C gave mainly $B_{12}H_{12}^{2-}$ an $B_{10}H_{10}^{2-}$, whereas at a higher temperature (230 °C), $B_9H_9^{2-}$, $B_{10}H_{10}^{2-}$, and $B_{12}H_{12}^{2-}$ formed.[98] In contrast, pyrolysis of $Pr_4NB_3H_8$ yields only $Pr_4NB_{12}H_{12}$.[132]

1.5.2. Solvent mediated synthesis of $B_{12}H_{12}^{2-}$

The solution-based method for synthesizing *closo* borates offers several advantages over gas-solid or solid-state approaches, primarily due to its high throughput and scalability. This method typically involves using borane precursors like B_2H_6, B_5H_9, or $B_{10}H_{14}$, which react with borohydrides to form intermediate complexes such as $[(CH_3)_3NH]_2B_{12}H_{12}$. Subsequent ion exchange with metal hydroxides yields $Na_2B_{12}H_{12}$, resulting in high-purity metal dodecaboranes. While solvent-free techniques have gained attention for direct producing anhydrous $B_{12}H_{12}^{2-}$ salts, however the inhomogeneous reactions often yield other boron-rich compounds alongside the desired product.[84,95]

The choice of solvent significantly influences the reaction efficiency and selectivity. Solvent-mediated reactions utilize solvent

properties to enhance reactant interactions, improve yields, and sometimes dictate reaction pathways. For example, $NaBH_4$ reaction with diborane in the presence of triethylamine at 180 °C yields $Na_2B_{12}H_{12}$ with a 90% yield. However, varying solvents can alter product distributions; dimethoxyethane yields a $B_{12}H_{12}^{2-}$ to $B_{11}H_{14}^{-}$ ratio of 50:40, while diethyl ether at 100 °C for 10 h produces a 40% $B_{12}H_{12}^{2-}$ yield. In dioxane at similar conditions, $B_{11}H_{14}^{-}$ anion is formed as only product.[95,133]

Solution-based methods often result in metal-$B_{12}H_{12}$ complexes in solvate form, which can complicate purification. Cation exchange with bulky singly charged cations like Cs^+, Et_3N^+ R_4N^+, R_4P^+, or R_3S^+ can yield water-insoluble $B_{12}H_{12}^{2-}$ salts suitable for analytical purposes. Triethylamine is a preferred cation in research work due to its effectiveness.[132]

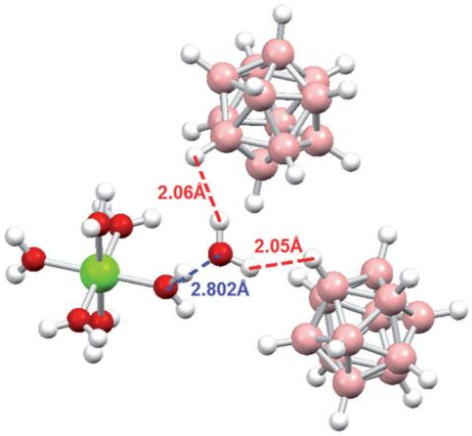

Figure 12. Structure of $Mg(H_2O)_6B_{12}H_{12}$. Color code: hydrogen, white; magnesium, green; oxygen, red.[135]

On the other hand, ion exchange between $(H_3O)_2B_{12}H_{12}$ and metal hydroxides yields hydrated metal-$B_{12}H_{12}$, which can be dehydrated to form anhydrous metal-$B_{12}H_{12}$.[134] Cation charge density,

determined by factors like charge, ionic radius, and coordination number, influences solvent coordination. Higher charge density cations exhibit stronger solvent coordination, making solvent removal challenging. Complexes with low charge density elements like Na^+ and K^+ can be dehydrated without decomposition, while those with high charge density elements like Mg^{2+} tend to decompose during desolvation. As shown in Figure 12, In the structures of hydrated $MgB_{12}H_{12}$, Specific B–H…H–O interactions between the hydrogen atoms of the BH groups of the polyhedron and hydrogen atoms from free water molecules are observed in the structure. Of the six water molecules coordinated to magnesium, only three are removed by heating to about 200 °C. Above 200 °C, competition between dehydration and hydrolysis/ dehydrogenation occur simultaneously to yield polyhydroxylated complexes. [135]

Compared to hydrated metal-$B_{12}H_{12}$ salts, there are limited data available on complexes containing ether-solvated metal-$B_{12}H_{12}$. Ethers are commonly employed as solvents in the synthesis of metal-$B_{12}H_{12}$, often resulting in ether-solvated metal-$B_{12}H_{12}$ as the primary product. Comprehensive data on the composition and coordination environment of the cations in these metal-$B_{12}H_{12}$ complexes could offer a straightforward approach to the preparation of anhydrous metal-$B_{12}H_{12}$ without the need for cation exchange. Understanding the coordination interactions of these ethers with metal cations in metal-$B_{12}H_{12}$ complexes can provide valuable insights into optimizing synthesis methods to directly yield anhydrous metal-$B_{12}H_{12}$, enhancing efficiency and purity in the production process.

1.5.3. Applications of $B_{12}H_{12}^{2-}$

Metal-$B_{12}H_{12}$ and its derivatives exhibit unique properties that

have opened up numerous applications across various fields, including solid state electrolytes, materials science, catalysis, and medicine.

In the field of solid-state electrolytes, $B_{12}H_{12}^{2-}$ salts exhibit good ionic conductivity under high-temperature conditions.[39] For instance, $Na_2B_{12}H_{12}$ can undergoes a phase transition from an ordered monoclinic phase to a disordered cubic phase at around 256 °C, the conductivity of the high-temperature phase $Na_2B_{12}H_{12}$ (HT-$Na_2B_{12}H_{12}$) is much higher (1000 times) than for low-temperature phase (LT-$Na_2B_{12}H_{12}$). Additionally, $B_{12}H_{12}^{2-}$ salts from solid solutions with different cations and anions (for example $B_{10}H_{10}^{2-}$ and $B_{12}H_{12}^{2-}$), also demonstrating excellent performance in terms of ion conductivity.[111,136] Figure 13 outlines the conductivity data for a few known boron clusters and other electrolytes with weak coordinating anions.

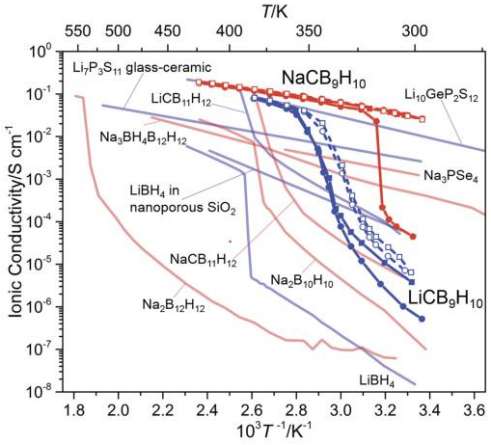

Figure 13. Comparison of the conductivities as a function of temperature for selected boron clusters with other popular electrolytes. [137]

Incorporation of $B_{12}H_{12}^{2-}$ and its derivatives into polymers and ceramics. These derivatives enhance the thermal stability, mechanical strength, and resistance to chemical degradation of these materials,

making them suitable for high performance applications. Furthermore, they are used in the development of materials for non-linear optics, which are essential for advanced optical technologies.[138]

$B_{12}H_{12}^{2-}$ also play a role in nuclear waste purification, helping to extract and stabilize radioactive elements, and in ion-selective electrodes, improving their sensitivity and selectivity for various ions. Additionally, they are involved in the production of boron carbide, a material known for its hardness and use in armor and abrasives. [139]

Medicine is perhaps the most prominent field for the application of $B_{12}H_{12}^{2-}$ derivatives (BSH, $B_{12}H_{11}SH^{-}$). Boron Neutron Capture Therapy (BNCT) is a targeted cancer treatment that utilizes the high neutron capture cross-section of boron atoms within the anion. This process selectively destroys cancer cells while sparing healthy tissue. Sodium borocaptate, a derivative of the $B_{12}H_{12}^{2-}$ anion, is one of the clinically used agents in BNCT. Beyond cancer treatment, BNCT has potential applications in treating localized diseases like rheumatoid arthritis through boron neutron capture synovectomy, targeting inflamed synovium.[140]

1.6. Objectives of the thesis

Polyhedral boranes are a well-known class of boron clusters with unique physical and chemical properties. However, existing synthetic methods suffer from low efficiency and selectivity, and there is a lack of understanding of the formation mechanism, which are crucial factors for the effective synthesis of *closo* boranes. The current primary method for synthesizing *closo* borates, especially $B_{12}H_{12}^{2-}$, involves the condensation reaction between borohydride and diborane in ethers. However, diborane is an expensive and commercially unavailable gas, making it necessary to seek alternative reagents with fewer handling issues. Additionally, the metal-$B_{12}H_{12}$ formed through solvent methods often coordinate with ethers, necessitating simpler methods to improve operational simplicity. To address these issues, the thesis work is organized according to the following objectives:

a) Finding an alternative to diborane: The first objective aims to identify a suitable substitute for diborane. We employed $DMS{\cdot}BH_3$ as a borane precursor. The condensation reaction between $DMS{\cdot}BH_3$ and borohydrides to form $B_{12}H_{12}^{2-}$ has never been attempted before, and the output of polyhedral boranes from solvothermal synthesis is often difficult to control, resulting in a mixture of borates. Thus, we systematically investigate the effect of key parameters such as reactant ratio, reaction time, temperature, and pressure, aiming to maximize the yield and purity of $B_{12}H_{12}^{2-}$. Moreover, published synthesis methods focus mainly on $Na_2B_{12}H_{12}$. Further extending the reaction to prepare other metal-$B_{12}H_{12}$ and even directly prepare organic-$B_{12}H_{12}$, we aim to gain more insights into the condensation reactions.

b) Developing an effective method for desolvation: The second

objective is to develop an effective method to remove solvents from ether-solvated metal-$B_{12}H_{12}$ complexes directly. Using heavy ethers such as glymes results in ether-solvated metal-$B_{12}H_{12}$ salts. There are limited reports on the structure and properties of ether-solvated metal-$B_{12}H_{12}$. Therefore, we aim to expand the understanding of these complexes by investigating their desolvation process and characterizing the resulting products.

c) Elucidating the reaction mechanism: The third objective is to uncover the detailed reaction mechanism underlying the condensation process that leads to the formation of $B_{12}H_{12}^{2-}$. Understanding the mechanistic pathway is crucial for optimizing the reaction conditions and improving the efficiency and selectivity of the synthesis.

1.7. Reference

(1) Tarhan, C.; Çil, M. A. A Study on Hydrogen, the Clean Energy of the Future: Hydrogen Storage Methods. *J. Energy Storage* **2021**, *40*, 102676.

(2) Arshad, M. Clean and Sustainable Energy Technologies. *Clean Energy Sustain. Dev.* **2017**, 73–89.

(3) Kresse, G.; Furthmüller, J. Efficient Iterative Schemes for Ab Initio Total-Energy Calculations Using a Plane-Wave Basis Set. *Phys. Rev. B* **1996**, *54* (16), 11169.

(4) Eberle, U.; Felderhoff, M.; Schüth, F. Chemical and Physical Solutions for Hydrogen Storage. *Angew. Chem. Int. Ed.* **2009**, *48* (36), 6608–6630.

(5) Hirscher, M. Handbook of Hydrogen Storage, **2010**.

(6) Ley, M. B.; Jepsen, L. H.; Lee, Y.-S.; Cho, Y. W.; Bellosta von Colbe, J. M.; Dornheim, M.; Rokni, M.; Jensen, J. O.; Sloth, M.; Filinchuk, Y.; Jørgensen, J. E.; Besenbacher, F.; Jensen, T. R. Complex Hydrides for Hydrogen Storage – New Perspectives. *Mater. Today* **2014**, *17* (3), 122–128.

(7) Çakanyıldırım, Ç.; Gürü, M. Hydrogen Cycle with Sodium Borohydride. *Int. J. Hydrogen Energy* **2008**, *33* (17), 4634–4639.

(8) Dincer, I.; Acar, C. Review and Evaluation of Hydrogen Production Methods for Better Sustainability. *Int. J. Hydrogen Energy* **2015**, *40* (34), 11094–11111.

(9) Younas, M.; Shafique, S.; Hafeez, A.; Javed, F.; Rehman, F. An Overview of Hydrogen Production: Current Status, Potential, and Challenges. *Fuel* **2022**, *316*, 123317.

(10) Faye, O.; Szpunar, J.; Eduok, U. A Critical Review on the Current Technologies for the Generation, Storage, and Transportation of Hydrogen. *Int. J. Hydrogen Energy* **2022**, *47* (29), 13771–13802.

(11) Møller, K. T.; Jensen, T. R.; Akiba, E.; Li, H. Hydrogen - A Sustainable Energy Carrier. *Prog. in Nat. Sci- Mater.* **2017**, *27* (1), 34–40.

(12) Li, J.-Q.; Li, J.-C.; Park, K.; Jang, S.-J.; Kwon, J.-T. An Analysis on the Compressed Hydrogen Storage System for the Fast-Filling Process of Hydrogen Gas at the Pressure of 82 MPa. *Energies* **2021**, *14* (9), 2635.

(13) Zheng, J.; Liu, X.; Xu, P.; Liu, P.; Zhao, Y.; Yang, J. Development of High Pressure Gaseous Hydrogen Storage Technologies. *Int. J. Hydrogen Energy* **2012**, *37* (1), 1048–1057.

(14) Ahluwalia, R. K.; Hua, T. Q.; Peng, J.-K.; Lasher, S.; McKenney, K.; Sinha, J.; Gardiner, M. Technical Assessment of Cryo-Compressed Hydrogen Storage Tank Systems for Automotive Applications. *Int. J. Hydrogen Energy* **2010**, *35* (9), 4171–4184.

(15) Lototskyy, M. V.; Yartys, V. A.; Pollet, B. G.; Bowman, R. C. Metal Hydride Hydrogen Compressors: A Review. *Int. J. Hydrogen Energy* **2014**, *39* (11), 5818–5851.

(16) Milanese, C.; Jensen, T. R.; Hauback, B. C.; Pistidda, C.; Dornheim, M.; Yang, H.; Lombardo, L.; Zuettel, A.; Filinchuk, Y.; Ngene, P.; de Jongh, P. E.; Buckley, C. E.; Dematteis, E. M.; Baricco, M. Complex Hydrides for Energy Storage. *Int. J. Hydrogen Energy* **2019**, *44*, 7860–7874.

(17) Orimo, S.; Nakamori, Y.; Eliseo, J. R.; Züttel, A.; Jensen, C. M. Complex Hydrides for Hydrogen Storage. *Chem. Rev.* **2007**, *107* (10), 4111–4132.

(18) Klopčič, N.; Grimmer I.; Winkler F.; Sartory M.; Trattner A. A review on metal hydride materials for hydrogen storage. *J. Energy Storage*, **2023**, *72*, 108456.

(19) Lan, R.; Irvine, J. T. S.; Tao, S. Ammonia and Related Chemicals as Potential Indirect Hydrogen Storage Materials. *Int. J. Hydrogen Energy* **2012**, *37* (2), 1482–1494.

(20) Juan-Juan, J.; Marco-Lozar, J. P.; Suárez-García, F.; Cazorla-Amorós, D.; Linares-Solano, A. A Comparison of Hydrogen Storage in Activated Carbons and a Metal–Organic Framework (MOF-5). *Carbon* **2010**, *48* (10), 2906–2909.

(21) Soulié, J.-P.; Renaudin, G.; Černý, R.; Yvon, K. Lithium Borohydride $LiBH_4$. *J. Alloys Compd.* **2002**, *346* (1–2), 200–205.

(22) Kim, J.-H.; Jin, S.-A.; Shim, J.-H.; Cho, Y. W. Thermal Decomposition Behavior of Calcium Borohydride $Ca(BH_4)_2$. *J. Alloys Compd.* **2008**, *461* (1–2), 20–22.

(23) Matsunaga, T.; Buchter, F.; Mauron, P.; Bielman, M.; Nakamori, Y.; Orimo, S.; Ohba, N.; Miwa, K.; Towata, S.; Züttel, A. Hydrogen Storage Properties of $Mg[BH_4]_2$. *J. Alloys Compd.* **2008**, *459* (1–2), 583–588.

(24) Hirscher, M.; Yartys, V. A.; Baricco, M.; Bellosta von Colbe, J.; Blanchard, D.; Bowman, R. C.; Broom, D. P.; Buckley, C. E.; Chang, F.; Chen, P.; Cho, Y. W.; Crivello, J.-C.; Cuevas, F.; David, W. I. F.; de Jongh, P. E.; Denys, R. V.; Dornheim, M.; Felderhoff, M.; Filinchuk, Y.; Froudakis, G. E.; Grant, D. M.; Gray, E. MacA.; Hauback, B. C.; He, T.; Humphries, T. D.; Jensen, T. R.; Kim, S.; Kojima, Y.; Latroche, M.; Li, H.-W.; Lototskyy, M. V.; Makepeace, J. W.; Møller, K. T.; Naheed, L.; Ngene, P.; Noréus, D.; Nygård, M. M.; Orimo, S.; Paskevicius, M.; Pasquini, L.; Ravnsbæk, D. B.; Veronica Sofianos, M.; Udovic, T. J.; Vegge, T.; Walker, G. S.; Webb, C. J.; Weidenthaler, C.; Zlotea, C. Materials for Hydrogen-Based Energy Storage – Past, Recent Progress and Future Outlook. *J. Alloys Compd.* **2020**, *827*, 153548.

(25) Osman, A. I.; Mehta, N.; Elgarahy, A. M.; Hefny, M.; Al-Hinai, A.; Al-Muhtaseb, A. H.; Rooney, D. W. Hydrogen Production, Storage, Utilisation and Environmental Impacts: A Review. *Environ. Chem. Lett*. **2022**, *20*, 153–188.

(26) Wang, L.-L.; Graham, D. D.; Robertson, I. M.; Johnson, D. D. On the Reversibility of Hydrogen-Storage Reactions in $Ca(BH_4)_2$: Characterization via Experiment and Theory. *J. Phys. Chem. C* **2009**, *113* (46), 20088–20096.

(27) Tarkowski, R. Underground Hydrogen Storage: Characteristics and Prospects. *Renew. Sust. Energ. Rev*. **2019**, *105*, 86–94.

(28) Hematpur, H.; Abdollahi, R.; Rostami, S.; Haghighi, M.; Blunt, M. J. Review of Underground Hydrogen Storage: Concepts and Challenges. *Adv. Geo-Energy Res.* **2023**, *7* (2), 111–131.

(29) Tarkowski, R.; Uliasz-Misiak, B. Towards Underground Hydrogen Storage: A Review of Barriers. *Renew. Sust. Energ. Rev*. **2022**, 162, 112451.

(30) Sakintuna, B.; Lamaridarkrim, F.; Hirscher, M. Metal Hydride Materials for Solid Hydrogen Storage: A Review. *Int. J. Hydrogen Energy* **2007**, *32* (9), 1121–1140.

(31) Rude, L. H.; Nielsen, T. K.; Ravnsbæk, D. B.; Bösenberg, U.; Ley, M. B.; Richter, B.; Arnbjerg, L. M.; Dornheim, M.; Filinchuk, Y.; Besenbacher, F.; Jensen, T. R. Tailoring Properties of Borohydrides for Hydrogen Storage: A Review. *Phys. Status Solidi A* **2011**, *208* (8), 1754–1773.

(32) Lee, S. Y.; Lee, J. H.; Kim, Y. H.; Kim, J. W.; Lee, K. J.; Park, S. J. Recent Progress Using Solid-State Materials for Hydrogen Storage: A Short Review.

Processes **2022**. *10* (2), 304.

(33) Falkowski, P.; Scholes, R. J.; Boyle, E.; Canadell, J.; Canfield, D.; Elser, J.; Gruber, N.; Hibbard, K.; Högberg, P.; Linder, S.; Mackenzie, F. T.; Moore III, B.; Pedersen, T.; Rosenthal, Y.; Seitzinger, S.; Smetacek, V.; Steffen, W. The Global Carbon Cycle: A Test of Our Knowledge of Earth as a System. *Science* **2000**, *290* (5490), 291–296.

(34) Michel, H. Editorial: The Nonsense of Biofuels. *Angew. Chemie - Int. Ed.* **2012**, *51* (11), 2516–2518.

(35) Modak, A.; Bhanja, P.; Dutta, S.; Chowdhury, B.; Bhaumik, A. Catalytic Reduction of CO_2 into Fuels and Fine Chemicals. *Green Chem.* **2020**, *22* (13), 4002–4033.

(36) Wang, J.; Tan, H.; Zhu, Y.; Chu, H.; Chen, H. M. Linking the Dynamic Chemical State of Catalysts with the Product Profile of Electrocatalytic CO_2 Reduction. *Angew. Chemie* **2021**, *133* (32), 17394–17407.

(37) Dovgaliuk, I.; Hagemann, H.; Leyssens, T.; Devillers, M.; Filinchuk, Y. CO_2 - Promoted Hydrolysis of KBH_4 for Efficient Hydrogen Co-Generation. *Int. J. Hydrogen Energy* **2014**, *39* (34), 19603–19608.

(38) Allendorf, M. D.; Stavila, V.; Snider, J. L.; Witman, M.; Bowden, M. E.; Brooks, K.; Tran, B. L.; Autrey, T. Challenges to Developing Materials for the Transport and Storage of Hydrogen. *Nat. Chem.* **2022**, *14*(11), 1214–1223.

(39) Udovic, T. J.; Matsuo, M.; Tang, W. S.; Wu, H.; Stavila, V.; Soloninin, A. V.; Skoryunov, R. V.; Babanova, O. A.; Skripov, A. V.; Rush, J. J.; Unemoto, A.; Takamura, H.; Orimo, S. Exceptional Superionic Conductivity in Disordered Sodium Decahydro- Closo -decaborate. *Adv. Mater.* **2014**, *26* (45), 7622–7626.

(40) Schlesinger, H. I.; Brown, H. C. Metallo Borohydrides. III. Lithium Borohydride. *J. Am. Chem. Soc.* **1940**, *62* (12), 3429–3435.

(41) Schlesinger, H. I.; Brown, H. C.; Finholt, A. E.; Gilbreath, J. R.; Hoekstra, H. R.; Hyde, E. K. Sodium Borohydride, Its Hydrolysis and Its Use as a Reducing Agent and in the Generation of Hydrogen 1. *J. Am. Chem. Soc.* **1953**, *75* (1), 215–219.

(42) Dematteis, E. M.; Amdisen, M. B.; Autrey, T.; Barale, J.; Bowden, M. E.; Buckley, C. E.; Cho, Y. W.; Deledda, S.; Dornheim, M.; de Jongh, P.; Grinderslev, J.

B.; Gizer, G.; Gulino, V.; Hauback, B. C.; Heere, M.; Heo, T. W.; Humphries, T. D.; Jensen, T. R.; Kang, S. Y.; Lee, Y.-S.; Li, H.-W.; Li, S.; Møller, K. T.; Ngene, P.; Orimo, S.; Paskevicius, M.; Polanski, M.; Takagi, S.; Wan, L.; Wood, B. C.; Hirscher, M.; Baricco, M. Hydrogen Storage in Complex Hydrides: Past Activities and New Trends. *Progress in Energy* **2022**, *4* (3), 032009.

(43) Suárez-Alcántara, K.; Tena García, J. R. Metal Borohydrides beyond Groups I and II: A Review. *Materials* **2021**, *14* (10), 2561.

(44) Singh, R. Reversible Chemical Hydrogen Storage in Borohydrides via Thermolysis and Hydrolysis: Recent Advances, Challenges, and Perspectives. *Int. J. Hydrogen Energy* **2022**, *47* (62), 26549–26573.

(45) Blanchard, D.; Shi, Q.; Boothroyd, C. B.; Vegge, T. Reversibility of Al/Ti Modified $LiBH_4$. *J. Phy. Chem. C* **2009**, *113* (31), 14059–14066.

(46) Mauron, P.; Buchter, F.; Friedrichs, O.; Remhof, A.; Bielmann, M.; Zwicky, C. N.; Züttel, A. Stability and Reversibility of $LiBH_4$. *J. Phys. Chem. B* **2008**, *112* (3), 906–910.

(47) Nielsen, T. K.; Bösenberg, U.; Gosalawit, R.; Dornheim, M.; Cerenius, Y.; Besenbacher, F.; Jensen, T. R. A Reversible Nanoconfined Chemical Reaction. *ACS Nano* **2010**, *4* (7), 3903–3908.

(48) Chong, M.; Matsuo, M.; Orimo, S. I.; Autrey, T.; Jensen, C. M. Selective Reversible Hydrogenation of $Mg(B_3H_8)_2/MgH_2$ to $Mg(BH_4)_2$: Pathway to Reversible Borane-Based Hydrogen Storage? *Inorg. Chem.* **2015**, *54* (8), 4120.

(49) Yan, Y.; Au, Y. S.; Rentsch, D.; Remhof, A.; de Jongh, P. E.; Züttel, A. Reversible Hydrogen Storage in $Mg(BH_4)_2$/Carbon Nanocomposites. *J. Mater. Chem. A Mater.* **2013**, *1* (37), 11177.

(50) Züttel, A.; Rentsch, S.; Fischer, P.; Wenger, P.; Sudan, P.; Mauron, Ph.; Emmenegger, Ch. Hydrogen Storage Properties of $LiBH_4$. *J. Alloys. Compd.* **2003**, 515–520.

(51) Vajo, J. J.; Skeith, S. L.; Mertens, F. Reversible Storage of Hydrogen in Destabilized $LiBH_4$. *J. Phys. Chem. B* **2005**, *109* (9), 3719–3722.

(52) Paskevicius, M.; Jepsen, L. H.; Schouwink, P.; Černý, R.; Ravnsbæk, D. B.; Filinchuk, Y.; Dornheim, M.; Besenbacher, F.; Jensen, T. R. Metal Borohydrides and

Derivatives – Synthesis, Structure and Properties. *Chem. Soc. Rev.* **2017**, *46* (5), 1565–1634.

(53) Grahame, A.; Aguey-Zinsou, K.-F. Properties and Applications of Metal (M) Dodecahydro-Closo-Dodecaborates ($M_{n=1,2}B_{12}H_{12}$) and Their Implications for Reversible Hydrogen Storage in the Borohydrides. *Inorganics* (Basel) **2018**, *6*, 106, 106.

(54) Liu, Y.; Giri, S.; Zhou, J.; Jena, P. Intermediate Phases During Decomposition of Metal Borohydrides, M $(BH_4)_n$ (M = Na, Mg, Y). *J. Phys. Chem. C* **2014**, *118* (49), 28456–28461.

(55) Au, M.; Jurgensen, A. R.; Spencer, W. A.; Anton, D. L.; Pinkerton, F. E.; Hwang, S.-J.; Kim, C.; Bowman, R. C. Stability and Reversibility of Lithium Borohydrides Doped by Metal Halides and Hydrides. *J. Phy. Chem. C* **2008**, *112* (47), 18661–18671.

(56) Wang, X.; Jia, Y.; Xiao, X.; Zhou, P.; Bi, J.; Qi, J.; Lv, L.; Xu, F.; Sun, L.; Chen, L. Robust Architecture of 2D Nano Mg-Based Borohydride on Graphene with Superior Reversible Hydrogen Storage Performance. *J. Mater. Sci. Technol.* **2023**, *146*, 121–130.

(57) Her, J.-H.; Yousufuddin, M.; Zhou, W.; Jalisatgi, S. S.; Kulleck, J. G.; Zan, J. A.; Hwang, S.-J.; Bowman, R. C.; Udovic, T. J. Crystal Structure of $Li_2B_{12}H_{12}$: A Possible Intermediate Species in the Decomposition of $LiBH_4$. *Inorg. Chem.* **2008**, *47* (21), 9757–9759.

(58) Callini, E.; Borgschulte, A.; Ramirez-Cuesta, A. J.; Züttel, A. Diborane Release and Structure Distortion in Borohydrides. *Dalton Trans.* **2013**, *42* (3), 719–725.

(59) Ohba, N.; Miwa, K.; Aoki, M.; Noritake, T.; Towata, S.; Nakamori, Y.; Orimo, S.; Züttel, A. First-Principles Study on the Stability of Intermediate Compounds of $LiBH_4$. *Phys. Rev. B* **2006**, *74* (7), 075110.

(60) Friedrichs, O.; Borgschulte, A.; Kato, S.; Buchter, F.; Gremaud, R.; Remhof, A.; Züttel, A. Low-Temperature Synthesis of LiBH 4 by Gas–Solid Reaction. *Chemistry – A European Journal* **2009**, *15* (22), 5531–5534.

(61) Yan, Y.; Li, H.-W.; Maekawa, H.; Aoki, M.; Noritake, T.; Matsumoto, M.; Miwa, K.; Towata, S.; Orimo, S. Formation Process of $B_{12}H_{12}^{2-}$ from BH_4^- during the Dehydrogenation Reaction of $Mg(BH_4)_2$. *Mater. Trans.* **2011**, *52* (7), 1443–1446.

(62) Pang, Y.; Liu, Y.; Gao, M.; Ouyang, L.; Liu, J.; Wang, H.; Zhu, M.; Pan, H. A Mechanical-Force-Driven Physical Vapour Deposition Approach to Fabricating Complex Hydride Nanostructures. *Nat. Commun.* **2014**, *5* (1), 3519.

(63) Yang, F.; Wang, J.; Zhang, Y.; Wu, Z.; Zhang, Z.; Zhao, F.; Huot, J.; Grobivć Novaković, J.; Novaković, N. Recent Progress on the Development of High Entropy Alloys (HEAs) for Solid Hydrogen Storage: A Review. *Int. J. Hydrogen Energy* **2022**, *47* (21), 11236–11249.

(64) Fletcher, C.; Jiang, Y.; Amal, R. Production of Formic Acid from CO_2 Reduction by Means of Potassium Borohydride at Ambient Conditions. *Chem. Eng. Sci.* **2015**, *137*, 301–307.

(65) Burr, J. G.; Brown, W. G.; Heller, H. E. The Reduction of Carbon Dioxide to Formic Aci. *J. Am. Chem. Soc.* **1950**, *72* (6), 2560–2562.

(66) Wartik, T.; Pearson, R. K. A New Type of Substituted Borohydride. *J. Am. Chem. Soc*. **1955**, *77* (4), 1075–1075.

(67) Kibar, M. E.; Akın, A. N. A Novel Process for CO_2 Capture by Using Sodium Metaborate. Part I: Effects of Calcination. *Environ. Sci. Pollut. Res.* **2018**, *25* (4), 3446–3457.

(68) Picasso, C. V.; Safin, D. A.; Dovgaliuk, I.; Devred, F.; Debecker, D.; Li, H.-W.; Proost, J.; Filinchuk, Y. Reduction of CO_2 with KBH_4 in Solvent-Free Conditions. *Int. J. Hydrogen Energy* **2016**, *41* (32), 14377–14386.

(69) Lombardo, L.; Ko, Y.; Zhao, K.; Yang, H.; Züttel, A. Direct CO_2 Capture and Reduction to High-End Chemicals with Tetraalkylammonium Borohydrides. *Angew. Chem. Inter. Ed*. **2021**, *60* (17), 9580–9589.

(70) Vitillo, J. G.; Groppo, E.; Bardají, E. G.; Baricco, M.; Bordiga, S. Fast Carbon Dioxide Recycling by Reaction with γ-$Mg(BH_4)_2$. *Phys. Chem. Chem. Phys.* **2014**, *16* (41), 22482–22486.

(71) Jeong, S.; Milner, P. J.; Wan, L. F.; Liu, Y.; Oktawiec, J.; Zaia, E. W.; Forse, A. C.; Leick, N.; Gennett, T.; Guo, J.; Prendergast, D.; Long, J. R.; Urban, J. J. Runaway Carbon Dioxide Conversion Leads to Enhanced Uptake in a Nanohybrid Form of Porous Magnesium Borohydride. *Adv. Mater.* **2019**, *31* (44), 1904252.

(72) Grinderslev, J. B.; Amdisen, M. B.; Skov, L. N.; Møller, K. T.; Kristensen, L.

G.; Polanski, M.; Heere, M.; Jensen, T. R. New Perspectives of Functional Metal Borohydrides. *J. Alloys Compd.* **2022**, *896*, 163014.

(73) Oh, H.; Tumanov, N.; Ban, V.; Li, X.; Richter, B.; Hudson, M. R.; Brown, C. M.; Iles, G. N.; Wallacher, D.; Jorgensen, S. W.; Daemen, L.; Balderas-Xicohténcatl, R.; Cheng, Y.; Ramirez-Cuesta, A. J.; Heere, M.; Posada-Pérez, S.; Hautier, G.; Hirscher, M.; Jensen, T. R.; Filinchuk, Y. Small-Pore Hydridic Frameworks Store Densely Packed Hydrogen. *Nat. Chem.* **2024**, *16* (5), 809-816.

(74) Li, X.; Yan, Y.; Jensen, T. R.; Filinchuk, Y.; Dovgaliuk, I.; Chernyshov, D.; He, L.; Li, Y.; Li, H.-W. Magnesium Borohydride $Mg(BH_4)_2$ for Energy Applications: A Review. *J. Mater. Sci. Technol.* **2023**, *161*, 170–179.

(75) Ahmad MA, Sazelee N, Ali NA, Ismail M. An overview of the recent advances of additive-improved Mg $(BH_4)_2$ for solid-state hydrogen storage material. *Energies* **2022**, *15*(3), 862.

(76) Filinchuk, Y.; Richter, B.; Jensen, T. R.; Dmitriev, V.; Chernyshov, D.; Hagemann, H. Porous and Dense Magnesium Borohydride Frameworks: Synthesis, Stability, and Reversible Absorption of Guest Species. *Angew. Chem.* **2011**, *123* (47), 11358–11362.

(77) Lane, C. F. Reduction of Organic Compounds with Diborane. *Chem. Rev.* **1976**, *76* (6), 773–799.

(78) Duncan, J. L.; Harper, J. The Structure of the Diborane Molecule. *Mol. Phys.* **1984**, *51* (2), 371–380.

(79) Kotlensky, W. V.; Schaeffer, R. Decomposition of Diborane in a Silent Discharge. Isolation of B_6H_{10} and B_9H_{15}. *J. Am. Chem. Soc.* **1958**, *80* (17), 4517–4519.

(80) Richter, B.; B. Grinderslev, J.; T. Møller, K.; Paskevicius, M.; R. Jensen, T. From Metal Hydrides to Metal Borohydrides. *Inorg. Chem.* **2018**, *57* (17), 10768–10780.

(81) Gremaud, R.; Borgschulte, A.; Friedrichs, O.; Züttel, A. Synthesis Mechanism of Alkali Borohydrides by Heterolytic Diborane Splitting. *J. Phy. Chem. C* **2011**, *115* (5), 2489–2496.

(82) Çakır, D.; de Wijs, G. A.; Brocks, G. Native Defects and the Dehydrogenation

of $NaBH_4$. *J. Phy. Chem. C* **2011**, *115* (49), 24429–24434.

(83) Gavrilova, L. A.; Titov, L. V; Petrovskii, P. V. Synthesis of $Bu_4NB_{11}H_{14}$ by the Reaction of Tetrabutylammonium Octahydrotriborate with Diborane in Diglyme. *Russ. J. Coord. Chem.* **2004**, 30, 307–308.

(84) A. Ellis, I.; F. Gaines, D.; Schaeffer, Riley. A Convenient Preparation of $B_{12}H_{12}^{2-}$ Salts. *J. Am. Chem. Soc.* **2002**, *85* (23), 3885–3885.

(85) H. Knoth, W.; C. Sauer, J.; H. Balthis, J.; Charles. Miller, H.; L. Muetterties, E. Chemistry of Boranes XXX. Carbonyl Derivatives of $B_{10}H_{10}^{2-}$ and $B_{12}H_{12}^{2-}$. *J. Am. Chem. Soc.* **2002**, *89* (19), 4842–4850.

(86) Panza, L.; Prosperi, D. Boron Chemistry. In Neutron Capture Therapy; Springer Berlin Heidelberg: Berlin, Heidelberg, **2012**, 77–98.

(87) Zhao, Q.; Li, J.; Hamilton, E. J. M.; Chen, X. The Continuing Story of the Diammoniate of Diborane. *J. Organomet. Chem.* **2015**, *798*, 24–29.

(88) Gaines, D. F.; Hildebrandt, S. J. Interactions of Metal Groups with the Octahydrotriborate(1−) Anion, $B_3H_8^-$. In Metal Interactions with Boron Clusters; Springer US: Boston, MA, **1982**, 119–143.

(89) Zheng, X.; Yang, Y.; Zhao, F.; Fang, F.; Guo, Y. Facile Preparation and Dehydrogenation of Unsolvated KB_3H_8. *Chem. Commun.* **2017**, *53* (80), 11083–11086.

(90) Chen, X.; Ma, N.; Liu, X.; Wei, C.; Cui, C.; Cao, B.; Guo, Y.; Wang, L.; Gu, Q.; Chen, X. Facile Synthesis of Unsolvated Alkali Metal Octahydrotriborate Salts MB_3H_8 (M=K, Rb, and Cs), Mechanisms of Formation, and the Crystal Structure of KB_3H_8. *Angew. Chem. Inter. Ed.* **2019**, *58* (9), 2720–2724.

(91) Hamilton, E. J. M.; Jordan; Meyers, E. A.; Shore, S. G. One-Step Preparation of Dimethyl Sulfide Substituted Icosahedral Boranes: The Crystal and Molecular Structures of 1,7-$(SMe_2)_2B_{12}H_{10}$, 1,12-$(SMe_2)_2B_{12}H_{10}$, and $[SMe_3][B_{12}H_{11}(SMe_2)]\cdot MeCN$. *Inorg. Chem.* **1996**, *35* (18), 5335–5341.

(92) Bykov, A. Yu.; Zhizhin, K. Yu.; Kuznetsov, N. T. The Chemistry of the Octahydrotriborate Anion $[B_3H_8]^-$. *Russ. J. Inorg. Chem.* **2014**, *59* (13), 1539–1555.

(93) H P Souza, D.; Moller, K. T.; Moggach, S. A.; Humphries, T. D.; D'Angelo, A. M.; Buckley, C. E.; Paskevicius, M. Hydrated Alkali-$B_{11}H_{14}$ Salts as Potential Solid-

State Electrolytes. *J. Mater. Chem. A* **2021**, *9*, 15027–15037.

(94) Mu, X.; Axtell, J. C.; Bernier, N. A.; Kirlikovali, K. O.; Jung, D.; Umanzor, A.; Qian, K.; Chen, X.; Bay, K. L.; Kirollos, M.; Rheingold, A. L.; Houk, K. N.; Spokoyny, A. M. Sterically Unprotected Nucleophilic Boron Cluster Reagents. *Chem* **2019**, *5* (9), 2461–2469.

(95) Pitochelli, A. R.; Hawthorne, F. M. The Isolation of The Icosahedral $B_{12}H_{12}^{-2}$ Ion. *J. Am. Chem. Soc.* **1960**, *82*, 3228.

(96) Muetterties, E. L.; Balthis, J. H.; Chia, Y. T.; Knoth, W. H.; Miller, H. C. Chemistry of Boranes. VIII. Salts and Acids of $B_{10}H_{10}^{-2}$ and $B_{12}H_{12}^{-2}$. *Inorg. Chem.* **1964**, *3* (3), 444–451.

(97) Klanberg, F.; Eaton, D. R.; Guggenberger, L. J.; Muetterties, E. L. Chemistry of Boranes. XXVIII. New Polyhedral Borane Anions, $B_8H_8^{2-}$, $B_8H_8^{-}$, and $B_7H_7^{2-}$. *Inorg. Chem*. **1967**, *6* (7), 1271–1281.

(98) Klanberg, F.; Muetterties, E. L. Chemistry of Boranes. XXVII. New Polyhedral Borane Anions, $B_9H_9^{2-}$ and $B_{11}H_{11}^{2-}$. *Inorg. Chem.* **1966**, *5* (11), 1955–1960.

(99) Edward Williams, R. Carboranes and Boranes; Polyhedra and Polyhedral Fragments. *Inorg. Chem*. **2002**, *10* (1), 210–214.

(100) Miller, H. C.; Muetterties, E. L.; Boone, J. L.; Garrett, P.; Hawthorne, M. F. *Borane Anions*; **1967**, 81–91.

(101) McKee, M. L.; Wang, Z. X.; Von Ragué Schleyer, P. Ab Initio Study of the Hypercloso Boron Hydrides $B_{(n)}H_{(n)}$ and $B_{(n)}H_{(n)}^{-}$. Exceptional Stability of Neutral $B_{13}H_{13}$. *J. Am. Chem. Soc.* **2000**, *122* (19), 4781–4793.

(102) Boron; Hnyk, D., McKee, M., Eds.; Springer International Publishing: Cham, 2015, 20.

(103) Hall, J. H.; Dixon, D. A.; Kleier, D. A.; Halgren, T. A.; Brown, L. D.; Lipscomb, W. N. Localized Molecular Orbitals for Polyatomic Molecules. II. Structural Relations and Charge Distributions for Open Boron Hydrides and Ions. *J. Am. Chem. Soc.* **1975**, *97* (15), 4202–4213

(104) Poater, J.; Solà, M.; Viñas, C.; Teixidor, F. Hückel's Rule of Aromaticity Categorizes Aromatic Closo Boron Hydride Clusters. *Chem. Europ. J.* **2016**, *22* (22), 7437–7443.

(105) Chen, Z.; King, R. B. Spherical Aromaticity: Recent Work on Fullerenes, Polyhedral Boranes, and Related Structures. *Chem. Rev.* **2005**, *105* (10), 3613–3642.

(106) Knapp, C. Weakly Coordinating Anions: Halogenated Borates and Dodecaborates. In Comprehensive Inorganic Chemistry II (Second Edition): From Elements to Applications, **2013**, 1.

(107) Geis, V.; Guttsche, K.; Knapp, C.; Scherer, H.; Uzun, R. Synthesis and Characterization of Synthetically Useful Salts of the Weakly-Coordinating Dianion $[B_{12}Cl_{12}]^{2-}$. *Dalton Tran.* **2009**, *15*, 2687.

(108) Alvarez, S. Coordinating Ability of Anions, Solvents, Amino Acids, and Gases towards Alkaline and Alkaline-Earth Elements, Transition Metals, and Lanthanides. *Chem. Eur. J.* **2020**, *26* (19), 4350–4377.

(109) Payandeh, S.; Rentsch, D.; Łodziana, Z.; Asakura, R.; Bigler, L.; Černý, R.; Battaglia, C.; Remhof, A. Nido-Hydroborate-Based Electrolytes for All-Solid-State Lithium Batteries. *Adv. Funct. Mater.* **2021**, *31* (18), 2010046.

(110) Carter, T. J.; Mohtadi, R.; Arthur, T. S.; Mizuno, F.; Zhang, R.; Shirai, S.; Kampf, J. W. Boron Clusters as Highly Stable Magnesium-Battery Electrolytes. *Angew. Chem.* **2014**, *126* (12), 3237–3241.

(111) Gigante, A.; Duchene, L.; Moury, R.; Pupier, M.; Remhof, A.; Hagemann, H. Direct Solution-Based Synthesis of $Na_4(B_{12}H_{12})(B_{10}H_{10})$ Solid Electrolyte. *ChemSusChem* **2019**, *12*, 4832.

(112) The Electronic Structure of the Borides MB_6. *Proc. R. Soc. Lond. A Math. Phys. Sci.* **1954**, *224* (1158), 336–347.

(113) C. Miller, H.; E. Miller, N.; L. Muetterties, E. Chemistry of Boranes. XX. Syntheses of Polyhedral Boranes. *Inorg. Chem.* **2002**, *3* (10), 1456–1463.

(114) Friedrichs, O.; Remhof, A.; Borgschulte, A.; Buchter, F.; Orimo, S. I.; Züttel, A. Breaking the Passivation—the Road to a Solvent Free Borohydride Synthesis. *Phy. Chem. Chem. Phy.* **2010**, *12* (36), 10919.

(115) M. Adams, R.; R. Siedle, A.; Grant, J. Convenient Preparation of the Dodecahydrododecaborate Ion. *Inorg. Chem.* **2002**, *3* (3), 461–461.

(116) Kuznetsov, N. T.; K. G. S. Mixed Dodecahydro-Closo-Dodecaborate Chlorides of Rubidium and Cesium. *Russ. J. Inorg. Chem.* **1971**, *16*.

(117) Remhof, A.; Yan, Y.; Rentsch, D.; Borgschulte, A.; Jensen, C. M.; Züttel, A. Solvent-Free Synthesis and Stability of $MgB_{12}H_{12}$. *J. Mater. Chem. A* **2014**, *2* (20), 7244–7249.

(118) He, L.; Li, H.-W.; Hwang, S.-J.; Akiba, E. Facile Solvent-Free Synthesis of Anhydrous Alkali Metal Dodecaborate $M_2B_{12}H_{12}$ (M = Li, Na, K). *J. Phys. Chem. C* **2014**, *118*, 6084.

(119) He, L.; Shao, H.; Felderhoff, M.; Li, H.-W.; Li, X.; Zhu, Q.; Zhang, D.; Wu, D.; Fu, Y.; Deng, Y.; Lu, Z. Facile Synthesis of Anhydrous $Li_2B_{12}H_{12}$ with High Purity by Solvent-Free Method. *Inorganica Chim. Acta* **2017**, *464*, 147–151.

(120) Caputo, R.; Garroni, S.; Olid, D.; Teixidor, F.; Surinach, S.; Baro, M. D. Can $Na_{(2)}[B_{(12)}H_{(12)}]$ Be a Decomposition Product of $NaBH_{(4)}$? *Phys. Chem. Chem. Phys.* **2010**, *12*, 15093.

(121) Geis, V.; Guttsche, K.; Knapp, C.; Scherer, H.; Uzun, R. Synthesis and Characterization of Synthetically Useful Salts of the Weakly-Coordinating Dianion $[B_{12}Cl_{12}]^{2-}$. *Dalton Trans.* **2009**, *15*, 2687.

(122) Colombier, M.; Atchekzaï, J.; Mongeot, H. Studies of the Pyrolysis of Tetraethylammonium Tetrahydroborate. *Inorganica Chim. Acta* **1986**, *115* (1), 11–16.

(123) Tran, B. L.; Allen, T. N.; Bowden, M. E.; Autrey, T.; Jensen, C. M. Effects of Glymes on the Distribution of $Mg(B_{10}H_{10})$ and $Mg(B_{12}H_{12})$ from the Thermolysis of $Mg(BH_4)_2$. *Inorganics (Basel)* **2021**, *9* (6), 41.

(124) Yan, Y.; Remhof, A.; Rentsch, D.; Zuttel, A. The Role of $MgB_{12}H_{12}$ in the Hydrogen Desorption Process of $Mg(BH_4)_2$. *Chem. Commun.* **2015**, *51*, 700.

(125) Yan, Y.; Rentsch, D.; Battaglia, C.; Remhof, A. Synthesis, Stability and Li-Ion Mobility of Nanoconfined $Li_2B_{12}H_{12}$. *Dalton Trans.* **2017**, *46* (37), 12434–12437.

(126) He, L.; Li, H.-W.; Tumanov, N.; Filinchuk, Y.; Akiba, E. Facile Synthesis of Anhydrous Alkaline Earth Metal Dodecaborates $MB_{12}H_{12}$(M = Mg, Ca) from $M(BH_4)_2$. *Dalton Trans.* **2015**, *44*, 15882.

(127) Bykov, A. Yu.; Mal'tseva, N. N.; Generalova, N. B.; Zhizhin, K. Yu.; Kuznetsov, N. T. Reactions of Sodium Tetrahydroborate with Alkyl and Aryl Halides: A New Approach to the Synthesis of $B_3H_8^-$ and $B_{12}H_{12}^{2-}$ Anions. *Russ. J. Inorg. Chem.* **2013**, *58* (11), 1321–1323.

(128) Chen, W.; Wu, G.; He, T.; Li, Z.; Guo, Z.; Liu, H.; Huang, Z.; Chen, P. An Improved Synthesis of Unsolvated NaB_3H_8 and Its Application in Preparing $Na_2B_{12}H_{12}$. *Int. J. Hydrogen Energy* **2016**, *41* (34), 15471–15476.

(129) Pylypko, S.; Ould-Amara, S.; Zadick, A.; Petit, E.; Chatenet, M.; Cretin, M.; Demirci, U. B. The Highly Stable Aqueous Solution of Sodium Dodecahydro-Closo-Dodecaborate $Na_2B_{12}H_{12}$ as a Potential Liquid Anodic Fuel. *Appl. Catal., B* **2018**, *222*,1.

(130) Wang, J.; Steenhaut, T.; Li, H.-W.; Filinchuk, Y. High Yield Autoclave Synthesis of Pure $M_2B_{12}H_{12}$ (M = Na, K). *Inorg. Chem.* **2023**, *62* (5), 2153–2160.

(131) Jing, Y.; Wang, X.; Han, H.; Liu, X.-R.; Yu, X.-C.; Chen, X.-M.; Wei, D.; Wang, L.-S.; Chen, X. Selective Synthesis of the $B_{11}H_{14}^-$ and $B_{12}H_{12}^{2-}$ Borane Derivatives and the General Mechanisms of the B-H Bond Condensation. *Sci. China Chem.* **2023**.

(132) Sivaev, I. B.; Bregadze, V. I.; Sjöberg, S. Chemistry of Closo-Dodecaborate Anion $[B_{12}H_{12}]^{2-}$: A Review. *Collection of Czechoslovak Chemical Communications.* **2002**.

(133) C. Miller, H.; R. Hertler, W.; L. Muetterties, E.; H. Knoth, W.; E. Miller, N. Chemistry of Boranes. XXV. Synthesis Andc Chemistry of Base Derivatives of $B_{10}H_{10}^{2-}$ and $B_{12}H_{12}^{2-}$. *Inorg. Chem.* **2002**, *4* (8), 1216–1221.

(134) Hansen, B. R. S.; Paskevicius, M.; Li, H.-W.; Akiba, E.; Jensen, T. R. Metal Boranes: Progress and Applications. *Coord. Chem. Rev.* **2016**, *323*, 60–70.

(135) Chen, X.; Liu, Y.; Alexander, A.; Gallucci, J. C.; Hwang, S.; Lingam, H. K.; Huang, Z.; Wang, C.; Li, H.; Zhao, Q.; Ozkan, U. S.; Shore, S. G.; Zhao, J. Desolvation and Dehydrogenation of Solvated Magnesium Salts of Dodecahydrododecaborate: Relationship between Structure and Thermal Decomposition. *Chem. Eur. J.* **2014**, *20* (24), 7325–7333.

(136) He, L.; Li, H.-W.; Nakajima, H.; Tumanov, N.; Filinchuk, Y.; Hwang, S.-J.; Sharma, M.; Hagemann, H.; Akiba, E. Synthesis of a Bimetallic Dodecaborate $LiNaB_{12}H_{12}$ with Outstanding Superionic Conductivity. *Chem. Mater.* **2015**, *27*, 5483.

(137) Tang, W. S.; Matsuo, M.; Wu, H.; Stavila, V.; Zhou, W.; Talin, A. A.; Soloninin, A. V.; Skoryunov, R. V.; Babanova, O. A.; Skripov, A. V.; Unemoto, A.; Orimo, S.;

Udovic, T. J. Liquid-Like Ionic Conduction in Solid Lithium and Sodium Monocarba- Closo -Decaborates Near or at Room Temperature. *Adv. Energy Mater.* **2016**, *6* (8).

(138) Zhao, X.; Wang, D.; Xiang, C.; Zhang, F.; Liu, L.; Zhou, X.; Zhang, H. Facile Synthesis of Boron Organic Polymers for Efficient Removal and Separation of Methylene Blue, Rhodamine B, and Rhodamine 6G. *ACS Sustain. Chem. Eng.* **2018**, *6* (12), 16777–16787.

(139) Bernard, R.; Cornu, D.; Grüner, B.; Dozol, J.-F.; Miele, P.; Bonnetot, B. Synthesis of $[B_{12}H_{12}]^{2-}$ Based Extractants and Their Application for the Treatment of Nuclear Wastes. *J. Organomet Chem.* **2002**, *657* (1–2), 83–90.

(140) Sivaev, I. B.; Bruskin, A. B.; Nesterov, V. V.; Antipin, M. Y.; Bregadze, V. I.; Sjöberg, S. Synthesis of Schiff Bases Derived from the Ammoniaundecahydro-Closo-Dodecaborate(1-) Anion, $[B_{12}H_{11}NH{=}CHR]^-$, and Their Reduction into Monosubstituted Amines $[B_{12}H_{11}NH_2CH_2R]^-$: A New Route to Water Soluble Agents for BNCT. *Inorg. Chem.* **1999**, *38* (25).

Chapter 2. Methodology

Abstract

In this chapter, we present a comprehensive overview of the experimental apparatus, including the autoclave and Schlenk line, followed by concise descriptions of the experimental devices and common characterization techniques employed in $B_{12}H_{12}^{2-}$ anion synthesis. We summarize various synthesis approaches for different metal-$B_{12}H_{12}^{2-}$ compounds within the thesis and provide detailed procedures and equipment details. Additionally, Nuclear Magnetic Resonance (NMR) and Powder X-ray Diffraction (PXRD) are introduced and the roles they played in this thesis are also emphasized. This chapter also covers other essential techniques, such as Thermogravimetric Analysis (TGA–DSC) and Fourier Transform Infrared Spectroscopy (FTIR).

Chapter 2

2.1. Synthesis Strategies

The experimental program was split into four areas:

i) Synthesis of $B_{12}H_{12}^{2-}$ (solvated form) through solvothermal synthesis either in Schlenk flask or in an autoclave;

ii) Structural and compositional characterization of the as-synthesized solvated $B_{12}H_{12}^{2-}$;

iii) Study of the thermal desolvation behavior of the solvated metal-$B_{12}H_{12}^{2-}$;

iv) Structural and compositional characterization of the anhydrous $B_{12}H_{12}^{2-}$ salts.

The flow diagram in Figure 1 illustrates the main characterization techniques employed in each part.

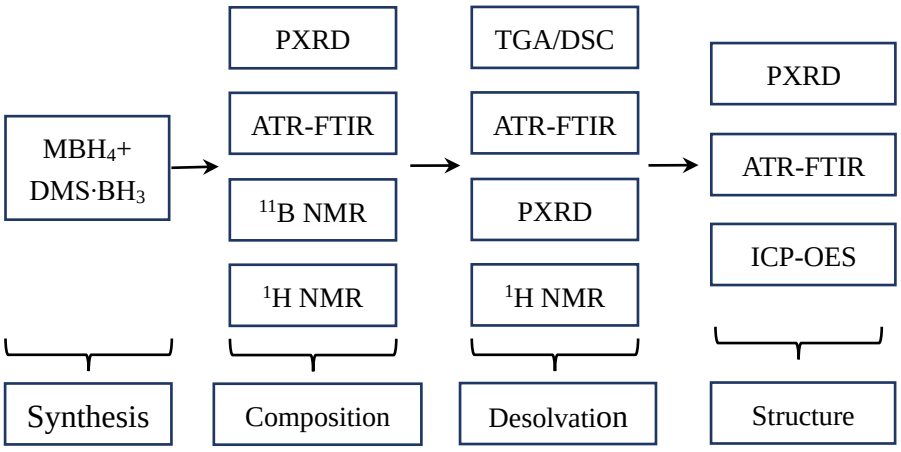

Figure 1. Diagram of experimental techniques used for the synthesis of $B_{12}H_{12}^{2-}$.

Solvothermal procedures involve the synthesis of precursor chemicals in a non-aqueous solvent at different temperatures and pressures. The equipment used in this thesis depends on the required

conditions. Autoclaves, for example, operate within sealed systems, allowing for greater pressure and temperature control. Schlenk synthesis, on the other hand, is performed at atmospheric pressure and inert conditions, allowing for rapid observation of the process. The appropriate equipment is determined by the properties of borohydrides, as well as the solvent's properties. An ideal solvent can dissolve both reactants and intermediates while leaving the final product to precipitate. Table 1 provides information on the solubility of metal borohydrides in commonly used organic solvents.

Table 1. Solubility of borohydrides in various solvents at 25 °C.[1]

	$LiBH_4$	**$NaBH_4$**	**KBH_4**	**$Ca(BH_4)_2$**	**$Mg(BH_4)_2$**
Et_2O (b. p. 34.6 °C)	4.28 g/ 100 g	Insoluble	Insoluble	n.d.	29 g/ 100 g
THF (b. p. 66 °C)	25 g/ 100 g	0.1 g/ 100 g	Insoluble	2 g/ 100 g	n.d.
Monoglyme (b. p. 85 °C)	9.81 g/ 100 g	0.8 g/ 100 g	n.d.	0.13 g/ 100 g	n.d.
1, 4−dioxane (b. p. 101.1 °C)	0.3 g/ 100 g	n. d.	Insoluble	0.1 g/ 100 g	n.d.
Diglyme (b. p. 162 °C)	9.64 g/ 100 g	5.5 g/ 100 g	n.d.	2.05 g/ 100 g	n.d.
DMSO (b. p. 189 °C)	n. d.	n. d.	7.6 g/ 100 g	1.94 g/ 100 g	0.56 g/ 100g

2.1.1. Autoclave Synthesis

The autoclave can provide an enclosed system and high pressure generated from dosing or the reaction itself as shown in Figure 2.

The autoclave is manufactured by Anhui Kemi Instrument Co., Ltd. (kmlabreactor.com). configuration includes a vessel constructed of 316 S stainless steel, and the pressure inside the autoclave can reach up to 250 bar at temperatures up to 300 °C. This vessel is safeguarded by a heated jacket, regulated by a temperature controller. A hot plate outfitted with a magnetic stirrer beneath the autoclave,

which permits stirring inside the vector during the experiment.

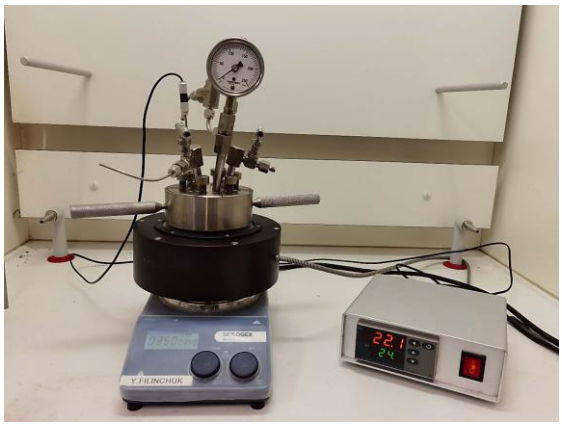

Figure 2. Autoclave used for synthesis.

The autoclave has a volume of 50 mL, and a quartz liner with a volume of 37.5 mL is used inside for convenient sample preparation in a glovebox. The reaction solution volume should be between 1/3 and 2/3 of the volume of the liner to ensure accurate temperature control and to prevent solvent overflow. Figure 3 shows a graphic illustration of the autoclave system.

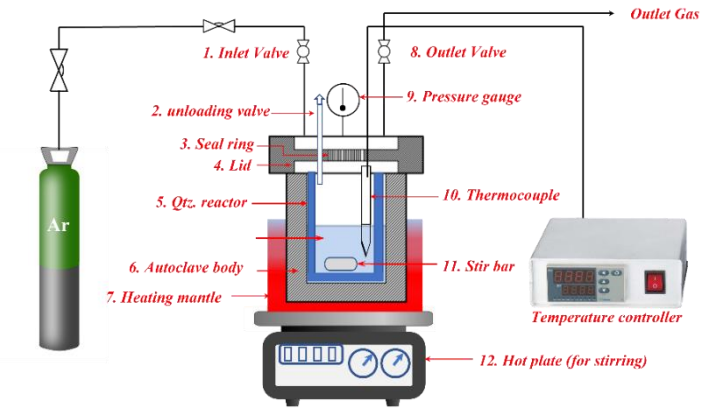

Figure 3. High-pressure autoclave used for the synthesis of $B_{12}H_{12}^{2-}$.

It is worth to mention that autoclave synthesis is a well-accepted method for the condensation reactions. The use of autoclave has several advantages:

i) To ensure safe synthesis, it is essential to conduct the experiment within a durable and sealed system.

ii) To elevate the boiling point of the employed solvents, consequently enhancing the solubility of borohydrides.

iii) To retain all generated gaseous active species inside (e.g., B_2H_6), thereby boosting the reaction yields.

2.1.2. Schlenk Synthesis

For the starting materials, like hydrides, metal borohydrides, as well as subsequent products such as lithium dodecaborates ($Li_2B_{12}H_{12}$) and sodium dodecaborates ($Na_2B_{12}H_{12}$), it is well documented in the literature that they are air and moisture sensitive. As a result, these compounds can only be synthesized and handled using modified Schlenk procedures in an inert argon environment. Schlenk flasks are typically used in conjunction with a Schlenk line for this purpose. A Schlenk flask consists of a round-bottom flask with a side arm for introducing or removing gases, liquids, or solids. This side arm has a valve that allows for the fine control of gas or liquid flowing into and out of the flask. A stopcock or a Teflon stopper is usually used to create a sealed environment. Our laboratory Schlenk flask (Figure 4) has a capacity of 100 mL and is an altered version of the classic Schlenk flask, with a P4 type filter (10–16 μm) frit on the side arm. This filter frit, which is commonly made of sintered glass, can be used for isolating solid precipitates from a solution, while maintaining an inert environment. The quartz reactor enclosed within the autoclave, has a limited volume of 37.5 mL. The volume of different reactors

determines the amount of available space for the reaction to occur.

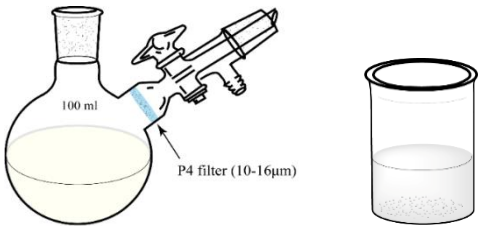

Figure 4. The comparison of the reactors used for Schlenk (left) and Autoclave synthesis (right).

When working with compounds that are sensitive to air and/or water, the Schlenk approach is more convenient than the autoclave method. Figure 5 depicts the Schlenk line, which can deliver vacuum and inert gas. The Schlenk system consists of a gas manifold that may deliver inert gases like argon or nitrogen, as well as a vacuum manifold that can purge the remaining air or moisture out of glassware. For this reason, a vacuum pump is linked to the vacuum manifold. The Schlenk line enables the careful control of the environment inside the flask and ensures that borohydrides are protected from the harmful effects of air and water and therefore retain their reactivity. Figure 5 and 6 show images of the Schlenk system used in various applications.

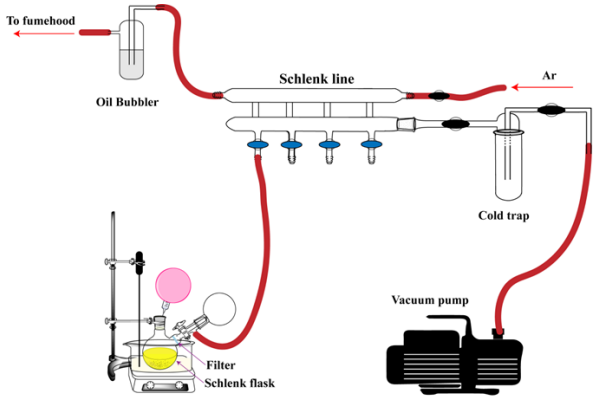

Figure 5. Complete Schlenk line setup used for the synthesis of $B_{12}H_{12}^{2-}$.

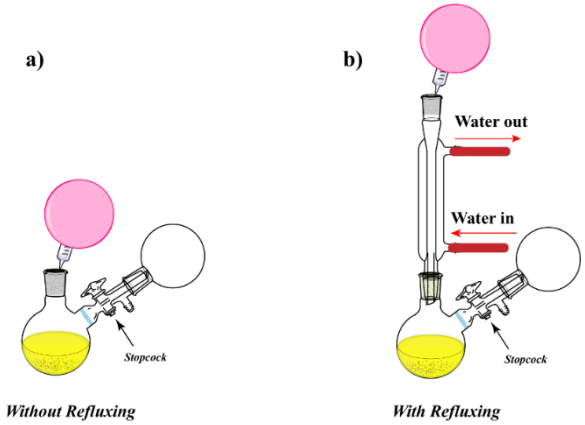

Figure 6. Scheme of the Schlenk setup used for $B_{12}H_{12}^{2-}$ synthesis a) without or b) with refluxing.

After the first step of synthesis mentioned above in Schlenk flask/ autoclave, the reaction mixture was filtered using a Schlenk filtration device in either the autoclave or the Schlenk. Following that, it was rinsed three times with solvents applied in the synthesis and then dried under vacuum. To get totally desolvated compounds, the samples were further heated under vacuum at either 200 or 150 °C, or dried under an argon flow, as shown in Figure 7.

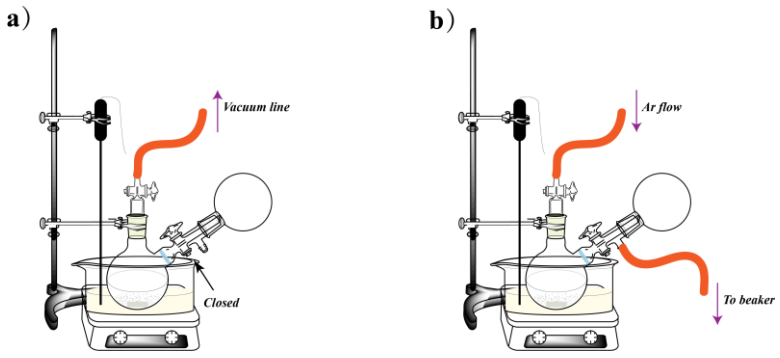

Figure 7. Scheme of the Schlenk setup used for $B_{12}H_{12}^{2-}$ synthesis thermal desolvation of solvents a) under Vacuum or b) under Argon flow.

2.1.3. Mechanochemical Synthesis

Figure 8. The ball milling machine used in the work of this thesis. Left: Fritsch Pulverisette P7, Right: schematic view of motion of the ball and powder mixture.[2]

Ball milling is a mechanical process that grinds and reduces the particle size of solid materials. The powder needs to be placed in a cylindrical container or drum, with grinding balls made of stainless steel, or flint (Figure 8). When the drum is turned on, the balls will engage with the powder, and lead to mechanical deformation, fracture and particle refining of the material.

In the thesis work, ball-milled MBH_4 (M = Li, Na, K) was produced by mechanically milling 0.5 g of MBH_4 at room temperature using a planetary ball mill (Fritsch Pulverisette P7) for the purpose of using small sized particles for the synthesis. The milling process used four steel balls (10 mm in diameter) loaded into a hardened steel vial (30 cm^3) within an argon-filled glovebox. Milling was conducted under 0.1 MPa of argon for a total duration of 2 h, consist of a 2 min of milling process and 3 min of pausing, and repeated for 24 cycles.

2.1.4. Glovebox Usage

In certain procedures, such as material loading, sample collection, and preparation of capillaries for XRD measurements, it is not possible to work in air. Therefore, these steps should be performed in a inert atmosphere such as in glovebox (under argon) to ensure the high-purity, water-free product. Gas analyzers of the glovebox can be used to test the quality of the inert gas, ensuring that both the water and oxygen content are less than 1 ppm. Samples can be transferred in and out of the glovebox through airtight evacuation chambers. To maintain a stable atmosphere within the glovebox, the evacuation chamber is generally evacuated and refilled at least three times in our lab.

2.2. Synthesis of $B_{12}H_{12}^{2-}$

Given that borate compounds are of deliquescent and hygroscopic nature, all synthetic procedures were carried out in an inert atmosphere with double manifold and Schlenk line techniques. All samples were stored in an argon-filled glovebox (Innovative Technology, <1 ppm H_2O, <1 ppm O_2), to ensure a moisture-free environment. Table 2 outlined sample synthesized in this thesis work. Detailed synthesis procedures are provided in separated chapters.

Table 2. Summary of high purity materials synthesized and their respective conditions in the thesis work.

Materials	Reactants	Solvents	Reactor	Conditions	Ref.
$Na_2B_{12}H_{12}$	$NaBH_4$ + 5.5 $DMS{\cdot}BH_3$	20 mL diglyme	Autoclave	160 °C	Chapter 3
			Schlenk	160 °C；refluxing diglyme	Chapter 4
$K_2B_{12}H_{12}$	KBH_4 + 5.5 $DMS{\cdot}BH_3$	20 mL diglyme	Autoclave	160 °C	Chapter 3
			Schlenk	160 °C；refluxing diglyme	Chapter 4
$Li_2B_{12}H_{12}$	KBH_4 + 5.5 $DMS{\cdot}BH_3$	20 mL diglyme	Autoclave	160 °C	Chapter 3
			Schlenk	160 °C；refluxing diglyme	Chapter 4
$LiB_{11}H_{14}$· n diglyme	$LiBH_4$ + 5.5 $DMS{\cdot}BH_3$	20 mL diglyme	Schlenk	i)120 °C; ii) 160 °C	Chapter 4
$LiB_{11}H_{14}$· n H_2O	$LiBH_4$ + 10 $DMS{\cdot}BH_3$	20 mL monoglyme	Schlenk	i)85 °C; ii) Et_2O extraction	Chapter 4
$NaB_{11}H_{14}$· n H_2O	$LiBH_4$ + 10 $DMS{\cdot}BH_3$	20 mL monoglyme	Schlenk	i)85 °C; ii) Et_2O extraction	Chapter 4
$CaB_{12}H_{12}$	$CaH_2(Ca(BH_4)_2)$ + $DMS{\cdot}BH_3$	monoglyme	Autoclave	120 °C, 24 h	Chapter 5
γ -$Mg(BH_4)_2$	$Mg(nBu)_2$ + $DMS{\cdot}BH_3$	Toluene	Schlenk	RT	Chapter 6
（$Me_4N)_2B_{12}H_{12}$	Me4NBH_4 + 5.5 $DMS{\cdot}BH_3$	diglyme	Autoclave	150 °C; 24 h	Chapter 7
$(Me_4N)_2B_{12}H_{12}$	2 Me_4NBr + $Na_2B_{12}H_{12}$	H_2O	Schlenk	RT	Chapter 7
$(Pr_4N)_2B_{12}H_{12}$	2 Pr_4NBr+ $Na_2B_{12}H_{12}$	H_2O	Schlenk	RT	Chapter 7
$(Bu_4N)_2B_{12}H_{12}$	2 Bu_4NI + $Na_2B_{12}H_{12}$	H_2O	Schlenk	RT	Chapter 7
$Me_4NB_3H_8$	Me_4NBH_4 + 2 $DMS{\cdot}BH_3$	THF	Schlenk	75 °C; 24 h	Chapter 7
$Bu_4NB_3H_8$	Bu_4NBH_4 + 2 $DMS{\cdot}BH_3$	monoglyme	Schlenk	85 °C; 72 h	Chapter 7

2.2.1. Autoclave synthesis of $M_2B_{12}H_{12}$ (M = Na, K)

The synthesis of alkali metal dodecahydrododecaborate started with sodium borohydride ($NaBH_4$) in diglyme (diethylene glycol dimethyl ether, $C_6H_{14}O_3$, b.p. 162 °C). The reaction was conducted in

a 37.5 mL quartz liner placed inside a stainless-steel autoclave (Figure 2).

During the reaction, 0.19 g of $NaBH_4$ (equivalent to 5 mmol, or 0.27 g of KBH_4) was weighed into the quartz liner reactor within a glovebox. The quartz reactor was then sealed by Parafilm. Before loading the quartz reactor into the autoclave, 16 mL of diglyme was added, followed by the addition of 27.5 mmol of borane dimethyl sulfide complex ($(CH_3)_2S{\cdot}BH_3$, 2.75 mL) to the borohydride. The reaction temperature and then maintained for 24 h. Subsequently, the system cooled down naturally to room temperature to collect crystalline samples.

The resulting reaction mixture was filtered using a Schlenk filtration apparatus (see Figure 6) and washed with diglyme (3 × 10 mL). The obtained product was then dried at 80 °C under vacuum for 2 h to convert the sticky powders into dry ones. The best conditions for $Na_2B_{12}H_{12}$ synthesis are 160 °C (85% yield), and 200 °C for $K_2B_{12}H_{12}$ (84% yield), the yields are calculated based on NMR and TGA analysis with final anhydrous sample obtained. The reaction follow equations below:

$$2\ MBH_4 + 10\ (CH_3)_2S{\cdot}BH_3 \xrightarrow{\text{diglyme, i)160 °C; ii) 80 °C vacuum}} M_2B_{12}H_{12}{\cdot}n\ (\text{diglyme}) + 10\ DMS + 13\ H_2\ (M = Na, K; \text{Autoclave}) \quad (1)$$

$$M_2B_{12}H_{12}{\cdot}n\ (\text{diglyme}) \xrightarrow{200\ °C,\ \text{vacuum}} M_2B_{12}H_{12} + n\ \text{diglyme}\ (M = Na, K; \text{Schlenk}) \quad (2)$$

Alternatively, the addition of 10 mL of H_2O prior to the drying process promotes the thermal removal of diglyme.

2.2.2. Synthesis of $M_2B_{12}H_{12}$ (M = Li, Na, K)

i) Synthesis of $Li_2B_{12}H_{12}$·n diglyme in autoclave

The experiment was conducted in a 50 mL stainless-steel autoclave with a 37.5 mL quartz liner. Typically, 5 mmol of $LiBH_4$ was weighed into the quartz liner reactor inside a glovebox and sealed with Parafilm. Before loading the quartz reactor into the autoclave, 20 mL of diglyme and subsequently 27.5 mmol of the borane dimethyl sulfide complex ($(CH_3)_2S{\cdot}BH_3$, 2.75 mL) were added to the borohydride. The autoclave was then sealed and purged with Ar for 30 s to remove air from the system. The reaction temperature was increased from room temperature to 120 °C at a rate of 2 °C/min, and then maintained for 24 h. After the system cooled down to room temperature, the reaction mixture was filtered using a Schlenk filtration apparatus and washed with diglyme (3 × 10 mL). The sample was dried at 80 °C under vacuum for 2 h. The yield was approximately 91% for $Li_2B_{12}H_{12}$.

$$2\ MBH_4 + 10\ (CH_3)_2S{\cdot}BH_3 \xrightarrow{\text{diglyme, i)120 °C; ii) 80 °C vacuum}} M_2B_{12}H_{12}{\cdot}n\ (\text{diglyme}) + 10\ DMS + 13\ H_2\ (M = Li, \text{autoclave}) \quad (3)$$

ii) Synthesis of $Li_2B_{12}H_{12}$·n diglyme in Schlenk line

The reaction was carried out in a 100 mL Schlenk flask (Figure 5). Typically, 5 mmol $LiBH_4$ was weighed into the Schlenk flask in a glovebox. Subsequently, 20 mL of diglyme and 27.5 mmol of borane dimethyl sulfide complex ($(CH_3)_2S{\cdot}BH_3$, 2.75 mL) were added to the borohydride. The initially colorless solution turned yellow after approximately 2 hours at 120 °C, followed by the appearance of a white precipitate. The reaction solution was then stirred at 120 °C for 24 h. After turning off the heat source, the system cooled down to

room temperature and the reaction mixture was filtered (10–16 μm) and washed with diglyme (3 × 10 mL), The sample was dried at 80 °C under vacuum for 2 h to remove residual diglyme. The solvated product $Li_2B_{12}H_{12}$·n $C_6H_{13}O_3$ was obtained as a white crystalline solid, with a $Li_2B_{12}H_{12}$ yield of ~ 40 %.

$$2\ MBH_4 + 10\ (CH_3)_2S{\cdot}BH_3 \xrightarrow{\text{diglyme}} M_2B_{12}H_{12}{\cdot}n\ (\text{diglyme}) + 10\ DMS + 13\ H_2\ (M=Li, Na, K) \quad (4)$$

The second step of the current method, the removal of diglyme from $Li_2B_{12}H_{12}$·n diglyme can be done by solvent exchange by dimethyl sulfoxide (DMSO, b. p. 189 ℃) or N, N-Diethylformamide (DEF, b. p. 178.3 ℃).

$$Li_2B_{12}H_{12}{\cdot}\ n(\text{diglyme})\ (s) + DMSO\ (sol) \xrightarrow{100\ ℃,\ \text{Vaccum}} Li_2B_{12}H_{12}\ {\cdot}n(DMSO)\ (s) + \text{diglyme}\ (g) \quad (5)$$

The synthesis of $Li_2B_{12}H_{12}$ can also begin with monoglyme (dimethoxyethane, DME, b. p. 85 ℃) as a solvent in an autoclave to obtain pure DME solvated $Li_2B_{12}H_{12}$. Chemical-grade pure $Li_2B_{12}H_{12}$·n H_2O can be obtained by substituting DME with H_2O without decomposition of the cluster.

$$Li_2B_{12}H_{12}{\cdot}\ n\ (\text{DME})\ (s) + H_2O\ (sol) \xrightarrow{40\ ℃,\ \text{Vaccum}} Li_2B_{12}H_{12}\ {\cdot}n\ (H_2O)\ (s) + \text{DME}\ (g) \quad (6)$$

iii) Improved synthesis of $Na_2B_{12}H_{12}$ and $K_2B_{12}H_{12}$ in Schlenk line

$NaBH_4$ (0.19 g, 5 mmol) or KBH_4 (0.27 g, 5 mmol) was weighed and added to a 100 mL of Schlenk flask in an argon-filled glovebox. The flask was connected to a Schlenk line and an argon-purged condenser. Then, 20 mL of diglyme and 27.5 mmol of borane dimethyl sulfide complex ($(CH_3)_2S{\cdot}BH_3$, 2.75 mL) were added to the borohydride. The reaction solution was stirred at 120 ℃ for 24 h.

Subsequently, the reaction mixture was filtered using a Schlenk filtration apparatus and washed with diglyme (3 × 10 mL), the sample was dried at 80 °C under vacuum for 4 h to convert the sticky powder to the unsolvated product. The raw product was obtained as a white substance. The yield is~ 92 % for $Na_2B_{12}H_{12}$ and ~ 88 % for $K_2B_{12}H_{12}$.

$$2\ MBH_4 + 10\ (CH_3)_2S{\cdot}BH_3 \xrightarrow{\text{refluxing diglyme, i)160 °C; ii) 80 °C vacuum}} M_2B_{12}H_{12}{\cdot}n\ (\text{diglyme}) + 10\ DMS + 13\ H_2\ (M = Na, K) \quad (7)$$

The formation mechanism of the $B_{12}H_{12}^{2-}$ anion, from the reaction between alkali metal borohydrides and borane complex, was investigated in this work:

The first step of the reaction, involving the formation of $B_{12}H_{12}^{2-}$, is the nucleophilic substitution of the B−H bond in BH_4^- by BH_3 to produce $B_2H_7^-$ (reaction 8), the terminal bond in $B_2H_7^-$ further substitutes BH_3 to form $B_3H_{10}^-$, which thermally decomposes into H_2 with $B_3H_8^-$ (reaction 9). Excess BH_3 in the system reacts further with $B_3H_8^-$ to produce $B_9H_{14}^-$ and $B_{11}H_{14}^-$ (reaction 10 and 11). Subsequently, the formation of $B_{12}H_{12}^{2-}$ is favored when the reaction temperature is in the range of 120 – 160 °C (reaction 12), when diglyme is used as a solvent. but the precipitation of solvated $B_{12}H_{12}^{2-}$ directly may leads to the formation of partially dehydrogenated $B_{12}H_{12-x}^{2-}$ anion. Thus, the synthesis of $Na_2B_{12}H_{12}$ in diglyme should be performed at a temperature lower than 200 °C, whereas for $Li_2B_{12}H_{12}$ it should be lower than 160 °C, and for $CaB_{12}H_{12}$ it should be lower than 120 °C, when diglyme used as solvents.

$$BH_4^- + BH_3 \rightarrow B_2H_7^- \quad (8)$$

$$B_2H_7^- + BH_3 \rightarrow B_3H_8^- + H_2 \quad (9)$$

$$B_3H_8^- + 6\ BH_3 \rightarrow B_9H_{14}^- + 6H_2 \quad (10)$$

$$B_9H_{14}^- + 2\ BH_3 \rightarrow B_{11}H_{14}^- + 3H_2 \quad (11)$$

$$B_{11}H_{14}^{-} + H^{-} + BH_3 \rightarrow B_{12}H_{12}^{2-} + 3H_2 \quad (12)$$

2.2.3. Autoclave synthesis of $CaB_{12}H_{12}$

The synthesis of alkali metal-earth dodecahydrododecaborate $MB_{12}H_{12}$ (M = Mg, Ca) leads to the formation of dehydrogenated anions ($B_{12}H_{12-x}^{2-}$) in diglyme during the synthetic process, the strong coordination ability between Ca^{2+}/Mg^{2+} and oxygen atoms in diglyme makes the thermal removal of diglyme impossible. These factors render diglyme an unsuitable choice for the synthesis of the $MB_{12}H_{12}$ (M = Ca, Mg).

However, it is known that hydrated $CaB_{12}H_{12}$ can be desolvated without forming dehydrogenated anions. Therefore, the synthesis of $CaB_{12}H_{12}$ can be designed by using light ethers such as THF or DME for the first step, followed by a solvent exchange with H_2O to obtain hydrated $CaB_{12}H_{12}$.

For the autoclave experiment in the synthesis of $CaB_{12}H_{12}$. Typically, 0.21 g of CaH_2 (5 mmol) was weighed into the plastic liner reactor (40 ml) in a glovebox and sealed with Parafilm. Before loading the plastic reactor into the autoclave, 8 mL of monoglyme and 8 mL of THF, and 60 mmol of the borane dimethyl sulfide complex ($(CH_3)_2S{\cdot}BH_3$, 6 mL), were added to the borohydride. The autoclave was then sealed and purged for 30s to remove air from the system.

The reaction temperature was increased from room temperature to 120 °C at a rate of 2 °C/min, and then maintained for 24 h. After the system cooled down to room temperature, the reaction mixture was filtered using a Schlenk filtration apparatus and washed with THF (3 × 10 mL) to remove residual $Ca(BH_4)_2$. The solvent was then replaced by water.

$$CaH_2 + 12\ (CH_3)_2S{\cdot}BH_3 \xrightarrow[120\ ^oC]{THF+DME} CaB_{12}H_{12}{\cdot}n\ DME + 10\ DMS + 12\ H_2 \quad (13)$$

The solvent was then replaced by water and the free water can be removed at 40 °C.

$$CaB_{12}H_{12}{\cdot}\ n\ (DME)\ (s) + H_2O\ (sol) \xrightarrow{40\ ℃,\ Vaccum} CaB_{12}H_{12}\ {\cdot}n\ (H_2O)\ (s) + DME\ (g) \quad (14)$$

The removal of H_2O from hydrated $CaB_{12}H_{12}$ can be done by thermal treatment at 200 °C under vacuum, resulting in the diffracting pure $CaB_{12}H_{12}$ in a yield of approximately 73%.

2.2.4. Synthesis of $(Me_4N)_2B_{12}H_{12}$

Tetraalkylammonium-$B_{12}H_{12}$ was synthesized in the autoclave according to the following procedures. Typically, 0.89 g of $(CH_3)_4NBH_4$ (10 mmol) was weighed into the quartz liner reactor in a glovebox and sealed with Parafilm. Before loading the quartz reactor into the autoclave, 16 mL of diglyme and 55 mmol of the borane dimethyl sulfide complex ($(CH_3)_2S{\cdot}BH_3$, 5.5 mL) were added to the borohydride. The autoclave was then sealed and purged for 30 s to remove air from the system. The reaction temperature increased from room temperature to 150 °C (melting point of Me_4NBH_4) at a rate of 2 °C/min, and then maintained for 24 h. After the system cooled down to room temperature, the reaction mixture was filtered using a Schlenk filtration apparatus and washed with diglyme (3 × 10 mL). The sample was dried at 200 °C under vacuum for 4 h.

The substitution method for the synthesis tetramethylammonium dodecaborate $[(CH_3)_4N]_2B_{12}H_{12}$ has been published. In this work, an improved substitution method for obtaining $[(CH_3)_4N]_2B_{12}H_{12}$ crystals has been developed as follows:

$$Na_2B_{12}H_{12} + 2\,(CH_3)_4NBr \xrightarrow{100\,℃,\ \text{fast cooling}} [(CH_3)_4N]_2B_{12}H_{12}\,(s) + 2\,NaBr\,(g) \quad (15)$$

2.3. Nuclear Magnetic Resonance

Nuclear Magnetic Resonance (NMR) spectroscopy is an important analytical tool for researchers who work with boron chemistry. In this work, NMR is important analytical technique used to gather information about purity and content of a material. In NMR, it's working principle is based on are producing signals by subjecting a sample to a strong magnetic field, which causes the nuclei to absorb energy and shift to a higher energy state. As the nuclei return to their original state by relaxing, they released energy in the form of electromagnetic radiation, which the NMR machine detects and quantifies. This is only possible for nuclei with a spin, *I*, of greater than zero and these nuclei are said to be "NMR active". Each NMR active element gives off its own characteristic frequency so different elements can be probed by detecting different frequencies. Figure 9 depicts a schematic representation of this procedure.

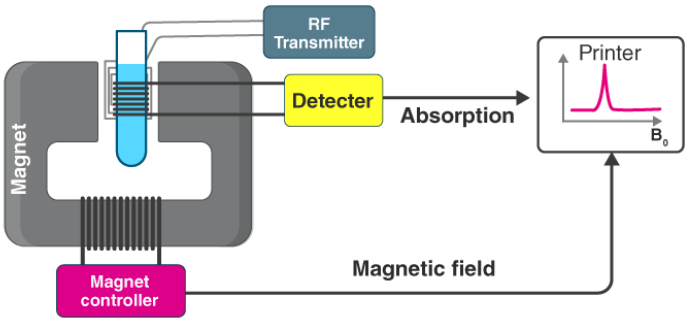

Figure 9. A schematic diagram of NMR measurement.[3,4]

In this project, we primarily utilized the ^{11}B NMR method. Both ^{10}B and ^{11}B isotopes are naturally occurring and NMR-active. However, ^{11}B, with a nuclear spin of $^{3}/_{2}$ and a natural abundance of 81.4%, offers higher sensitivity and narrower lines due to its smaller quadrupole moment, making it more commonly used for analyzing boron containing compounds, which makes ^{11}B is favored over ^{10}B for NMR investigations.

Solution-state NMR spectroscopy is mainly used in this work, which involves the dissolution or dilution of the sample or reaction mixture in a deuterated solvent for the first step. Many of the $B_{12}H_{12}^{2-}$ salts exhibit very high solubility in solvents like DMSO or water, making deuterated DMSO-d_6 and D_2O the preferred choices for solution state NMR testing. Solid-state NMR spectroscopy is used to investigate materials in their solid state, such as powders or crystals. The material is compressed into a rotor and placed within a magnetic field. Solid-state NMR is very useful for studying big molecules and insoluble solid.

All NMR spectra in this work were recorded at room temperature (298 K) on a Bruker Avance 500 spectrometer operating at 500.13 MHz for ^{1}H and 160.46 MHz for ^{11}B, using a BBFO {^{1}H, X} probehead equipped with a z-gradient coil. The experiments were conducted under the TopSpin program (version 1.3; Bruker). ^{1}H chemical shifts were referenced to the residual DMSO-d_6 signal (δ = 2.50 ppm), and ^{11}B NMR signals were externally referenced to $BF_3 \cdot Et_2O$ (δ = 0.00 ppm). All experiments were performed using quartz NMR tubes (i.d. = 5 mm).

2.4. Diffraction Studies

2.4.1. X-ray Diffraction and Bragg's Law

X-ray diffraction is a powerful technique for crystalline structure and composition determination of the synthesized materials. X-rays are a form of high-energy electromagnetic radiation with short wavelength (size similar to the distance between atoms in solids). When an X-ray pulse interacts with a long range ordered crystal structure, a physical process known as diffraction occurs. The electrons surrounding the atoms within the crystal become secondary sources of X-ray beams. The waves scattered by individual electrons interact with each other according to Bragg's law, due to the regular arrangement of the crystal's atoms. This interaction causes significant peaks to emerge at specific scattering angles. These intense peaks are determined by several factors, including the X-ray wavelength, crystal size, and orientation.

1. Diffraction Conditions

Figure 10 illustrates how diffraction of X-rays by crystal planes allows us to derive lattice spacings by using Bragg equation.

$$n\lambda = 2d \sin\theta$$

where:

n = the diffraction order (n = 1, 2, 3…)

λ = the wavelength of X-rays

d = crystal plane spacing

θ = angle between X-ray and crystal lattice planes

In the detection of diffraction patterns, the measurement were performed using a MAR345 image plate detector and an Incoatec Microfocus Source^{HIGHBRILLIANCE} (IμS^{HIGHBRILLIANCE}) Mo ELM47 operating at 50 kV and 1000 μA. By measuring the angles, represented as 2θ, at which X-rays constructively interfere and exit the crystal, we can estimate the relevant lattice spacings. The resulting diffraction pattern is then represented by the intensity of diffracted X-rays as a function of the angle 2θ. To describe the crystal structure and the orientation of lattice planes, we utilize Miller indices designated as h, k, and l consisting of integers. These indices play a crucial role in specifying both the dimensionality of the crystal lattice and the orientation of specific planes within the lattice, as visually depicted in Figure 10.

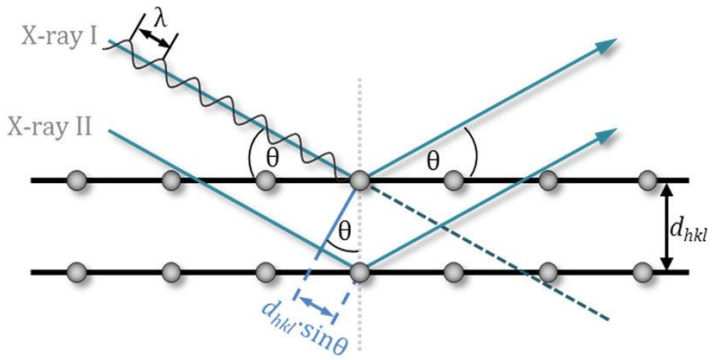

Figure 10. Graphical representation of the Bragg equation.[6]

2.4.2. Single Crystal X-ray Diffraction

Diffraction investigations can be performed on single crystals or powders. A monochromatic X-ray beam is focused on a single crystal mounted on a goniometer in the case of single crystals, as shown in Figure 11. The goniometer permits exact rotation of the crystal at certain angles, allowing for the reflection intensities from each lattice

plane to be measured. These reflections are captured on a two-dimensional surface with a film or electronic detector.

High-quality crystals refract X-rays effectively, allowing for the identification of atomic locations within the crystal. As a result, a high-resolution crystal structure is obtained. SC-XRD is an effective tool for studying materials that have a single, well-defined structure.[7]

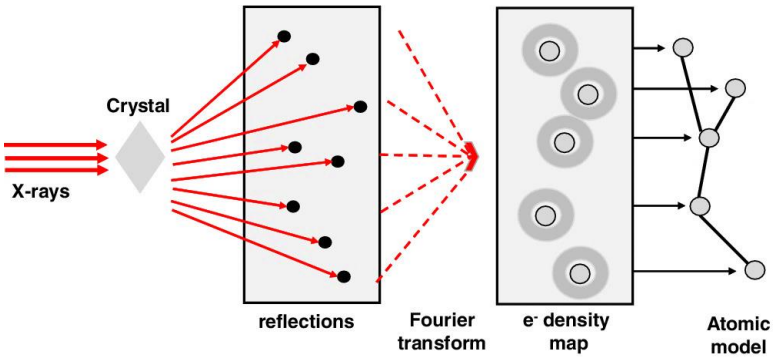

Figure 11. Single crystal XRD instrumentation.[8]

The SC-XRD measurements in this work were performed on a MAR345 image plate detector with Mo Ka radiation (λ = 0.71073 Å) at either room temperature, or by fast cooling to 150 °C in a flow of gaseous nitrogen (N_2). The diffraction pattern was indexed, and the total number of images were integrated using the CrysAlis^{PRO} software. During data processing step, an empirical absorption correction was applied.

For structure determination, the SHELXT program was employed, and subsequent refinement was carried out using full-matrix least squares based on $|F^2|$ with SHELXL 2014/7. Non-hydrogen atoms were refined anisotropically, while hydrogen atoms were positioned in riding mode, with temperature factors constrained to 1.2 times Ueq (the equivalent isotropic temperature factor) for parent atoms and 1.5

times Ueq for methyl groups. Mercury software was used to generate structural figures.

The comprehensive preparation and specific information for each crystals in the thesis work can be found in appendix.

2.4.3. Powder X-ray Diffraction

Powder X-ray Diffraction (PXRD) is a crucial method for understanding the crystal structure of materials. When the material cannot be grown into large enough crystal for single crystal diffraction but is still presented as crystalline material. As shown in Figure 12, a powder sample is made up of a large amount of small single crystals that are randomly aligned.

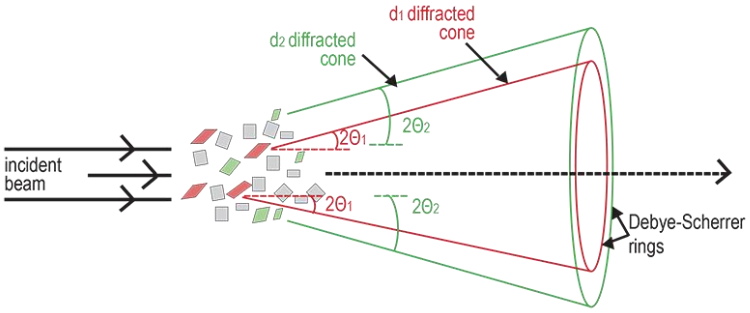

Figure 12. A schematic picture of powder diffraction with cones in red and green representing diffraction peaks having different *h k l* indices.[9,10]

In PXRD measurement, the powdered sample is slowly rotated, allowing it to pass through various orientations where diffraction can occur. An X-ray-sensitive camera or detector captures the diffraction rings, as shown in Figure 13a. Each ring corresponds to a specific diffraction angle. The data from the 2-D detector is integrated, summing the values from all pixels corresponding to a given angle, resulting in an intensity versus angle plot, as depicted in Figure 12b. Each diffraction peak corresponds to scattering from a specific lattice

plane can be denoted as h k l.

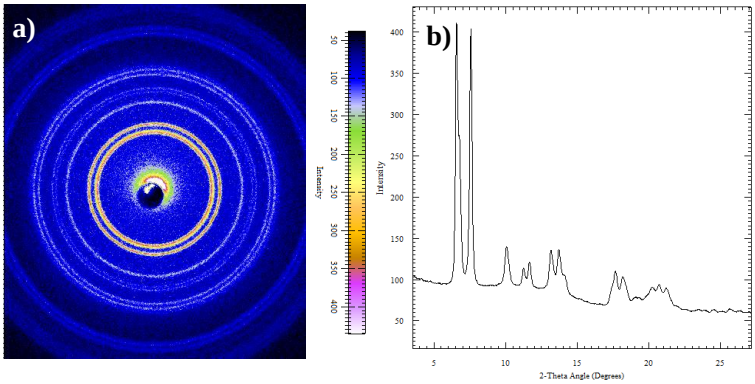

Figure 13. (a) The diffraction rings on a 2-D detector and (b) intensity versus diffraction angle, 2θ, obtained from integration of one sector. ($CaB_{12}H_{12}$ in thesis work)

In our laboratory, X-rays are generated using X-ray tubes, with high-speed cathode electrons continually targetting a metallic Mo (Molybdenum) anode target material in X-ray diffraction (XRD) measurements. When the electrons have enough energy, they collide with the anode material after being accelerated in an electric field with a potential difference of at least 30 kV. The electronic configuration of the atoms is excited and collided, resulting in the creation of characteristic high-energy X-ray emission lines, known as K lines during the de-excitation process.

The in-house X-ray diffractometers are equipped with two Incoatec X-ray generators, producing Mo Kα radiation with a wavelength of λ = 0.71073 Å. They are coupled with MAR345 image plate detectors. For SC-XRD measurements, a microfocus beam setup with an Incoatec source is used. PXRD is performed on capillary samples in transmission mode, using a high-brilliance Incoatec source with a parallel beam (focus on detector surface). Reference structures

were obtained in the form of Crystallographic information files (.cif) from the Cambridge Crystallographic Data Centre (CCDC) and Crystallography Open Database (COD).

2.4.4. Synchrotron Radiation X-ray Diffraction

To achieve high-resolution X-ray diffraction, measurements can be conducted at synchrotrons. Synchrotron radiation offers significant advantages compared to the X-ray tubes used in laboratory. These advantages include high intensity, a highly collimated beam, and a tunable energy range. Because of its monochromatic high flux and well-focused beams, synchrotron X-ray diffraction (SR-XRD) offers several benefits, including the absence of $K\alpha_2$ diffraction peaks, a high signal-to-noise ratio, and high angular resolution. These advantages are particularly valuable for analyzing complex structural details. The exceptionally high signal-to-noise ratio in the diffraction pattern is especially beneficial for Rietveld refinement of the data.

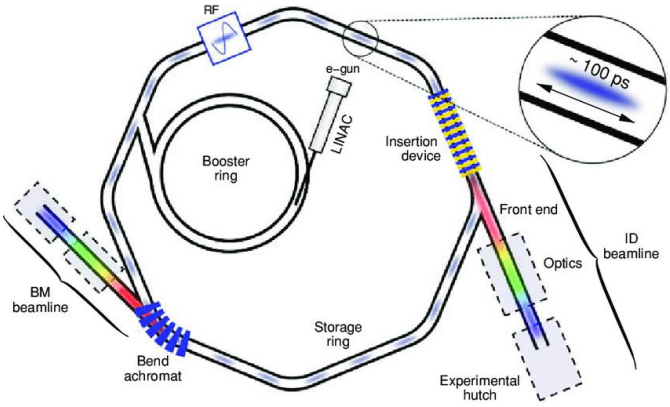

Figure 14. A schematic diagram of the basic components of a modern synchrotron facility.[11]

Figure 14 shows a synchrotron facility. In this facility, electrons are first generated in an electron gun and then accelerated in a linear

accelerator to almost the speed of light. After reaching high energy levels in the booster, these fast electrons are injected into a large storage ring, which is several kilometers in circumference and kept in ultra-high vacuum conditions. In the storage ring, the electrons travel at very high speeds and are forced to change direction by magnetic fields. This process makes the electrons produce a strong X-ray beam using devices called undulators and wigglers. Finally, the X-ray radiation is controlled by optical elements and directed to the experimental setup.

In this work, all SR-XRD diffraction data were collected at the SNBL beamline (BM 01) at the European Synchrotron Radiation Facility (ESRF) in Grenoble, France. Following a major upgrade (EBS), ESRF now boasts the world's first fourth-generation high-energy synchrotron (6 GeV). BM01 is equipped with a pixel PILATUS2M detector, which combines the advantages of pixel detector technology (low noise, fast readout, no correlation between pixels) with flexible goniometry. This detector and goniometer can be easily repositioned in both vertical and horizontal directions, making it suitable for fast measurements, such as phase transformations and reaction kinetics, often adopting a capillary geometry with rapid detectors.

2.4.5. *In situ* Powder X-ray Diffraction

Understanding the behavior of materials and tracking the chemical and structural changes during the reaction can be crucial. It is also a challenge to analyze samples without access to synchrotron beam time. Our X-ray Platform offers several in-situ chambers that enable on-site XRD studies of materials under various conditions, including:

i) Variable temperature ranges from RT to 500 °C.

ii) Controlled environments such as CO_2, air, or vacuum (other gases) during the reaction.

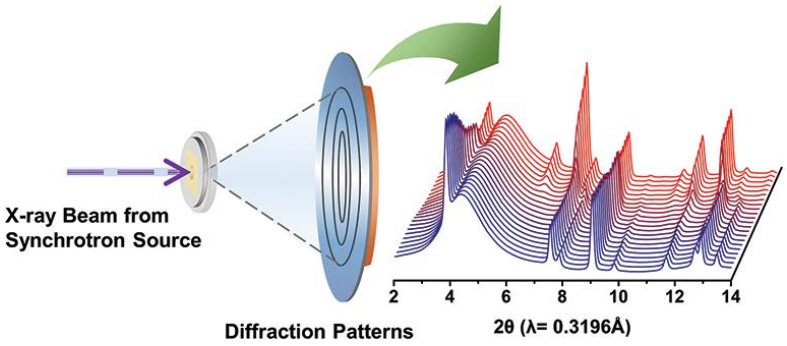

Figure 15. A schematic diagram of synchrotron radiation-based X-ray scattering.[12]

The in-situ synchrotron radiation powder X-ray diffraction (Figure 15) data were collected at the Swiss-Norwegian beamline BM1A at the European Synchrotron Radiation Facility (ESRF) in Grenoble, using a Dectris PILATUS 2M single-photon counting pixel area detector Wavelengths employed in various experiments ranged from 0.70 to 0.75 Å, while the sample-to-detector distances varied from 200 to 400 mm. These parameters, along with image plate tilt angles, were calibrated using a standard LaB_6 sample. Samples were sealed under argon within thin-walled glass capillaries. Two-dimensional diffraction images were azimuthally integrated using the ESRF Fit2D program.

2.5. Thermogravimetric Analysis and Differential Scanning Calorimetry

Thermogravimetric analysis and Differential Scanning Calorimetry (TGA–DSC) were employed to determine the phase

changes and the decomposition temperatures for various synthesized materials. DSC measures changes in heat flow, both exothermic (heat-releasing) and endothermic (heat-absorbing), when a sample is heated. This enables the determination of key phase transition temperatures, including crystallization, melting and solid-solid polymorphic transitions. TGA tracks the variations in mass when a sample is heated. It is valuable for assessing thermal stability, solvent content, and decomposition of materials.

The TGA–DSC analyses were conducted using a NETZSCH STA 449 F3 Jupiter instrument equipped with a stainless-steel oven, placed within an argon-filled glovebox. Measurements were carried out at a heating rate of 5 °C /min under a continuous argon flow (total flow rate of 100 mL/min), with the temperature ranges from 25 to 1000 °C. Approximately 5–10 mg of samples were weighted within the argon-filled glovebox and loaded into aluminum crucibles. These crucibles were securely sealed by cold-welding. Just before insertion into the instrument, the aluminum crucibles were punctured, and a vacuum was applied to ensure the removal of air and moisture from the furnace for accurate and reliable measurements.

2.6. Vibration spectroscopy

Fourier transform infrared spectroscopy (FTIR) is a vibrational technique employed for the identification of functional groups like B–H, O–H, C–H, etc. In FTIR, infrared radiation is directed through a sample (transmission), leading to the generation of an absorption spectrum. This spectrum contains distinct IR absorption bands that correspond to the wavenumbers of the infrared-active vibrational

modes present in the sample. FTIR spectroscopy is a valuable tool for both qualitative and quantitative analyses.

In ATR-FTIR spectroscopy, the sample comes into direct contact with the ATR crystal. An IR beam passes through the crystal from underneath and interacts with the sample placed on the crystal's surface. Because of the differences in the refractive indices of both materials, total internal reflection occurs. This leads to some penetration of reflectance into the material, generating an "evanescent wave." When the evanescent wave interacts with the sample, a small portion of the infrared light is absorbed by the material, resulting in a slight attenuation of total reflection. The basic setup is depicted in Figure 16. ATR-FTIR spectroscopy minimizes the requirement for extensive sample preparation. It has become the preferred method for acquiring IR spectra of solid materials.

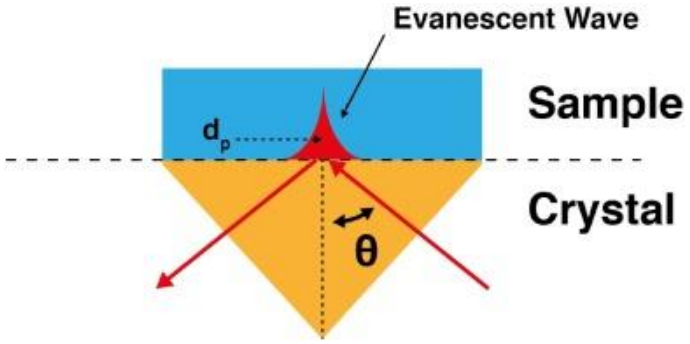

Figure 16. A schematic of the single bounce ATR used in this work.[13]

In this study, the ATR-FTIR spectra were acquired using a Bruker Alpha II spectrometer, which was operated in an argon-filled glovebox. The spectrometer was equipped with a Platinum ATR module (Bruker), featuring a diamond crystal with a single bounce configuration. Spectral data were collected in the wavenumber range of 370 to 4000 cm^{-1} with a spectral resolution of 4 cm^{-1}, averaged from16 scans.

2.7. Reference

(1) Bugaris, D. E.; Ibers, J. A. Syntheses and Characterization of Some Solid-State Actinide (Th, U, Np) Compounds. *Dalt. Trans.* **2010**, *39* (26), 5949–5964.

(2) Tsamos, D.; Krestou, A.; Papagiannaki, M.; Maropoulos, S. An Overview of the Production of Magnetic Core-Shell Nanoparticles and Their Biomedical Applications. *Metals (Basel).* **2022**, *12* (4), 1–22 .

(3) Zia, K.; Siddiqui, T.; Ali, S.; Farooq, I.; Zafar, M. S.; Khurshid, Z. Nuclear Magnetic Resonance Spectroscopy for Medical and Dental Applications: A Comprehensive Review. *Eur. J. Dent.* **2019**, *13* (1), 124–128.

(4) https://Byjus.Com/Chemistry/Nmr-Spectroscopy/

(5) Nesbitt, G. J. Principles of NMR Microscopy. *TrAC Trends Anal. Chem.* **1992**, *11* (6), XVIII.

(6) Paula, C. In Situ Solid-State NMR and XRD Investigations of Structural Transformations in Crystalline Porous Solids, **2021**.

(7) Suter, R. M.; Hennessy, D.; Xiao, C.; Lienert, U. Forward Modeling Method for Microstructure Reconstruction Using X-Ray Diffraction Microscopy: Single-Crystal Verification. *Rev. Sci. Instrum.* **2006**, *77* (12), 1–12.

(8) Khan, H.; Yerramilli, A. S.; D'Oliveira, A.; Alford, T. L.; Boffito, D. C.; Patience, G. S. Experimental Methods in Chemical Engineering: X-Ray Diffraction Spectroscopy—XRD. *Can. J. Chem. Eng.* **2020**, *98* (6), 1255–1266.

(9) Mabey, P. A; Study on Dense Plasmas Using Molecular Dynamics and X-Ray Scattering Techniques, **2016**.

(10)https://www.Diamond.Ac.Uk/Industry/Industry-News/Latest-News/Synchrotron-Industry-News-Powder-Diffraction.html.

(11) Joly, L. Magnetism and Accelerator-Based Light Sources. **2021**, 262.

(12) Muhammad, S.; Kim, H.; Yoon, W. S. Synchrotron Radiation-Based X-Ray Study on Energy Storage Materials. *IntechOpen*. **2017**.

(13) Saukel, J. Spectrochimica Acta Part A : Molecular and Biomolecular Spectroscopy Apparent Penetration Depth in Attenuated Total Re Fl Ection Fourier-Transform Infrared (ATR-FTIR) Spectroscopy of Allium Cepa L. *Epidermis and Cuticle*. **2020**, *224*, 1–6.

Chapter 3. High Yield Autoclave Synthesis of Pure $M_2B_{12}H_{12}$ (M = Na, K)

Jian Wang,[a] *Timothy Steenhaut,*[a] *Hai-Wen Li,*[b] *Yaroslav Filinchuk,*[a*]

[a] Institute of Condensed Matter and Nanosciences, Université Catholique de Louvain, 1348 Louvain-la-Neuve, Belgium

[b] Hefei General Machinery Research Institute, Hefei 230031, China

*Corresponding Author. E-mail: yaroslav.filinchuk@uclouvain.be (Y. Filinchuk)

This chapter has been published in *Inorg. Chem.* 2023, 62, 5, 2153–2160.

Chapter 3

Abstract

In this chapter, we report a simple, efficient, and environmentally benign solvothermal method to prepare diffraction and ^{11}B NMR pure $Na_2B_{12}H_{12}$ (85% yield) and $K_2B_{12}H_{12}$ (84% yield) using autoclave method. This new synthetic approach is based on the use of the borane dimethyl sulfide complex ($DMS{\cdot}BH_3$) and borohydrides ($NaBH_4$, KBH_4) heated at different temperatures in diglyme in an autoclave. It was found that high purity $Na_2B_{12}H_{12}$·diglyme solvate is obtained via an intermediate formation of $B_3H_8^-$, $B_9H_{14}^-$, $B_{11}H_{14}^-$, which are all soluble in diglyme. Heating under vacuum is shown to be efficient for removing the coordinated diglyme, allowing the formation of unsolvated $Na_2B_{12}H_{12}$. Autoclave synthesis starting from KBH_4 directly yields solvent-free $K_2B_{12}H_{12}$, and ball-milling KBH_4 prior to the synthesis enabling us to significantly improve the final yield. The new synthetic method paves the way for large-scale synthesis of $M_xB_{12}H_{12}$ derivatives, enabling to envisage a wider scope of practical applications.

3.1. Introduction

Complex hydrides containing light elements are considered promising materials for solid-state hydrogen storage. Among these, metal borohydrides having high volumetric and gravimetric hydrogen densities, primarily $LiBH_4$, $Mg(BH_4)_2$ and $Ca(BH_4)_2$, [1-3] have attracted considerable attention. This includes reactive hydride composites with binary hydrides, such as $LiBH_4$ and MgH_2, which are capable of storing hydrogen reversibly.[4] However, the major problem are the side reactions transforming BH_4^- anions into more stable dodecaborates, $B_{12}H_{12}^{2-}$, that cannot be easily rehydrogenated, therefore, these compounds are often called "boron sinks" in this context.[5]

On the other hand, metal dodecaborates are interesting compounds as they find applications in cancer treatment, polymer chemistry, and, more recently, as solid-state ionic conductors.[6-11] They contain closed icosahedral boron clusters with 12 terminal hydrogen atoms in each corner, and have remarkable chemical and thermal stability.[12,13] However, dodecaborates, such as $Li_2B_{12}H_{12}$ and $Na_2B_{12}H_{12}$, are commercially available, but at a very high price (e.g., 5 g of $Na_2B_{12}H_{12}$ cost around 500 €).[14, 15] The investigation of the sizeable scale synthesis of $M_xB_{12}H_{12}$ has therefore been subject to a great effort of many research groups over the past few decades.

The $B_{12}H_{12}^{2-}$ anion was first obtained by Hawthorn in 1960, in very low yields, as a byproduct of the reaction between triethylamine and 2-iododecaborane in benzene.[16] Since then, synthetic methods for obtaining dodecaborate salts have been continuously developed and improved.[13, 17-19] However, these methods still suffer from low yields or the use of toxic and flammable boranes (B_2H_6 and $B_{10}H_{14}$) as

precursors. The main synthetic methods developed so far are based on two types of reactions.

The first method is the reaction of borohydrides with boranes (B_2H_6 or $B_{10}H_{14}$), which produces a series of boron-rich anions. The reaction between B_2H_6 and $NaBH_4$ in triethylamine at room temperature leads to the formation of NaB_3H_8 with a higher yield than the method described above. By rising the temperature to 180 °C, $Na_2B_{12}H_{12}$ is obtained in a high yield of around 90 %. Below this temperature, lower borane anion species, such as $B_{11}H_{14}^-$, are formed instead.[20] Generally, higher temperatures favor the formation of B–B bonds, forming polyhedral boranes that tend to become larger and more stable with increasing reaction temperatures.[21] Solvent-free methods, like annealing in sealed tubes, were employed for the reaction between solid state decaborane ($B_{10}H_{14}$) and borohydrides. However, in this case, the reaction leads to the formation of $B_{12}H_{12}^{2-}$ together with other B−H compounds.[18,22] The $B_{12}H_{12}^{2-}$ anion can also be formed by the reaction between boranes (B_2H_6 or $B_{10}H_{14}$) and borane triethylamine complex precursors.[20,21] Since nowadays green chemistry is gaining attention for chemical syntheses, the use of toxic and expensive compounds such as B_2H_6 and $B_{10}H_{14}$ should be avoided whenever possible.

The second method is a two-step synthesis that relies on the oxidation of borohydrides by iodine.[17,23] During the first step, $NaBH_4$ reacts with I_2 in diglyme (diethylene glycol dimethyl ether), giving NaB_3H_8 as main intermediate. $Na_2B_{12}H_{12}$ can then be obtained as one of the pyrolysis products of NaB_3H_8, at 150 °C (equation 1 and 2). This route can be made cheap and specific, but the yield is not high (between 50 and 60 %) due to low conversion of $NaBH_4$ and the difficulty of the purification process.

$$3\ NaBH_4 + I_2 \rightarrow NaB_3H_8 + 2\ NaI + 2\ H_2 \quad (1)$$

$$5\ NaB_3H_8 \rightarrow Na_2B_{12}H_{12} + 3\ NaBH_4 + 8\ H_2 \quad (2)$$

In this study, we propose a new and convenient route for the one pot synthesis of sodium and potassium dodecaborates from their respective borohydrides and the borane dimethyl sulfide complex ($DMS{\cdot}BH_3$) in an autoclave. The use of an autoclave not only provides an enclosed system to keep all gaseous species confined, but also enables increasing the boiling point of diglyme, which is used as a solvent, thereby increasing the solubility of the used borohydrides. We first investigated the effect of reaction temperature on the synthesis, exploiting sodium as cation.

Previous research showed that diglyme is easily chelated with dodecaborate salts with smaller cations, such as Na^+ and Li^+.[24] To obtain non-solvated dodecaborates with those cations, synthesis can be undertaken with larger monovalent cations such as trimethylammonium, yielding water-insoluble products ($[(CH_3)_3NH]_2B_{12}H_{12}$) with no coordinating diglyme. $Na_2B_{12}H_{12}$ can then be obtained by simple cation exchange between $[(CH_3)_3NH]_2B_{12}H_{12}$ and NaOH in water.[19] For the present work, the desolvation of diglyme by thermal treatment of the obtained diglyme-solvated $Na_2B_{12}H_{12}$ was studied. Once optimized for the sodium derivative, the method was further developed to obtain $K_2B_{12}H_{12}$ from KBH_4 and $DMS{\cdot}BH_3$. All the obtained samples were characterized by means of powder X-ray diffraction (PXRD), Fourier-transform infrared, nuclear magnetic resonance and inductively coupled plasma optical emission spectroscopies (FTIR, NMR and ICP-OES). Their thermal properties were assessed by thermal gravimetric and differential scanning calorimetric (TGA/DSC) methods.

3.2. Experimental Section

3.2.1. Chemicals

Sodium borohydride ($NaBH_4$, anhydrous, 95%), potassium borohydride (KBH_4, anhydrous, 98%), Borane triethylamine complex ($(C_2H_5)_3N{\cdot}BH_3$, 97%), borane dimethyl sulfide complex ($(CH_3)_2S{\cdot}BH_3$, analytical) and diethylene glycol dimethyl ether (diglyme, $C_6H_{14}O_3$, anhydrous, 99.5%) were obtained from Sigma-Aldrich. Deuterated dimethyl sulfoxide (DMSO-d_6, anhydrous, 99.9 atom% D) was obtained from Eurisotop. All the above chemicals were used without further purification. Commercial $Na_2B_{12}H_{12}$ (99.5%) was purchased from Katchem and was dried at 150 °C under vacuum for 2 h before PXRD and FTIR measurements.

3.2.2. General Synthetic Procedure

The reaction was performed in a 37.5 mL quartz liner fitted inside a stainless steel autoclave (Anhui Kemi Instrument Co., Ltd., the volume of the autoclave is 50 mL. Typically, 0.19 g $NaBH_4$ (5 mmol, or 0.27 g of KBH_4) was weighted into the quartz liner reactor in a glovebox, and the glass reactor was sealed by Parafilm. Before loading the quartz reactor into the autoclave, 16 mL of diglyme (the solubility of $NaBH_4$ in diglyme at room temperature is reported to be 0.55 g/g),[25] and subsequently 27.5 mmol of borane dimethyl sulfide complex $(CH_3)_2S{\cdot}BH_3$ (2.75 mL) were added to the borohydride. The autoclave was then sealed and the system was purged with argon for 30 s to remove air in the system, and the solution was then stirred further at room temperature for another 10 min. The reaction temperature was controlled by a programmed system and was

increased at a heating rate of 2 °C/min from RT to the final reaction temperature, at which it was maintained for 24 h. Subsequently, the system was naturally cooled down to room temperature. The reaction mixture was then filtered, using a Schlenk filtration apparatus, and washed with diglyme (3 × 10 mL), followed by drying at 80 °C under vacuum for 2 h to transform sticky powders into dry ones for PXRD and ATR-FTIR measurements. The raw product was obtained as a white substance. The desolvated samples were obtained by heating at 200 or 150 °C under vacuum for 12 h.

In this work, different temperatures were investigated for both reaction and desolvation. The obtained samples were labelled as MD-X-Y, where M = alkali ion (Na or K), and D is the abbreviation of $DMS{\cdot}BH_3$, X stands for the reaction temperature (in °C, ranging from 90 to 200 °C), and Y denotes the desolvation temperature (in °C, either 150 or 200 °C). The raw product was obtained as a white solid substance.

Purified $K_2B_{12}H_{12}$ was obtained by refluxing samples in boiling demineralized water (100 °C, 1 h). Samples were then filtrated and dried at 120 °C under vacuum for 4 h.

Ball milled KBH_4 (bm-KBH_4) was produced by mechanical milling of 0.5 g of KBH_4 at room temperature using a planetary ball mill (Fritsch Pulverisette P7) upon loading with 4 steel balls (10 mm in diameter) in a hardened steel vials (30 cm^3 in volume) in an argon-filled glovebox. Milling was performed under 0.1 MPa of Ar for 2 h (2 min of milling cycles, 3 min of pausing, 24 cycles).

3.2.3. Characterization

Powder X-ray diffraction (PXRD) patterns were collected using a MAR 345 image plate detector, utilizing Mo Kα radiation (λ =

0.71073 Å) from Incoatec Microfocus Source Mo ELM47 operating at 50 kV and 1000 µA. Samples were rotated 180° during exposure for 10 min. Samples were loaded into thin-walled glass capillaries (0.7 mm diameter, Hilgenberg, GmbH) under argon in a glovebox. The capillaries were sealed with grease in the glovebox. Once removed from the glovebox, they were cut and immediately placed into molten wax on goniometric heads and measured immediately after preparation to avoid sample degradation. The data were integrated by the Fit2D software (ESRF) using LaB_6 as calibrant.

TGA–DSC analyses were performed on a NETZSCH STA 449 F3 Jupiter instrument equipped with a stainless steel oven, housed inside an argon-filled glovebox. Measurements were performed at a heating rate of 5 K/min under constant Ar flow (total flow of 100 mL/min), from 25 to 500 °C.

The attenuated total reflectance Fourier transform infrared (ATR-FTIR) spectra were measured on a Bruker Alpha II spectrometer set in an argon-filled glovebox. For the measurements, the spectrometer was equipped with a Platinum ATR module (Bruker, diamond crystal, single bounce).

All NMR spectra were recorded at room temperature (295 K) on a Bruker Avance 500 spectrometer operating at 500.13 MHz for ^{1}H and 160.46 MHz for ^{11}B, using a BBFO {^{1}H, X} probehead equipped with a *z*-gradient coil. Experiments were run under the *TopSpin* program (1.3 version; Bruker). ^{1}H chemical shifts were referenced to the residual DMSO-d_5 signal (δ = 2.50 ppm), and ^{11}B NMR signals were referenced externally to $BF_3{\cdot}Et_2O$ (δ = 0.00 ppm). All experiments were conducted using a quartz NMR tube (internal diameter = 5 mm)

ICP-OES analyses were carried out on an ICAP-6500 apparatus from ThermoFisher Scientific, upon dissolution of the samples in

purified water.

3.3. Results and Discussion

3.3.1. Influence of the reaction temperature on the reaction products in the synthesis of $Na_2B_{12}H_{12}$·diglyme

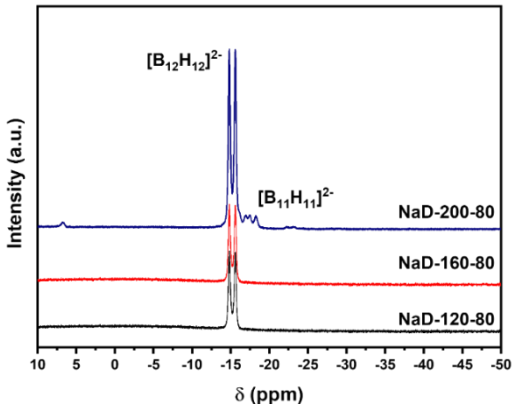

Figure 1. ^{1}H-coupled ^{11}B NMR spectra of the solid precipitates formed in the reaction conditions used for NaD-X-80 (X = 120, 160, 200).

Borane complexes have proven exceedingly useful for hydroboration reactions. They offer similar reactivity to diborane (B_2H_6) but have fewer storage and handling issues. Among the available complexes, the borane tetrahydrofuran complex ($THF{\cdot}BH_3$), borane triethylamine complex ($Et_3N{\cdot}BH_3$) and $DMS{\cdot}BH_3$ are the most popular agents. Although $THF{\cdot}BH_3$ is more reactive than $DMS{\cdot}BH_3$ and $Et_3N{\cdot}BH_3$, it is commercially available only as a solution in THF. In contrast, $DMS{\cdot}BH_3$ and $Et_3N{\cdot}BH_3$ are more stable and readily available as neat reagents. However, $Et_3N{\cdot}BH_3$ has a million times lower dissociation constant than $DMS{\cdot}BH_3$.[26] This is the reason of its

lower reactivity with borohydrides: indeed, we observed in our first experimental attempts that $NaBH_4/KBH_4$ and $Et_3N{\cdot}BH_3$ at 180 °C in an autoclave did not yield any dodecaborates. Hence, we focused on using $DMS{\cdot}BH_3$ in the reaction with $NaBH_4$, studying the effect of the reaction temperature (90, 120, 160 and 200 °C) on the obtained products. Once the reaction was completed in an autoclave, the products were initially dried at 80 °C, transforming sticky powders into dry samples, i.e., removing most of the free diglyme and allowing easy characterization of the samples. Figure 1 depicts the proton coupled ^{11}B NMR spectra of as-prepared NaD-X-80 (X = 120, 160 and 200) samples. A reaction at a temperature of 90 °C (sample NaD-90-80) did not lead to the formation of any solid precipitate. The NMR spectrum of the reaction solution of NaD-90-80 (Figure S1) shows that mainly $B_3H_8^-$ was formed, together with some boron clusters with higher nuclearity ($B_9H_{14}^-$ and $B_{11}H_{14}^-$), which are all soluble in diglyme.[23, 27, 28] This is consistent with earlier reports of the formation of $B_9H_{14}^-$ and $B_{11}H_{14}^-$ by dehydrocondensation of $B_3H_8^-$ with diborane in diglyme at low temperatures around 70–90 °C.[27] When higher reaction temperatures are used (120 and 160 °C), solid precipitates appear after cooling the autoclave. The ^1H-coupled ^{11}B NMR spectra of NaD-120-80 and NaD-160-80 dissolved in DMSO-d_6 show doublet peaks at approximately –15 ppm, which indicates the presence of $B_{12}H_{12}^{2-}$. The ^{11}B NMR spectra do not show the formation of any other solid boron compounds under those reaction conditions.[13, 28] For NaD-200-80, an additional multiplet is present at –17.2 ppm, partly overlapping the doublet of $B_{12}H_{12}^{2-}$. It can be assigned to $B_{11}H_{11}^{2-}$, likely forming due to the decomposition of intermediates, such as $B_{11}H_{14}^-$, at high temperatures, as indicated by previous works.[9] These results show that temperature is a crucial factor for the outcome of the synthesis, as it usually is for the synthesis of

polyhedral borates.

TGA–DSC analyses were performed to investigate the thermal stability and composition of the NaD-X-80 (X = 120, 160, 200) samples, which were compared to commercial $Na_2B_{12}H_{12}$. Figure 2(a) shows that commercial $Na_2B_{12}H_{12}$ displays an endothermic signal on the DSC curve, accompanied by a small mass loss of about 1 wt. % on TGA, around 100 °C, which is ascribed to the loss of physically adsorbed water. The DSC curve furthermore shows an endothermic peak with a maximum at 266 °C, without mass loss, which is explained by a well-known phase transition of $Na_2B_{12}H_{12}$.[29] For the synthesized samples, the loss of some diglyme can be observed from the DSC curves, starting around 110 °C. The DSC curves of all the synthesized samples show an intense endothermic peak around 142 °C, accompanied by a weight loss, attributed to the liberation of the remaining coordinated diglyme. A separate experiment consisting of drying the sample at 150 °C under vacuum was performed, showing that the PXRD pattern (Figure S2) has changed upon this treatment, which confirms that the weight loss is due to the departure of diglyme inside the structure. A similar endothermic peak and weight loss are also present around 201 °C, which is attributed to the release of the coordinated diglyme, which is known to form chelates with small cations such as Na^+ and Li^+.[24]

The DSC curve of NaD-120-80 shows the typical endothermic peak related to the phase transition of the solvent-free $Na_2B_{12}H_{12}$ at 266 °C (Figure 2b), in agreement with the behavior of the commercial sample. This phase transition peak is however not observed on the DSC curves of NaD-160-80 and NaD-200-80. XRD data (Figure 4) shown below indicate that solvated $Na_2B_{12}H_{12}$ obtained at 120 °C has a different structure than products obtained at higher synthesis

temperatures (160 °C). The decomposition of the high temperature (HT) form of $Na_2B_{12}H_{12}$·diglyme likely leads directly to the HT form of $Na_2B_{12}H_{12}$, thus explaining the absence of the DSC peak at 266 °C. In addition, a new endothermic peak at 220 °C is observed on the DSC curve of NaD-200-80, which is due to the desolvation of $Na_2B_{11}H_{11}$·diglyme that is present as a secondary product.

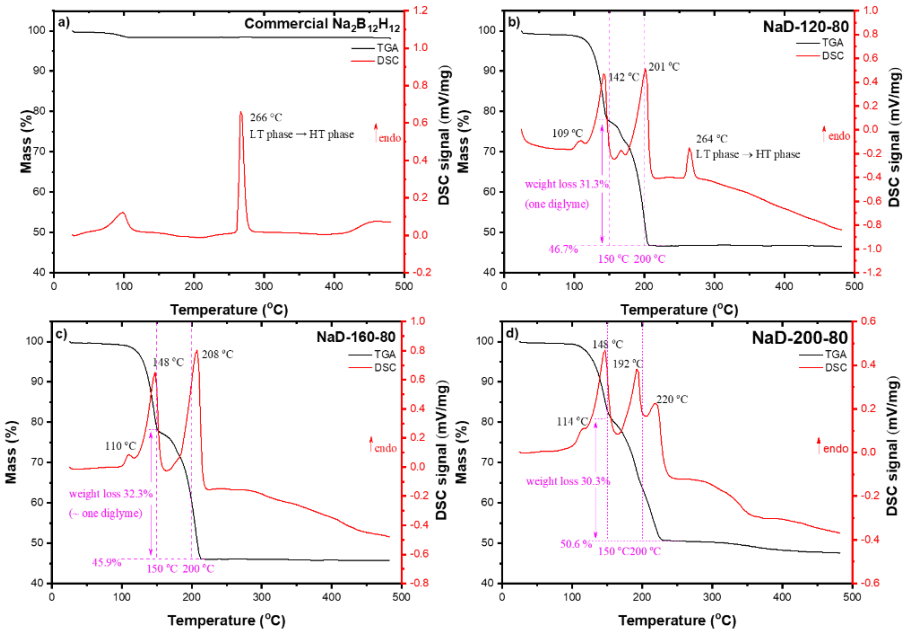

Figure 2. TGA–DSC curves of a) commercial $Na_2B_{12}H_{12}$, b) NaD-120-80, c) NaD-160-80 and d) NaD-200-80 samples, measured under argon at a heating rate of 5 K/min from RT to 500 °C.

3.3.2. Removal of diglyme from $Na_2B_{12}H_{12}$·diglyme

Based on the results of the TGA–DSC experiments, we decided to investigate drying temperatures of 150 and 200 °C in order to obtain desolvated $Na_2B_{12}H_{12}$. The solvent removal was performed in a Schlenk flask connected to a vacuum pump, and the obtained dried samples were analyzed by FTIR (Figure 3) and PXRD (Figure 4).

Typical signals of the $B_{12}H_{12}^{2-}$ anion are observed for all samples: 1074 cm^{-1} (vibration of the B−B bond), 2467 cm^{-1} (B−H symmetric and antisymmetric stretchings), 713 and 539 cm^{-1} (B−H bending and rocking vibrations).[19] The absorption bands located at 3000−2750 and 1500−1300 cm^{-1} present in the spectra of the sample dried at 80 °C are attributed to C−H and C−O stretching modes of diglyme, respectively. The disappearance of these bands from the FTIR spectrum upon drying the samples at 200 °C proves that this temperature enables effective removal of all the coordinated diglyme.

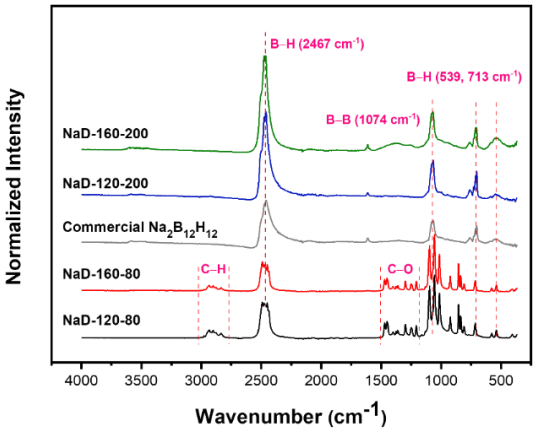

Figure 3. FTIR spectra of the NaD-X-Y (X=120, 160; Y=150, 200) samples.

All samples before and after drying were analyzed with PXRD. As shown in Figure 4, the PXRD patterns of the as-prepared NaD-120-200 and NaD-160-200 are in good agreement with the commercial $Na_2B_{12}H_{12}$, having a monoclinic *P*21/*n* structure corresponding to the low temperature (LT) phase (ICSD 164649). A peak shift and broadening are observed for the NaD-160-200 sample in the zoomed diffraction pattern (Figure 4b). All patterns were measured under the same conditions, and the observed shift and broadening can likely be attributed to a higher number of structural defects resulting from the higher reaction temperature. The solvated samples, obtained by drying

the reaction products at 80 °C and 150 °C, show very different diffraction patterns (Figure S2), indicating that the diglyme-solvated $Na_2B_{12}H_{12}$ phases corresponding to NaD-120-80 and NaD-160-80 are not the same.

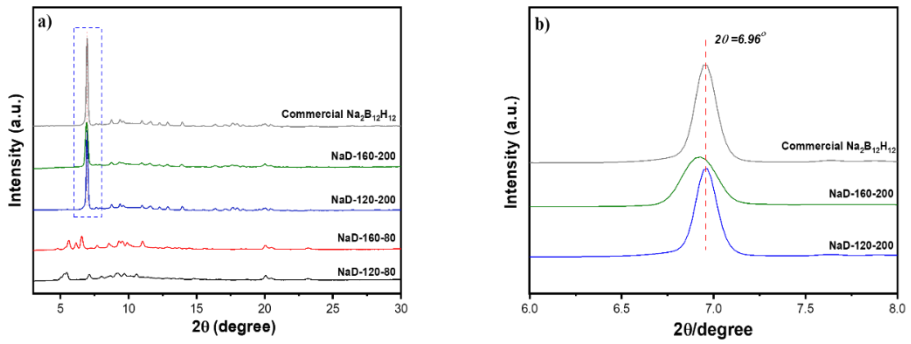

Figure 4. a) PXRD patterns of the NaD-X-Y (X=120, 160; Y=150, 200) samples; b) zoom between 6 and 8º.

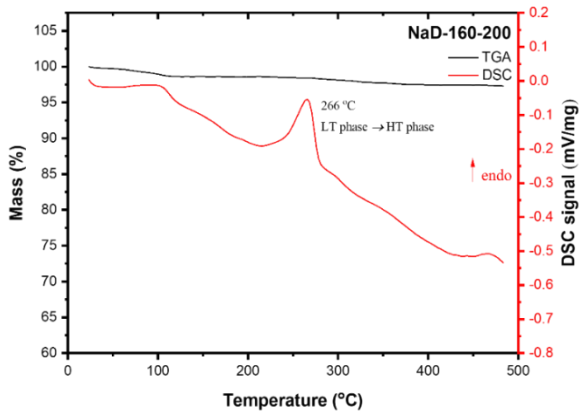

Figure 5. TGA–DSC analysis of NaD-160-200, measured under argon, with a heating rate of 5 K/min from RT to 500 °C.

The desolvated NaD-160-200 was further characterized by ICP-OES. As shown in Table S1, the experimentally determined Na/B ratio is in very good agreement with the expected value for $Na_2B_{12}H_{12}$. Figure 5 shows the TGA and DSC curves for the same sample. The

total weight loss is about 2.5 % on heating from room temperature to 500 °C, including the weight loss below 110 °C due to the departure of physically absorbed water. The gradual and small weight loss after 150 °C is ascribed to the removal of the remaining traces of diglyme. This residual diglyme (~2 mol%) was also observed in the ^{1}H NMR spectrum (Figure S4). The DSC curve shows a remarkable endothermic peak at 264 °C, characteristic for the LT to HT phase transition of $Na_2B_{12}H_{12}$. The yield of desolvated $Na_2B_{12}H_{12}$ is calculated as being 85% for NaD-160-200, and 72% for NaD-120-200.

Our synthesis likely follows the equation with the following stoichiometry (eq. 3):

$$2\ NaBH_4 + 10\ (CH_3)_2S{\cdot}BH_3 \rightarrow Na_2B_{12}H_{12} + 10\ (CH_3)_2S + 13\ H_2 \quad (3)$$

This equation is consistent with the amount of formed gas measured by the pressure build up in the autoclave once it is cooled down to room temperature, see Table S2. The mechanism of the reaction most likely involves, as the first step, the formation of $B_3H_8^-$ (eq. 4):

$$BH_4^- + 2\ BH_3 \rightarrow B_3H_8^- + H_2 \quad (4)$$

This reaction pathway has previously been demonstrated for the synthesis of alkali metal octohydrotriborate salts,[30, 31] with an excess of $(CH_3)_2S{\cdot}BH_3$ being advantageous in improving the yield of $B_3H_8^-$. This first step would then be followed by the condensation of $B_3H_8^-$ with $(CH_3)_2S{\cdot}BH_3$ to form $B_{12}H_{12}^{2-}$ (eq. 5):

$$2\ B_3H_8^- + 6\ BH_3 \rightarrow \text{LT-phase } Na_2B_{12}H_{12} + 11\ H_2 \quad (5)$$

At temperatures above 120 °C, other boranes are also produced. $(CH_3)_2S{\cdot}BH_3$ is in equilibrium with B_2H_6, known to undergo pyrolysis.[31] Indeed, for NaD-120-200, the reaction is dominated by the

dehydrocondensation of BH_4^- by BH_3. An increased yield of $Na_2B_{12}H_{12}$ is observed only when the synthesis is performed at a higher temperature, namely 160 °C, leading to the decomposition of NaB_3H_8 according to eq. 2.[19] $Na_2B_{12}H_{12}$ and $NaBH_4$ are formed during the decomposition of NaB_3H_8, and the newly formed $NaBH_4$ is recycled into NaB_3H_8 by reacting with the remaining $DMS{\cdot}BH_3$, subsequently transforming into $Na_2B_{12}H_{12}$. The involved reactions can be described as follows:

$$BH_4^- + 2\ BH_3 \rightarrow B_3H_8^- + H_2 \quad (6)$$

$$5\ NaB_3H_8 \rightarrow \text{HT phase}\ Na_2B_{12}H_{12} + 3\ NaBH_4 + 8\ H_2 \quad (7)$$

3.3.3. Synthesis of $K_2B_{12}H_{12}$

Since the synthesis worked well for the sodium salt, we further optimized the procedure for obtaining $K_2B_{12}H_{12}$. Despite the solubility of KBH_4 in diglyme is low, the yield of $K_2B_{12}H_{12}$ by using our approach reached 84%, and the real yield is even higher, as $K_2B_{12}H_{12}$ is slightly soluble in diglyme not enabling full recovery of the formed product. On the other hand, K^+ has a lower charge density than Na^+ and is less frequently coordinating with diglyme in the solid state, allowing for the formation of unsolvated $K_2B_{12}H_{12}$ upon drying at only 150 °C under vacuum.[24] The synthesis of $K_2B_{12}H_{12}$ was carried out at 120 °C and 200 °C. We also used ball-milled KBH_4 as reactant, as it enables a higher contact surface with the solution during synthesis. Figure S3 shows the PXRD pattern of commercially supplied KBH_4 and ball-milled KBH_4, the peak intensities and widths are the same. The size reduction achieved by ball milling is revealed by optical microscopy (Figure S5), showing that the procedure is efficient. Ball milling is effective in reducing the size of KBH_4; the difference is not visible in PXRD patterns, as the long-range ordered of the crystal structure is not affected by ball milling.

Figure 6 shows the ^{11}B NMR spectra and ^{1}H NMR patterns of the obtained samples upon drying at 150 °C (KD-X-150), synthesized by reacting $DMS{\cdot}BH_3$ with either commercially supplied KBH_4, or ball-milled KBH_4. The yields of $K_2B_{12}H_{12}$ are summarized in Table S3 and Table S4. The NMR spectra clearly shows that non-milled KBH_4 mainly converts into $K_2B_{12}H_{12}$, although there is a small amount of KBH_4 remaining upon reaction (about 11 wt.% for reaction at 120 °C). The bm-KD-120-150 sample showed a much higher yield and purity (97%) than KD-120-150 (89%). This indicates that larger contact surface of KBH_4 particles leads to improved reactions between KBH_4 and $DMS{\cdot}BH_3$. With increasing reaction temperatures, the yields of $K_2B_{12}H_{12}$ also significantly increase, demonstrating again that temperature plays a key role in the formation of B−B bonds. The ^{1}H NMR spectrum (Figure 6b) showed a similar tendency with ^{11}B NMR spectra.

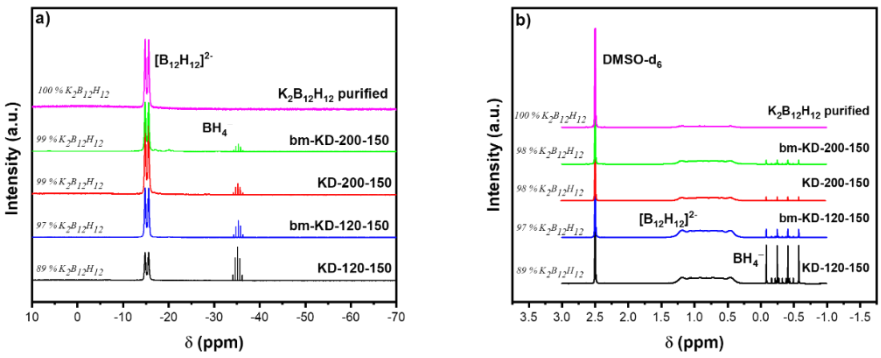

Figure 6. a) ^{11}B NMR and b) ^{1}H NMR spectra of synthesized KD-X-150 (X=120; 200) samples, purities of $K_2B_{12}H_{12}$ are calculated from ^{11}B NMR peak integration.

Figure 7 shows the PXRD patterns of the KD-X-150 (bm-KD-X-150) samples and $K_2B_{12}H_{12}$ purified by refluxing in hot water (see experimental section). The PXRD patterns clearly show the presence of $K_2B_{12}H_{12}$ (COD 1533614) and KBH_4 as the only diffracting phases in the as-synthesized samples. For the sample purified in water,

$K_{12}B_{12}H_{12}$ is the only phase present, demonstrating that this purification approach is efficient.

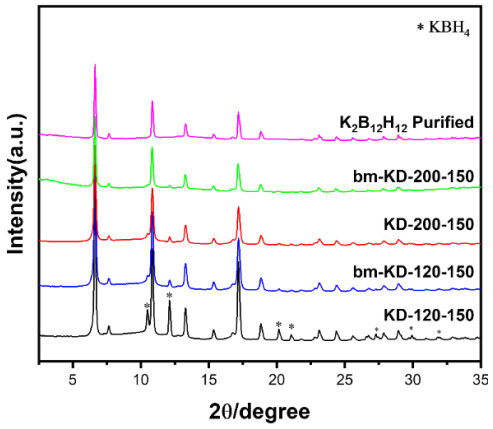

Figure 7. PXRD patterns of as-synthesized $K_2B_{12}H_{12}$ samples.

3.4. Conclusions

We demonstrated a new solvothermal synthesis method for obtaining high-purity $Na_2B_{12}H_{12}$ and $K_2B_{12}H_{12}$. This new approach is based on the reaction between the corresponding alkali borohydrides and the $DMS{\cdot}BH_3$ complex in diglyme in an autoclave. The solubility of the borohydrides increases with temperature, thus leading to a higher yield of $B_{12}H_{12}^{2-}$: the best conditions for $Na_2B_{12}H_{12}$ synthesis are at 160 °C (85% yield), and 200 °C for $K_2B_{12}H_{12}$ (84% yield), producing X-ray and ^{11}B NMR pure samples. Lower temperatures led to the incomplete conversion of $NaBH_4$ into $Na_2B_{12}H_{12}$, attributed to the formation of diglyme-soluble species such as $B_3H_8^-$, $B_9H_{14}^-$, $B_{11}H_{14}^-$, whereas higher temperatures led to the formation of various impurities, including $B_{11}H_{11}^{2-}$. Moreover, the different reaction temperatures lead to the formation of different diglyme-solvated $Na_2B_{12}H_{12}$ phases. When using temperatures higher than 160 °C, the final desolvated product contains a higher number of structural defects. The desolvation of $Na_2B_{12}H_{12}{\cdot}$diglyme is efficient in vacuum at 200 °C. Since KBH_4 is insoluble in diglyme, reducing the particle size of KBH_4 by ball-milling allows us to increase the yields of $K_2B_{12}H_{12}$. The temperature was also shown to be crucially important, similar to the synthesis of $Na_2B_{12}H_{12}$. $K_2B_{12}H_{12}$ presents some solubility in diglyme; the totality of the formed product is thus not recovered in the precipitate, but the mother liquor may be recycled for a subsequent batch to further increase the yield. The new method that we developed for the synthesis of $Na_2B_{12}H_{12}$ and $K_2B_{12}H_{12}$ presents an important improvement compared to previous strategies that are more difficult to implement and usually lead to lower yields and higher production costs.

3.5. References

(1) Li, H.-W.; Yan, Y.; Orimo, S.-i.; Züttel, A.; Jensen, C. M., Recent Progress in Metal Borohydrides for Hydrogen Storage. *Energies* **2011**, *4* (1), 185−214.

(2) Paskevicius, M.; Jepsen, L. H.; Schouwink, P.; Černý, R.; Ravnsbæk, D. B.; Filinchuk, Y.; Dornheim, M.; Besenbacher, F.; Jensen, T. R. Metal Borohydrides and Derivatives – Synthesis, Structure and Properties. *Chem. Soc. Rev.* **2017**, *46*, 1565–1634.

(3) Milanese, C.; Jensen, T. R.; Hauback, B. C.; Pistidda, C.; Dornheim, M.; Yang, H.; Lombardo, L.; Zuettel, A.; Filinchuk, Y.; Ngene, P.; de Jongh, P. E.; Buckley, C. E.; Dematteis, E. M.; Baricco, M., Complex Hydrides for Energy Storage. *Int. J. Hydrogen Energy* **2019**, *44* (15), 7860–7874.

(4) Jepsen, J.; Milanese, C.; Girella, A.; Lozano, G. A.; Pistidda, C.; Bellosta von Colbe, J. M.; Marini, A.; Klassen, T.; Dornheim, M., Compaction Pressure Influence on Material Properties and Sorption Behaviour of $LiBH_4$–MgH_2 Composite. Int. J. *Hydrogen Energy* **2013**, *38* (20), 8357–8366.

(5) Grahame, A.; Aguey-Zinsou, K.-F., Properties and Applications of Metal (M) dodecahydro-closo-dodecaborates ($Mn=_{1,2}B_{12}H_{12}$) and Their Implications for Reversible Hydrogen Storage in the Borohydrides. *Inorganics* **2018**, *6* (4).

(6) He, L.; Li, H.-W.; Nakajima, H.; Tumanov, N.; Filinchuk, Y.; Hwang, S.-J.; Sharma, M.; Hagemann, H.; Akiba, E., Synthesis of a Bimetallic Dodecaborate $LiNaB_{12}H_{12}$ with Outstanding Superionic Conductivity. *Chem. Mater.* **2015**, *27* (16), 5483–5486.

(7) Barth, R. F.; Mi, P.; Yang, W., Boron Delivery Agents for Neutron Capture Therapy of Cancer. *Cancer Commun (Lond)* **2018**, *38* (1), 35.

(8) Li, J.; Janouskova, O.; Fernandez-Alvarez, R.; Mesikova, S.; Tosner, Z.; Kereiche, S.; Uchman, M.; Matejicek, P., Designed Boron-Rich Polymeric Nanoparticles Based on Nano-ion Pairing for Boron Delivery. *Chemistry* **2020**, *26* (63), 14283–14289.

(9) Gigante, A.; Duchene, L.; Moury, R.; Pupier, M.; Remhof, A.; Hagemann, H., Direct Solution-Based Synthesis of $Na_4(B_{12}H_{12})(B_{10}H_{10})$ Solid Electrolyte. *ChemSusChem* **2019**, *12* (21), 4832–4837.

(10) Guzik, M. N.; Mohtadi, R.; Sartori, S. Lightweight Complex Metal Hydrides for Li-, Na-, and Mg-Based Batteries. *J. Mater. Res.* **2019**, *34* (6), 877–904.

(11) Brighi, M.; Murgia, F.; Černý, R. Closo-Hydroborate Sodium Salts as an Emerging Class of Room-Temperature Solid Electrolytes. *Cell Reports Phys. Sci.* **2020**, *1* (10), 100217.

(12) Yan, Y.; Remhof, A.; Rentsch, D.; Zuttel, A., The Role of $MgB_{12}H_{12}$ in the Hydrogen Desorption Process of $Mg(BH_4)_2$. *Chem. Commun. (Camb)* **2015**, *51* (4), 700–702.

(13) Moury, R.; Gigante, A.; Hagemann, H. An Alternative Approach to the Synthesis of NaB_3H_8 and $Na_2B_{12}H_{12}$ for Solid Electrolyte Applications. *Int. J. Hydrogen Energy* **2017**, *42*, 22417–22421.

(14) Katchem. http://www.katchem.cz.

(15) Boron Specialties. https://www.boron.com.

(16) Pitochelli, A. R.; Hawthorne, F. M. The Isolation of The Icosahedral $B_{12}H_{12}^{-2}$ Ion. *J. Am. Chem. Soc.* **1960**, *82*, 3228–3229.

(17) Geis, V.; Guttsche, K.; Knapp, C.; Scherer, H.; Uzun, R., Synthesis and Characterization of Synthetically Useful Salts of the Weakly-Coordinating Dianion $[B_{12}Cl_{12}]^{2-}$. *Dalton Trans.* **2009**, (15), 2687–2694.

(18) He, L.; Li, H.-W.; Tumanov, N.; Filinchuk, Y.; Akiba, E. Facile Synthesis of Anhydrous Alkaline Earth Metal Dodecaborates $MB_{12}H_{12}$ (M = Mg, Ca) from $M(BH_4)_2$. *Dalton Trans.* **2015**, *44*, 15882–15887.

(19) Pylypko, S.; Ould-Amara, S.; Zadick, A.; Petit, E.; Chatenet, M.; Cretin, M.; Demirci, U. B. The Highly Stable Aqueous Solution of Sodium Dodecahydro-Closo-Dodecaborate $Na_2B_{12}H_{12}$ as a Potential Liquid Anodic Fuel. *Appl. Catal., B* **2018**, *222*, 1–8 .

(20) Miller, H. C., Miller, N. E., & Muetterties, E. L., Synthesis of Polyhedral Boranes. *J. Am. Chem. Soc.***1963**, *85*(23), 3885–3886.

(21) Hansen, B. R. S.; Paskevicius, M.; Li, H.-W.; Akiba, E.; Jensen, T. R. Metal Boranes: Progress and Applications. *Coord. Chem. Rev.* **2016**, *323*, 60–70.

(22) He, L.; Li, H.-W.; Hwang, S.-J.; Akiba, E. Facile Solvent-Free Synthesis of Anhydrous Alkali Metal Dodecaborate $M_2B_{12}H_{12}$ (M = Li, Na, K). *J. Phys. Chem. C* **2014**, *118*, 6084–6089.

(23) Caputo, R.; Garroni, S.; Olid, D.; Teixidor, F.; Surinach, S.; Baro, M. D., Can $Na_{(2)}[B_{(12)}H_{(12)}]$ Be a Decomposition Product of $NaBH_{(4)}$? *Phys. Chem. Chem. Phys.* **2010**, *12*, 15093– 15100.

(24) Souza, D. H. P.; Moller, K. T.; Moggach, S. A.; Humphries, T. D.; D'Angelo, A. M.; Buckley, C. E.; Paskevicius, M. Hydrated Alkali-$B_{11}H_{14}$ Salts as Potential Solid-State Electrolytes. *J. Mater. Chem. A* **2021**, *9*, 15027– 15037 .

(25) Hagemann, H.; Cerny, R., Synthetic Approaches to Inorganic Borohydrides. *Dalton Trans.* **2010**, *39* (26), 6006–6012.

(26) Zhdanko, A.; Worp, B. A.; Lemaire, S., Coordination Chemistry of Borane in Solution: Application to a STING Agonist. *Eur. J. Org. Chem.* **2022**, *2022* (13).

(27) Gavrilova, L. A.; Titov L. V.; Petrovskii P. V. Synthesis of $Bu_4NB_{11}H_{14}$ by the Reaction of Tetrabutylammonium Octahydrotriborate with Diborane in Diglyme." *Russ. J. Coord. Chem.* **2004**, *30*, 307–308.

(28) Moury, R.; Gigante, A.; Hagemann, H. An Alternative Approach to the Synthesis of NaB_3H_8 and $Na_2B_{12}H_{12}$ for Solid Electrolyte Applications. *Int. J. Hydrogen Energy* **2017**, *42*, 22417– 22421.

(29) Verdal, N.; Her, J.-H.; Stavila, V.; Soloninin, A. V.; Babanova, O. A.; Skripov, A. V.; Udovic, T. J.; Rush, J. J., Complex High-Temperature Phase Transitions in $Li_2B_{12}H_{12}$ and $Na_2B_{12}H_{12}$. *J. Solid State Chem.* **2014**, *212*, 81–91.

(30) Chen, X.; Liu, X. R.; Wang, X.; Chen, X. M.; Jing, Y.; Wei, D., A Safe and Efficient Synthetic Method for Alkali Metal Octahydrotriborates, Unravelling a General Mechanism for Constructing the Delta B_3 Unit of Polyhedral Boranes. *Dalton Trans.* **2021,** *50* (39), 13676–13679.

(31) Chen, X.-M.; Ma, N.; Zhang, Q.-F.; Wang, J.; Feng, X.; Wei, C.; Wang, L.-S.; Zhang, J.; Chen, X., Elucidation of the Formation Mechanisms of the Octahydrotriborate Anion ($B_3H_8^-$) through the Nucleophilicity of the B–H Bond. *J. Am. Chem. Soc.* **2018,** *140* (21), 6718–6726.

Chapter 4. A Simple and Efficient Preparation of High-Purity and High-Yield Unsolvated Lithium Dodecaborate

Jian Wang,[a] *Timothy Steenhaut,*[a] *Koen Robeyns,*[a] *Hai-Wen Li,*[b] *Yaroslav Filinchuk*[a*]

[a] Institute of Condensed Matter and Nanosciences, Université catholique de Louvain, 1348 Louvain-la-Neuve, Belgium

[b] Hefei General Machinery Research Institute, Hefei 230031, China

* Corresponding Author. E-mail: yaroslav.filinchuk@uclouvain.be (Y. Filinchuk)

Chapter 4

Abstract

In this chapter, we present a new and simple approach for the synthesis of lithium dodecaborate ($Li_2B_{12}H_{12}$) in high purity and high yield, based on the reaction between borane dimethyl sulfide complex ($DMS{\cdot}BH_3$) and lithium borohydride ($LiBH_4$) in glymes (monoglyme or diglyme). The reaction can conveniently be performed either in a Schlenk flask with or without reflux, or in an autoclave. This strategy exhibits various advantages over existing methods, including high product purity, high reaction yields (up to 96%), and operational simplicity. The enclosed system provided by an autoclave is shown to be more favorable for the synthesis of the $B_{12}H_{12}^{2-}$ anion and enables obtaining the highest yields. The reaction mechanism has been investigated by ^{11}B NMR spectroscopy, revealing a stepwise formation of $B_2H_7^-$, $B_3H_8^-$, $B_9H_{14}^-$, $B_{11}H_{14}^-$ and $B_{11}H_{13}^{2-}$ intermediates. This synthesis method is extended to the $M_2B_{12}H_{12}$ (M = Li, Na, K) series, yielding metal dodecaboranes coordinated with glymes, characterized by single crystal X-ray diffraction. We show that glymes can be removed through simple exchange with weaker coordinating solvents like DMSO or H_2O, followed by heating under vacuum.

4.1. Introduction

Efficient synthesis of boron-hydrogen based compounds has garnered considerable interest in recent years, especially in the context of energy-related applications.[1–10] Notably, the dodecahydro-closo-dodecaborate anion, $B_{12}H_{12}^{2-}$, possesses unique bonding configurations typified by electron delocalization, remarkable chemical and thermal stabilities and salt-like behavior.[9,11] Those properties have contributed to its increasing importance in areas such as polymer chemistry,[12] cancer treatment,[13] nuclear waste extraction[14] and solid state electrolytes.[15–18]

$B_{12}H_{12}^{2-}$ features a high-symmetry structure of closed icosahedral boron cluster with terminal hydrogen atoms and was initially predicted by Longuet-Higgins and Roberts in 1955 based on calculations.[19] Its isolation by Hawthorn in 1960 initiated extensive research efforts towards its large-scale synthesis over the next decades.[20] However, up to now, the high commercial cost of metal-salt derivatives of $B_{12}H_{12}^{2-}$ remains an important constraint for its broader application.

The current synthesis pathways towards $B_{12}H_{12}^{2-}$ rely on solution-based and solvent-free techniques. The former involves the use of borane precursors, such as B_2H_6, B_5H_9 or $B_{10}H_{14}$, that are reacted with a borane triethylamine complex, leading to $[(CH_3)_3NH]_2B_{12}H_{12}$. Ion-exchange of this compound with metal hydroxides subsequently enables to obtain $Na_2B_{12}H_{12}$.[21] While this method yields high-purity metal dodecaboranes in a solvated form and has been the preferred choice in earlier studies, its main drawbacks are the complexity of operation and high cost.[9,22–24] More recent solvent-free approaches,

based on ball-milling or annealing, have gained popularity in recent years due to their ability to produce anhydrous $B_{12}H_{12}^{2-}$ salts in a single step.[4,5,25] However, these approaches lead to formation of the $B_{12}H_{12}^{2-}$ with other boron-rich compounds. Furthermore, both approaches present concerns about the yield and purity of the product, as well as regarding toxicity and reactivity of specific borane precursors, which continue to pose significant challenges.

Incremental improvements of synthetic approaches towards $B_{12}H_{12}^{2-}$ have been mainly focusing on the replacement of diborane by reducing agents presenting less handling issues.[3,26,27] As mentioned in former chapter, we represent the synthesis of unsolvated sodium and potassium dodecaborates ($Na_2B_{12}H_{12}$ and $K_2B_{12}H_{12}$) by reacting borane dimethyl sulfide complex ($DMS{\cdot}BH_3$) with the corresponding borohydride ($NaBH_4$ or KBH_4) in diglyme by heating in an autoclave. The use of diglyme was found to facilitate the removal of all intermediate products formed during the reaction, leading to high-purity $M_2B_{12}H_{12}$ (M = Na or K).[26]

The formation mechanism of $B_{12}H_{12}^{2-}$ from BH_4^- has long been discussed without a definitive conclusion to date, which is not helping in the development of more efficient synthetic strategies. Since the observation of its formation as a "boron sink" during the dehydrogenation of BH_4^-, extensive experimental and computational work has been carried out to demystify the conversion process into $B_{12}H_{12}^{2-}$.[25,28–30] These works demonstrate that BH_4^- features a wealth of pathways to higher monovalent anions such as $B_3H_8^-$, $B_9H_{14}^-$ and $B_{11}H_{14}^-$. The stepwise formation of larger polyhedral boranes from smaller boron clusters can be described as a series of reactions involving the incorporation of neutral boron hydrides, such as B_2H_6, into the BH_4^- anion. Indeed, the small charged boron species, such as

BH_4^- and $B_3H_8^-$ tend to react with strongly electrophilic neutral boron hydrides like $L{\cdot}BH_3$ (L= Lewis base), B_2H_6, B_4H_{10}, $B_{10}H_{14}$ due to their nucleophilicity.[28,31,32] However, the formation mechanism of the final dianion ($B_{12}H_{12}^{2-}$) from monovalent anions and neutral boron hydrides has not yet been experimentally understood.

In contrast to sodium and potassium dodecaborates, limited research has been conducted concerning direct synthetic approaches in solution to obtain $Li_2B_{12}H_{12}$. The latter is recently seen as a very important precursor for producing Li-ion solid-state electrolytes.[7] Due to the tendency of Li^+ towards strong coordination with ethereal solvents used for the synthesis, the production of unsolvated $Li_2B_{12}H_{12}$ is very challenging.[4,25,27,33] One alternative consists in exchanging Li^+ by large monovalent cations, such as trimethylammonium, to yield water-insoluble products, enabling the removal of diglyme (eq. 1). Anhydrous $Li_2B_{12}H_{12}$ can then be obtained through a second cation substitution in the resulting $[(CH_3)_3NH]_2B_{12}H_{12}$ using LiOH in water, which can be readily removed through heat treatment (eq. 2).[34] However, this approach proceeds in several steps and, if the amount of LiOH is not carefully controlled, may bring in impurities.

$$Li_2B_{12}H_{12}{\cdot}\ (diglyme)_n\ (sol) + 2\ (CH)_3NN{\cdot}HCl\ (sol) \xrightarrow{water} [(CH)_3NH]_2B_{12}H_{12}\ (s) + 2\ LiCl\ (sol) + n\ diglyme\ (sol) \quad (1)$$

$$[(CH)_3NH]_2B_{12}H_{12}\ (s) + 2\ LiOH(s) \xrightarrow{water} Li_2B_{12}H_{12}(sol) + 2\ (CH)_3N\ (g) + 2\ H_2O \quad (2)$$

In this contribution, we present a novel and convenient two-step synthetic approach towards anhydrous $Li_2B_{12}H_{12}$. The first step is based on reacting $LiBH_4$ with $DMS{\cdot}BH_3$ under heating in a solvent using either conventional Schlenk techniques or in an autoclave. In the second step, a solvent exchange strategy coupled with a thermal treatment is used to desolvate the product. Finally, the formation

mechanism of $B_{12}H_{12}^{2-}$ is experimentally investigated by solution-state ^{11}B nuclear magnetic resonance spectroscopy (^{11}B NMR).

4.2. Experimental Section

4.2.1. Chemicals

Lithium borohydride ($LiBH_4$, anhydrous, 95%), sodium borohydride ($NaBH_4$, anhydrous, 95%), potassium borohydride (KBH_4, anhydrous, 98%), borane dimethyl sulfide complex (~ 10−10.2 M, $(CH_3)_2S{\cdot}BH_3$, BMS, analytical), borane tetrahydrofuran complex solution ($THF{\cdot}BH_3$, 1 M in THF, <0.005 M sodium borohydride as stabilizer), diethylene glycol dimethyl ether (diglyme, $C_6H_{14}O_3$, anhydrous, 99.5%), dimethoxymethane (monoglyme, DME, $C_4H_{10}O_2$, anhydrous, 99.5%), dimethyl sulfoxide (DMSO, anhydrous, 99.9%), *N*,*N*-Diethylformamide ($C_5H_{11}NO$, DEF, 99%), Toluene (C_7H_8, 99.85%) and dichloromethane (CH_2Cl_2, 99.8%) were obtained from Sigma-Aldrich. Deuterated dimethyl sulfoxide (DMSO-d_6, 99.9 atom% D), deuterated dimethyl sulfoxide with TMS (DMSO-d_6 with TMS (0.03 vol.%), 99.8 atom% D), deuterated acetonitrile (CD_3CN-d_3, 99.8 atom% D), deuterated tetrahydrofuran, (THF-d_8, 99.5 atom% D) and deuterated dichloromethane (CD_2Cl_2, 99.8 atom% D) were obtained from Eurisotop. All the above chemicals were used without further purification.

4.2.2. Characterization

All NMR spectra were acquired on a Bruker Avance 500 spectrometer (^1H: 500.13 MHz, ^{11}B:160.46 MHz) at room temperature,

utilizing a {^{1}H, X} probehead fitted with a *z*-gradient coil. The TopSpin 1.3 software (Bruker) was employed to run the experiments. Unless state otherwise, solid samples were dissolved and filtrates diluted (0.35 ml of filtrate mixed with 0.2 ml of DMSO-d_6; the NMR samples containing filtrate were prepared under Ar protection) in deuterated DMSO (alternatively deuterated acetonitrile was used for samples in which DMSO was quantified). ^{1}H chemical shifts were calibrated using the residual peaks of the deuterated solvents (δ = 2.50 ppm for DMSO-d_6, 0 ppm for TMS, 1.94 ppm for CD_3CN-d_3). External referencing to $BF_3{\cdot}Et_2O$ (δ = 0.00 ppm) was performed for the ^{11}B NMR signals. All experiments were carried out using quartz NMR tubes with an internal diameter of 5 mm. The splitting patterns in NMR spectra are reported as follows: s = singlet; d = doublet; t = triplet; m = multiplet.

Standard and *in situ* laboratory powder X-ray diffraction experiments were performed using a MAR345 image plate detector, with Mo Kα radiation (λ = 0.71073 Å) generated by an Incoatec Microfocus Source Mo ELM47 operating at 50 kV and 1000 µA. The powdered samples were loaded inside thin-walled glass capillaries (0.7 mm diameter, Hilgenberg, GmbH) which were sealed with grease under the protective atmosphere of an argon-filled glovebox. After being removed from the glovebox, the capillaries were cut and promptly placed into molten wax on goniometric heads, followed by immediate measurements to prevent sample degradation. Samples were rotated by 180° during a 10-minute exposure. For in-situ powder X-ray diffraction, the samples underwent a 60° rotation over a 10-minute exposure period. The procedure involved heating the capillary containing the sample, utilizing a Leister LE MINI SENSOR KIT hot air blower from Leister Technologies Benelux B.V. The air blower was calibrated using a thermocouple housed in a capillary, and the

determined error in sample temperature was ± 5 °C. Data were integrated using the Fit2D software (ESRF), using LaB_6 as calibrant.

The single crystal X-Ray diffraction data were acquired on a MAR345 image plate detector using Mo Kα radiation (λ = 0.71073 Å), either at ambient temperature or after flash cooling to 150 K in a nitrogen gas stream. Data indexation, integration and reduction was done with the CrysAlis^{PRO} software, incorporating an empirical absorption correction. Structures were solved by dual space direct methods (SHELXT), followed by refinement using full-matrix least squares based on $|F^2|$ with SHELXL 2014/ 7. Non-hydrogen atoms were anisotropically refined, while hydrogen atoms were positioned at calculated positions and refined in riding mode, with temperature factors constrained to 1.2 times Ueq of the parent atoms (1.5 times Ueq for methyl and OH hydrogens. The Vesta software was used to generate figures of crystal structures.

Single scan and *in situ* synchrotron radiation powder X-ray diffraction (SR-PXRD) data were collected at the Swiss-Norwegian beamline BM1A at the European Synchrotron Radiation Facility (ESRF) in Grenoble, using a PILATUS@SNBL diffractometer at, which was equipped with a Dectris PILATUS 2M single-photon counting pixel area detector (λ = 0.77509 Å). Powder patterns were generated through the utilization of raw data processed by the SNBL Toolbox software, employing information from the LaB_6 standard.

Attenuated total reflectance Fourier transform infrared (ATR-FTIR) spectra were obtained using a Bruker Alpha II spectrometer housed in an argon-filled glovebox. The spectrometer was equipped with a Platinum ATR module (Bruker, diamond crystal, single bounce) for measurements. Each spectrum was recorded within the 370-4000 cm^{-1} range at a resolution of 4 cm^{-1}, averaged over 24 scans.

Thermogravimetric analysis/differential scanning calorimetry (TGA/DSC) was carried out using a NETZSCH STA 449 F3 Jupiter instrument equipped with a stainless steel oven housed within an argon-filled glovebox. Measurements were conducted at a heating rate of 5 K/min under a constant Ar flow (total flow of 100 mL/min), spanning a temperature range of 25 to 500 °C. Alternatively, the TGA measurement to evaluate the thermal stability of $Li_2B_{12}H_{12}$·n diglyme (S6) was conducted on a Mettler Toledo TGA/DSC 3+ system equipped with a sample robot. A nitrogen (N_2) flow rate of 100 mL/min was used for the measurement. Prior to heating, an initial isotherm at 27 °C was maintained for 15 minutes, and the sample was then heated to 500 °C at a rate of 10 K/min.

Ball-milled $LiBH_4$ ($NaBH_4$) was produced by mechanically milling 1.0 g of borohydrides at room temperature using a planetary ball mill (Fritsch Pulverisette P7). Four steel balls (10 mm in diameter) were loaded into a hardened steel vial (30 cm^3 in volume) in an argon-filled glovebox. Milling was conducted under 0.1 MPa of Ar for 2 h (2 min of milling cycles, 3 min of pausing, 24 cycles).

The detailed information about experimental setup and synthesis can be found in **Chapter II**.

4.3. Results and Discussion

4.3.1. Synthesis of $Li_2B_{12}H_{12}$ from $LiBH_4$ and $DMS{\cdot}BH_3$ in a Schlenk flask and its optimization

In the first step of our new synthetic method, $LiBH_4$ is reacted with $DMS{\cdot}BH_3$ in diglyme to produce $Li_2B_{12}H_{12}$, following eq. 3. This reaction was firstly investigated using a classical Schlenk setup at a reaction temperature of 120 °C with a molar ratio of 1: 5.5 (10 % excess of $DMS{\cdot}BH_3$) (Figure S1).

$$2MBH_4 + 10(CH_3)_2S{\cdot}BH_3 \xrightarrow{diglyme} M_2B_{12}H_{12}{\cdot}n\ \text{diglyme} + 10\ (CH_3)_2S + 13\ H_2\ (M = Li, Na, K) \quad (3)$$

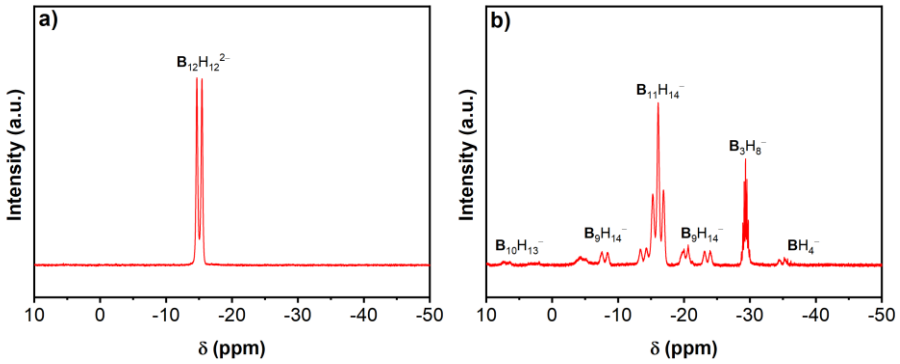

Figure 1. Proton-coupled ^{11}B NMR spectra of a) solid precipitate and b) filtrate after reaction at 120°C for 24 h in a Schlenk setup (5 mmol $LiBH_4$ + 27.5 mmol $DMS{\cdot}BH_3$ in 20 ml diglyme)

In 24 hours the yield of $B_{12}H_{12}^{2-}$ found in the solid product reaches 45 %, as shown by the sole presence of a doublet around -15.2 ppm on the proton-coupled ^{11}B solution-state NMR spectrum of the solid product dissolved in DMSO-d_6 (Figure 1a).[22,35,36] NMR analysis

of the filtrate (Figure 1b) reveals the presence of residual intermediates such as $B_3H_8^-$ and higher nuclearity boron clusters including $B_9H_{14}^-$, $B_{10}H_{13}^-$ and $B_{11}H_{14}^-$, all of which are soluble in diglyme.[1,3,37,38]

To optimize the reaction conditions, the DMS·BH_3 ratio was varied while maintaining all other reaction parameters constant (5 mmol $LiBH_4$, 20 mL of diglyme and 24 h of heating at 120 °C). Experiments were carried out with $LiBH_4$/DMS·BH_3 molar ratios of 1:2 and 1:10. The 1:2 ratio stoichiometry for the synthesis of $B_3H_8^-$ provided the yield of $Li_2B_{12}H_{12}$ around 11 %, based on the used amount of $LiBH_4$, with $B_3H_8^-$ remaining as the main boron species in the filtrate (Figure S2−3 and Table S2−3). In contrast, the 1:10 ratio resulted in the lowest yield (30%) and produced $B_{11}H_{14}^-$ as main boron species in the filtrate. Excessive concentrations of DMS·BH_3 thus lead to low yields, likely due to the formation of higher nuclearity boron clusters ($B_9H_{14}^-$, $B_{11}H_{14}^-$), which likely prevent the two reactants from interacting efficiently.[3]

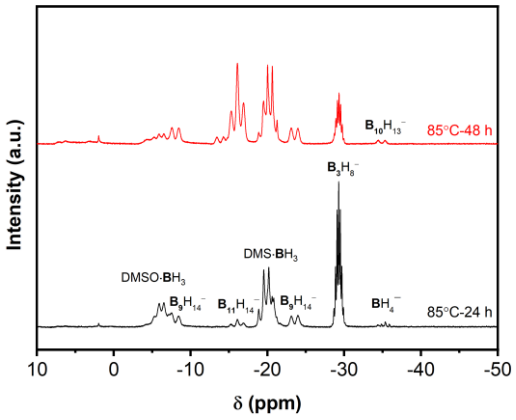

Figure 2. Proton-coupled ^{11}B NMR spectra of mixture containing $LiBH_4$ with 5 equiv (10% excess) of DMS·BH_3 after 24 h (black) and 48 h (red) of reaction at 85 °C in a Schlenk flask.

Temperature has always been regarded as being a crucial factor for the synthesis of polyhedral borates,[9] and has thus been investigated for our new approach as well. In our synthetic procedure, when a lower temperature (85 °C) was used, an incomplete conversion of BH_4^- and DMS·BH_3 into $B_3H_8^-$, $B_9H_{14}^-$, $B_{10}H_{13}^-$ and $B_{11}H_{14}^-$ occurred after 24 hours, as shown by ^{11}B NMR in Figure 2, leading to a yellow reaction solution without a precipitate. By prolonging the reaction to 48 hours, a very small amount of precipitate appeared, and the ^{11}B NMR spectrum of the reaction mixture (Figure 2) indicates weak signals of $B_{12}H_{12}^{2-}$ and nearly complete depletion of $LiBH_4$. Applying a higher reaction temperature (160 °C), without condenser, led directly to the formation of a complicated borate anion (Figure S4). We speculate that the formation of complicated borate anion might be due to the reaction between $B_{11}H_{14}^-$ and the dehydrogenated $B_{12}H_{12-x}^{2-}$ anion. The dehydrogenation occurring in the icosahedral $B_{12}H_{12}^{2-}$ results in a change in charge, no longer identical, and symmetry of the twelve BH vertices. This leads to the formation of a disubstituted anion when reacted with electrophilic compounds.[39]

Performing the same experiment at 160 °C but using a setup equipped with a condenser resulted in the formation of $B_{12}H_{12}^{2-}$, along with some $B_{10}H_{10}^{2-}$ and partially dehydrogenated $B_{12}H_{12-x}^{2-}$ anion (Figure S4).[40] The use of a condenser also increases the yield when performing the reaction at 120 °C, as indicated in Table S4. Additionally, the presence of $B_{11}H_{14}^-$ as the main boron species in the filtrate (Figure S5) indicates that refluxing promotes the conversion of lower boranes to $B_{12}H_{12}^{2-}$.

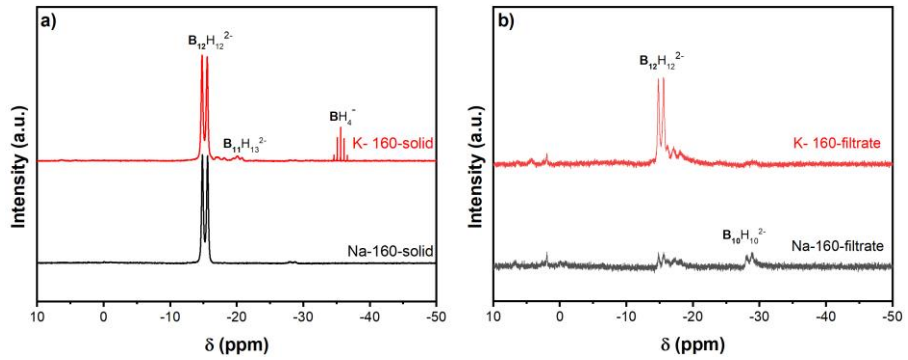

Figure 3. Proton-coupled ^{11}B NMR spectra of a) solid precipitates and b) filtrates obtained upon reaction of 5 mmol $NaBH_4$ (black) and KBH_4 (red) with 5 equiv (10% excess) of $DMS{\cdot}BH_3$ for 24 hours at 160 °C in a Schlenk setup in refluxing diglyme.

Similar reactions at 160 °C in Schlenk flasks (Figure 3 and Table S4) equipped with a condenser, where $LiBH_4$ was substituted by $NaBH_4$ and KBH_4, produced $Na_2B_{12}H_{12}$ and $K_2B_{12}H_{12}$ in isolated yields of 92% and 88%, respectively. In this case, higher temperature favors the formation of $B_{12}H_{12}^{2-}$, which is in line with previous research showing that the thermal decomposition of BH_4^- and $B_3H_8^-$ salts can lead to the formation of closo-boranes such as $B_{10}H_{10}^{2-}$ and $B_{12}H_{12}^{2-}$.[33,41–44] Furthermore, on the contrary to diglyme solvated $Li_2B_{12}H_{12}$, the solvates of $Na_2B_{12}H_{12}$ and $K_2B_{12}H_{12}$ are much more stable at this temperature.[26] The small amounts of $B_{10}H_{10}^{2-}$ impurities in $Na_2B_{12}H_{12}$ and $K_2B_{12}H_{12}$ obtained by this procedure can be completely removed by washing with diglyme. These results indicate that using a Schlenk setup equipped with a condenser is a proper choice for the synthesis of $Na_2B_{12}H_{12}$ and $K_2B_{12}H_{12}$ but is not ideal for obtaining $Li_2B_{12}H_{12}$ in high yield.

4.3.2. Synthesis of $Li_2B_{12}H_{12}$ from $LiBH_4$ and $DMS{\cdot}BH_3$ in an autoclave

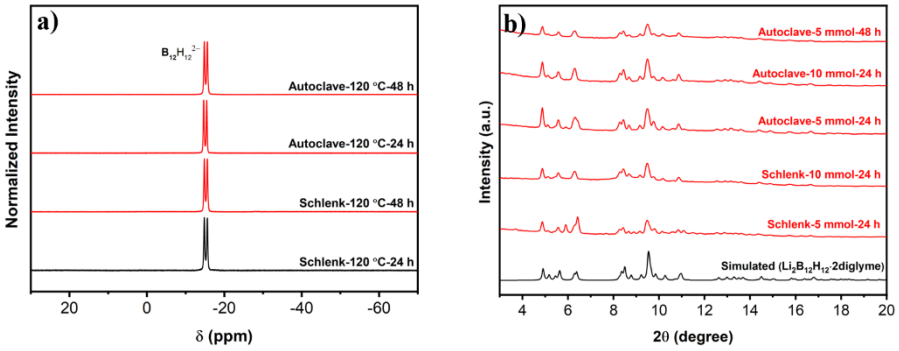

Figure 4. a) Proton-coupled ^{11}B NMR spectra of solid precipates obtained from the reaction of $LiBH_4$ with 5 equiv. (10% excess) of $DMS{\cdot}BH_3$ at 120 °C during 24 or 48 h in a Schlenk setup or in an autoclave; b) PXRD patterns of selected as-synthesized $Li_2B_{12}H_{12}{\cdot}$n diglyme samples (λ = 0.71073 Å).

Further optimization of the synthesis conditions was performed by varying reactants concentrations and reaction times. Additionally, the reactions were performed either in a Schlenk setup without condenser or in an autoclave, as the use of the latter enables keeping all generated gaseous species, such as B_2H_6 and DMS, confined in the volume. Indeed, we speculate that B_2H_6 could highly accelerate the hydroboration reaction from BH_4^- to $B_{11}H_{14}^-$, thus improving the yields of $B_{12}H_{12}^{2-}$.[22,37] Detailed reaction conditions are summarized in Tables S3−7 and Figures 4 and Figure S6−7. To prevent the loss of the volatile during the argon flush of the autoclave system, an excess amount of 10 % $DMS{\cdot}BH_3$ was used. As a general trend, the yields of $Li_2B_{12}H_{12}$ obtained in the autoclave were much higher than in the Schlenk setup. In addition, longer reaction times allowed complete

conversion of the reactants, resulting in higher yields. Remarkably, an isolated 96% yield of pure $Li_2B_{12}H_{12}$ was achieved in the autoclave, representing the highest yield achieved thus far in the preparation of metal dodecaborates, to the best of our knowledge. When the concentration of reactants in the autoclave was increased, a decrease in yield was observed. This contrasts with the reactions in the Schlenk setup, for which increasing reactant concentrations or reaction times did not have significant impact on the final yield of $B_{12}H_{12}^{2-}$.

Signals of $B_{10}H_{13}^-$ were not observed in the ^{11}B NMR spectra (Figure S8) of filtrates resulting from autoclave experiments. The autoclave keeps all gaseous species confined under high pressure inside the reactor system, and the B_2H_6 dimer can thus be retained in the reaction mixture. We speculate that the pyrolysis of B_2H_6 directly leads to the formation of higher boranes, such as B_4H_{10} or B_6H_{10}, resulting in an increased content of $B_{11}H_{14}^-$ in the solution and a slow reaction between $B_3H_8^-$ and $B_{11}H_{14}^-$.[45,46] Remaining $DMS{\cdot}BH_3$ can be observed in NMR spectra of products obtained in the autoclave system but not on those resulting from reactions performed in a Schlenk flask.

The synthesis of $Li_2B_{12}H_{12}$ in an autoclave can also be carried out using a lighter ether, such as monoglyme (b. p. of 85 °C), as solvent. Figure 5 shows the ^{11}B NMR spectrum of the solid precipitate and the filtrate obtained upon reaction of 10 mmol $LiBH_4$ with 55 mmol $DMS{\cdot}BH_3$ in 20 ml monoglyme. The ^{11}B NMR spectra (Figure 5a and Figure S9) demonstrate that under those conditions pure monoglyme solvated $Li_2B_{12}H_{12}$ is obtained, with an isolated yield of 42%. However, a considerable amount of $Li_2B_{12}H_{12}$ remains as small particles in the filtrate (Figure 5b), which makes full recovery of the formed product difficult. Cooling the reaction solution in the fridge at 10 °C overnight before filtration allows addressing this issue, by

increasing the crystallite size. By doing so and washing the product with cold monoglyme (10 °C), a monoglyme-rich solvated $Li_2B_{12}H_{12}$ was obtained with an isolated yield of 89%.

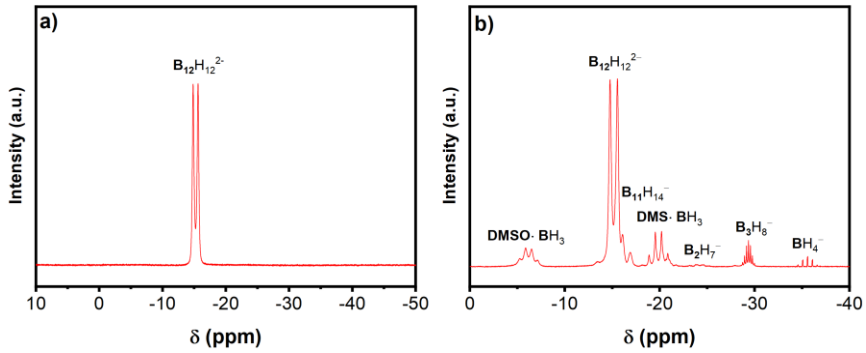

Figure 5. Proton-coupled ^{11}B NMR spectra of a) solid precipitate and b) filtrate (10 mmol $LiBH_4$, autoclave, 24 h). The particles of $Li_2B_{12}H_{12}$ that remained suspended in the filtrate were fully dissolved by addition of DMSO-d_6 prior to analysis.

4.3.3. Thermal behavior and desolvation of as synthesized $M_2B_{12}H_{12}$

After initial drying, the crude products contained a variable amount of diglyme molecules per formula unit, as evidenced by NMR spectroscopy (see above). Attempts to remove coordinated solvent from $Li_2B_{12}H_{12}$·n diglyme by thermal treatment were unsuccessful. Thermogravimetric analysis (TGA) was performed to investigate the thermal stability and composition of $Li_2B_{12}H_{12}$·n diglyme (Figure 6). The thermal decomposition occurs in three steps: removal of free diglyme starts at 25 °C (9.5 wt.%), followed by a larger mass loss of 15.5 wt.% starting around 150 °C and a third mass loss of 5 wt.% between 200 °C and 300 °C, the two latter steps corresponding to removal of coordinated diglyme.

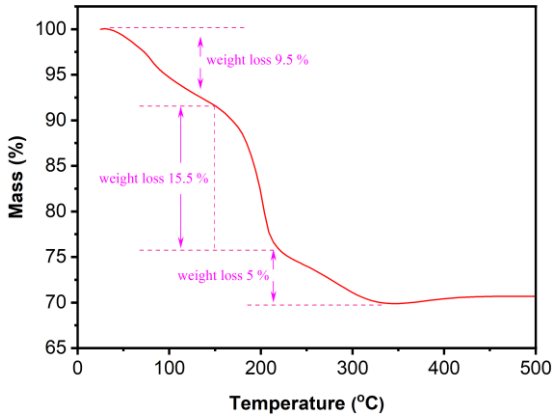

Figure 6. TGA analysis of as-synthesized $Li_2B_{12}H_{12}$.n diglyme.

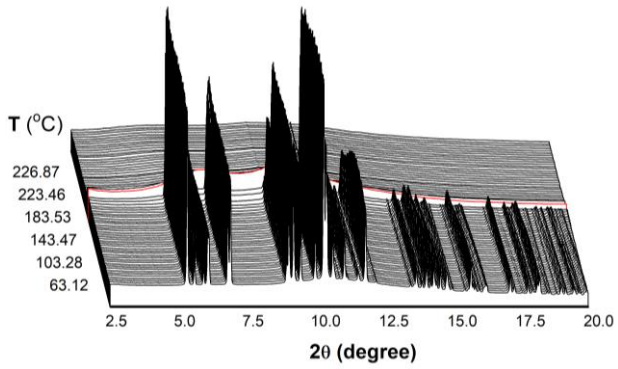

Figure 7. In-situ synchrotron radiation powder X-ray diffraction data of $Li_2B_{12}H_{12}$·2 diglyme. Heating rate = 10 °C/min (λ = 0.77509 Å).

An *in situ* synchrotron radiation powder X-ray diffraction (SR-PXD) experiment was performed to further investigate the behavior of $Li_2B_{12}H_{12}$·n diglyme during thermal treatment (Figure 7). The only crystalline phase observed on the diffraction patterns corresponds to $Li_2B_{12}H_{12}$·2 diglyme, which is thermally stable until 179 °C and then decomposes into an amorphous phase.

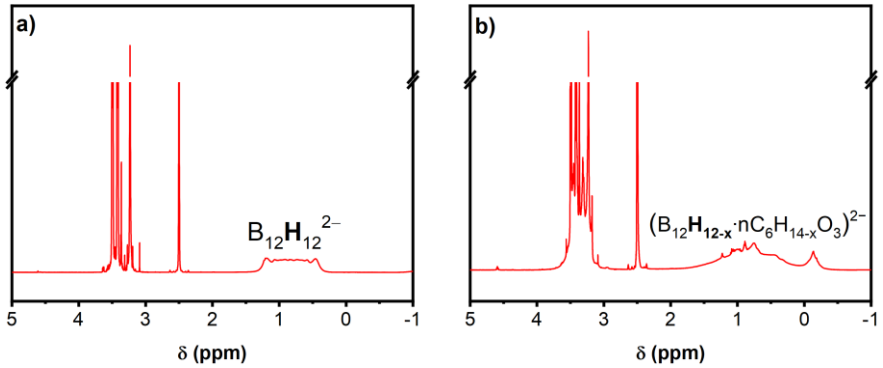

Figure 8. ^{1}H NMR spectra of diglyme solvated $Li_2B_{12}H_{12}$ a) before and b) after heat treatment at 170 °C under vacuum. The characteristic multiplet of $B_{12}H_{12}^{2-}$ (1.6 – 0 ppm) disappears upon thermal treatment.

The loss of hydrogen from the boron cages was evidenced by ^{1}H NMR (Figure 8) and ^{11}B NMR (Figure S10-11), as the characteristic asymmetric multiplet of $B_{12}H_{12}^{2-}$ (1.6–0 ppm) disappears after thermal treatment at 170 °C under vacuum for 12 h, indicating competition between desolvation and dehydrogenation.[47] This suggests that direct removal of diglyme by thermal treatment is not possible.

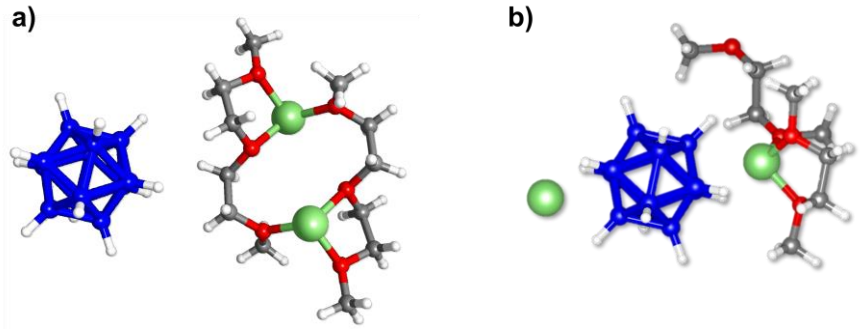

Figure 9. Fragments of the crystal structures of a) $Li_2B_{12}H_{12}{\cdot}2$ diglyme and b) $Li_2B_{12}H_{12}{\cdot}1.5$ monoglyme, illustrating the coordination modes of the glymes to Li^{+}. Color code: **Li**, green; **B**, dark blue; **H**, light grey; **O**, red; **C**: dark grey.

The structure of $Li_2B_{12}H_{12}{\cdot}2$ diglyme was resolved by single

crystal X-ray diffraction (SC-XRD, see Figure 9 and SI). In this solvate, two Li ions are threefold coordinated with three O atoms from two diglyme molecules, evidencing strong interaction with the solvent molecules. It is noteworthy that when reaching the decomposition temperature, the solid sample starts melting and bubbling.

Single crystals of diglyme solvated $Na_2B_{12}H_{12}$ and $K_2B_{12}H_{12}$ were isolated from the reaction mixtures upon synthesis as well, and their structures determined by SC-XRD as being $Na_2B_{12}H_{12}$·4 diglyme and $K_2B_{12}H_{12}$·4 diglyme (Figure 10). Unlike Li^+, Na^+ and K^+ possess a lower charge density and larger cation size, resulting in a higher cation-to-anion size ratio.[48] This leads to a different coordination environment for Na^+ and K^+, with $M^+\cdots O$ bonds ($Na^+\cdots O$ = 2.378−2.446 Å, $K^+\cdots O$ = 2.728−2.844 Å) longer than $Li^+\cdots O$ = 1.958−2.039 Å, meaning that less energy will be needed to break these coordination bonds. This explains why direct heat treatment of diglyme solvated $Na_2B_{12}H_{12}$ (150 °C) and $K_2B_{12}H_{12}$ (200 °C) under vacuum was effective for direct removal of diglyme in our previous work, while it is ineffective for the Li^+ derivative.[26]

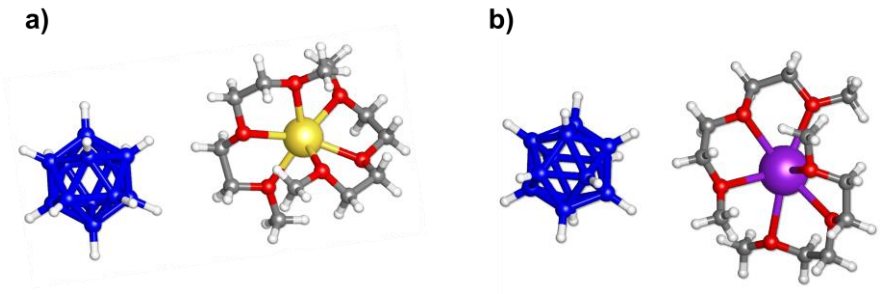

Figure 10. Fragments of the single crystal structures of a) $Na_2B_{12}H_{12}$· 4 diglyme (RT) and b) $K_2B_{12}H_{12}$·4 diglyme, illustrating the coordination modes of the glymes to the alkali metal cations. Color code: **Na**, Yellow; **K**, purple; **B**, dark blue; **H**, light grey; **O**, red; **C**: dark grey.

Interestingly, by drying crystals of the diglyme solvated $Na_2B_{12}H_{12}$ at 80 °C for 2 h, a single crystal to single crystal transformation occurred, leading to a high temperature (HT) diglyme solvated form of $Na_2B_{12}H_{12}$ (Figure 11).

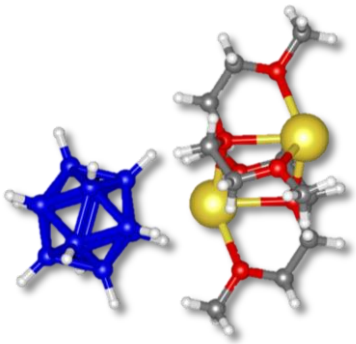

Figure 11. Fragment of the single crystal structure of the HT form of $Na_2B_{12}H_{12}$·2 diglyme, illustrating the coordination mode of diglyme to Na^+. Color code: **Na**, Yellow; **B**, dark blue; **H**, light grey; **O**, red; **C**: dark grey.

Initial washing and drying at room temperature resulted in the reduction partial desolvation from $Na_2B_{12}H_{12}$·4 diglyme to $Na_2B_{12}H_{12}$·7/2 diglyme. TGA/DSC analyses data in Figure 12 revealed that the loss of diglyme from $Na_2B_{12}H_{12}$·7/2 diglyme occurs in three distinct steps: the first one resulted in the formation of $Na_2B_{12}H_{12}$·5/3 diglyme, in the second step, about 2/3 molecules of diglyme are removed, resulting in $Na_2B_{12}H_{12}$·diglyme, and in the final stage, all diglyme molecules are removed, leading to anhydrous $Na_2B_{12}H_{12}$. Those three solvent removal steps are accompanied by intense endothermic peaks on the DSC curve at around 86 °C, 151 °C and 206 °C, respectively. These results indicate that diglyme solvated metal dodecaborates are metastable compounds which lose diglyme molecules in a stepwise manner upon heating. The decomposition of the HT form of $Na_2B_{12}H_{12}$·2 diglyme leads directly to the disordered

HT phase of $Na_2B_{12}H_{12}$, as indicated in chapter 3 and Figures 12−16.

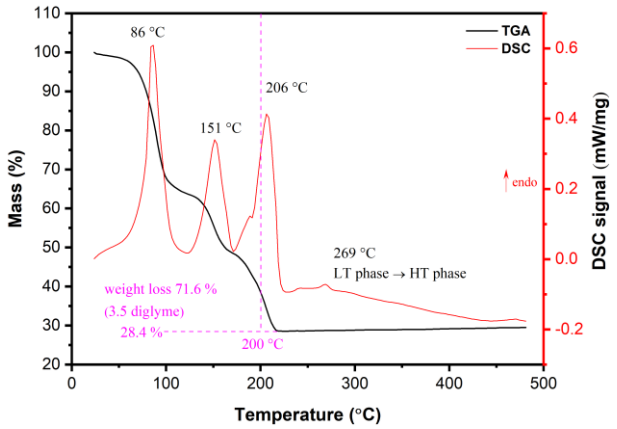

Figure 12. TGA-DSC analysis of as-synthesized $Na_2B_{12}H_{12}$.n diglyme, after initial drying under vacuum at room temperature.

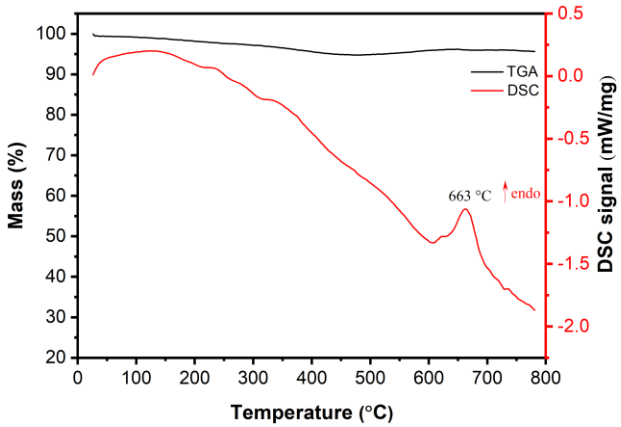

Figure 13. TGA-DSC analysis of purified $K_2B_{12}H_{12}$ after initial drying at 150 °C.

The TGA-DSC analysis of $K_2B_{12}H_{12}$ in Figure 13 reveals an evident endothermic peak at 663 °C, typical of the decomposition of $K_2B_{12}H_{12}$ and the polymerization of $K_2B_{12}H_{12}$ to $(K_2B_{12}H_n)_m$. However, it is worth noting that a phase transition of $K_2B_{12}H_{12}$ is

expected to occur at a lower temperature based on a previous report. $K_2B_{12}K_{12}$ can be purified according to a procedure reported in our earlier work, consisting in removing $B_{11}H_{13}^{2-}$ and BH_4^- through treatment with hot water. This leads to a solid residue containing $B_{12}H_{12}^{2-}$ and $B_{12}H_{12-x}^{2-}$ (closomers), which can be separated by extraction with a less polar solvent like alcohol for instance. To minimize the formation of $B_{12}H_{12-x}^{2-}$ during the synthesis of $K_2B_{12}H_{12}$, milling of KBH_4 to smaller-sized crystallites prior to use for synthesis has been proven to be advantageous. It should be noted that when KBH_4 is used for the synthesis of higher boranes, traces of KBH_4 may still be detected in the final products, due to its low solubility in most ethereal solvents.

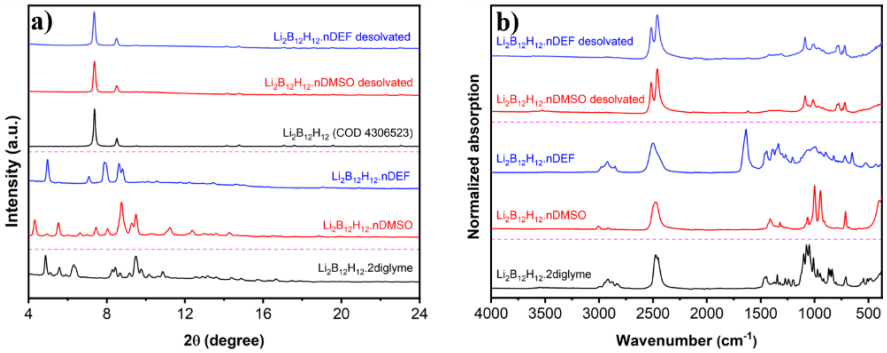

Figure 14. a) PXRD patterns of $Li_2B_{12}H_{12}$·n diglyme, and DMSO- and DEF-substituted samples before and after drying at 200 °C under vacuum, together with simulated pattern of $Li_2B_{12}H_{12}$. b) FTIR spectra of $Li_2B_{12}H_{12}$·n diglyme, and DMSO- and DEF-substituted samples before and after drying at 200 °C under vacuum.

We investigated a new method to obtain anhydrous $Li_2B_{12}H_{12}$ from the glymes solvates, eliminating the need for the inconvenient previously utilized ion exchange strategy, by using dimethyl sulfoxide

(DMSO) or *N*, *N*-Diethylformamide (DEF) as solvent exchange agents. This approach is aimed to overcome the strong chelation of diglyme with dodecaborate salts containing small cations such as Li^+ and Na^+. The methodology consisted of adding 10 ml of DMSO or DEF to 1 g of the diglyme solvated product and drying the solution under vacuum at 100 °C for 12 h. Upon this treatment, the formation of completely exchanged DMSO or DEF solvated $Li_2B_{12}H_{12}$ is achieved, as demonstrated by PXRD and FTIR analyses in Figure 14.

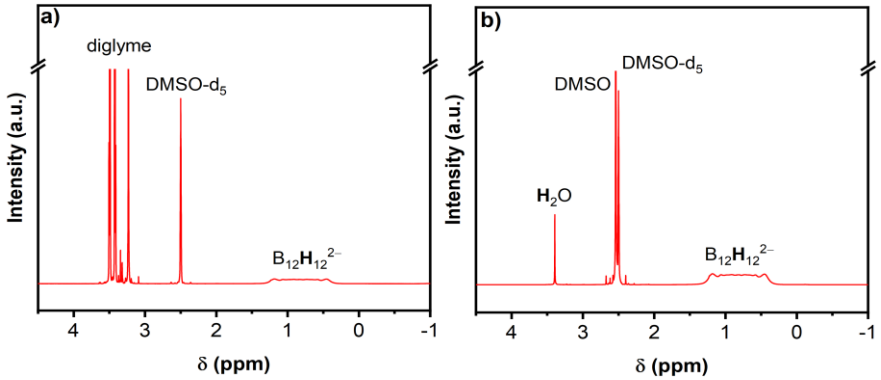

Figure 15. ^{1}H NMR spectra of a) $Li_2B_{12}H_{12}$·n diglyme and b) $Li_2B_{12}H_{12}$· n DMSO.

Figure 15 shows the ^{1}H NMR analysis of $Li_2B_{12}H_{12}$·n DMSO before and after desolvation indicates that DMSO completely substitutes diglyme. Additionally, DMSO can be removed from the solvate by thermal treatment without decomposition of the $B_{12}H_{12}^{2-}$ anion. This suggests that DMSO can be used as an effective solvent for the removal of diglyme in $Li_2B_{12}H_{12}$. Subsequently, drying the solvent-exchanged products at 200 °C under vacuum resulted in the formation of unsolvated $Li_2B_{12}H_{12}$, as shown by (*in situ*) PXRD and NMR (Figures S17−21). The choice of DMSO and DEF for the solvent exchange is justified by their higher boiling points and weaker

coordinating strength compared to diglyme.[49] Although both solvents can effectively substitute diglyme, DMSO is the more economically viable option given the much higher price of DEF.

It is worth noting that lighter solvents were investigated for the removal of diglyme. CH_2Cl_2 was able to lower the amount of free diglyme in the final product and to facilitate the recrystallization of $Li_2B_{12}H_{12}$.2 diglyme, but it also resulted in sample loss. Toluene was only able to partially lower the amount of free diglyme. The use of H_2O was not as effective to remove diglyme. Although H_2O has a higher polarity than diglyme and is able to lower the amount of coordinated diglyme, its lower boiling point and vapor pressure made it difficult to remove the latter completely from the product. The use of H_2O combined with rotary evaporation is more effective in lowering the amount of diglyme, although it requires a much longer duration for complete solvent removal. Organic solvents, such as ethyl acetate or Et_2O, can be used to extract the diglyme from the aqueous solution of diglyme solvated $Li_2B_{12}H_{12}$ before evaporation, but such a process requires more steps and does not enable to remove the totality of the diglyme. A system enabling to achieve higher vacuum for solvent removal by using a turbomolecular pump was also investigated for the desolvation of $Li_2B_{12}H_{12}$·n diglyme but was ineffective.

As a general trend, the diglyme-solvated form of $Li_2B_{12}H_{12}$ exhibits relatively low solubility in lighter ethers such as Et_2O, THF, and DME, making it challenging to use those solvents for diglyme substitution. The choice of solvent for the removal of coordinated solvent from diglyme solvated $Li_2B_{12}H_{12}$ must thus be carefully considered to ensure maximum efficiency.

When monoglyme is used for the synthesis, the crystalline phase

of the obtained solvate corresponds to $Li_2B_{12}H_{12}$·1.5 monoglyme, as evidenced by its structure determined by SC-XRD (see Figure 9b and SI). In this structure, monoglyme shows a similar coordinating ability to Li^+ as diglyme in solvated $Li_2B_{12}H_{12}$, and thus poses similar challenges for desolvation.

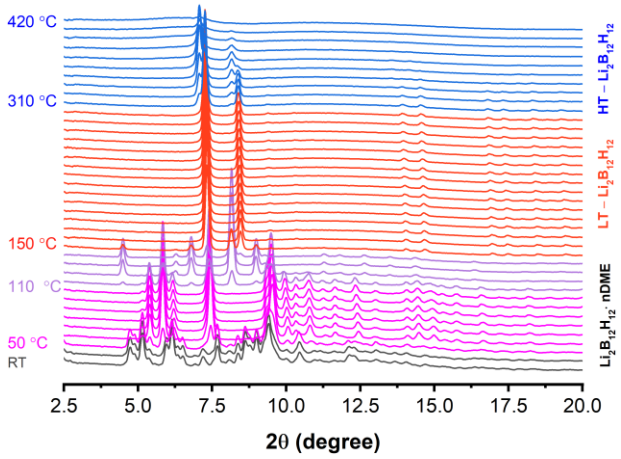

Figure 16. In situ powder X-ray diffraction data of a monoglyme-rich $Li_2B_{12}H_{12}$·n DME sample (λ = 0.71073 Å).

However, compared to diglyme solvated $Li_2B_{12}H_{12}$, in situ PXRD data (Figure 16) reveals that monoglyme solvated $Li_2B_{12}H_{12}$ exhibits different phase changes during thermal desolvation before leading to $Li_2B_{12}H_{12}$. Diffraction peaks of monoglyme solvated $Li_2B_{12}H_{12}$ disappear at around 150 °C, while $Li_2B_{12}H_{12}$ is formed at this temperature. At 310 °C, the phase transition from the α-$Li_2B_{12}H_{12}$ to the β-$Li_2B_{12}H_{12}$ polymorph is observed, and decomposition to a hydrogen poor γ-$Li_2B_{12}H_{12-x}$ phase occurs at higher temperatures.[50,51] This last phase transition occurs about 50 °C below the previously reported temperature, likely due to the experiment being performed under vacuum. An attempt to directly remove monoglyme from solvated $Li_2B_{12}H_{12}$ by heating at 180 °C under vacuum for 12 h resulted in a small amount of $Li_2B_{12}H_{12-x}$·n monoglyme, as observed

in the ^{11}B NMR spectrum (Figure S22).

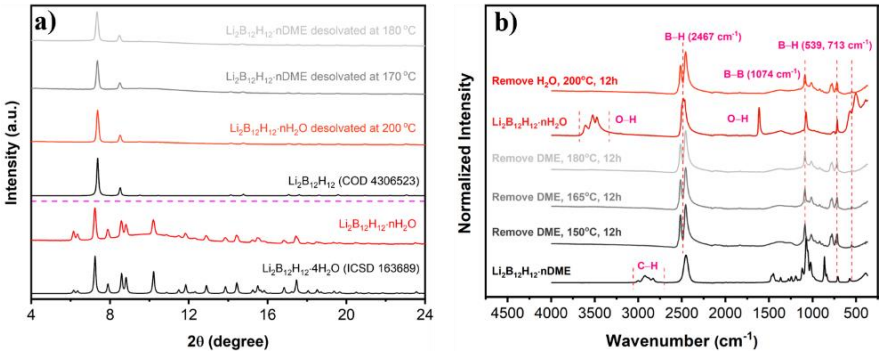

Figure 17. a) Experimental PXRD patterns of $Li_2B_{12}H_{12}$·n DME, $Li_2B_{12}H_{12}$·n H_2O and unsolvated $Li_2B_{12}H_{12}$ obtained after heat treatment, along with simulated patterns of anhydrous and tetrahydrated $Li_2B_{12}H_{12}$ (λ = 0.71073 Å). b) FTIR spectra of $Li_2B_{12}H_{12}$·n DME, $Li_2B_{12}H_{12}$·n H_2O and unsolvated $Li_2B_{12}H_{12}$ obtained after various heat treatments.

Residual DME present in the samples obtained after heat treatment of $Li_2B_{12}H_{12}$·n DME can be observed on the FTIR spectra. Complete removal of DME at high temperature (180 °C) is accompanied by the formation of partially dehydrogenated $B_{12}H_{12-x}^{2-}$, as shown in Figure S22. The ^1H NMR spectrum (Figure S23−24) indicates that DME can be completely removed by treating the sample with H_2O, and H_2O can subsequently easily be removed by thermal treatment. By combining the results of PXRD and FTIR (Figure 17) and ^1H NMR (Figure S25) analyses of desolvated $Li_2B_{12}H_{12}$·n H_2O, it can be concluded that $Li_2B_{12}H_{12}$ is completely anhydrous after the thermal treatment, as the vibration bonds for H_2O disappear from the FTIR spectrum.

Although complete removal of monoglyme from $Li_2B_{12}H_{12}$ through direct heating is difficult, our above proposed solvent

exchange strategy can in this case be carried out even lighter, more abundant and greener solvents, such as H_2O, as compared to DMSO and DEF for the diglyme solvated dodecaborate. Indeed, upon exchange with water and applying vacuum at 40°C, monoglyme can be completely removed, as shown by ^1H NMR, PXRD and FTIR analyses, and pure hydrated $Li_2B_{12}H_{12}$ can be obtained. Water can then be easily removed from the hydrated $Li_2B_{12}H_{12}$ without damaging the $B_{12}H_{12}^{2-}$ clusters. It is worth noting that $Li_2B_{12}H_{12}$ is commercially available in its hydrated form, which can be simply obtained by our solvent exchange strategy, without the last heating step.

4.3.4. Synthesis in Toluene

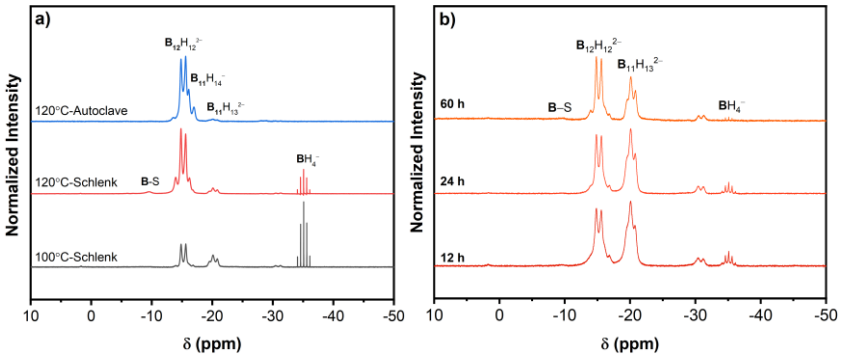

Figure 18. Proton coupled ^{11}B NMR spectra of (a) solid compounds obtained from 5 mmol $LiBH_4$ + 27.5 mmol $DMS{\cdot}BH_3$ in 20 ml toluene at 100 °C and 120 °C for 24 h, in a Schlenk flask or autoclave and (b) of 5 mmol ball milled $LiBH_4$ with 27.5 mmol of $DMS{\cdot}BH_3$ after various reaction times at 120 °C in a Schlenk flask.

The reactions were also attempted in toluene, a non-coordinating solvent, with the aim of obtaining directly unsolvated $Li_2B_{12}H_{12}$.[4,5,25] The NMR spectra (Figure 18 and Figures S26−27) of the solid sample obtained from reaction in a Schlenk setup shows the presence of the desired $B_{12}H_{12}^{2-}$ along with BH_4^-, $B_{11}H_{14}^-$, and $B_{11}H_{13}^{2-}$ and in the

final solid. The formation of $B_{12}H_{11}S(CH_3)^{2-}$ can be attributed to the self-condensation of $DMS{\cdot}BH_3$.[52]

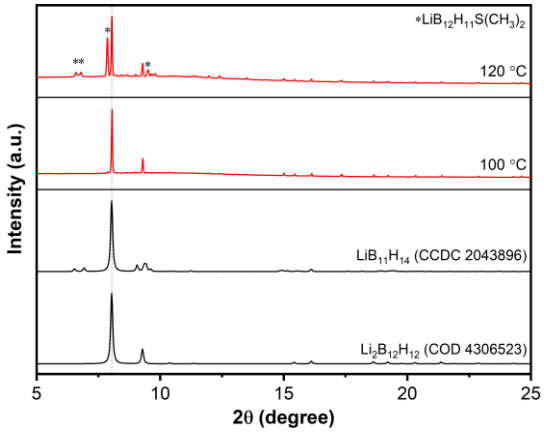

Figure 19. Synchrotron radiation powder X-ray diffraction (SR-PXRD) patterns of solid samples obtained by reaction of 5 mmol ball milled $LiBH_4$ with 27.5 mmol (10% excess) of $DMS{\cdot}BH_3$ in 20 ml toluene for 24 h at 100 °C or 120 °C

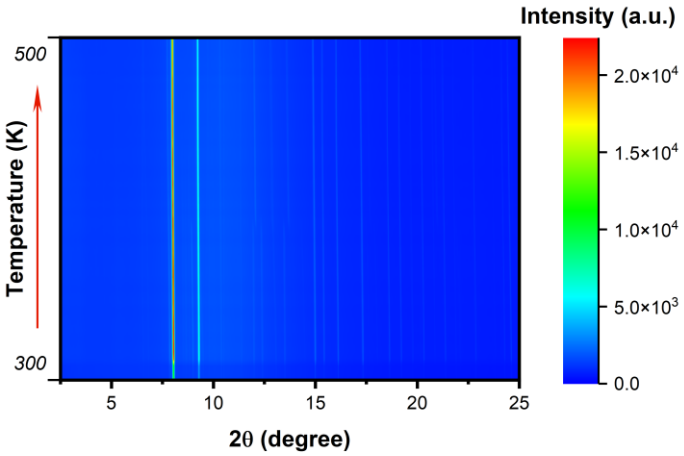

Figure 20. *In situ* SR-PXRD data of solid samples obtained by reaction of 5 mmol ball milled $LiBH_4$ with 27.5 mmol (10% excess) of $DMS{\cdot}BH_3$ in 20 ml toluene for 24 h at 100 °C. Heating rate = 10 °C/min.

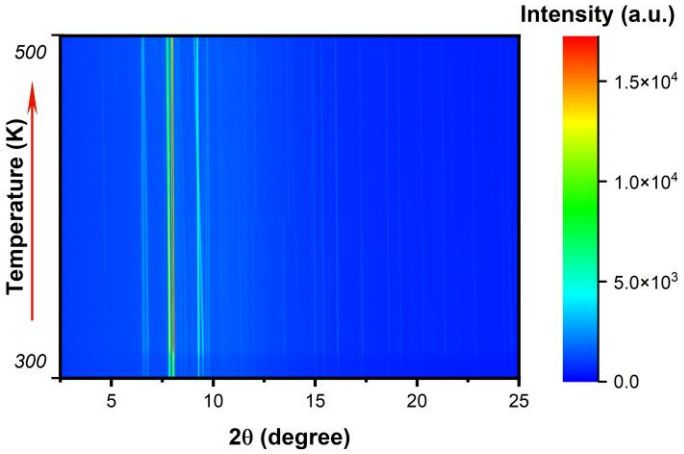

Figure 21. *In situ* SR-PXRD data of solid samples obtained by reaction of 5 mmol ball milled $LiBH_4$ with 27.5 mmol (10% excess) of $DMS{\cdot}BH_3$ in 20 ml toluene for 24 h at 120 °C. Heating rate = 10 °C/min.

The diffraction patterns (Figures 19−21) of the sample obtained by running the reaction at 100 °C however indicates the presence of $Li_2B_{12}H_{12}$ as only crystalline phase. A higher temperature of 120 °C leads to a solid showing diffraction peaks of impurity phases along the desired phase. In contrast, experiments performed in an autoclave enabled the complete conversion of BH_4^- into $B_{11}H_{14}^-$, $B_{11}H_{13}^{2-}$ and $B_{12}H_{12}^{2-}$.

We also ball milled $LiBH_4$ prior to the synthesis in toluene in the Schlenk setup to further improve the synthesis, as this reactant exhibits insolubility in this solvent. ^{11}B NMR spectra (Figure 18b and Figures S28−31) shows that this led to the presence of only BH_4^- and $B_{11}H_{13}^{2-}$ along with $B_{12}H_{12}^{2-}$ in the final solid. A considerable amount of $B_{11}H_{13}^{2-}$ is obtained after 24 hours and a longer reaction time is required for its conversion into $B_{12}H_{12}^{2-}$. As we observed that $B_{11}H_{13}^{2-}$ is insoluble in THF-d_8 (Figure S32), its isolation was attempted by washing the synthesized sample with excess THF (Figure S33).

However, we did not succeed in purifying the desired product, as $B_{12}H_{12}^{2-}$ and BH_4^- were still present after this washing procedure, completely isolating unsolvated $B_{11}H_{13}^{2-}$ without other boron-hydrogen compounds is challenging. It is noteworthy that similar reactions performed with ball milled $NaBH_4$ instead of $LiBH_4$ resulted in the formation of $NaB_{12}H_{11}S(CH_3)_2$ as the main product, as shown in Figure 22 and Figure S34.

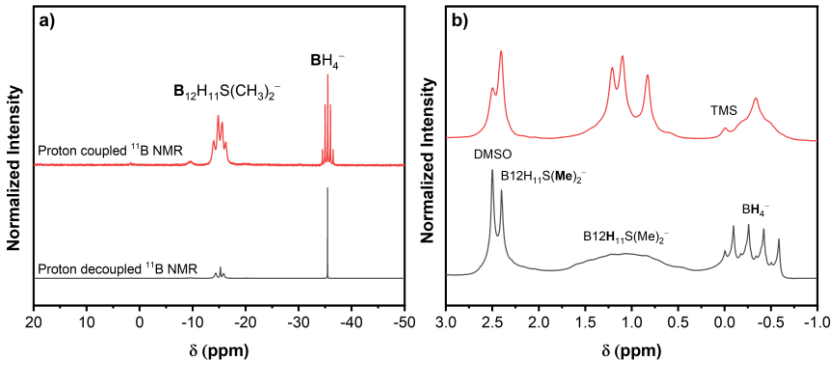

Figure 22. (a) Proton-coupled and decoupled ^{11}B NMR and (b) ^{1}H and $^{1}H\{^{11}B\}$ NMR spectra of solid samples obtained by reaction of 5 mmol ball milled $NaBH_4$ with 27.5 mmol (10% excess) of $DMS{\cdot}BH_3$ in 20 ml toluene for 24 h at 120 °C in a Schlenk flask.

4.3.5. Elucidation of the formation mechanism of $B_{12}H_{12}^{2-}$

To gain insight into the formation mechanism of $B_{12}H_{12}^{2-}$, ^{11}B NMR was employed to monitor the composition of the reaction mixture over the course of the synthesis. Figure 23 shows the ^{11}B NMR spectra of aliquots of a mixture of $LiBH_4$ and $DMS{\cdot}BH_3$ in diglyme collected before heating (0 h) and at different reaction times during solvothermal reaction at 120 °C.

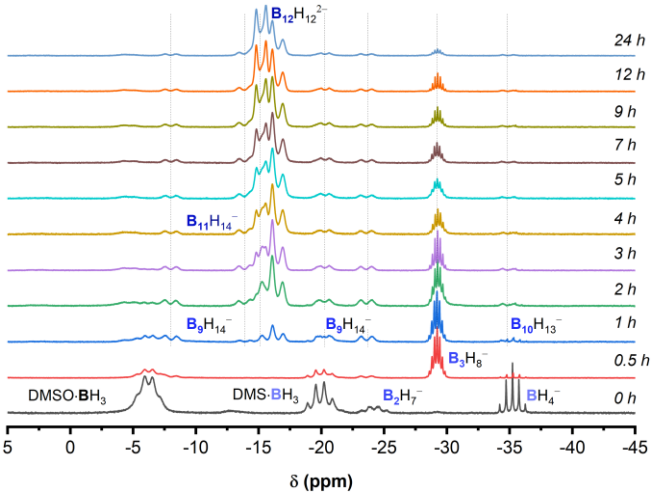

Figure 23. ^{1}H-coupled ^{11}B NMR spectra of aliquots taken from a reaction mixture containing $LiBH_4$ and $DMS{\cdot}BH_3$ in diglyme at 120 °C at different time intervals (t = 0 h was sampled before heating the mixture and intensities were normalized to the most intense signal).

In the initial mixture at room temperature, a signal at −24 ppm can be observed together with those of the reactants, which is ascribed to $B_2H_7^-$.[37] This intermediate is then quickly converted into $B_3H_8^-$, in accordance with previous observations, together with $B_9H_{14}^-$, during the first half hour of the solvothermal reaction. Notably, the intensities of the BH_4^- and $DMS{\cdot}BH_3$ signals drop rapidly after initiating heating, coupled to an increase in the concentration of $B_9H_{14}^-$ and $B_{11}H_{14}^-$ during the first hour of the reaction, consistent with earlier reports on the dehydrocondensation of $B_3H_8^-$ with B_2H_6.[53] Notably, the appearance of the characteristic doublet of $B_{12}H_{12}^{2-}$ can be observed already after 2 h of reaction, and its intensity then constantly increases while the reaction progresses. In contrast, the intensities of the $B_9H_{14}^-$ and $B_{11}H_{14}^-$ signals remain almost constant over the whole duration of the reaction, while slow consumption of $B_3H_8^-$ is observed. The constant concentration of $B_9H_{14}^-$ and $B_{11}H_{14}^-$ over nearly the whole

reaction time indicates that those species act as intermediates in a chemical equilibrium, being consumed rapidly after their formation to yield the final product. The reaction pathway for $B_{12}H_{12}^{2-}$ from BH_4^- is represented in Figure 24.

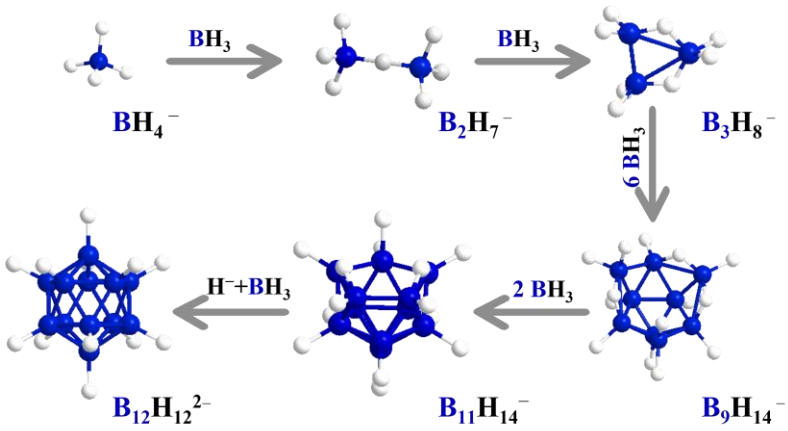

Figure 24. Proposed mechanism for the stepwise buildup of $B_{12}H_{12}^{2-}$ from BH_4^-.

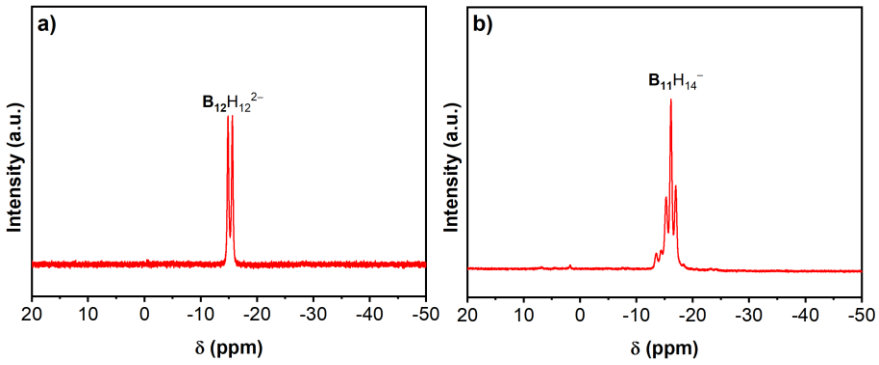

Figure 25. Proton-coupled ^{11}B NMR spectra (a) solid precipitate and (b) reaction solution obtained by further heat treatment reaction solution from $LiBH_4$ with 5 equiv. (10% excess) $DMS{\cdot}BH_3$ in diglyme at 160 °C for 4 h.

The above experiment demonstrates that $B_3H_8^-$, $B_9H_{14}^-$ and $B_{11}H_{14}^-$ are stable intermediates in the sequential buildup of $B_{12}H_{12}^{2-}$ from BH_4^- and BH_3. To understand the final step of the formation

mechanism of lithium dodecaborate, the isolation of the intermediate, $B_{11}H_{14}^-$, is critical. After various trials (see SI, Figures S35–39), we achieved this by subjecting the reaction filtrate obtained from the initial synthetic step to thermal treatment at 160 °C (Figures 25).

In order to understand what species adds to $B_{11}H_{14}^-$ to form dodecaborate, a solution of the isolated $LiB_{11}H_{14}$ in diglyme was reacted with various lower boranes, including $DMS{\cdot}BH_3$ and BH_4^-, at 120 °C in a Schlenk flask for 3 hours. As shown in Figure 26, direct reaction of $LiB_{11}H_{14}$ with BH_4^- did not yield $B_{12}H_{12}^{2-}$, but instead led to $B_{11}H_{13}^{2-}$ through the deprotonation of $B_{11}H_{14}^-$ by BH_4^-. On the other hand, the reaction of $B_{11}H_{14}^-$ with $DMS{\cdot}BH_3$ resulted in the successful formation of $B_{12}H_{12}^{2-}$. Previous reports have demonstrated the isolation of the $B_{12}H_{12}^{2-}$ anion through similar reactions, such as the one between $B_{11}H_{14}^-$ and triethylamine borane at 150 °C. $Na_2B_{12}H_{12}$ could however be obtained through reaction of $NaB_{11}H_{14}$ with $NaBH_4$ in boiling diglyme (b.p. = 162 °C).[3,24,27,54,55] Our results indicate that at a lower reaction temperature of 120 °C, deprotonation is likely favored over direct hydroboration.

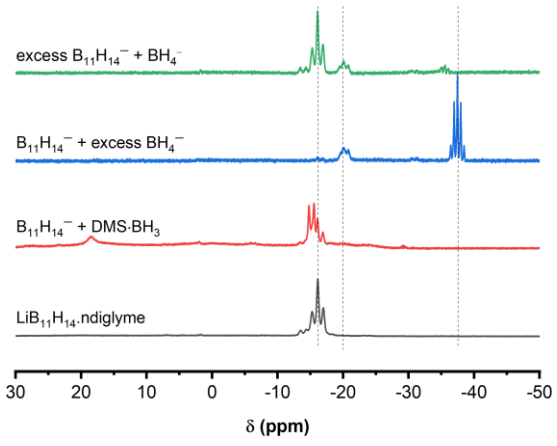

Figure 26. Proton coupled ^{11}B NMR spectra of reaction mixtures containing $LiB_{11}H_{14}$ and $DMS{\cdot}BH_3$ or $LiBH_4$ in diglyme.

4.4. Conclusions

We developed a simple solvothermal synthesis method enabling the synthesis of $Li_2B_{12}H_{12}$ and, by extension, its Na^+ and K^+ counterparts, in high purity and yield. Our innovative approach involves the reaction between the respective alkali borohydride and $DMS{\cdot}BH_3$ in glymes, either in an autoclave or in a Schlenk flask.

The yield of $B_{12}H_{12}^{2-}$ increases with temperature and reaction time, with optimal conditions for obtaining $Li_2B_{12}H_{12}$ being 120 °C in an autoclave for 48 hours, resulting in a 96% yield. Lower reaction temperatures resulted in incomplete conversion of BH_4^- to $B_{12}H_{12}^{2-}$, due to the slow reaction kinetics between $B_3H_8^-$ on the one hand, and $B_9H_{14}^-$ and $B_{11}H_{14}^-$ on the other hand. Higher temperatures led to the direct formation of partially dehydrogenated $Li_2B_{12}H_{12-x}{\cdot}$ n diglyme. The closed system of the autoclave, enabling a higher (autogenous) pressure of DMS, prevented decomposition of BH_3 into higher boranes and facilitated the reaction between $B_3H_8^-$ and $B_{11}H_{14}^-$. In turn, the conditions in the Schlenk flask favored the formation of $B_{11}H_{14}^-$. For the syntheses of $Na_2B_{12}H_{12}$ and $K_2B_{12}H_{12}$, refluxing diglyme in a Schlenk flask at 160 °C led to 92 % and 88 % yields, respectively.

The use of glymes as solvents resulted in the formation of glyme-solvated $Li_2B_{12}H_{12}$, with strong coordination with Li^+, evidenced by single crystal X-ray diffraction. Thermal treatment was ineffective to diglyme from the solvate. In that case, a methodology consisting in exchange of diglyme by higher boiling point polar solvents such as DMSO or *N*, *N*-diethylformamide followed by heating under vacuum was demonstrated as being successful for obtaining unsolvated

$Li_2B_{12}H_{12}$. In addition, substitution of diglyme by monoglyme as reaction solvent in an autoclave led to pure DME-solvated $Li_2B_{12}H_{12}$, which, in contrast to the diglyme solvate could be converted into unsolvated $Li_2B_{12}H_{12}$ by a simple heat treatment. Additionally, substitution of DME by H_2O allows for the preparation of chemically pure $Li_2B_{12}H_{12}$·n H_2O. Performing the reaction in toluene can yield crystalline pure $Li_2B_{12}H_{12}$, similar to the solvent-free synthetic method, but a further purification or extraction steps are required.

Finally, the formation mechanism of $B_{12}H_{12}^{2-}$ under the developed reaction conditions was elucidated through ex situ follow up of reaction intermediates using ^{11}B NMR. This evidenced a stepwise buildup mechanism of $B_{12}H_{12}^{2-}$ from BH_4^- through $B_2H_7^-$, $B_3H_8^-$, $B_9H_{14}^-$, $B_{11}H_{14}^-$intermediates. Furthermore, $B_{11}H_{13}^{2-}$ was proposed as the final intermediate based on experiments starting from isolated $B_{11}H_{14}^-$.

The developed synthetic method represents a significant improvement compared to previous strategies in terms of yield, purity, and cost-effectiveness for lithium and other alkali metal dodecaborates under their solvated and desolvated forms.

4.5. References

(1) Dunks, G. B.; Barker, Kathryn.; Hedaya, Eddie.; Hefner, Catherine.; Palmer-Ordonez, Kathy.; Remec, Peter. Simplified Synthesis of Decaborane (14) from Sodium Tetrahydroborate via Tetradecahydroundecaborate (1-) Ion. *Inorg. Chem.* **1981**, *20* (6), 1692–1697.

(2) Getman, T. D.; Krause, J. A.; Shore, S. G. Synthesis of the New Boron Hydride Nido-Undecaborane (15), $B_{11}H_{15}$, and the X-Ray Structure of Its Conjugate Base Tetradecahydroundecaborate (1-), $[B_{11}H_{14}]^-$. *Inorg. Chem.* **1988**, *27* (14), 2398–2399.

(3) Jing, Y.; Wang, X.; Han, H.; Liu, X.-R.; Yu, X.-C.; Chen, X.-M.; Wei, D.; Wang, L.-S.; Chen, X. Selective Synthesis of the $B_{11}H_{14}^-$ and $B_{12}H_{12}^{2-}$ Borane Derivatives and the General Mechanisms of the B-H Bond Condensation. *Sci. China Chem.* **2023**.

(4) He, L.; Shao, H.; Felderhoff, M.; Li, H.-W.; Li, X.; Zhu, Q.; Zhang, D.; Wu, D.; Fu, Y.; Deng, Y.; Lu, Z. Facile Synthesis of Anhydrous $Li_2B_{12}H_{12}$ with High Purity by Solvent-Free Method. *Inorganica Chim. Acta* **2017**, *464*, 147–151.

(5) Remhof, A.; Yan, Y.; Rentsch, D.; Borgschulte, A.; Jensen, C. M.; Züttel, A. Solvent-Free Synthesis and Stability of $MgB_{12}H_{12}$. *J. Mater. Chem. A* **2014**, *2* (20), 7244–7249.

(6) Garcia, A.; Müller, G.; Černý, R.; Rentsch, D.; Asakura, R.; Battaglia, C.; Remhof, A. $Li_4B_{10}H_{10}B_{12}H_{12}$ as Solid Electrolyte for Solid-state Lithium Batteries. *J. Mater. Chem. A.* **2023**, 11(35), 18996–19003.

(7) Payandeh, S.; Rentsch, D.; Łodziana, Z.; Asakura, R.; Bigler, L.; Černý, R.; Battaglia, C.; Remhof, A. *Nido*-Hydroborate-Based Electrolytes for All-Solid-State Lithium Batteries. *Adv. Funct. Mater.* **2021**, *31* (18), 1–12.

(8) Souza, D. H. P.; D'Angelo, A. M.; Humphries, T. D.; Buckley, C. E.; Paskevicius, M. $Na_2B_{11}H_{13}$ and $Na_{11}(B_{11}H_{14})_3(B_{11}H_{13})_4$ as Potential Solid-State Electrolytes for Na-Ion Batteries. *Dalton Trans.* **2022**, *51* (36), 13848–13857.

(9) Hansen, B. R. S.; Paskevicius, M.; Li, H.-W.; Akiba, E.; Jensen, T. R. Metal Boranes: Progress and Applications. *Coord. Chem. Rev*. **2016**, *323*, 60–70.

(10) Huang, Z.; Wang, S.; Dewhurst, R. D.; Ignat'ev, N. V.; Finze, M.; Braunschweig, H. Boron: Its Role in Energy-Related Processes and Applications. *Angew. Chemie - Int. Ed.* **2020**, *59* (23), 8800–8816.

(11) Sivaev, I. B.; Bregadze, V. V. Polyhedral Boranes for Medical Applications: Current Status and Perspectives. *Eur. J. Inorg. Chem.* **2009**, *2009* (11), 1433–1450.

(12) Li, J.; Janouskova, O.; Fernandez-Alvarez, R.; Mesikova, S.; Tosner, Z.; Kereiche, S.; Uchman, M.; Matejicek, P. Designed Boron-Rich Polymeric Nanoparticles Based on Nano-Ion Pairing for Boron Delivery. *Chem. – Eur. J.* **2020**, *26*, 14283–14289.

(13) Sivaev, I. B.; Bruskin, A. B.; Nesterov, V. V.; Antipin, M. Y.; Bregadze, V. I.; Sjöberg, S. Synthesis of Schiff Bases Derived from the Ammoniaundecahydro-Closo-Dodecaborate(1-) Anion, $[B_{12}H_{11}NH{=}CHR]^-$, and Their Reduction into Monosubstituted Amines $[B_{12}H_{11}NH_2CH_2R]^-$: A New Route to Water Soluble Agents for BNCT. *Inorg. Chem.* **1999**, *38* (25), 5887–5893.

(14) Zhao, X.; Wang, D.; Xiang, C.; Zhang, F.; Liu, L.; Zhou, X.; Zhang, H. Facile Synthesis of Boron Organic Polymers for Efficient Removal and Separation of Methylene Blue, Rhodamine B, and Rhodamine 6G. *ACS Sustain. Chem. Eng.* **2018**, *6* (12), 16777–16787.

(15) He, L.; Li, H.-W.; Nakajima, H.; Tumanov, N.; Filinchuk, Y.; Hwang, S.-J.; Sharma, M.; Hagemann, H.; Akiba, E. Synthesis of a Bimetallic Dodecaborate $LiNaB_{12}H_{12}$ with Outstanding Superionic Conductivity. *Chem. Mater.* **2015**, *27*, 5483–5486.

(16) Campos dos Santos, E.; Sato, R.; Kisu, K.; Sau, K.; Jia, X.; Yang, F.; Orimo, S.; Li, H. Explore the Ionic Conductivity Trends on $B_{12}H_{12}$ Divalent Closo-Type Complex Hydride Electrolytes. *Chem. Mater.* **2023**, *35* (15), 5996–6004.

(17) Duchêne, L.; Kühnel, R. S.; Stilp, E.; Cuervo Reyes, E.; Remhof, A.; Hagemann, H.; Battaglia, C. A Stable 3 V All-Solid-State Sodium-Ion Battery Based on a Closo-Borate Electrolyte. *Energy Environ. Sci.* **2017**, *10* (12), 2609–2615.

(18) Duchêne, L.; Kim, D. H.; Song, Y. B.; Jun, S.; Moury, R.; Remhof, A.; Hagemann, H.; Jung, Y. S.; Battaglia, C. Crystallization of Closo-Borate Electrolytes from Solution Enabling Infiltration into Slurry-Casted Porous Electrodes for All-Solid-State Batteries. *Energy Storage Mater.* **2020**, *26*, 543–549.

(19) Longuet-Higgins, H. C.; Roberts M. V. The Electronic Structure of the Borides MB_6. *Proc. R. Soc. Lond A* **1954**, *224* (1158), 336–347.

(20) Pitochelli, A. R.; Hawthorne, F. M. The Isolation of The Icosahedral $B_{12}H_{12}^{-2}$ Ion. *J. Am. Chem. Soc.* **1960**, *82*, 3228–3229.

(21) Miller, H. C.; Muetterties, E. L.; Boone, J. L.; Garrett, P.; Hawthorne, M. F. Borane Anions, **1967**, 81–91.

(22) Chen, W.; Wu, G.; He, T.; Li, Z.; Guo, Z.; Liu, H.; Huang, Z.; Chen, P. An Improved Synthesis of Unsolvated NaB_3H_8 and Its Application in Preparing $Na_2B_{12}H_{12}$. *Int. J. Hydrogen Energy* **2016**, *41* (34), 15471–15476.

(23) Moury, R.; Gigante, A.; Hagemann, H. An Alternative Approach to the Synthesis of NaB_3H_8 and $Na_2B_{12}H_{12}$ for Solid Electrolyte Applications. *Int. J. Hydrogen Energy* **2017**, *42*, 22417–22421.

(24) Miller, H. C.; Miller, N. E.; Muetterties, E. L. Synthesis of Polyhedral Boranes. *J. Am. Chem. Soc.* **1963**, *85*, 3885–3886.

(25) He, L.; Li, H.-W.; Hwang, S.-J.; Akiba, E. Facile Solvent-Free Synthesis of Anhydrous Alkali Metal Dodecaborate $M_2B_{12}H_{12}$ (M = Li, Na, K). *J. Phys. Chem. C* **2014**, *118*, 6084–6089.

(26) Wang, J.; Steenhaut, T.; Li, H.-W.; Filinchuk, Y. High Yield Autoclave Synthesis of Pure $M_2B_{12}H_{12}$ (M = Na, K). *Inorg. Chem.* **2023**, *62* (5), 2153–2160.

(27) Souza, D. H. P.; Moller, K. T.; Moggach, S. A.; Humphries, T. D.; D'Angelo, A. M.; Buckley, C. E.; Paskevicius, M. Hydrated Alkali-$B_{11}H_{14}$ Salts as Potential Solid-State Electrolytes. *J. Mater. Chem. A* **2021**, *9*, 15027–15037.

(28) Johnson, S. I.; DeMaria, J. M.; Ginovska, B.; Edvenson, G. M.; Hagemann, H.; Autrey, S. T. Exploring Detailed Reaction Pathways for Hydrogen Storage with Borohydrides Using DFT Calculations. *Energ. Fuel.* **2022**, *36* (10), 5513–5527.

(29) Sethio, D.; Daku, L. M. L.; Hagemann, H.; Kraka, E. Quantitative Assessment of B−B−B, B−H_b−B, and B−H_t Bonds: From BH_3 to $B_{12}H_{12}^{2-}$. *ChemPhysChem* **2019**, *20* (15), 1967–1977.

(30) Yan, Y.; Remhof, A.; Rentsch, D.; Zuttel, A. The Role of $MgB_{12}H_{12}$ in the Hydrogen Desorption Process of $Mg(BH_4)_2$. *Chem. Commun.* **2015**, *51*, 700–702.

(31) Chen, X.; Liu, X.-R.; Wang, X.; Chen, X.-M.; Jing, Y.; Wei, D. A Safe and Efficient Synthetic Method for Alkali Metal Octahydrotriborates, Unravelling a General Mechanism for Constructing the Delta B3 Unit of Polyhedral Boranes. *Dalton Trans.* **2021**, *50* (39), 13676–13679.

(32) Zhao, Q.; Dewhurst, R. D.; Braunschweig, H.; Chen, X. A New Perspective on Borane Chemistry: The Nucleophilicity of the B−H Bonding Pair Electrons. *Angew. Chemie - Int. Ed.* **2019**, *58* (11), 3268–3278.

(33) Fu, H.; Wang, X.; Shao, Y.; Chen, J.; Zhang, X.; Fu, H.; Zheng, J.; Li, X. Synthesis of Lithium Octahydrotriborate and Investigation on Its Thermal Decomposition. *Int. J. Hydrogen Energy* **2016**, *41* (1), 384–391.

(34) Huang, Z.; Gallucci, J.; Chen, X.; Yisgedu, T.; Lingam, H. K.; Shore, S. G.; Zhao, J.-C. $Li_2B_{12}H_{12}\cdot 7NH_3$: A New Ammine Complex for Ammonia Storage or Indirect Hydrogen Storage. *J. Mater. Chem.* **2010**, *20* (14), 2743–2745.

(35) Avdeeva, V. V.; Malinina, E. A.; Sivaev, I. B.; Bregadze, V. I.; Kuznetsov, N. T. Silver and Copper Complexes with Closo-Polyhedral Borane, Carborane and Metallacarborane Anions: Synthesis and X-Ray Structure. *Crystals*. **2016**, *6*, 60–61.

(36) Ďorďovič, V.; Tošner, Z.; Uchman, M.; Zhigunov, A.; Reza, M.; Ruokolainen, J.; Pramanik, G.; Cígler, P.; Kalíková, K.; Gradzielski, M.; Matějíček, P. Stealth Amphiphiles: Self-Assembly of Polyhedral Boron Clusters. *Langmuir* **2016**, *32* (26), 6713–6722.

(37) Chen, X.-M.; Ma, N.; Zhang, Q.-F.; Wang, J.; Feng, X.; Wei, C.; Wang, L.-S.; Zhang, J.; Chen, X. Elucidation of the Formation Mechanisms of the Octahydrotriborate Anion ($B_3H_8^-$) through the Nucleophilicity of the B–H Bond. *J. Am. Chem. Soc.* **2018**, *140*, 6718–6726.

(38) Siedle, A. R.; Bodner, G. M.; Todd, L. J. Studies in Boron Hydrides—V. *J. Inorg. Nucl. Chem.* **1971**, *33* (11), 3671–3676.

(39) Kultyshev, R. G.; Liu, J.; Meyers, E. A.; Shore, S. G. Synthesis and Characterization of Sulfide, Sulfide−Sulfonium, and Bissulfide Derivatives of $[B_{12}H_{12}]^{2-}$. Additivity of Me_2S and MeS^- Substituent Effects in ^{11}B NMR Spectra of Disubstituted Icosahedral Boron Clusters. *Inorg. Chem.* **2000**, *39* (15), 3333–3341.

(40) Gigante, A.; Duchene, L.; Moury, R.; Pupier, M.; Remhof, A.; Hagemann, H. Direct Solution-Based Synthesis of $Na_4(B_{12}H_{12})(B_{10}H_{10})$ Solid Electrolyte.

ChemSusChem **2019**, *12*, 4832–4837.

(41) Zheng, X.; Yang, Y.; Zhao, F.; Fang, F.; Guo, Y. Facile Preparation and Dehydrogenation of Unsolvated KB_3H_8. *Chem. Commun.* **2017**, *53* (80), 11083–11086.

(42) Chong, M.; Autrey, T.; Jensen, C. Lewis Base Complexes of Magnesium Borohydride: Enhanced Kinetics and Product Selectivity upon Hydrogen Release. *Inorganics* **2017**, *5* (4), 89.

(43) Caputo, R.; Garroni, S.; Olid, D.; Teixidor, F.; Suriñach, S.; Baró, M. D. Can $Na_2[B_{12}H_{12}]$ Be a Decomposition Product of $NaBH_4$? *Phys. Chem. Chem. Phys.* **2010**, *12* (45), 15093–15100.

(44) Hwang, S.-J.; C. Bowman, R.; W. Reiter, J.; , J.; L. Soloveichik, G.; Zhao, J.-C.; Kabbour, H.; C. Ahn, C. NMR Confirmation for Formation of $[B_{12}H_{12}]^{2-}$ Complexes during Hydrogen Desorption from Metal Borohydrides. *J. Phys. Chem. C* **2008**, *112* (9), 3164–3169.

(45) Long, L. H. The Mechanisms of Thermal Decomposition of Diborane and of Interconversion of the Boranes. *J. Inorg. Nucl. Chem.* **1970**, *32* (4), 1097–1115

(46) Kotlensky, W. V.; Schaeffer, R. Decomposition of Diborane in a Silent Discharge. Isolation of B_6H_{10} and B_9H_{15}. *J. Am. Chem. So.c* **1958**, *80* (17), 4517–4519.

(47) Chen, X.; Liu, Y.; Alexander, A.; Gallucci, J. C.; Hwang, S.; Lingam, H. K.; Huang, Z.; Wang, C.; Li, H.; Zhao, Q.; Ozkan, U. S.; Shore, S. G.; Zhao, J. Desolvation and Dehydrogenation of Solvated Magnesium Salts of Dodecahydrododecaborate: Relationship between Structure and Thermal Decomposition. *Chem. – Eur. J.* **2014**, *20* (24), 7325–7333.

(48) Payandeh, S.; Rentsch, D.; Łodziana, Z.; Asakura, R.; Bigler, L.; Černý, R.; Battaglia, C.; Remhof, A. *Nido*-Hydroborate-Based Electrolytes for All-Solid-State Lithium Batteries. *Adv. Funct. Mater.* **2021**, *31* (18), 1–12.

(49) Alvarez, S. Coordinating Ability of Anions, Solvents, Amino Acids, and Gases towards Alkaline and Alkaline-Earth Elements, Transition Metals, and Lanthanides. *Chem. – Eur. J.* **2020**, *26* (19), 4350–4377.

(50) Paskevicius, M.; Pitt, M. P.; Brown, D. H.; Sheppard, D. A.; Chumphongphan,

S.; Buckley, C. E. First-Order Phase Transition in the $Li_2B_{12}H_{12}$ System. *Phys. Chem. Chem. Phys.* **2013**, *15* (38), 15825–15828.

(51) Yan, Y.; Wang, H.; Zhu, M.; Cai, W.; Rentsch, D.; Remhof, A. Direct Rehydrogenation of LiBH4 from H-Deficient $Li_2B_{12}H_{12-x}$. *Crystals* **2018**, *8* (3), 131.

(52) Hamilton, E. J. M.; Jordan; Meyers, E. A.; Shore, S. G. One-Step Preparation of Dimethyl Sulfide Substituted Icosahedral Boranes: The Crystal and Molecular Structures of 1,7-$(SMe_2)_2$ $B_{12}H_{10}$, 1,12-$(SMe_2)_2B_{12}H_{10}$, and $[SMe_3][B_{12}H_{11}(SMe_2)]$·MeCN. *Inorg. Chem.* **1996**, *35* (18), 5335–5341.

(53) Gavrilova, L. A.; Titov, L. V; Petrovskii, P. V. Synthesis of $Bu_4NB_{11}H_{14}$ by the Reaction of Tetrabutylammonium Octahydrotriborate with Diborane in Diglyme. *Russ. J. Coord. Chem.* **2004**, *30*, 307–308.

(54) Volkov, O.; Paetzold, P. The Chemistry of the Undecaborates. *J. Organomet. Chem.* **2003**, *680* (1–2), 301–311.

(55) Adams, R. M.; Siedle, A. R.; Grant, J. Convenient Preparation of the Dodecahydrododecaborate Ion. *Inorg Chem* **1964**, *3* (3), 461–461.

Chapter 4

Chapter 5. Autoclave-Mediated Synthesis of Calcium Dodecaborate in a Mixture of Ethers

Jian Wang,[a] Timothy Steenhaut,[a] Koen Robeyns,[a] Torben René Jensen,[b] Hai-Wen Li,[c] Yaroslav Filinchuk[a]*

[a] Institute of Condensed Matter and Nanosciences, Université catholique de Louvain, 1348 Louvain-la-Neuve, Belgium

[b] Department of Chemistry and Interdisciplinary Nanoscience Center, Aarhus University, Langelandsgade 140, Aarhus C 8000, Denmark

[c] Hefei General Machinery Research Institute, Hefei 230031, China

* Corresponding author. E-mail: yaroslav.filinchuk@uclouvain.be (Y. Filinchuk)

Chapter 5

Abstract

In this chapter, we introduce a simple and cost effective solvothermal pathway to achieve high purity of $CaB_{12}H_{12}$ with a yield of 73%. The synthetic process involves the reaction of borane dimethyl sulfide complex with calcium hydride, in a mixture of tetrahydrofuran (THF) and dimethoxyethane (DME) with ratio of 1:1. The use of DME can ensure a stronger bidentate configuration with Ca^{2+}, minimizing the risk of $B_{12}H_{12-x}^{2-}$ anion formation. By further optimizing the conditions, we found that, combining DME with THF can provide adequate solubility of lower borane clusters, thereby preventing the formation of unwanted higher borane clusters. The synthesis was closely monitored using X-ray diffraction, Fourier transform infrared (FTIR) and nuclear magnetic resonance (NMR) spectroscopies. The results show that, we can obtain $CaB_{12}H_{12}$ by using this newly developed strategy, but it cannot be applied for the synthesis of $MgB_{12}H_{12}$, due to the extreme oxophylicity of Mg^{2+}. This study contributes valuable insights into the synthesis of useful alkali-earth metal dodecaborates.

5.1. Introduction

The increasing demand for better energy storage systems, with higher capacity and more robust battery cells, has attracted attention both in academia and industry.[1–4] Although the rechargeable Li-ion batteries has been commercialized as dominance, the society still requires continuous study for developing energy-intensive technologies.[5] Compared to the traditional Li-ion counterparts, the divalent cations, like Ca^{2+} and Mg^{2+} have received special attention, due to the higher theoretical energy densities.[6–8]

Salts of Ca^{2+} or Mg^{2+} with weak coordinating anions are particularly desirable to achieve high ion mobility in the electrolytes.[9,10] The dodecaborate dianion, $B_{12}H_{12}^{2-}$, characterized by an icosahedral boron cluster with spherical electron delocalization, is such an anion.[11,12] The properties of $MB_{12}H_{12}$ (M = Ca, Mg) salts have not been fully understood yet, mainly due to their challenging synthesis, and very limited work has been reported.[13,14]

The reported synthetic work has primarily focused on alkali metal $M_2B_{12}H_{12}$ (M = Na, K) salts. Our efforts in this area are also presented in the preceding chapters (Chapters 3 and 4). Those salts can be synthesized by solvothermal reactions between their borohydride (BH_4^-) and boranes (B_2H_6, $B_{10}H_{14}$ or $L{\cdot}BH_3$ (L = Et_3N or DMS)), followed by a desolvation or a dehydration process.[15–18] However, the stronger interactions between divalent cations and coordinating species result in relatively higher desolvation barriers. Therefore, the synthesis route towards $MB_{12}H_{12}$ (M = Ca, Mg) has to be well considered. The described syntheses of $CaB_{12}H_{12}$ include sintering of calcium borohydride ($Ca(BH_4)_2$) with $B_{10}H_{14}$ in sealed tubes,[19] and

similar reactions in pentadecane at 160 °C for 4 h.[20] However, those approaches all lead to the formation of $CaB_{12}H_{12}$ along with other B−H impurities, requiring more further isolation and purification processes. Also, the use of expensive and toxic boranes, like B_2H_6 and $B_{10}H_{14}$, should be avoided. Similarly, attempts to synthesize the solvent-free $MgB_{12}H_{12}$ by ball milling $Mg(BH_4)_2$/carbon nanocomposite under a B_2H_6/H_2 atmosphere or by sintering $Mg(BH_4)_2$ with $B_{10}H_{14}$ were also hindered by impurities.[19,21] Furthermore, the preparation of anhydrous $MgB_{12}H_{12}$ from various solvated forms (with H_2O, NH_3, and CH_3OH) failed, due to the competition between desolvation and dehydrogenation, leading to the formation of polyhydro(metho)xylated complexes.[22]

The search for suitable solvents for enabling the solvothermal synthesis of $MB_{12}H_{12}$ (M = Ca, Mg) is thus of paramount importance, as it could significantly impact the solubility and dispersibility of borohydrides during synthesis, the purity of the final product, and the ease of solvent removal after reaction.[17] Although ethereal solvents play a crucial role in the condensation reactions for the synthesis of $B_{12}H_{12}^{2-}$, their use has not been investigated yet for the synthesis of alkali earth derivatives.[17,23] The physicochemical properties of ethereal solvents is summarized in Table S1. Light ethers, such as diethyl ether and tetrahydrofuran, have low boiling points and enable controlled and efficient reactions involving boron-based reagents. Those solvents are for example particularly advantageous for condensation reactions leading to the synthesis of BH_4^- from hydrides or $B_3H_8^-$ from BH_4^-.[24,25] In contrast, heavier ethers like glymes and dioxane offer higher boiling point and better thermal stability, making them favorable for condensation reaction, especially in the synthesis of higher boranes.[17,18,26] Furthermore, the stability of metal cation-solvent complexes increases with the denticity of the used ether,

leading to better availability of reactive anions, thus facilitating the formation of $B_{12}H_{12}^{2-}$. Our prior research into the synthesis of $M_2B_{12}H_{12}$ (M = Li, Na, K) revealed the utility of glymes in facilitating the synthesis of $B_{12}H_{12}^{2-}$ through intermediate formations of $B_3H_8^-$, $B_9H_{14}^-$, and $B_{11}H_{14}^-$.[17,27] The elevated boiling point of diglyme enables the feasibility of conducting the reaction within ambient pressure vessels. With this in mind, we investigated the use of various ethers to develop a more efficient route towards alkali-earth metal dodecaborates.

5.2. Experimental Section

5.2.1. Chemicals

Calcium borohydride bis(tetrahydrofuran) ($Ca(BH_4)_2{\cdot}2THF$, anhydrous, 100%), calcium hydride (CaH_2, anhydrous, 95%), borane dimethylsulfide complex ($(CH_3)_2S{\cdot}BH_3$, neat), diethylene glycol dimethyl ether (diglyme, anhydrous, 99.5%) tetrahydrofuran (C_4H_8O, anhydrous, 99.9%), 1,2-dimethoxyethane (monoglyme, DME, $C_4H_{10}O_2$, anhydrous, 99.5 %) were obtained from Sigma-Aldrich. Deuterated dimethyl sulfoxide (DMSO-d_6, anhydrous, 99.9 atom% D) and deuterium oxide (D_2O, anhydrous, 99.9%) were obtained from Eurisotop. CaH_2 underwent manual grinding with an agate mortar and pestle for 10 minutes until a small powder was obtained before use. All the other above chemicals were used without further purification.

$Ca(BH_4)_2$ was obtained through the thermal removal of tetrahydrofuran (THF) from $Ca(BH_4)_2{\cdot}2THF$ at 180 °C under vacuum for 12 h. Powder X-ray diffraction (PXRD) confirmed that the resulting powder consisted of β-$Ca(BH_4)_2$ (Figure S1).

γ-$Mg(BH_4)_2$ was synthesized according to a published method, by reaction of dibutylmagnesium with borane dimethylsulfide ($DMS{\cdot}BH_3$) complex, followed by vacuum removal of DMS from the obtained $Mg(BH_4)_2{\cdot}1/2$ DMS.[28]

5.2.2. General synthetic procedure for $CaB_{12}H_{12}$

The reaction was conducted in a 40 mL plastic (PTFE) liner fitted inside a 50 mL stainless steel autoclave (Anhui Kemi Instrument Co., Ltd.). Typically, 0.21 g of CaH_2 (5 mmol) was weighed into the liner reactor within a glovebox, which was sealed with Parafilm®. Prior to loading the PTFE reactor into the autoclave, 8 mL of DME and 8 mL of THF were added. Then, 60 mmol of borane dimethyl sulfide complex ($(CH_3)_2S{\cdot}BH_3$, concentration: 10 −10.2 M, 6 mL) was added to the mixture and the autoclave was sealed, followed by purging the system with argon for 30 seconds to remove air. The reaction temperature was controlled using a programmed system, increased at a rate of 2 °C/min from room temperature to 120 °C, at which it was maintained for 24 h. Subsequently, the system was naturally cooled down to room temperature. After synthesis, the pressure in the autoclave reached 29−31 bar on average. Excess pressure was bled of the reactor and the obtained suspension was transferred to a Schlenk filtration apparatus to isolate the obtained solid. The product was washed with THF (3 × 10 mL) to eliminate residual $Ca(BH_4)_2$, and then dried at room temperature under vacuum for 2 h. The raw product was obtained as a white dry substance.

High purity $CaB_{12}H_{12}$ was obtained by adding 15 mL of H_2O to the raw product. The obtained solution was heated to boiling, and then filtered to remove boric acid and $Ca(OH)_2$. The filtrate containing $CaB_{12}H_{12}$ was subsequently evaporated at 40 °C under vacuum to

remove ethers. Anhydrous $CaB_{12}H_{12}$ was obtained by further drying the white suspension at 200 °C for 12 h. The reaction yielded approximately 0.63 g of anhydrous $CaB_{12}H_{12}$ (73% yield). Repeating the described solvent exchange two more times enhanced the removal of light ethers.

5.2.3. Characterization

Powder X-ray diffraction (PXRD) patterns were acquired in-house using a MAR 345 image plate detector with Mo Kα radiation (wavelength λ = 0.71073 Å) generated from an performed using a MAR345 image plate detector and an Incoatec Microfocus Source^{HIGHBRILLIANCE} (IμS^{HIGHBRILLIANCE}) Mo ELM47 operating at 50 kV and 1000 μA. During exposure, samples were rotated 180° for a duration of 10 minutes. All samples were loaded into thin-walled glass capillaries (0.7 mm diameter, Hilgenberg, GmbH), which were sealed with grease under argon in a glovebox. The sealed capillaries were taken out of the glovebox and were cut and promptly placed into molten wax on goniometric heads before analysis, ensuring immediate measurement after preparation to prevent sample degradation. Data integration was conducted using the Fit 2D software (ESRF), using LaB_6 as a calibrant.

Attenuated total reflectance-Fourier transform infrared (ATR-FTIR) spectra were collected on a Bruker Alpha II spectrometer (with Bruker Platinum ATR module, diamond crystal, single bounce) set in an argon-filled glovebox, in the 4000 − 370 cm^{-1} range, with 16 scans.

in situ synchrotron radiation powder X-ray diffraction (SR-PXRD) were gathered at the Swiss-Norwegian beamline BM1A within the European Synchrotron Radiation Facility (ESRF) in Grenoble. Employing a PILATUS@SNBL diffractometer equipped

with a Dectris PILATUS 2M single photon counting pixel area detector (λ = 0.77509 Å), the collection process took place. The SNBL Toolbox software was utilized to process the raw data, utilizing calibration details sourced from the LaB_6 standard, to generate the powder patterns.

Liquid state NMR spectra were recorded at room temperature (295 K) on a Bruker Avance 500 spectrometer operating at 500.13 MHz for ^{1}H and 160.46 MHz for ^{11}B, using a BBFO {^{1}H, X} probehead equipped with a *z*-gradient coil. Experiments were run under the *TopSpin* program (1.3 version; Bruker). ^{1}H chemical shifts were referenced to the residual DMSO-d_5 signal (δ = 2.50 ppm) and ^{11}B NMR signals were referenced externally to $BF_3{\cdot}Et_2O$ (δ = 0.00 ppm). All experiments were conducted using quartz NMR tubes (i.d. = 5 mm). All solvated $CaB_{12}H_{12}$ samples were observed to not completely dissolve in DMSO-d_6.

5.3. Results and Discussion

5.3.1. Attempt to synthesize $CaB_{12}H_{12}$ in diglyme

The first attempt to obtain $CaB_{12}H_{12}$ in ethereal solvents involved reacting 5 mmol bulk calcium borohydride ($Ca(BH_4)_2$) and 50 mmol $DMS{\cdot}BH_3$ in 16 ml of diglyme (b.p. 162 °C) in a Schlenk flask, resulting in the precipitation of a white solid, which was then filtered.[17] Figure 1 shows the proton-coupled ^{11}B NMR spectra of the as-prepared $CaB_{12}H_{12}$ dissolved in D_2O and in DMSO-d_6. NMR was measured in DMSO and D_2O, and then immediately add that the product was fully soluble in D_2O but that some solid was not soluble in DMSO. Both spectra reveal a doublet at around −15.2 ppm,

indicating the successful predominant formation of $B_{12}H_{12}^{2-}$.[15,29,30] The ^{11}B NMR spectra however also indicate the presence of $B_{11}H_{13}^{2-}$ and $B_{12}H_{12-x}^{2-}$ anions as impurities.[22,31] The presence of the latter species is likely due to hydrogen loss of the formed diglyme-solvated $CaB_{12}H_{12}$ under the demanding thermal conditions.

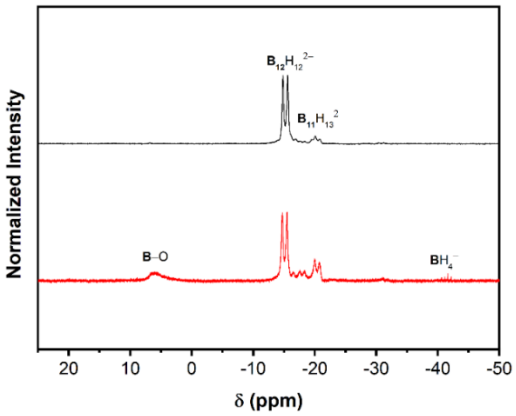

Figure 1. Proton-coupled ^{11}B NMR spectra of the solid precipitate obtained by reaction between 5 mmol $Ca(BH_4)_2$ and 10 equiv. $DMS{\cdot}BH_3$ at 120 °C in an autoclave, dissolved in D_2O (red line) and DMSO−d_6 (black line).

Furthermore, the presence of BH_4^- in the spectra measured in D_2O (Figure 1) is attributed to unreacted $Ca(BH_4)_2$. Overall, the ^1H NMR spectra in Figures S2 and S3 align with the observations of ^{11}B NMR, although an additional strong singlet is present in the ^1H spectra, with a chemical shift of 2.86 ppm in DMSO−d_6 and 2.89 ppm in D_2O. This signal can be assigned to $(CH_3)_3S^+$, which presence might be due to the low solubility of $Ca(BH_4)_2$ in diglyme, leading to the self-condensation of $DMS{\cdot}BH_3$.[32,33]

The existence of B−H impurities, notably $B_{11}H_{13}^{2-}$ and the dehydrogenated anion $B_{12}H_{12-x}^{2-}$, together with the additional cation $(CH_3)_3S^+$, makes the synthesis of pure $CaB_{12}H_{12}$ in diglyme challenge. Additionally, the extraction of high-purity $CaB_{12}H_{12}$ from this

complex mixture is intrinsically difficult, as shown by several unsuccessful attempts. Heating to remove diglyme from the obtained solvated $CaB_{12}H_{12}$ was failed, as demonstrated by synchrotron radiation studies (Figure S4).

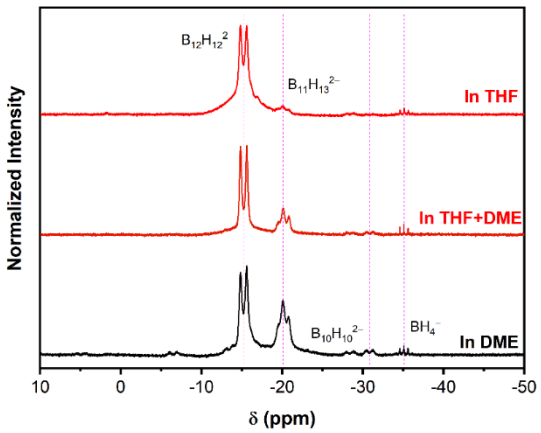

Figure 2. Proton-coupled ^{11}B NMR spectra of the solid precipitate obtained upon reaction of 5 mmol CaH_2 with 12 equiv. $DMS{\cdot}BH_3$ in different ethereal solvents (samples dissolved in DMSO−d_6).

We previously demonstrated the efficiency of an alternative technique, which enabled desolvation of diglyme from $Li_2B_{12}H_{12}$ by substitution with DMSO or *N*, *N*-diethylformamide, which can then be eliminated thermally. A similar method was attempted here to obtain DMSO or *N*, *N*- diethylformamide solvated $CaB_{12}H_{12}$ from the crude product. However, the strong interaction of Ca^{2+} with both solvents rendered their direct thermal removal impossible as demonstrated by ^1H NMR and PXRD (Figure S5 and S6). Therefore, we investigated the use of the lighter and less coordinating ethers DME (b.p. = 85 °C, bidentate coordinating) and THF (b.p. = 66°C, monodentate coordinating) for the synthesis. These solvents not only increase the solubility of $Ca(BH_4)_2$, but they are also less coordinating than diglyme (tridentate coordination). Given the very high cost of calcium

borohydride, subsequent investigations were carried out using much cheaper calcium hydride (CaH_2), reducing the cost of this synthesis by several orders of magnitude.[34]

The autoclave experiments with 5 mmol of calcium hydride and 60 mmol of $DMS.BH_3$ were further carried out in either THF, DME, or a THF/DME mixture in 1:1 (v/v) ratio. Figure 2 representing the ^{11}B NMR spectra of the obtained solid precipitates reveal the predominant formation of the desired $B_{12}H_{12}^{2-}$, along with other boron-hydrogen compounds such as $B_{11}H_{13}^{2-}$ and $B_{10}H_{10}^{2-}$. The highest proportion of $B_{11}H_{13}^{2-}$ is observed for the reactions performed in DME, which is explained by the limited solubility of CaH_2 and the newly formed $Ca(BH_4)_2$ in this solvent, affecting the reaction rate significantly. Interestingly, a single crystal could be isolated from the reaction in DME, and that it was identified as being $CaB_{12}H_{12}{\cdot}2DME$, showing bidentate coordination of two DME molecules on each Ca^{2+} cation (Figure 3). Although the product obtained in THF contains less of the boron-hydrogen impurities, an additional quartet is observed at around −17 ppm (Figure S7 and S8), which is attributed to the presence of a $B_{12}H_{12-x}^{2-}$ anion. The formation of this latter is likely due to the low boiling point of THF and its unstable monodentate coordination mode towards Ca^{2+}, resulting in the precipitation of the THF solvated $CaB_{12}H_{12}$ phase. This in turn leads to dehydrogenation reactions, as the temperature for the formation of $B_{12}H_{12-x}^{2-}$ anions may closely associated with the coordinating ability of the used solvent towards the cations.[22] A similar phenomenon was also observed in our previous work on the synthesis of $Li_2B_{12}H_{12}$ and $Na_2B_{12}H_{12}$.

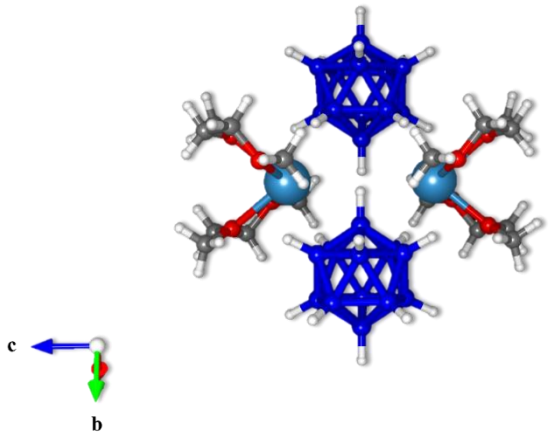

Figure 3. Crystal structure of $CaB_{12}H_{12}$·2DME. Color code: Ca, light blue; B, dark blue; H, white; O, red; C: dark grey.

In contrast to reactions conducted in THF and DME, the ^{11}B NMR spectrum of the solid precipitates and filtrate (Figure S9) indicate that $CaB_{12}H_{12}$ and $CaB_{11}H_{13}$ are completely insoluble in the mixture of THF and DME, facilitating their isolation from the target product. No formation of $THF{\cdot}BH_3$ was observed upon the synthesis, indicating that borane dimethyl sulfide is more stable under ambient conditions, even in the presence of THF, which is a stronger Lewis base. Using 3 x 10 mL of THF for washing the as-synthesized samples allowed for an efficient removal of residual BH_4^- from the obtained product, as shown by ^{11}B NMR spectra (Figure S10). The reaction in THF/DME mixtures 1:1 (v/v) ratio furthermore led to the formation of less B−H impurities and the absence of $B_{12}H_{12-x}^{2-}$ anions (Figure 2). This can be attributed to the higher boiling point of DME compared to THF, and to the more stable bidentate coordination mode of DME towards Ca^{2+}.

5.3.2. Desolvation of crude $CaB_{12}H_{12}$

The PXRD patterns revealed that the product obtained in the solvent mixture composed of THF and DME is a crystalline phase of

DME-solvated $CaB_{12}H_{12}$, as shown in Figures S11 and S12, regardless of the presence of THF. Heating up the sample up to 180 °C systematically leads to the formation of $CaB_{12}H_{12}$·2DME, which structure is show in Figure 3, without further desolvation. Direct attempts to remove THF and DME from the obtained $CaB_{12}H_{12}$ at 200 °C proved impractical (Figure S13).[36]

To remove THF and DME, substitution with H_2O was explored, as hydrated $CaB_{12}H_{12}$ is known to be easily desolvated, and the boiling point of water is higher than that of both ethers. The solvent exchange procedure was completed by drying the filtrate obtained from the heat treatment of DME-solvated $CaB_{12}H_{12}$ in 15 ml H_2O under vacuum, and the resulting dried samples were subjected to FTIR analysis (Figure 4, Figure S14-16). Typical signals of the $B_{12}H_{12}^{2-}$ anion were observed for all samples, including vibrations of the B−B bond at 1074 cm^{-1}, B−H stretching at 2467 cm^{-1}, and B−H bending at 713 cm^{-1}. In the FTIR spectra of Figure 4a, the absorption bands within the 3000−2750 cm^{-1} and 1500−1300 cm^{-1} correspond to the C−H and C−O stretching modes of DME or THF, respectively.[17] The disappearance of these bands and the simultaneous appearance of O−H stretching at 3700−3500 cm^{-1} and 1700−1600 cm^{-1} in Figure 4b indicates successful removal of all coordinated ethers and their exchange with H_2O. Upon drying the samples at 200 °C for 12 h, these O−H bands disappear from the FTIR spectrum (Figure 4c), proving that heating at this temperature enables effective removal of all the coordinated H_2O.

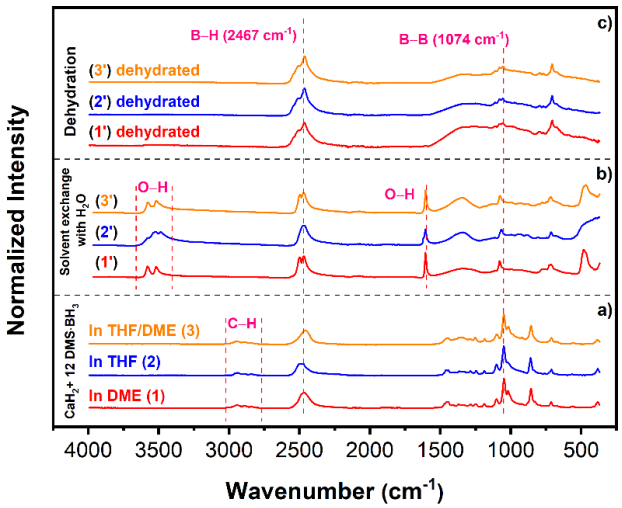

Figure 4. FTIR spectra of the (a) as-synthesized samples obtained in DME, THF, THF/DME at 120 °C in an autoclave, (b) after solvent exchange with H_2O and (c) after thermal dehydration at 200 °C under vacuum.

Furthermore, all as-synthesized, solvent-exchanged and dehydrated samples were analyzed by PXRD (Figure 5). The as-prepared samples display diffraction peaks expected for $CaB_{12}H_{12}$·2DME, with some additional peaks supposedly assigned to solvated species containing $B_{11}H_{13}^{2-}$. Upon solvent exchange with water, PXRD patterns reveal that the main phase is $CaB_{12}H_{12}$·$3H_2O$ in all samples.[35] Upon thermal dehydration, all samples display similar diffraction patterns, corresponding to pure $CaB_{12}H_{12}$, with some small impurity peaks for the product obtained from the synthesis in DME. Our repeat experiments (see Figure 5b) indicate that this process is reproducible. [35]

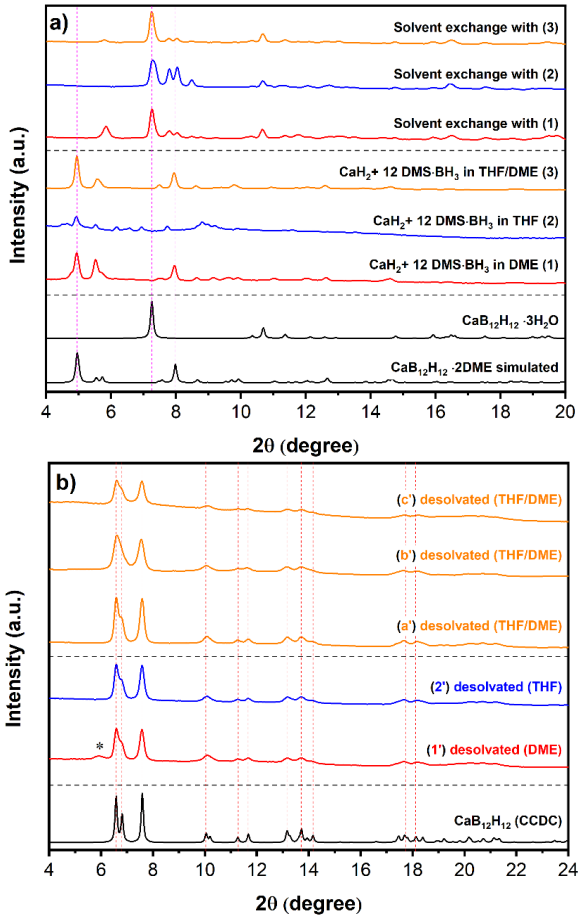

Figure 5. PXRD patterns of the as-synthesized samples obtained in DME, THF, THF/DME at 120 °C in an autoclave (a) before and after solvent exchange with H_2O and b) after thermal dehydration at 200 °C under vacuum, (a'), (b') and (c') are repeated experiments on desolvation of sample obtained from mixing ethers.

5.3.3. Adapting the synthesis towards $MgB_{12}H_{12}$

We investigated whether our new synthetic approach to synthesize $CaB_{12}H_{12}$ could be modified to obtain $MgB_{12}H_{12}$. This was first attempted by starting from both anhydrous and solvated $Mg(BH_4)_2$, which were reacted with $DMS{\cdot}BH_3$ at 120 °C for 24 h in ethers

(monoglyme, diglyme, or mixture of ethers) as solvents. ^{11}B NMR spectra of all obtained samples (Figure 6) show a doublet at −15.2 ppm, indicating the formation of $B_{12}H_{12}^{2-}$, together with the signal of the $B_{12}H_{12-x}^{2-}$ at −17 ppm. Other species, such as $B_3H_8^-$ (−29.2 ppm), $B_{10}H_{10}^{2-}$ (−0.5 and −28.5 ppm), and $B_{11}H_{11}^{2-}$ (−16.5 ppm) were also observed. It is noteworthy that when $Mg(BH_4)_2 \cdot {}^1/_2$ DMS was used as starting material, a black, insoluble material was formed.

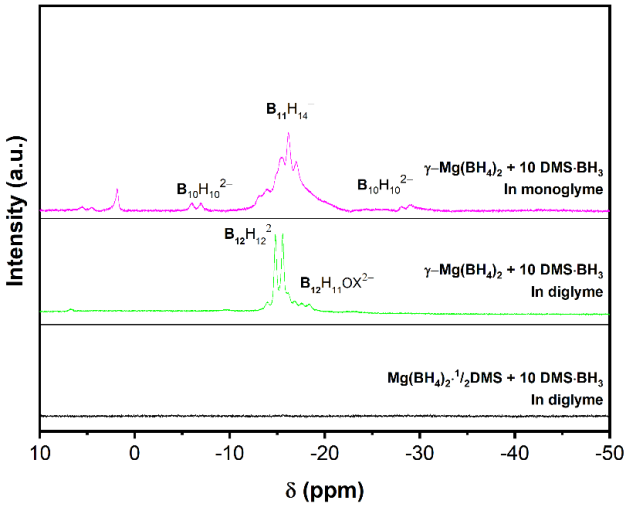

Figure 6. Proton-coupled ^{11}B NMR spectra of the solid precipitates formed under various reaction conditions between $Mg(BH_4)_2$ (solvate) and 10 equiv. DMS·BH_3 in ethereal solvents (measurements performed on samples dissolved in DMSO-d_6).

Experiments were conducted at various temperatures in a Schlenk flask starting from $Mg(BH_4)_2$, with higher temperatures favoring the conversion of BH_4^-, as shown by ^{11}B NMR (Figure 7). However, the main generated anion was $B_{12}H_{11}S(CH_3)_2^-$, characterized by a singlet at around −9 ppm, attributed to B−S bonds, and a quartet at around −15 ppm, accounting for the remaining 10 boron atoms, even when the reaction was carried out in an autoclave. The ^{1}H NMR spectrum of the sample is also consistent with earlier

reports on $[B_{12}H_{11}S(CH_3)_2][S(CH_3)_3]$, displaying two resonances in a 3:2 ratio (Figure S17, 18), corresponding to the number of methyl groups in the $S(CH_3)_3^+$ and SMe_2 substituents.[39] No signals were however observed for Mg-based borates, suggesting that they were not formed or that the corresponding signals may be overlapped with the ones of $B_{12}H_{11}S(CH_3)_2^-$.

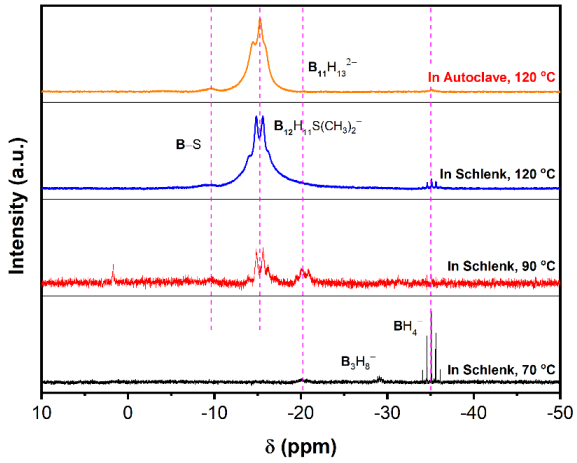

Figure 7. Proton-coupled ^{11}B NMR spectra of the solid precipitates formed under various reaction conditions between $Mg(BH_4)_2$ (solvate) and 10 equiv. $DMS{\cdot}BH_3$ in toluene (measurements performed on samples dissolved in DMSO-d_6). Signals of $MgB_{12}H_{12}$ are overlapped with $B_{12}H_{11}S(CH_3)_2^-$.

Due to the strong coordination affinity between Mg and O atoms, the removal of solvents from solvated $MgB_{12}H_{12}$ poses a significant challenge. Attempts to realize desolvation through similar procedures as the ones described above for $CaB_{12}H_{12}$ were unsuccessful with $MgB_{12}H_{12}$ ether solvates. It is noteworthy that current described synthesis procedures for $MgB_{12}H_{12}$ are therefore generally conducted without solvents to avoid the need of a desolvation step. As an alternative, we further pushed the limits of our synthetic approach by attempting the synthesis in toluene as non-coordinating solvent. Final

confirmation that $[SMe_3][B_{12}H_{11}S(CH_3)_2]$ was formed was given by isolation of a single crystal from the mixture obtained after reaction in toluene at 120 °C, The obtained sample consisted of a mixture of needle shaped crystals, which were used for the analysis, and hygroscopic amorphous compounds. The solved structure is displayed in Figure 8, the structure exhibit disorder of the $[SMe_3]^+$ moiety.[32]

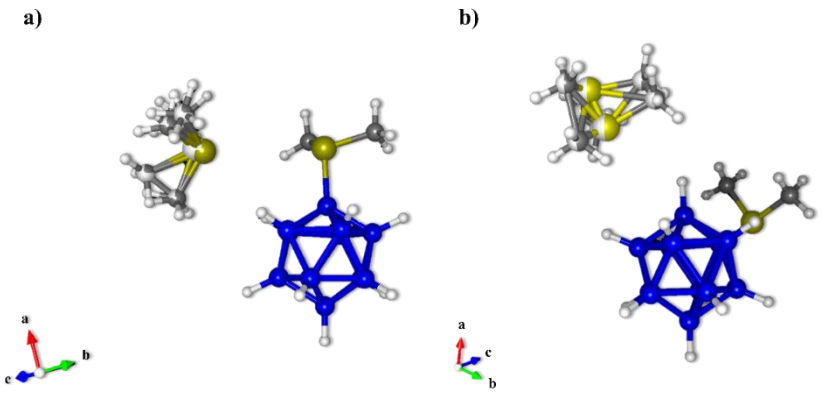

Figure 8. Single crystal structure of (a) LT phase (100 K) and (b) RT (298 K) phase of $[(CH_3)_3S][B_{12}H_{11}S(CH_3)_2]$. Color code: S, yellow; B, dark blue; H, white; C: dark grey.

5.4. Conclusions

In conclusion, we developed a novel solvothermal synthesis approach for producing high-purity $CaB_{12}H_{12}$ from cheap CaH_2 and relatively safe $DMS{\cdot}BH_3$ as boron source, using a carefully selected combination of THF and DME as solvents. This method successfully eliminates the usually encountered problem of the simultaneous formation of other unwanted borane clusters, while simultaneously ensuring the solubility of smaller borane clusters. This facilitates the interaction of the latter with calcium hydride and the $DMS{\cdot}BH_3$ complex, which is required for the formation of the final product. In addition, the presence of dimethoxyethane (DME) in the reaction improves coordination between the solvent and Ca^{2+}, lowering the risk of producing $B_{12}H_{12-x}^{2-}$ anions. This new facile synthetic technique yields $CaB_{12}H_{12}$ samples that are not only X-ray pure, but also show high purity ^{11}B NMR spectra.

To broaden the scope of our synthetic approach, we attempted to synthesize $MgB_{12}H_{12}$. However, difficulties arose due to the strong coordination between Mg^{2+} ions and oxygen donors, which resulted in the irreversible coordination to ethers, limiting their use as solvents. Furthermore, utilizing toluene as the solvent led to the insolubility of borohydrides and spurred the self-condensation of $DMS{\cdot}BH_3$, leading to the formation of $B_{12}H_{11}S(CH_3)_2^-$, as demonstrated by the formation of $(CH_3)_3S$ $B_{12}H_{11}S(CH_3)_2$ single crystals. Future work could delve deeper into selective production or separation of this material and investigate its possible applications.

5.5. References

(1) Gür, T. M. Review of Electrical Energy Storage Technologies, Materials and Systems: Challenges and Prospects for Large-Scale Grid Storage. *Energy Environ. Sci.* **2018**, *11* (10), 2696–2767.

(2) He, L.; Li, H.-W.; Nakajima, H.; Tumanov, N.; Filinchuk, Y.; Hwang, S.-J.; Sharma, M.; Hagemann, H.; Akiba, E. Synthesis of a Bimetallic Dodecaborate $LiNaB_{12}H_{12}$ with Outstanding Superionic Conductivity. *Chem. Mater.* **2015**, *27* (16), 5483–5486.

(3) He, L.; Lin, H.; Li, H.-F.; Filinchuk, Y.; Zhang, J.; Liu, Y.; Yang, M.; Hou, Y.; Deng, Y.; Li, H.-W.; Shao, H.; Wang, L.; Lu, Z. $Na_3NH_2B_{12}H_{12}$ as High Performance Solid Electrolyte for All-Solid-State Na-Ion Batteries. *J. Power Sources* **2018**, *396*, 574–579.

(4) Hagemann, H. Boron Hydrogen Compounds: Hydrogen Storage and Battery Applications. *Molecules* **2021**, *26* (24), 7425.

(5) Fouquet, R. Path Dependence in Energy Systems and Economic Development. *Nat. Energy* **2016**, *1* (8), 1–5.

(6) Kisu, K.; Dorai, A.; Kim, S.; Hamada, R.; Kumatani, A.; Horiguchi, Y.; Sato, R.; Sau, K.; Takagi, S.; Orimo, S. Fast Divalent Conduction in $MB_{12}H_{12}{\cdot}12H_2O$ (M = Zn, Mg) Complex Hydrides: Effects of Rapid Crystal Water Exchange and Application for Solid-State Electrolytes. *J. Mater. Chem. A Mater.* **2022**, *10* (46), 24877–24887.

(7) Campos dos Santos, E.; Sato, R.; Kisu, K.; Sau, K.; Jia, X.; Yang, F.; Orimo, S.; Li, H. Explore the Ionic Conductivity Trends on $B_{12}H_{12}$ Divalent Closo-Type Complex Hydride Electrolytes. *Chem. Mater.* **2023**, *35* (15), 5996–6004.

(8) Koettgen, J.; Bartel, C. J.; Shen, J.-X.; Persson, K. A.; Ceder, G. First-Principles Study of $CaB_{12}H_{12}$ as a Potential Solid-State Conductor for Ca. *Phy. Chem. Chem. Phys.* **2020**, *22* (47), 27600–27604.

(9) Carter, T. J.; Mohtadi, R.; Arthur, T. S.; Mizuno, F.; Zhang, R.; Shirai, S.; Kampf, J. W. Boron Clusters as Highly Stable Magnesium-Battery Electrolytes. *Angew. Chemie* **2014**, *126* (12), 3237–3241.

(10) Huang, Z.; Wang, S.; Dewhurst, R. D.; Ignat'ev, N. V.; Finze, M.; Braunschweig, H. Boron: Its Role in Energy-Related Processes and Applications. *Angew. Chemie - Int. Ed.* **2020**, *59* (23), 8800–8816.

(11) Hansen, B. R. S.; Paskevicius, M.; Li, H.-W.; Akiba, E.; Jensen, T. R. Metal Boranes: Progress and Applications. *Coord. Chem. Rev.* **2016**, *323*, 60–70.

(12) Knoth, W. H.; Sauer, J. C.; Balthis, J. H.; Miller, H. C.; Muetterties, E. L. Chemistry of Boranes. XXX. Carbonyl Derivatives of $B_{10}H_{10}^{2-}$ and $B_{12}H_{12}^{2-}$. *J. Am. Chem. Soc.* **2002**, *89* (19), 4842–4850.

(13) Li, H.-W.; Miwa, K.; Ohba, N.; Fujita, T.; Sato, T.; Yan, Y.; Towata, S.; Chen, M. W.; Orimo, S. Formation of an Intermediate Compound with a $B_{12}H_{12}$ Cluster: Experimental and Theoretical Studies on Magnesium Borohydride $Mg(BH_4)_2$. *Nanotechnology* **2009**, *20* (20), 204013.

(14) Hwang, S.-J.; C. Bowman, R.; W. Reiter, J.; J.; L. Soloveichik, G.; Zhao, J.-C.; Kabbour, H.; C. Ahn, C. NMR Confirmation for Formation of $[B_{12}H_{12}]^{2-}$ Complexes during Hydrogen Desorption from Metal Borohydrides. J. Phys. Chem. C **2008**, *112* (9), 3164–3169.

(15) Ellis, I. A.; Gaines, D. F.; Schaeffer, R. A Convenient Preparation of $B_{12}H_{12}^{2-}$ Salts. *J. Am. Chem. Soc.* **2002**, *85* (23), 3885–3885.

(16) Pitochelli, A. R.; Hawthorne, M. F. The Isolation of the Icosahedral $B_{12}H_{12}^{-2}$ Ion. *J. Am. Chem. Soc.* **1960**, *82*(12), 3228–3229.

(17) Wang, J.; Steenhaut, T.; Li, H.-W.; Filinchuk, Y. High Yield Autoclave Synthesis of Pure $M_2B_{12}H_{12}$ (M = Na, K). *Inorg. Chem.* **2023**, 62 (5), 2153–2160.

(18) Jing, Y.; Wang, X.; Han, H.; Liu, X.-R.; Yu, X.-C.; Chen, X.-M.; Wei, D.; Wang, L.-S.; Chen, X. Selective Synthesis of the $B_{11}H_{14}^-$ and $B_{12}H_{12}^{2-}$ Borane Derivatives and the General Mechanisms of the B-H Bond Condensation. *Sci. China Chem.* **2023**, *67*(3).

(19) He, L.; Li, H.-W.; Tumanov, N.; Filinchuk, Y.; Akiba, E. Facile Synthesis of Anhydrous Alkaline Earth Metal Dodecaborates $MB_{12}H_{12}$ (M = Mg, Ca) from $M(BH_4)_2$. *Dalton Trans.* **2015**, *44*, 15882–15887.

(20) Sharma, M. Experimental and Theoretical Studies of Boron and Hydrogen Containing Compounds in Relation to Potential Hydrogen Storage and Ionic Conduction Applications. **2017**.

(21) Yan, Y.; Au, Y. S.; Rentsch, D.; Remhof, A.; de Jongh, P. E.; Züttel, A. Reversible Hydrogen Storage in $Mg(BH_4)_2$/Carbon Nanocomposites. *J. Mater. Chem. A Mater.* **2013**, *1* (37), 11177–11183.

(22) Chen, X.; Liu, Y.; Alexander, A.; Gallucci, J. C.; Hwang, S.; Lingam, H. K.; Huang, Z.; Wang, C.; Li, H.; Zhao, Q.; Ozkan, U. S.; Shore, S. G.; Zhao, J. Desolvation and Dehydrogenation of Solvated Magnesium Salts of Dodecahydrododecaborate: Relationship between Structure and Thermal Decomposition. *Chem. – Eur. J.* **2014**, *20* (24), 7325–7333.

(23) Richter, B.; B. Grinderslev, J.; T. Møller, K.; Paskevicius, M.; R. Jensen, T. From Metal Hydrides to Metal Borohydrides. *Inorg. Chem.* **2018**, *57* (17), 10768–10780.

(24) Moury, R.; Gigante, A.; Hagemann, H. An Alternative Approach to the Synthesis of NaB_3H_8 and $Na_2B_{12}H_{12}$ for Solid Electrolyte Applications. *Int. J. Hydrogen Energy* **2017**, *42* (35), 22417–22421.

(25) Chen, X.-M.; Ma, N.; Zhang, Q.-F.; Wang, J.; Feng, X.; Wei, C.; Wang, L.-S.; Zhang, J.; Chen, X., Elucidation of the Formation Mechanisms of the Octahydrotriborate Anion ($B_3H_8^-$) through the Nucleophilicity of the B–H Bond. *J. Am. Chem. Soc.* **2018,** *140* (21), 6718–6726.

(26) Souza, D. H. P.; Moller, K. T.; Moggach, S. A.; Humphries, T. D.; D'Angelo, A. M.; Buckley, C. E.; Paskevicius, M. Hydrated Alkali-$B_{11}H_{14}$ Salts as Potential Solid-State Electrolytes. *J. Mater. Chem. A* **2021**, *9*, 15027–15037.

(27) Jing, Y.; Wang, X.; Han, H.; Liu, X.-R.; Yu, X.-C.; Chen, X.-M.; Wei, D.; Wang, L.-S.; Chen, X. Selective Synthesis of the $B_{11}H_{14}^-$ and $B_{12}H_{12}^{2-}$ Borane Derivatives and the General Mechanisms of the B-H Bond Condensation. *Sci. China Chem.* **2023**, *67*(3).

(28) Filinchuk, Y.; Richter, B.; Jensen, T. R.; Dmitriev, V.; Chernyshov, D.; Hagemann, H. Porous and Dense Magnesium Borohydride Frameworks: Synthesis, Stability, and Reversible Absorption of Guest Species. *Angew. Chemie* **2011**, *123* (47), 11358–11362.

(29) Sivaev, I. B.; Bregadze, V. I.; Kuznetsov, N. T. Derivatives of the Closo-Dodecaborate Anion and Their Application in Medicine. *Russ. Chem. B+* **2002**, *51* (8), 1362–1374.

(30) Pylypko, S.; Ould-Amara, S.; Zadick, A.; Petit, E.; Chatenet, M.; Cretin, M.; Demirci, U. B. Liquid Anodic Fuel. *Appl. Catal. B* **2018**, *222*, 1–8.

(31) Souza, D. H. P.; D'Angelo, A. M.; Humphries, T. D.; Buckley, C. E.; The Highly Stable Aqueous Solution of Sodium Dodecahydro-Closo-Dodecaborate $Na_2B_{12}H_{12}$ as a Potential Paskevicius, M. $Na_2B_{11}H_{13}$ and $Na_{11}(B_{11}H_{14})_3(B_{11}H_{13})_4$ as Potential Solid-State Electrolytes for Na-Ion Batteries. *Dalton Trans.* **2022**, *51* (36), 13848–13857.

(32) Hamilton, E. J. M.; Jordan; Meyers, E. A.; Shore, S. G. One-Step Preparation of Dimethyl Sulfide Substituted Icosahedral Boranes: The Crystal and Molecular Structures of 1,7-$(SMe_2)_2B_{12}H_{10}$, 1,12-$(SMe_2)_2B_{12}H_{10}$, and $[SMe_3][B_{12}H_{11}(SMe_2)]$·MeCN. *Inorg. Chem.* **1996**, 35 (18), 5335–5341.

(33) Kultyshev, R. G.; Liu, J.; Meyers, E. A.; Shore, S. G. Synthesis and Characterization of Sulfide, Sulfide−Sulfonium, and Bissulfide Derivatives of $[B_{12}H_{12}]^{2-}$. Additivity of Me_2S and MeS^- Substituent Effects in ^{11}B NMR Spectra of Disubstituted Icosahedral Boron Clusters. *Inorg. Chem.* **2000**, *39* (15), 3333–3341.

(34) https://www.sigmaaldrich.com/BE/.

(35) Stavila, V.; Her, J.-H.; Zhou, W.; Hwang, S.-J.; Kim, C.; Ottley, L. A. M.; Udovic, T. J. Probing the Structure, Stability and Hydrogen Storage Properties of Calcium Dodecahydro-Closo-Dodecaborate. *J. Solid State Chem.* **2010**, *183* (5), 1133–1140.

(36) Filinchuck, Y.; Ronnebro, E.; Chandra, D. Crystal Structures and Phase Transformations in $Ca(BH_4)_2$. *Acta Mater.* **2009**, *57* (3), 732–738.

(37) Volkov, O.; Paetzold, P. The Chemistry of the Undecaborates. *J. Organomet. Chem.* **2003**, *680* (1–2), 301–311.

(38) Volkov, O.; Dirk, W.; Englert, U.; Paetzold, P. Undecaborates $M_2[B_{11}H_{11}]$: Facile Synthesis, Crystal Structure, and Reactions. *Z. Anorg. Allg. Chem.* **1999**, *625* (7), 1193–1200.

(39) Lane, C. F. Reduction of Organic Compounds with Diborane. Chem. Rev. 1976, 76 (6), 773–799.

Chapter 6. Conversion of Carbon Dioxide into Hydrocarbons by Reaction with γ-$Mg(BH_4)_2$

Jian Wang,[a] Nikolay Tumanov,[a] Antoine Raillliet,[a] Jakob Grinderslev,[b] Jørgen Skibsted,[b] Torben René Jensen,[b] Yaroslav Filinchuk[a]*

[a] *Institute of Condensed Matter and Nanosciences, Université catholique de Louvain, 1348 Louvain-la-Neuve, Belgium*

[b] *Department of Chemistry and Interdisciplinary Nanoscience Center, Aarhus University, Langelandsgade 140, Aarhus C 8000, Denmark*

** Corresponding Author. E-mail: yaroslav.filinchuk@uclouvain.be (Y. Filinchuk)*

Chapter 6

Abstract

The gamma-phase of magnesium borohydride, γ-$Mg(BH_4)_2$, features a nanoporous framework structure with hydride atoms accessible to gas molecules. In this chapter, we illustrate the ability of γ-$Mg(BH_4)_2$ to adsorb CO_2 under ambient conditions, followed by its reduction to formate and methoxy compounds. Both mechanochemical and thermally induced solid-gas reactions between γ-$Mg(BH_4)_2$ and CO_2 lead to the formation of formatoborohydride ($[H_{4-x}B(OCHO)_x]^-$) intermediates. These reactions were investigated through thermogravimetric analysis (TGA), Infrared spectroscopy (FTIR) and Nuclear magnetic resonance (NMR) measurements.

6.1. Introduction

Carbon dioxide is the most important long-lived greenhouse gas contributing to global climate change.[1] The manufacture of valuable hydrocarbons from CO_2, a product arising from combustion processes, would encourage its recovery and help to avoid its emission, thereby forming a carbon-neutral cycle.[2–4] Although electrochemical and thermal catalytic reduction of carbon dioxide is of significance for the development of carbon recycling technologies at present. However, achieving complete conversions typically demands high temperatures (250–300 °C) and pressures (50–100 atm), and utilization of highly efficient heterogeneous catalysts.[5] An ideal scheme under mild conditions for reducing CO_2 into energy molecules remains as desirable target.[6]

A potentially alternative route attracting growing attention is the reduction of CO_2 by metal hydrides at ambient conditions.[7–11] These hydrides contains negatively charged hydrogen (H^-), which exhibits stronger reducibility compared to molecular hydrogen, allowing for the reduction of CO_2 without the need for a catalyst and an extra hydrogen source.[12] The first report of the reaction between hydrides and CO_2 can dates back to 1955, involving sodium borohydride ($NaBH_4$) and CO_2 in dimethyl ether at room temperature (RT), yielding triformatoborohydride ($[HB(OCHO)_3]^-$) as main product, which converts to formic acid upon treatment with sulfuric acid.[13] In the following decades, the interactions of alanates (AlH_4^-) or borohydrides (BH_4^-) with CO_2 have been preliminarily studied. It has already been reported that valuable chemical products such as formic acid, acyloxyborohydrides and formatomethoxyborate or

triformatoborohydride are formed in the reaction between CO_2 and hydrides.[13–16]

The gamma phase of magnesium borohydride, (γ-$Mg(BH_4)_2$), is notable for being the first hydride with functional porosity of 33% in its structure, featuring a high theoretical surface area of 1160 m^2/g. Unlike other known porous solids, its framework lacks open metal sites for gas molecule coordination, but its pores are comprised of hydridic hydrogen atoms, showing excellent adsorption capacities for small molecules such as hydrogen, methane and CH_2Cl_2.[3,17] Earlier works have shown that γ-$Mg(BH_4)_2$ exhibits significant CO_2 adsorption capacity (theoretical CO_2 uptake of 37 mmol/g, calculated based 1:1 reaction between BH_4^- unit with CO_2), and possible to reduce CO_2 into formate and alkoxide-like compounds with unprecedentedly fast kinetics at 30 °C and 1 bar.[18] More recently, the CO_2 uptake by γ-$Mg(BH_4)_2$ demonstrated rapid CO_2 uptake of up to 19.9 mmol/g at low partial pressures and temperatures, with enhanced CO_2 uptake observed from porous nanocrystals on reduced graphene oxides.[16,18] Further investigation to understand the reaction pathway and intermediate products of CO_2 in the porous γ-$Mg(BH_4)_2$ are required and are currently being carried out in this work.

6.2. Experimental Section

Synthesis of *γ*-$Mg(BH_4)_2$.

The synthesis of *γ*-$Mg(BH_4)_2$ was performed using a modified procedure from the reference.[17] Typically, to a stirred solution of 3 mL borane dimethyl sulfide complex ($(CH_3)_2S{\cdot}BH_3$, 10−10.2 M, 30 mmol) in 15 mL toluene in a 100 ml Schlenk flask (modified with a filter) under inert atmosphere, subsequently 9.5 mL Di-*n*-butylmagnesium solution ($Mg(n\text{-}Bu)_2$, 1 M solution in heptane) was added at room temperature, the adding of $Mg(n\text{-}Bu)_2$ was done dropwise and slowly, the exothermic reaction is carefully monitored by adding a 5-minute break for every 1 ml $Mg(n\text{-}Bu)_2$ added. After stirring the reaction solution at room temperature for 1.5 ~ 2 h, the reaction mixture was filtered using a Schlenk filtration apparatus and subsequently washed with toluene (3 × 10 mL). The solvated product $Mg(BH_4)_2{\cdot}½S(CH_3)_2$ was obtained as a white crystalline solid, collected and dried for 12−16 hours at room temperature on a vacuum line ($2{\cdot}10^{-2}$ mbar). Then the flask was placed in oil bath and heated to 72 °C. Solvent removal was done by using a turbo pump reaching residual pressures down to 10^{-5} mbar for 60 hours, yielding porous crystalline *γ*-$Mg(BH_4)_2$.

The isotopic, *γ*-$Mg(^{11}BD_4)_2$, containing deuterium and ^{11}B, was prepared for NPD experiments, by starting with $^{11}BD_3{\cdot}DMS$ for the synthesis.

The dense amorphous $Mg(BH_4)_2$ (am-$Mg(BH_4)_2$) was prepared using the referenced method. This involved compressing the γ-$Mg(BH_4)_2$ at 1 GPa.[19] The entire compression operation lasted about 5 minutes. Subsequently, the die containing the sample was returned

inside the glovebox for extraction of the pellet, which was then hand-milled into powder for further use.

More experimental section can be seen in **Appendix IV**

6.3. Results and Conclusions

6.3.1. Thermally induced reactions

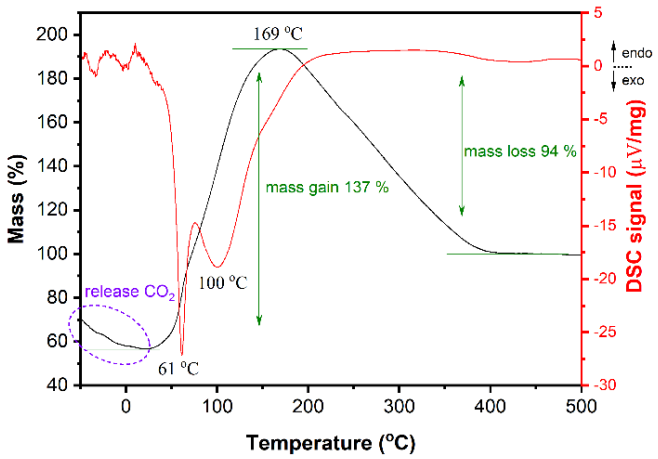

Figure 1. TGA-DSC analysis of the solid gas reaction of

γ-$Mg(BH_4)_2$ with CO_2.

To assess the reactivity of γ-$Mg(BH_4)_2$ with CO_2, the reaction was thermally initiated in a CO_2/He mixed atmosphere with a 20/80 ratio at a flow rate of 100 mL/min. As shown in Figure 1, the thermalgravimetric analysis (TGA) combined with mass spectrum (MS) was applied to examine the gas phase products. About 20% weight loss was observed at the initial heating stage (from −50 °C to 25 °C), which is attributed to the desorption of physically absorbed CO_2 within the porous structure of γ-$Mg(BH_4)_2$. Subsequently, a

significant smooth weight gain occurring between 25 °C and 169 °C, accompanied by two prominent exothermic peaks in the differential scanning calorimetry (DSC) curve, indicting the reactions between CO_2 with γ-$Mg(BH_4)_2$ (exothermic at 61 °C) and the active intermediates (exothermic at 100 °C), respectively. The total uptake of 137% of mass gain, showed a CO_2 uptake of 13.1 mmol/g.

As shown in mass spectra presented in Figure S1, signals corresponding to methanol (m/z = 31), methyl formate (m/z = 60), and $B(OMe)_3$ in the gas phase (m/z = 72, 73, 89) were detected during the weight loss process when the temperature higher than 169 °C, which is generated from the decomposition of the solid intermediates.

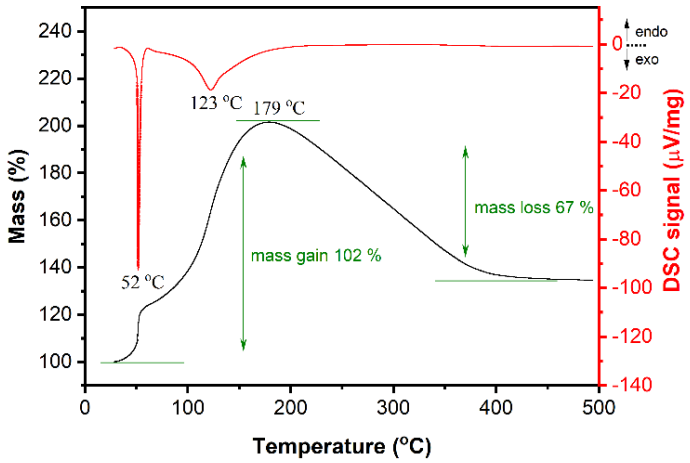

Figure 2. TGA-DSC analysis of the solid gas reaction of am-$Mg(BH_4)_2$ with CO_2.

The sample of γ-$Mg(BH_4)_2$ obtained in a solid comprises both porous crystalline and dense polymorph (amorphous) phase from synthetic process, distinguishing the contribution of each phase to the CO_2 reducing ability is of great importance. To facilitate a direct comparison between these phases, the amorphous $Mg(BH_4)_2$ (am-$Mg(BH_4)_2$) was prepared by compressing the porous γ-$Mg(BH_4)_2$ at 1

GPa into nonporous phase, as outlined in the experimental section.

As shown in Figure 2, the TGA and DSC curves shows that the structure collapsed am-$Mg(BH_4)_2$ exhibit enhanced reactivity compared to its porous counterparts. Typically, the TGA curve representing a distinct mass increase of 22% along with an abrupt heat release at around 52 °C on the DSC curve. The evolution of methanol (m/z = 31), formic acid (m/z = 29), and $B(OMe)_3$ (m/z = 72, 73, 89) in the gas phases are observed in the mass spectra (Figure S2), indicating the as formed intermediate between $Mg(BH_4)_2$ and CO_2 is quickly decomposed due to the intense heat release from the reaction. The reaction between CO_2 and am-$Mg(BH_4)_2$, is likely due to the intense heat generated from the reaction triggered a phase transition of am-$Mg(BH_4)_2$ back to porous γ-$Mg(BH_4)_2$ phase, and which subsequently react with CO_2 aggressively.[19] Upon interaction with CO_2, the second weight gain centered at around 123 °C, which can be attributed to the reaction with dense phase of $Mg(BH_4)_2$, as formed due to a phase transition induced by intense heat generated from earlier step. The total uptake of 102% of mass gain, indicating CO_2 uptake of 11.5 mmol/g.

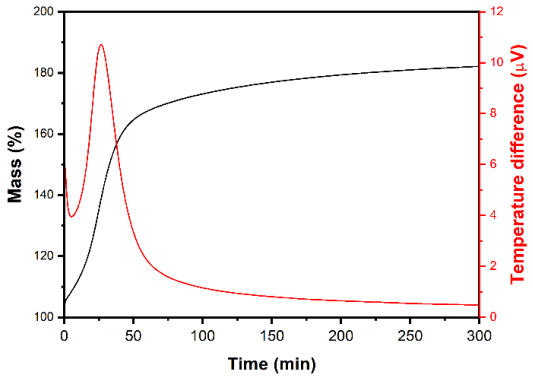

Figure 3. TG-DTA analysis of the solid gas reaction of γ-$Mg(BH_4)_2$ in constant CO_2 flow.

The reaction of γ-$Mg(BH_4)_2$ in a constant CO_2 flow was monitored by means of TG combined with different thermal analysis (DTA) in a constant CO_2 flow at room temperature. As shown in Figure 3, the TG curve shows a total mass increase about 80% during the measurement (300 minutes), indicating a CO_2 capacity of 10.1 mmol/g, which is slightly lower than earlier report on a maximum CO_2 uptake of 12 mmol/g at under 1 bar of CO_2 at 30 °C for 7 days.[18] The CO_2 uptake is not thermodynamic equilibrium in our conditions. A difference on the system temperature is observed after γ-$Mg(BH_4)_2$ exposed in CO_2 for 25 minutes, which can be ascribed to chemical equilibrium of CO_2 molecules in γ-$Mg(BH_4)_2$. The distribution of the CO_2 molecules along the channels of the porous polymorph of magnesium borohydride was determined by X-ray and neutron diffraction techniques in Figure 4.

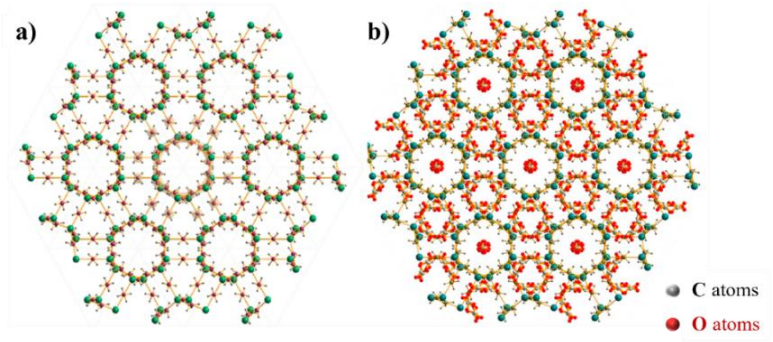

Figure 4. Fragments of the crystal structures of (a) porous γ-$Mg(BH_4)_2$ and with (b) adsorbed CO_2.

As shown in Figure 4a, in the crystal structure of γ-$Mg(BH_4)_2$, each Mg ion is coordinated to four BH_4^- groups, forming a distorted tetrahedron. This arrangement results in an assembly with symmetry characterized by the space group Ia-3d. The continuous measurement with CO_2 uptake by γ-$Mg(BH_4)_2$ in Figure 4b does not induce any

phase transition, while CO_2 atoms in the structure can be occupied by two distinct adsorption sites.

6.3.2. Mechanochemically induced reactions

The mechanochemical reaction between γ-$Mg(BH_4)_2$ and solid CO_2 was carried out in a stainless steel grinding bowl with stainless steel balls. The pressure and temperature during reaction were monitored, as represented in Figure S3. The reaction between γ-$Mg(BH_4)_2$ and solid CO_2 occurred after 6 milling cycles (36 minutes). The proton coupled and decoupled ^{11}B NMR spectra of the obtained grey product in Figure S 4a representing a dominating quintet at −35.1 ppm, which is characteristic peaks to the BH_4^- anion. Minor signals were observed at lower field at −9.41, 0.96 ppm, which can be assigned four coordinated $[H_3B(OCHO)]^-$ anion. A board singlet peaks observed at around can be assigned to tri-coordinated boron anion. The proton decoupled ^{11}B NMR spectrum exhibits a negligible signal at around -29.1 ppm, which can be assigned to the $B_3H_8^-$ anion. The ^{13}C NMR (Figure S4c) spectrum of the product contains a negligible singlet signal with a very low intensity at 48.62 ppm, in combination of the doublet at 3.16 ppm and quintet at 4.01 ppm observed in ^1H NMR spectrum (Figure S4d), which can be assigned to methanol (CH_3OH). The zoomed ^1H NMR spectrum of the product contains sharp peaks at 8.04, 8.14 and 8.22 ppm, assigned to the OCHO protons in $[HB(OCHO)_3]^-$, $[H_2B(OCHO)_2]^-$ and $[H_3B(OCHO)]^-$ anions, respectively. Signals for formatoborohydride were not observed in ^{11}B and ^{13}C NMR spectra, is likely due to boron and carbon nuclei have smaller nuclear magnetic moments compared with hydrogen, making them relatively less sensitive.

Similar reaction performed in a closed system at 0.5 bar CO_2 with γ-$Mg(BH_4)_2$ in different reaction times, the FTIR spectra of γ-$Mg(BH_4)_2$ before and after interact with CO_2 (Figure 5) indicate the simultaneous formation of formate (1630 cm^{-1}) and methoxy (3000−2800 cm^{-1}) species from the reaction, along with the consume of BH_4^- (bands at 2270 cm^{-1}), the observation of B−H stretchings at 2479 cm^{-1} indicating formation of closo-borates. Additionally, Figure S5 illustrates the PXRD patterns of γ-$Mg(BH_4)_2$ before and after the reaction with CO_2. The disappearance of most diffraction peaks observed in the pattern of γ-$Mg(BH_4)_2$ suggests the complete collapse of the porous crystalline structure and the formation of a amorphous intermediate phase.

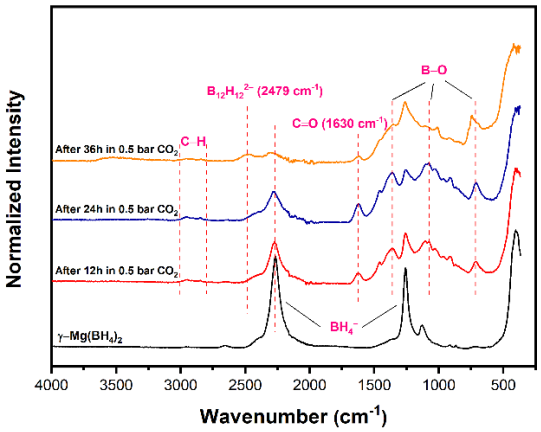

Figure 5. FTIR spectra of γ-$Mg(BH_4)_2$ before and after interaction with 0.5 bar CO_2 at RT and for 12 h, 24 h and 36 h.

The samples were further studied using ^{1}H, $^{11}B\{^{1}H\}$, and ^{13}C cross-polarization magic angle spinning (CP-MAS) solid-state NMR spectroscopy. Figure 6a shows the ^{1}H NMR spectrum in, three main broad singlets centered at 0, 5, and 11 ppm are observed, which is corresponding to the protons from methoxy (CH_3OX), formate

(HCOOX), and formylhydroborate $[H_xB(OCHO)_{4-x}]^-$ groups, respectively. [15,18]

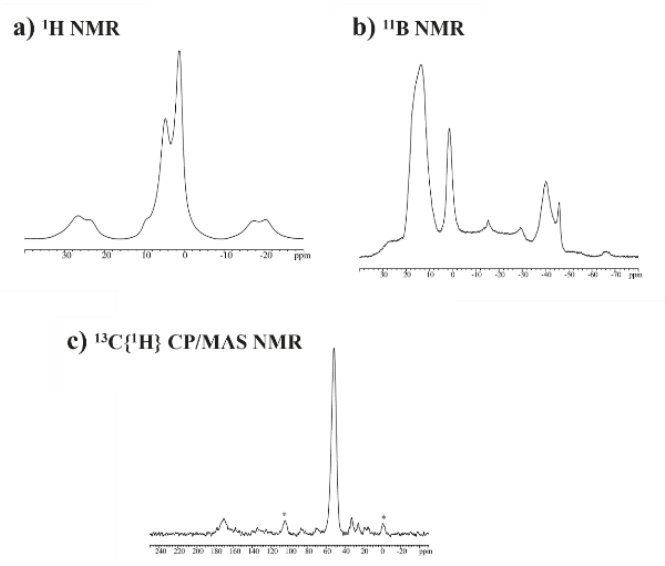

Figure 6. Solid state NMR spectra of γ-$Mg(BH_4)_2$ sample after CO_2 interaction at RT and 0.5 bar for 72 h.

The $^{11}B\{^1H\}$ MAS NMR spectrum of the same sample shows two broad singlets centered at 1 and 18 ppm (Figure 6b). The high-field signal corresponds to boron nuclei of the $[HB(OCHO)_3]^-$, $[H_2B(OCHO)_2]^-$, and $[H_3B(OCHO)]^-$ anions, while the low-field signal arises from boron nuclei in the O_3 environment, such as trimethyl borate $B(OMe)_3$, as suggested by TG-MS data. Additionally, broad singlets around −40 ppm, along with two singlets at −29 ppm and −15 ppm, were attributed to BH_4^-, $B_3H_8^-$, and $B_{12}H_{12}^{2-}$.[18] The formation of higher nuclearity boranes indicates the generation of B_2H_6 during the reduction of CO_2, which reacts with borohydrides

subsequently. CO_2 may enhances the hydrogen desorption kinetics of the $Mg(BH_4)_2$ while it's reduced at the meantime.

Peaks are observed at 170, 86, 50, and approximately 33−13 ppm (33.3, 19.3, and 13.8 ppm) in the ^{13}C CP-MAS NMR spectrum (Figure 6c), which correspond to C=O, OC−H, OCH_3, and aliphatic groups, respectively.[18] Furthermore, NMR enables the quantification of the relative abundance of the reaction products. Interestingly, the methoxy species (seen as a large peak at 50 ppm) are found to be the most abundant groups.

6.4. Conclusion

Adsorption of CO_2 in porous hydride, γ-$Mg(BH_4)_2$ was primary investigated at ambient conditions. The solid gas reaction were investigated by thermally and mechanochemically induced. Both methods revealed the spontaneous character of the reaction at room temperature. The formation of magnesium formylhydroborates, $Mg[H_xB(OCHO)_{4-x}](x = 1−3)$, was identified as main intermediates by ^{11}B NMR, and it's decomposition lead to the generation of diborane, as well as $B(OME)_3$ and hydrocarbon such as methanol and formate. Localization of CO_2 in the porous structure in the initial stages of the interaction was characterized by neutron and synchrotron X-ray powder diffraction.

6.5. References

(1) Marland, E.; Marland, G. The Treatment of Long-Lived, Carbon-Containing Products in Inventories of Carbon Dioxide Emissions to the Atmosphere. *Environ. Sci. Policy.* **2003**, *6* (2), 139–152.

(2) Graetz, J. New Approaches to Hydrogen Storage. *Chem. Soc. Rev.* **2009**, *38* (1), 73–82.

(3) Li, X.; Yan, Y.; Jensen, T. R.; Filinchuk, Y.; Dovgaliuk, I.; Chernyshov, D.; He, L.; Li, Y.; Li, H.-W. Magnesium Borohydride $Mg(BH_4)_2$ for Energy Applications: A Review. *J. Mater. Sci. Technol.* **2023**, *161*, 170–179.

(4) Ozkan, M.; Akhavi, A.-A.; Coley, W. C.; Shang, R.; Ma, Y. Progress in Carbon Dioxide Capture Materials for Deep Decarbonization. *Chem* **2022**, *8* (1), 141–173.

(5) Sun, X.; Cao, X.; Hu, P. Theoretical Insight into the Selectivities of Copper-Catalyzing Heterogeneous Reduction of Carbon Dioxide. *Sci. China Chem.* **2015**, *58* (4), 553–564.

(6) Wu, J.; Huang, Y.; Ye, W.; Li, Y. CO2 Reduction: From the Electrochemical to Photochemical Approach. *Advan. Sci.* **2017**, *4* (11).

(7) Yang, J. Y.; Kerr, T. A.; Wang, X. S.; Barlow, J. M. Reducing CO_2 to HCO_2^- at Mild Potentials: Lessons from Formate Dehydrogenase. *J. Am. Chem. Soc.* **2020**, *142* (46), 19438–19445.

(8) Qian, C.; Sun, W.; Hung, D. L. H.; Qiu, C.; Makaremi, M.; Hari Kumar, S. G.; Wan, L.; Ghoussoub, M.; Wood, T. E.; Xia, M.; Tountas, A. A.; Li, Y. F.; Wang, L.; Dong, Y.; Gourevich, I.; Singh, C. V.; Ozin, G. A. Catalytic CO_2 Reduction by Palladium-Decorated Silicon–Hydride Nanosheets. *Nat. Catal.* **2018**, *2* (1), 46–54.

(9) Doherty, M. D.; Grills, D. C.; Muckerman, J. T.; Polyansky, D. E.; Fujita, E. Toward More Efficient Photochemical CO_2 Reduction: Use of $ScCO_2$ or Photogenerated Hydrides. *Coord. Chem. Rev.* **2010**, *254* (21–22), 2472–2482.

(10) Kato, S.; Matam, S. K.; Kerger, P.; Bernard, L.; Battaglia, C.; Vogel, D.; Rohwerder, M.; Züttel, A. The Origin of the Catalytic Activity of a Metal Hydride in CO_2 Reduction. *Angew. Chem. Int. Ed.* **2016**, *55* (20), 6028–6032.

(11) Waldie, K. M.; Ostericher, A. L.; Reineke, M. H.; Sasayama, A. F.; Kubiak, C. P. Hydricity of Transition-Metal Hydrides: Thermodynamic Considerations for CO_2 Reduction. *ACS Catal.* **2018**, *8* (2), 1313–1324.

(12) Zhao, J.; Teng, Y.-L.; Dong, B.-X. Thermal Reduction of CO_2 with Activated Alkali Metal Aluminum Hydrides for Selective Methanation. *Energ. Fuel* **2020**, *34* (9), 11210–11218.

(13) Wartik, T.; Pearson, R. K. A New Type of Substituted Borohydride. *J. Am. Chem. Soc.* **1955**, *77* (4), 1075–1075.

(14) Eisenberg, F.; Bolden, A. H. Formate Contamination in Borohydride Reduction. *Carbohydr. Res.* **1967**, *5* (3), 349–350.

(15) Picasso, C. V.; Safin, D. A.; Dovgaliuk, I.; Devred, F.; Debecker, D.; Li, H.-W.; Proost, J.; Filinchuk, Y. Reduction of CO_2 with KBH_4 in Solvent-Free Conditions. *Int. J. Hydrogen Energy* **2016**, *41* (32), 14377–14386.

(16) Jeong, S.; Milner, P. J.; Wan, L. F.; Liu, Y.; Oktawiec, J.; Zaia, E. W.; Forse, A. C.; Leick, N.; Gennett, T.; Guo, J.; Prendergast, D.; Long, J. R.; Urban, J. J. Runaway Carbon Dioxide Conversion Leads to Enhanced Uptake in a Nanohybrid Form of Porous Magnesium Borohydride. *Advan. Mater.* **2019**, *31* (44).

(17) Filinchuk, Y.; Richter, B.; Jensen, T. R.; Dmitriev, V.; Chernyshov, D.; Hagemann, H. Porous and Dense Magnesium Borohydride Frameworks: Synthesis, Stability, and Reversible Absorption of Guest Species. *Angew. Chem.* **2011**, *123* (47), 11358–11362.

(18) Vitillo, J. G.; Groppo, E.; Bardají, E. G.; Baricco, M.; Bordiga, S. Fast Carbon Dioxide Recycling by Reaction with γ-$Mg(BH_4)_2$. *Phys. Chem. Chem. Phys.* **2014**, *16* (41), 22482–22486.

(19) Ban, V.; Soloninin, A. V.; Skripov, A. V.; Hadermann, J.; Abakumov, A.; Filinchuk, Y. Pressure-Collapsed Amorphous $Mg(BH_4)_2$: An Ultra dense Complex Hydride Showing a Reversible Transition to the Porous Framework. *J. Phys. Chem. C* **2014**, *118* (40), 23402–23408.

Chapter 6

Chapter 7. Preparation of Organic Dodecaborate and Octahydrotriborate Compounds

Jian Wang,[a] *Koen Robeyns,*[a] *Igor Golub,*[b] *Yaroslav Filinchuk*[a*]

[a] Institute of Condensed Matter and Nanosciences, Université catholique de Louvain, 1348 Louvain-la-Neuve, Belgium

[b] Institut des Matériaux Poreux de Paris, Ecole Normale Supérieure, ESPCI Paris, CNRS, PSL Université, 75005 Paris, France

*Corresponding Author. E-mail: yaroslav.filinchuk@uclouvain.be (Y. Filinchuk)

Chapter 7

Abstract

Previous sections detailed the synthesis of alkali and alkaline earth metal-$B_{12}H_{12}$ using the borane dimethyl sulfide complex ($DMS{\cdot}BH_3$) and corresponding borohydrides. Although metal-$B_{12}H_{12}$ complexes have garnered significant attention in solvothermal syntheses, the resulting products are commonly obtained coordinated with solvents. Direct synthesis of borates with non-coordinating cations will have fewer issues with removal of solvents. In this chapter, we present the direct synthesis of non-coordinating tetraalkylammonium Octahydrotriborate ($B_3H_8^-$) and $B_{12}H_{12}^{2-}$ using substitution or autoclave techniques. The primary focus lies in the synthesis and structural analysis of $(Me_4N)_2B_{12}H_{12}$ alongside the synthesis of larger cationic tetraalkylammonium $B_{12}H_{12}$ derivatives. Furthermore, the synthesis of two organic $B_3H_8^-$ anions is also presented. Notably, $(Me_4N)_2B_{12}H_{12}$ was observed to exhibit isolated pores in the structure. Though without interconnecting channels, it is still very promising for gas adsorption, particularly with CO_2.

7.1. Introduction

Borohydrides have a long history of use as reducing agents in chemical synthesis.[1–3] However, recent interest in these materials has been sparked by their potential as hydrogen storage media. For instance, light metal borohydrides such as $LiBH_4$ (18.4 wt.% H) are viewed as attractive candidates for solid-state hydrogen storage because of their exceptional gravimetric hydrogen capacity.[4–7] Beyond hydrogen storage, borohydride materials have found diverse applications, including polymer chemistry,[8] diborane sources,[9] cancer treatment,[10] and for CO_2 capture and reduction.[11] Furthermore, certain metal-ion containing borohydrides have demonstrated significant ion conductivity, expanding their utility in electrochemical applications.[12-15]

Compared to metal-ion based borohydrides, less attention has been paid to organic borohydrides, such as ammonium borohydride (NH_4BH_4, 24.5 wt.% H), which have attracted significant interest in the hydrogen storage community due to their impressive hydrogen gravimetric content and their ability to release hydrogen at relative low temperatures.[16] Furthermore, other organic borohydrides such as tetraalkylammonium borohydrides also found playing a crucial role as important components of ionic liquids and for CO_2 reduction.[11,17] These compounds are typically composed of light elements from the first and second periods of the periodic table, presenting a promising avenue in applications compared to conventional borohydride salts. Furthermore, these organic cations (R_4N^+, R = CH_3, C_2H_5, C_3H_7, C_4H_9) are commonly known as non-coordinating and their $B_{12}H_{12}^{2-}$ salts are soluble in most of organic solvents, which makes organic-$B_{12}H_{12}$ can serve as precursors in the substitution synthesis of alkaline and

alkaline earth $M_xB_{12}H_{12}$ (M = metal cations), and even as stabilizers to stabilize highly reactive species such as the $B_2H_7^-$ anion.[18]

In this chapter, we report a direct synthesis and new substitution methods of a few tetraalkylammonium $B_3H_8^-$ and $B_{12}H_{12}^-$ salts. The procedure employs a simple setup but may open a new avenue for large-scale production of $B_3H_8^-$ and $B_{12}H_{12}^-$ salts.

7.2. Experimental Section

7.2.1. Chemicals

Tetramethylammonium borohydride ($(CH_3)_4NBH_4$, SIGMA, purity ≥ 95%), tetrabutylammonium borohydride ($(C_4H_9)_4NBH_4$, SIGMA, purity ≥ 98%), tetramethylammonium bromide $(CH_3)_4NBr$ (SIGMA, purity ≥ 98%), tetrabutylammonium Iodide $(C_4H_9)_4NBr$ (ACROS, purity ≥ 98%), borane dimethyl sulfide complex ($(CH_3)_2S{\cdot}BH_3$, analytical), diethylene glycol dimethyl ether (diglyme, $C_6H_{14}O_3$, anhydrous, 99.5%), Tetrahydropyran (THF, $C_5H_{10}O$, anhydrous, purity ≥ 99.5%), 1, 2-Dimethoxyethane (monoglyme, $C_4H_{10}O_2$, anhydrous, purity ≥ 99.5%), deuterated dimethyl sulfoxide (DMSO-d_6, anhydrous, 99.9 atom% D) and deuterated Acetonitrile (CD_3CN-d_3, anhydrous, 99.9 atom% D) was obtained from Eurisotop. All the above chemicals were used without further purification. sodium dodecahydrododecaborate ($Na_2B_{12}H_{12}$) was synthesized according to reference method.[19]

7.2.2. Characterization

Powder X-ray diffraction (PXRD) patterns were acquired employing a MAR 345 image plate detector, with Mo Kα radiation (λ = 0.71073 Å) sourced from an Incoatec Microfocus Source Mo ELM47 operating at 50 kV and 1000 µA. During the 10 min exposure, samples were rotated over 180°. Samples were encapsulated in thin-walled glass capillaries (0.7 mm diameter, Hilgenberg, GmbH) in an argon filled glovebox. These capillaries were then hermetically sealed with grease and measured immediately to prevent any degradation. Data integration was performed using the Fit2D software (ESRF),

with LaB_6 utilized as calibrant.

Attenuated total reflectance Fourier transform infrared (ATR-FTIR) spectra were obtained using a Bruker Alpha II spectrometer, housed within an argon-filled glovebox. The spectrometer was configured with a Platinum ATR module (Bruker, featuring a diamond crystal, single bounce) for the measurements. Infrared spectra were recorded with a spectral resolution of 4 cm^{-1}, with 30 scans in the range 370−4000 cm^{-1}.

All NMR spectra were acquired at room temperature (295 K) utilizing a Bruker Avance 500 spectrometer, operating at frequencies of 500.13 MHz for ^{1}H nuclei and 160.46 MHz for ^{11}B nuclei. A BBFO {^{1}H, X} probehead with a z-gradient coil was employed for the experiments. The experiments were conducted using the TopSpin program (version 1.3; Bruker). Chemical shifts for ^{1}H nuclei were referenced to the residual DMSO-d_5 signal (δ = 2.50 ppm), while ^{11}B NMR signals were referenced externally to $BF_3{\cdot}Et_2O$ (δ = 0.00 ppm). All experiments were carried out in quartz NMR tubes with an internal diameter of 5 mm.

The single crystal X-Ray diffraction data were acquired on a MAR345 image plate detector using Mo Kα radiation (λ = 0.71073 Å), either at ambient temperature or after flash cooling to 150 K in a nitrogen gas stream. Data indexation, integration and reduction was done with the CrysAlis^{PRO} software, incorporating an empirical absorption correction. Structures were solved by dual space direct methods (SHELXT), followed by refinement using full-matrix least squares based on $|F^2|$ with SHELXL 2014/7.[20] Non-hydrogen atoms were anisotropically refined, while hydrogen atoms were positioned at calculated positions and refined in riding mode, with temperature factors constrained to 1.2 times Ueq of the parent atoms (1.5 times

Ueq for methyl and OH hydrogens. Structural figures were generated using Mercury.[21]

7.3. Synthesis, Results and Discussions

7.3.1. Synthesis of tetraalkylammonium-$B_{12}H_{12}$

i) Synthesis of $(Me_4N)_2B_{12}H_{12}$

a) Typically, 0.89 g of Me_4NBH_4 (10 mmol) was precisely weighed and deposited in a quartz liner reactor under inert atmosphere within a glovebox, followed by sealing with Parafilm. A solution of 16 mL diglyme and 55 mmol of the borane dimethyl sulfide complex ($(CH_3)_2S{\cdot}BH_3$, 5.5 mL) was added to the borohydride before inserting the quartz reactor into the autoclave. After sealing, the autoclave was purged by Ar for 30 s to remove any remaining air. The reaction began at room temperature and steadily increased to 150 °C (the melting point of Me_4NBH_4) at a regulated rate of 2 °C/min, where it was sustained for 24 h. After completion, the reaction mixture was cooled naturally to room temperature, then filtered using a Schlenk filtering system and washed with diglyme (3 × 5 mL). The final product was then vacuum dried at 150 °C for 4 h.

b) The substitution method is inspired by a published approach for synthesizing $(Me_4N)_2B_{12}H_{12}$.[22] In this study, an improved substitution method for obtaining crystalline $(Me_4N)_2B_{12}H_{12}$ has been developed as follows: without the use of an ion-exchange resin and titration, the simplified substitution method involves reacting Me_4NBr and $Na_2B_{12}H_{12}$ (or diglyme solvated $Na_2B_{12}H_{12}$) in water. This reaction is followed by a heating and rapid cooling process to obtain single

crystal samples:

$$Na_2B_{12}H_{12} + 2\ Me_4NBr \xrightarrow{H_2O,\ 100\ ℃,\ \text{fast cooling}} (Me_4N)_2B_{12}H_{12}(s) + NaBr\ (g) \quad (1)$$

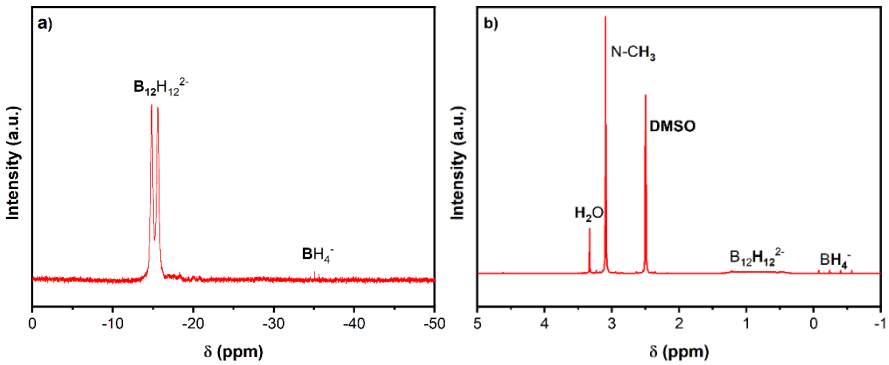

Figure 1. a) Proton-decoupled 11B NMR spectra of solid precipitate; b) ^{1}H NMR after reaction of Me_4NBH_4 with 5 equiv. of DMS·BH_3 for 24 h at 150 °C in an autoclave.

In the new synthetic route, $(Me_4N)_2B_{12}H_{12}$ can be synthesized directly by reacting 5 mmol Me_4NBH_4 and 27.5 mmol DMS·BH_3 (10 % excess) in an autoclave. The ^{11}B NMR spectrum (Figure 1a) of the as-synthesized compound in DMSO-d_6 shows a doublet peak at around -15.2 ppm, which is in good agreement with previously report on $B_{12}H_{12}^{2-}$.[23–25] The remaining BH_4^- can also be observed, this observation is similar to our previous work on the synthesis of $K_2B_{12}H_{12}$; the low solubility of borohydrides in diglyme results in incomplete conversion.[19] For further investigation, the ^{1}H NMR of the product was measured, confirming the presence of $-CH_3$ groups, spectrum is shown in Figure 1b.[11]

Since the synthesis starting from BH_4^- results in the formation of $B_{12}H_{12}^{2-}$ with residual impurities, employing a substitution method may yield higher purity samples of $(Me_4N)_2B_{12}H_{12}$. The method of

obtaining single crystals of $(Me_4N)_2B_{12}H_{12}\cdot CH_3CN$ was reported in the literature by Albert et al. in 2000.[22] $(Me_4N)_2B_{12}H_{12}$ was synthesized by reacting hydrated $Na_2B_{12}H_{12}$ with an acidic ion-exchange resin, leading to the formation of free acid $(H_3O)_2B_{12}H_{12}$, which was titrated by $N(CH_3)_4OH$ solution. However, they were not able to resolve the single crystal structure of $(Me_4N)_2B_{12}H_{12}$ due to the lack of symmetry. In this work, a simple and efficient substitution method has been developed by reacting $N(CH_3)_4Br$ and $Na_2B_{12}H_{12}$ in boiling water. The large and highly symmetric tetraalkylammonium cation is non-coordinating, which means that glymes-solvated $Na_2B_{12}H_{12}$ can also be used instead of $Na_2B_{12}H_{12}$ as starting materials.

The single crystal X-ray data of the crystal with $(Me_4N)_2B_{12}H_{12}$ in Figure 2 reveals a similar structure to that of alkali metal dodecaborates (such as $K_2B_{12}H_{12}$). The room temperature data can be indexed in a cubic *F*23 system with a lattice parameter of a = 13.4 Å, where the Me_4N^+ cations occupy the tetrahedral interstices of the FCC cubic packing in the lattice. The molecular ion is arranged according to the anti-CaF_2 type, as indicated in Figure 2. Detailed information about the crystal is summarized in Table 1. Interestingly, the simulation of the crystal in Mercury found the existence of isolated pores in the structure (Figure 2, upper right). The structure features isolated pores with a pore diameter of 6.7 Å and a volume of 4 × 134 $Å^3$, resulting in a porosity of 22.5 %.

In-situ X-ray diffraction experiments of $(Me_4N)_2B_{12}H_{12}$ were performed in the temperature range of 25−400 °C with a heating rate of 10 °C min^{-1} to observe the decomposition of the structure as a function of temperature. Figure 2 shows the patterns of the experiments, revealing that $(Me_4N)_2B_{12}H_{12}$ thermal stable until 315 °C and does not undergo a phase transition below this temperature range.

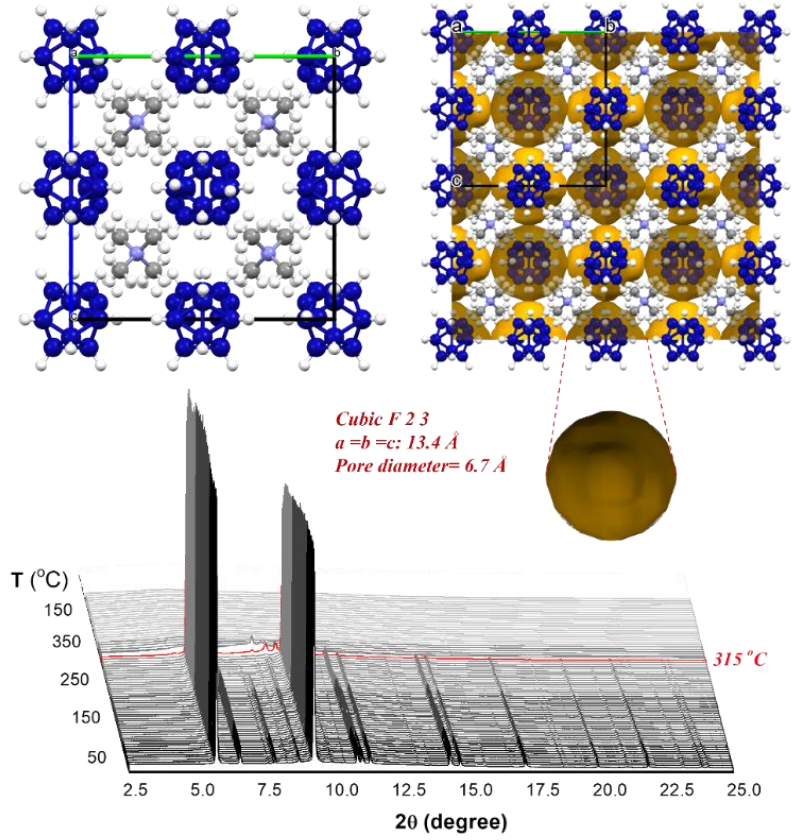

Figure 2. Selected parts of the crystal structures of $(Me_4N)_2B_{12}H_{12}$. Color code: **N**, blue; **B**, dark blue; **H**, light grey; **C**: dark grey. (upper), and in-situ SR-PXD diffraction measurements of $(Me_4N)_2B_{12}H_{12}$ (from autoclave synthesis, bottom picture)

Table 1. Single crystal structure parameters for $[(Me_4N)_2B_{12}H_{12}]$

Identification code	**$[Me_4N]_2B_{12}H_{12}$**
Empirical formula	C8 H36 B12 N2
Formula weight	290.11
Temperature (K)	297(2)
Wavelength (Å)	0.71073
Crystal system	Cubic
Space group	*F*23
Unit cell dimensions (Å)	a = 13.3887(12)
Volume ($Å^3$)	2400.0(7)
Z	4
Density (calculated) (g/cm^3)	0.803
Absorption coefficient (mm^{-1})	0.039
F(000)	632
Crystal size (mm^3)	0.15x 0.10 x 0.06
Theta range for data collection (°)	5.050 to 20.800
Reflections collected	1921
Independent reflections	222 [R(int) = 0.0746]
Completeness to q = 21.257° (%)	97.7
Absorption correction	None
Max. and min. transmission	Full-matrix least-squares on F2
Refinement method	222 / 12 / 29
Data / restraints / parameters	1.121
Goodness-of-fit on F^2	R1 = 0.0476, wR2 = 0.1321
Final R indices [I>2s(I)]	R1 = 0.0584, wR2 = 0.1377
R indices (all data)	10.0(10)
Dr (max,min)($e.Å^{-3}$)	0.057, -0.046

Though the pores inside the $(Me_4N)_2B_{12}H_{12}$ are isolated without interconnection, our attempt with CO_2 adsorption shows that CO_2 enter the structure at slow kinetics. The CO_2 adsorption experiments were performed at ambient conditions, wherein the sample was exposed to 42 bar CO_2, and the diffraction patterns were collected every 10 s for 3 h. The in-situ data show significant changes in the peak intensities in the XRD patterns of $(Me_4N)_2B_{12}H_{12}$ with the CO_2 adsorption time (see Figure 3).

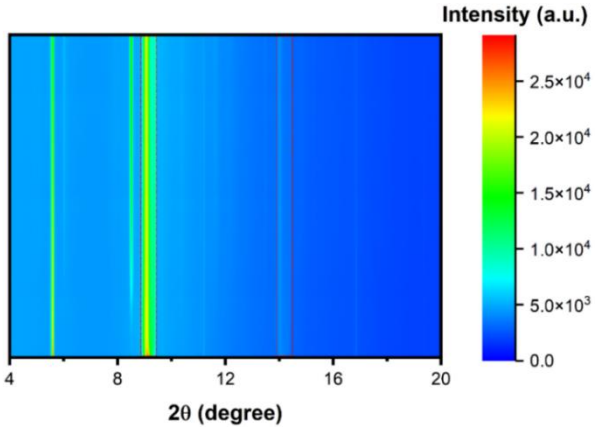

Figure 3. Time-dependent powder diffraction from $(Me_4N)_2B_{12}H_{12}$ loaded with CO_2 gas (p (CO_2) = 42 bar, T = 25 °C, λ = 0.75334 Å). The significant change of the intensities of Bragg peaks correlates with the amount of the adsorbed gas (measured with $(Me_4N)_2B_{12}H_{12}$ obtained from autoclave experiment).

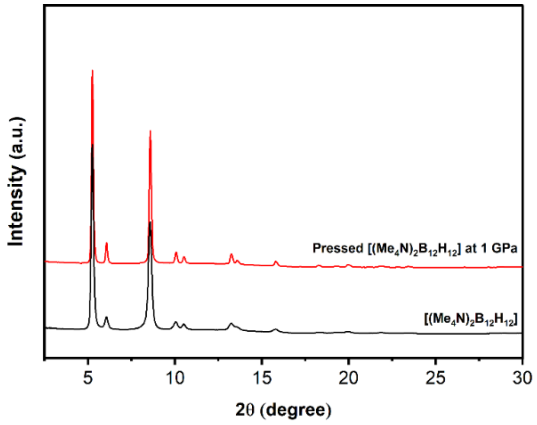

Figure 4. PXRD patterns of $(Me_4N)_2B_{12}H_{12}$ from substitution and pressed at 1 GPa by press.

Pressure-induced phase transitions can occur in some porous materials, as demonstrated in our previous work with γ-$Mg(BH_4)_2$, where the cubic porous phase can be collapsed by 0.8 GPa pressure into a dense amorphous phase.[26] In this case, we attempted a similar

experiment with $(Me_4N)_2B_{12}H_{12}$, but no phase transition was observed even when the pressure was increased up to 1 GPa (see Figure 4).

ii) Synthesis of $(Pr_4N)_2B_{12}H_{12}$ and $(Bu_4N)_2B_{12}H_{12}$

Upon discovering that the pores within the material were isolated, we considered whether it would be possible to obtain internally interconnected porous materials by acquiring $B_{12}H_{12}^{2-}$ salts with a different ammonium ion. The structure data with $B_{12}H_{12}^{2-}$ salts of ammonium (NH_4^+) and tetraethylammonium (Et_4N^+) were known, with lattice parameters of a = 10.87 (8) Å and a = 14.20 (5) Å, respectively. Their synthetic methods can also be found in published literature.[27,28] We think $(Et_4N)_2B_{12}H_{12}$ can be obtained through substitution by reacting Et_4NBr with $Na_2B_{12}H_{12}$ in water.

We also attempted to obtain the $B_{12}H_{12}^{2-}$ salts of tetrapropylammonium (Pr_4N) and tetrabutylammonium (Bu_4N) through a substitution reaction between $Na_2B_{12}H_{12}$ and stoichiometric excess of Pr_4NBr and Bu_4NI at ambient conditions, as illustrated in eq.2 and eq 3.

$$Na_2B_{12}H_{12}\,(sol) + 2\,Pr_4NBr\,(sol) \xrightarrow{H_2O,\ RT} (Pr_4N)_2B_{12}H_{12}(s) + NaBr\,(sol) \qquad (2)$$

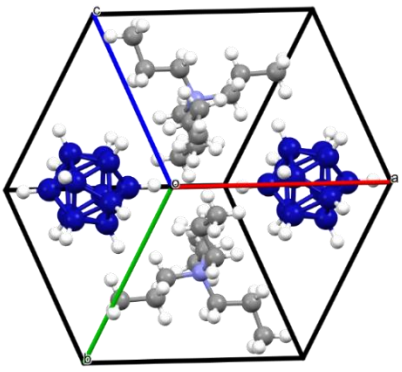

Figure 5. Selected parts of the crystal structures of $[(Pr_4N)_2B_{12}H_{12}]$.

The single crystal of $(Pr_4N)_2B_{12}H_{12}$ from experimental was obtained, the crystal structure indexed in a triclinic *P*-1 system, the crystal structure and structural parameters are represented in Figure 5 and Table 2.

Table 2. Single crystal structure parameters for $[(Pr_4N)_2B_{12}H_{12}]$

Identification code	**$(Pr_4N)_2B_{12}H_{12}$**
Empirical formula	C12 H34 B6 N
`Formula weight	257.26
Temperature (K)	297(2)
Wavelength (Å)	0.71073
Crystal system	Triclinic
Space group	*P*-1
Unit cell dimensions (Å,°)	a = 9.352(5)
	b = 9.611(3)
	c = 11.496(4)
	a = 92.18(3)
	β= 106.85(4)
	γ= 114.67(4)
Volume ($Å^3$)	883.4(7)
Z	2
Density (calculated) (g/cm^3)	0.967
Absorption coefficient (mm^{-1})	0.049
F(000)	286
Crystal size (mm^3)	0.08 x 0.04 x 0.01
Theta range for data collection (°)	3.441 to 20.815
Reflections collected	4498
Independent reflections	1766 [R(int) = 0.0861]
Completeness to q = 21.257° (%)	95.3
Absorption correction	Semi-empirical from equivalents
Max. and min. transmission	1.00000 and 0.80137
Refinement method	Full-matrix least-squares on F2
Data / restraints / parameters	1766 / 0 / 194
Goodness-of-fit on F^2	1.061
Final R indices [I>2s(I)]	R1 = 0.0716, wR2 = 0.1403
R indices (all data)	R1 = 0.1417, wR2 = 0.1672
Dr (max,min)($e.Å^{-3}$)	0.135, -0.142

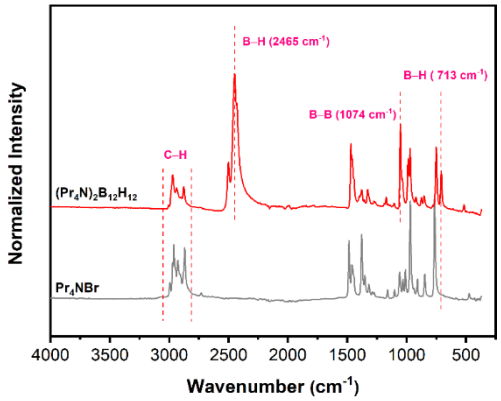

Figure 6. FTIR spectrum of Pr_4NBr and $(Pr_4N)_2B_{12}H_{12}$.

Figure 6 shows the comparison of FTIR spectrum of the sample before and after substitution, the successful acquisition of $(Pr_4N)_2B_{12}H_{12}$ is confirmed by the characteristic B−H stretching observed at 2465 cm^{-1}. Additionally, the cation exchange between Pr_4NBr and $Na_2B_{12}H_{12}$ is effective under ambient conditions.

$$Na_2B_{12}H_{12}\ (sol) + 2\ Bu_4NI\ (sol) \xrightarrow{H_2O,\ RT} (Bu_4N)_2B_{12}H_{12}\ (s) + NaI\ (sol) \quad (3)$$

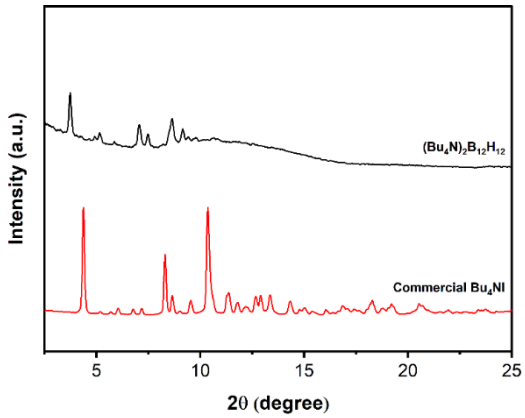

Figure 7. PXRD patterns of Bu4NI and $(Bu_4N)_2B_{12}H_{12}$ from substitution.

We also try to obtain $(Bu_4N)_2B_{12}H_{12}$ through the substitution between Bu_4NI and $Na_2B_{12}H_{12}$ in accordance with eq.3, Figure 7

shows the PXRD pattern of the product in comparison to commercial Bu_4NI, representing a successful obtained of $(Bu_4N)_2B_{12}H_{12}$ through the substitution reaction.

Among the series of tetraalkylammonium borohydrides, it is known that the borohydrides with larger cations exhibit lower melting points, due to the decreased lattice energy. We also attempted to synthesize $(Bu_4N)_2B_{12}H_{12}$ through an autoclave experiment by using Bu_4NBH_4 and $DMS{\cdot}BH_3$ in diglyme. Figure 8 below shows the ^{11}B NMR spectrum of the final product obtained by reacting 5 mmol of Bu_4NBH_4 and 27.5 mmol (10% excess) $DMS{\cdot}BH_3$ in diglyme in an autoclave at different temperatures. The final product obtained at 150 °C decomposes into unknown boron compounds, whereas a lower reaction temperature (120 °C) leads to the formation of a diffraction pure $(Bu_4N)_2B_{12}H_{12}$, as confirmed by the ^1H NMR spectra depicted in Figure 9.

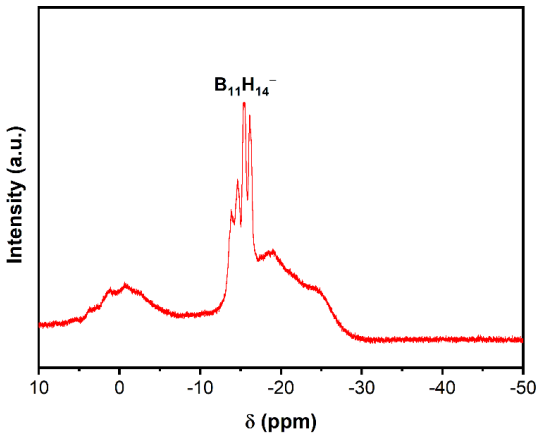

Figure 8. Proton coupled ^{11}B NMR spectra of solid precipitate after reaction of 5mmol Bu_4NBH_4 with 27.5 mmol (10% excess) of $DMS{\cdot}BH_3$ for 24 h at 150 °C in autoclave.

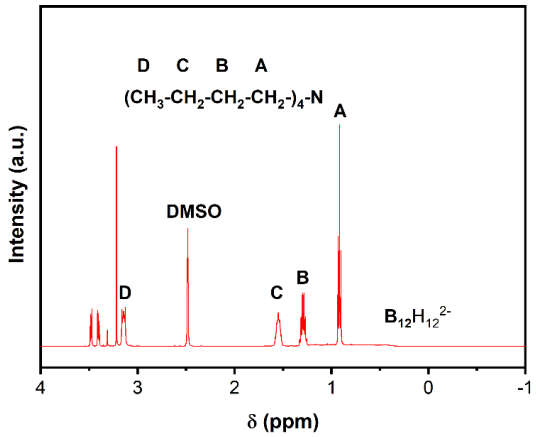

Figure 9. ^{1}H NMR spectra of solid precipitate after reaction of Bu_4NBH_4 with 5 equiv (10 % excess) of $DMS{\cdot}BH_3$ for 24 h at 120 °C in autoclave.

Figures 10 and 11 compare $(Bu_4N)_2B_{12}H_{12}$ obtained from an autoclave experiment and through substitution between Bu_4NI and $Na_2B_{12}H_{12}$. The PXRD and FTIR results confirm the effectiveness of both synthetic methods.

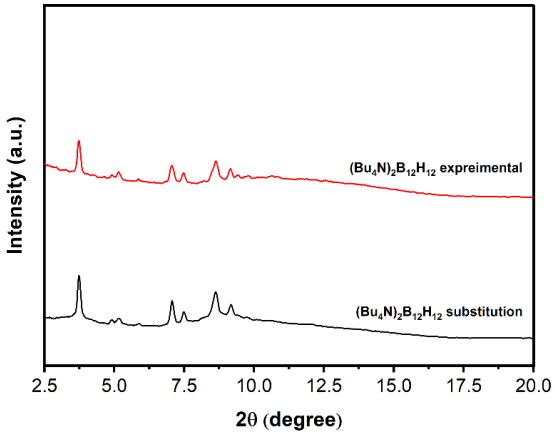

Figure 10. PXRD patterns of $(Bu_4N)_2B_{12}H_{12}$ from substitution and from autoclave experiment (120 °C)

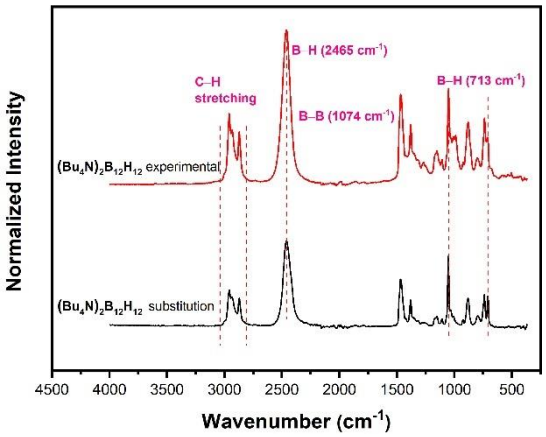

Figure 11. FTIR spectrum of $(Bu_4N)_2B_{12}H_{12}$ from substitution and from autoclave experiment (120 °C)

The FTIR spectrum (Figure 12) of the substituted tetraalkylammonium-$B_{12}H_{12}$ salt exhibits the characteristic B−H stretching peak at 2465 cm^{-1}. Peaks within the range of 2800−3000 cm^{-1} can be attributed to C−H stretching.

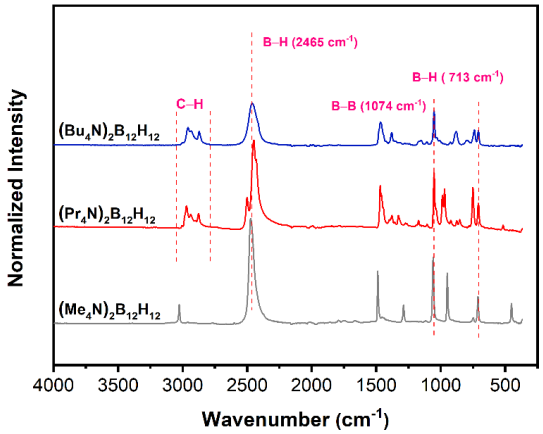

Figure 12. FTIR spectra of tetraalkylammonium-$B_{12}H_{12}$ compounds synthesized via substitution.

7.3.2. Synthesis of tetraalkylammonium-B_3H_8

i) Synthesis of $Bu_4NB_3H_8$

The synthesis is inspired from a reported method.[29] Typically, 1.22 g of Bu_4NBH_4 (5 mmol) was combined with 1.2 ml of $DMS{\cdot}BH_3$ (12 mmol, 20% excess) in 20 ml of THF in a Schlenk flask, and the mixture was heated to 75 °C for 24 h. After the reaction was complete, all the solvent was evaporated by vacuum drying at room temperature, resulting in a white-colored powder.

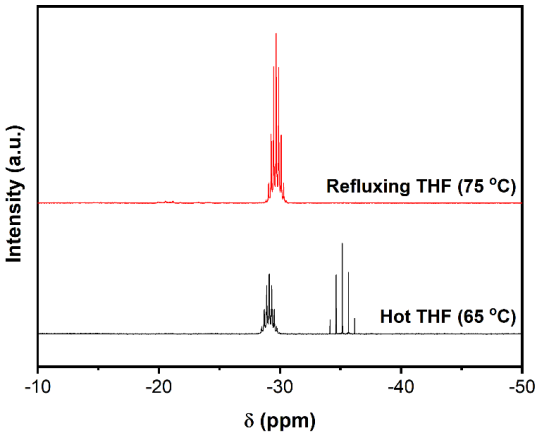

Figure 13. Proton coupled ^{11}B NMR spectra of solid precipitate after reaction of 5mmol Bu_4NBH_4 with 2 equiv (20% excess) of $DMS{\cdot}BH_3$ for 24 h with the oil bath temperature set at 65 °C (75 °C) in THF. (The measurement was conducted in DMSO-d_6 (black), and CD_3CN-d_3 (red)).

Figure 14 displays the proton-coupled ^{11}B NMR of the resulting product obtained from experiments conducted in THF at 65 °C and 75 °C, the NMR spectrum shows a multiplet peaks at around −29.2 ppm, which can be assigned to $B_3H_8^-$.[29] Although the boiling point of THF is 66 °C, at higher reaction temperature in THF, the increased refluxing rate significantly impacts the conversion rate of BH_4^-. This

phenomenon aligns with previous reports on the synthesis of $B_3H_8^-$, where refluxing promotes the conversion of BH_4^- into $B_3H_8^-$.[29] Figure 14 shows the ^1H NMR spectra of the as-synthesized $Bu_4NB_3H_8$, further confirming the presence $B_3H_8^-$ anion and the presence of -CH_3 and $-CH_2$ groups. The PXRD pattern of as-synthesized $Bu_4NB_3H_8$ is representing in Figure 15.

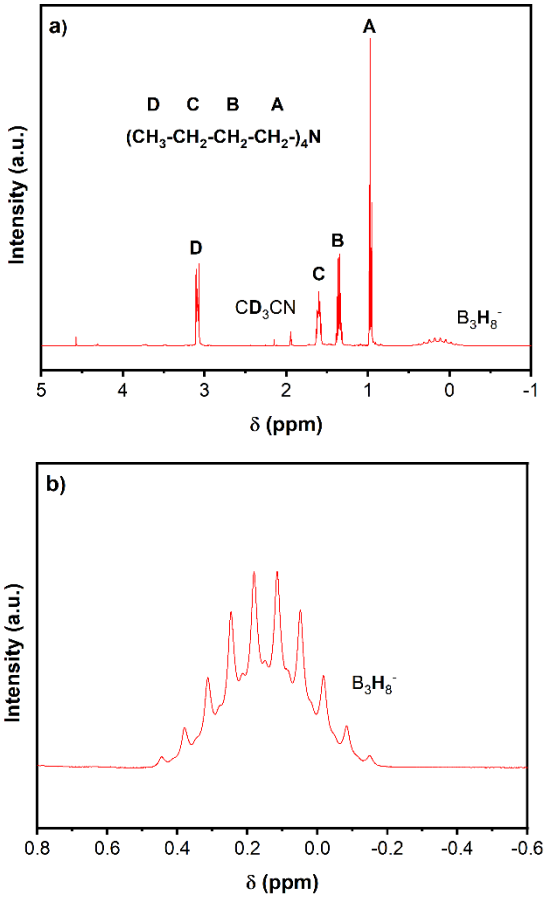

Figure 14. a) ^1H NMR spectra of $Bu_4NB_3H_8$ obtained from reaction of 5 mmol Bu_4NBH_4 with 2 equiv. (20% excess) of DMS·BH_3 for 24 h with the oil bath temperature at 75 °C in refluxing THF; b) zoom between −0.6~0.8 ppm.

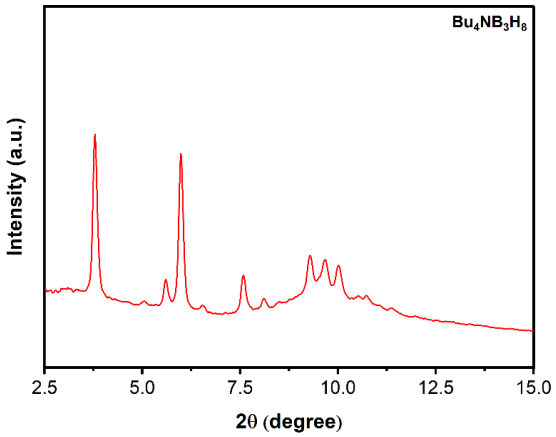

Figure 15. PXRD patterns of $Bu_4NB_3H_8$ obtained from reaction of 5 mmol Bu_4NBH_4 with 2 equiv. (20% excess) of $DMS{\cdot}BH_3$ for 24 h at 75 °C in refluxing THF.

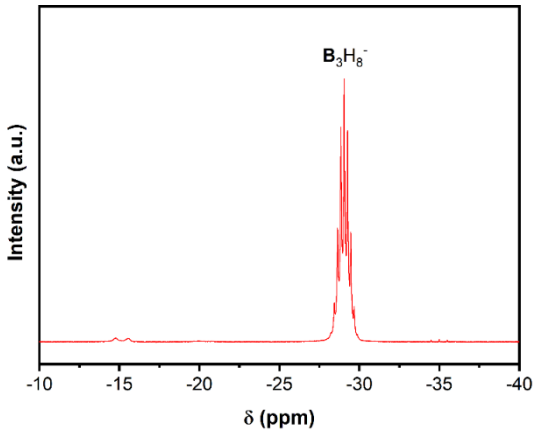

Figure 16. Proton coupled ^{11}B NMR spectra of solid precipitate after reaction of 5mmol Me_4NBH_4 with 2 equiv. (20% excess) of $DMS{\cdot}BH_3$ for 72 h at 85 °C in DME. (The measurement was conducted in DMSO-d_6 (red))

Figure 17 shows the ^{11}B NMR spectra of the obtained $Me_4NB_3H_8$ samples when monoglyme was used as the solvent. Typically, 0.45 g of Me_4NBH_4 (5 mmol) was combined with 1.2 ml of $DMS{\cdot}BH_3$ (12 mmol, 20% excess) in 20 ml of monoglyme in a Schlenk flask, and

the mixture was heated to 85 °C for 72 h. The characteristic multiplet peaks at around −29 ppm confirms the high-purity $B_3H_8^-$ obtained.

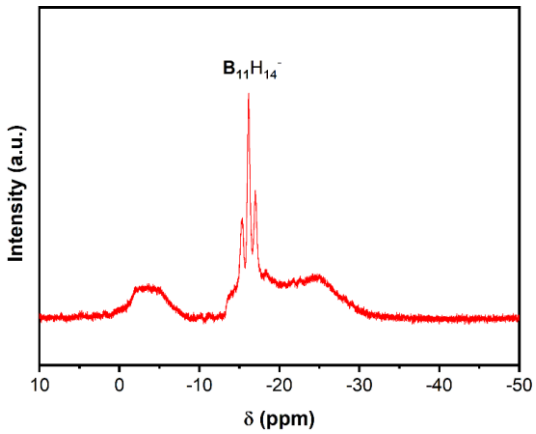

Figure 17. Proton coupled ^{11}B NMR spectra of solid precipitate after reaction of 2.5 mmol $Bu_4NB_3H_8$ with 3 equiv. of $DMS{\cdot}BH_3$ for 24 h at 120 °C in diglyme in autoclave.

In this thesis work, we also attempted to react $B_3H_8^-$ and $DMS{\cdot}BH_3$ for the synthesis of $B_{12}H_{12}^{2-}$. Figure 17 represents the ^{11}B NMR spectra of the solid samples, wherein the main species formed was observed to be $B_{11}H_{14}^-$. The absence of a signal for $B_{12}H_{12}^{2-}$ may be relevant to the decomposition of crucial intermediates, as indicated by the signal for amorphous boron compounds.[18]

7.4. Conclusions

In this chapter, we are presenting autoclave synthesis/substitution methods for producing high purity tetraalkylammonium $B_{12}H_{12}$ and B_3H_8 salts. We begin by detailing two distinct methods for synthesizing $(Me_4N)_2B_{12}H_{12}$. Notably, this compound exhibits intriguing isolating pores within its crystal structure. Although these pores lack interconnection, they hold significant promise for applications such as CO_2 gas adsorption. This initial investigation sets the stage for exploring the structural properties and potential applications of tetraalkylammonium borohydride compounds. Next, we delve into the autoclave synthesis/substitution method applied to $(Pr_4N)_2B_{12}H_{12}$ and $(Bu_4N)_2B_{12}H_{12}$. The single crystal structure of $(Pr_4N)_2B_{12}H_{12}$ adopts a triclinic structure without pores inside. Furthermore, we provide a synthesis process for $Bu_4NB_3H_8$ and $Me_4NB_3H_8$, the improved synthesis pathway towards tetraalkylammonium $B_{12}H_{12}$ and B_3H_8 salts may support in developing substitution methods for metal $B_{12}H_{12}$ and B_3H_8 salts based on differences in solubility.

7.5. References

(1) Burkhardt, E. R.; Matos, K. Boron Reagents in Process Chemistry: Excellent Tools for Selective Reductions. *Chem. Rev.* **2006**, *106* (7), 2617–2650.

(2) Nakamori, Y.; Orimo, S. Borohydrides as Hydrogen Storage Materials. *Solid-State Hydrogen Storage*, **2008**, 420–449.

(3) Paskevicius, M.; Jepsen, L. H.; Schouwink, P.; Černý, R.; Ravnsbæk, D. B.; Filinchuk, Y.; Dornheim, M.; Besenbacher, F.; Jensen, T. R. Metal Borohydrides and Derivatives – Synthesis, Structure and Properties. *Chem. Soc. Rev.* **2017**, *46*, 1565–1634.

(4) Yan, Y.; Li, H. W.; Maekawa, H.; Miwa, K.; Towata, S. I.; Orimo, S. I. Formation of Intermediate Compound $Li_2B_{12}H_{12}$ during the Dehydrogenation Process of the $LiBH_4$-MgH_2 System. *J. Phys. Chem. C* **2011**, *115* (39), 19419–19423.

(5) Javadian, P.; Sheppard, D. A.; Buckley, C. E.; Jensen, T. R. Hydrogen Storage Properties of Nanoconfined $LiBH_4$–$Ca(BH_4)_2$. *Nano Energy* **2015**, *11*, 96–103.

(6) Jepsen, J.; Milanese, C.; Girella, A.; Lozano, G. A.; Pistidda, C.; Bellosta von Colbe, J. M.; Marini, A.; Klassen, T.; Dornheim, M. Compaction Pressure Influence on Material Properties and Sorption Behaviour of $LiBH_4$–MgH_2 Composite. *Int. J. Hydrogen Energy* **2013**, *38*, 8357–8366.

(7) Züttel, A.; Rentsch, S.; Fischer, P.; Wenger, P.; Sudan, P.; Mauron, Ph.; Emmenegger, Ch. Hydrogen Storage Properties of $LiBH_4$. *J. Alloys Compd.* **2003**, *356–357*, 515–520.

(8) Palard, I.; Schappacher, M.; Soum, A.; Guillaume, S. M. Ring-opening Polymerization of E-caprolactone Initiated by Rare Earth Alkoxides and Borohydrides: A Comparative Study. *Polym. Int.* **2006**, *55* (10), 1132–1137.

(9) Callini, E.; Borgschulte, A.; Ramirez-Cuesta, A. J.; Züttel, A. Diborane Release and Structure Distortion in Borohydrides. *Dalton Trans.* **2013**, *42* (3), 719–725.

(10) Sivaev, I. B.; Bruskin, A. B.; Nesterov, V. V.; Antipin, M. Y.; Bregadze, V. I.; Sjöberg, S. Synthesis of Schiff Bases Derived from the Ammoniaundecahydro-Closo-Dodecaborate (1-) Anion, $[B_{12}H_{11}NH{=}CHR]^-$, and Their Reduction into

Monosubstituted Amines $[B_{12}H_{11}NH_2CH_2R]^-$: A New Route to Water Soluble Agents for BNCT. *Inorg. Chem*. **1999**, *38* (25), 5887–5893.

(11) Lombardo, L.; Ko, Y.; Zhao, K.; Yang, H.; Züttel, A. Direct CO_2 Capture and Reduction to High-End Chemicals with Tetraalkylammonium Borohydrides. *Angew. Chemie - Int. Ed.* **2021**, *60* (17), 9580–9589.

(12) Carter, T. J.; Mohtadi, R.; Arthur, T. S.; Mizuno, F.; Zhang, R.; Shirai, S.; Kampf, J. W. Boron Clusters as Highly Stable Magnesium-Battery Electrolytes. *Angew. Chemie* **2014**, *126* (12), 3237–3241.

(13) Asakura, R.; Duchêne, L.; Kühnel, R. S.; Remhof, A.; Hagemann, H.; Battaglia, C. Electrochemical Oxidative Stability of Hydroborate-Based Solid-State Electrolytes. *ACS Appl. Energy Mater.* **2019**, 2 (9), 6924–6930.

(14) Asakura, R.; Remhof, A.; Battaglia, C. Hydroborate-Based Solid Electrolytes for All-Solid-State Batteries, **2022**, 353–393.

(15) Souza D. H. P.; Moller, K. T.; Moggach, S. A.; Humphries, T. D.; D'Angelo, A. M.; Buckley, C. E.; Paskevicius, M. Hydrated Alkali-$B_{11}H_{14}$ Salts as Potential Solid-State Electrolytes. *J. Mater. Chem. A* **2021**, *9*, 15027–15037.

(16) Andersson, M. S.; Grinderslev, J. B.; Jensen, T. R.; García Sakai, V.; Häussermann, U.; Udovic, T. J.; Karlsson, M. Interplay of NH_4^+ and BH_4^- reorientational dynamics in NH_4BH_4. *Phys. Rev. Mater.* **2020**, *4* (8), 085002.

(17) Klindtworth, E.; Delidovich, I.; Palkovits, R. Borohydride in Ionic Liquids for Tailored Hydrogen Release. *Int. J. Hydrogen Energy* **2018**, *43* (45), 20772–20782.

(18) Miller H. C.; Miller N. E.; Muetterties E. L. Chemistry of Boranes. XX. Syntheses of Polyhedral Boranes. *Inorg. Chem.* **2002**, *3* (10), 1456–1463.

(19) Wang, J.; Steenhaut, T.; Li, H.-W.; Filinchuk, Y. High Yield Autoclave Synthesis of Pure $M_2B_{12}H_{12}$ (M = Na, K). *Inorg. Chem.* **2023**, *62* (5), 2153–2160.

(20) Sheldrick, G. M. SHELXT – Integrated Space-Group and Crystal-Structure Determination. *Acta Crystallogr. A Found. Adv.* **2015**, *71* (1), 3–8.

(21) Macrae, C. F.; Sovago, I.; Cottrell, S. J.; Galek, P. T. A.; McCabe, P.; Pidcock, E.; Platings, M.; Shields, G. P.; Stevens, J. S.; Towler, M.; Wood, P. A. Mercury 4.0: From Visualization to Analysis, Design and Prediction. *J. Appl. Crystallogr.* **2020**,

53 (1), 226–235.

(22) Hofmann, K.; Albert, B. Synthesis, Characterization, and Crystal Structures of $[N(CH_3)_4]_2[B_{12}H_{12}]$ and $[N(CH_3)_4]_2[B_{12}H_{12}]\cdot CH_3CN$. *Z. Anorg. Allg. Chem.* **2001**, *627* (5), 1055–1058.

(23) Ellis, I. A.; Gaines, D. F.; Schaeffer, R. A Convenient Preparation of $B_{12}H_{12}^{2-}$ Salts. *J. Am. Chem. Soc.* **2002**, *85* (23), 3885–3885.

(24) Peymann, T.; Knobler, C. B.; Khan, S. I.; Hawthorne, M. F. Dodecahydroxy-Closo-Dodecaborate(2-). *J. Am. Chem. Soc.* **2001**, *123* (10), 2182–2185.

(25) He, L.; Li, H.-W.; Tumanov, N.; Filinchuk, Y.; Akiba, E. Facile Synthesis of Anhydrous Alkaline Earth Metal Dodecaborates $MB_{12}H_{12}$ (M = Mg, Ca) from $M(BH_4)_2$. *Dalton Trans.* **2015**, *44*, 15882–15887.

(26) Ban, V.; Soloninin, A. V.; Skripov, A. V.; Hadermann, J.; Abakumov, A.; Filinchuk, Y. Pressure-Collapsed Amorphous $Mg(BH_4)_2$: An Ultradense Complex Hydride Showing a Reversible Transition to the Porous Framework. *J. Phys. Chem. C* **2014**, *118* (40), 23402–23408.

(27) Yisgedu, T. B.; Huang, Z.; Chen, X.; Lingam, H. K.; King, G.; Highley, A.; Maharrey, S.; Woodward, P. M.; Behrens, R.; Shore, S. G.; Zhao, J.-C. The Structural Characterization of $(NH_4)_2B_{10}H_{10}$ and Thermal Decomposition Studies of $(NH_4)_2B_{10}H_{10}$ and $(NH_4)_2B_{12}H_{12}$. *Int. J. Hydrogen Energy* **2012**, *37* (5), 4267–4273.

(28) Sivaev, I. B.; Bregadze, V. I.; Sjöberg, S. Chemistry of Closo-Dodecaborate Anion $[B_{12}H_{12}]^{2-}$: A Review. *ollect. Czech. Chem. Commun.* **2002**, *67*, 679–727.

(29) Chen, X.-M.; Ma, N.; Zhang, Q.-F.; Wang, J.; Feng, X.; Wei, C.; Wang, L.-S.; Zhang, J.; Chen, X. Elucidation of the Formation Mechanisms of the Octahydrotriborate Anion ($B_3H_8^-$) through the Nucleophilicity of the B–H Bond. *J. Am. Chem. Soc.* **2018**, *140* (21), 6718–6726.

Chapter 8. Conclusions and Perspectives

Conclusions

The discovery of high cation mobility in the systems containing disordered dodecaborate anion, $B_{12}H_{12}^{2-}$, at the beginning of the century sparked intense research into hydroborates as solid electrolytes for all-solid-state batteries. However, the high commercial cost of $B_{12}H_{12}^{2-}$ salts remains a significant constraint for broader application. Consequently, the investigation of large scale synthesis of $M_xB_{12}H_{12}$ has become a focus of numerous research groups over the past few decades. The reported synthesis pathways towards $B_{12}H_{12}^{2-}$ involve both solution-based and solvent-free techniques. The former entails the use of borane precursors such as B_2H_6, B_5H_9, or $B_{10}H_{14}$, reacted with a borane triethylamine complex to yield $[(CH_3)_3NH]_2B_{12}H_{12}$. Subsequent cation exchange of this compound with metal hydroxides facilitates the production of $M_xB_{12}H_{12}$. While this method yields high-purity solvated $M_xB_{12}H_{12}$ and has been preferred in earlier studies, it is complex and costly. Conversely, more recent solvent-free approaches, based on ball-milling or annealing, have gained popularity due to their ability to produce anhydrous $B_{12}H_{12}^{2-}$ salts in a single step. However, these methods often result in the formation of $B_{12}H_{12}^{2-}$ alongside other boron-rich compounds. Additionally, concerns exist regarding the yield and purity of the product, as well as the toxicity and reactivity of specific borane precursors, presenting significant challenges. Thus, the ease of

synthesis and the optimization of processes to obtain pure $B_{12}H_{12}^{2-}$ salts in high yield emerge as crucial tasks.

The main goal of this thesis was to develop novel, simple, and efficient approaches for the synthesis of $B_{12}H_{12}^{2-}$ salts using cheaper and more manageable borane precursors, rather than conventional methods that rely on B_2H_6 and $B_{10}H_{14}$. We used the $DMS{\cdot}BH_3$ and borohydrides as a precursor to obtain a series of high-purity $B_{12}H_{12}^{2-}$ compounds through solvothermal synthesis. This thesis covers the solvothermal synthesis process, sample analysis, and experimental design.

Our research highlights the critical roles of temperature, solvents, reaction duration, and the role of the enclosed system in synthesizing high purity solvated metal-$B_{12}H_{12}$ compounds. Subsequently, we explored the desolvation processes and proposed solvent exchange as an alternative to conventional cation exchange to obtain anhydrous metal-$B_{12}H_{12}$ salts. In addition, the stepwise buildup for the formation of $B_{12}H_{12}^{2-}$ has been proposed in this experimental work.

Our initial efforts focused on autoclave conditions for reacting sodium borohydrides with $DMS{\cdot}BH_3$, as we believed that relatively harsh conditions, such as high temperatures and pressures, were necessary. We also considered the closed system essential for containing the volatile reagents, thus improving control over the yield and purity. The results of the studies with autoclave conditions are described in **Chapter 3**, where we detail the successful synthesis of $Na_2B_{12}H_{12}$ and $K_2B_{12}H_{12}$ in an autoclave, achieving high yield and purity. The synthesis of $Na_2B_{12}H_{12}$ and $K_2B_{12}H_{12}$ from their respective borohydrides and $DMS{\cdot}BH_3$ in diglyme follows a two-step process: synthesis and desolvation. We found that temperature is a critical factor for the synthesis: low temperatures led to incomplete

conversion of $NaBH_4$ into $Na_2B_{12}H_{12}$, attributed to the formation of diglyme-soluble species such as $B_3H_8^-$, $B_9H_{14}^-$, and $B_{11}H_{14}^-$, while higher temperatures resulted in the formation of various impurities, including dehydrogenated $B_{12}H_{12-x}^{2-}$ anion. Moreover, different reaction temperatures led to formation of different diglyme solvated $Na_2B_{12}H_{12}$ phases. Complete removal of diglyme from $Na_2B_{12}H_{12}$ solvates is efficient in vacuum at 200 °C. Exploring the synthetic methods to $K_2B_{12}H_{12}$, we found that reducing the particle size of the starting KBH_4 by ball-milling allowed us to increase the yields of $K_2B_{12}H_{12}$, which would be otherwise low due to the insolubility of KBH_4 in diglyme. $K_2B_{12}H_{12}$ shows some solubility in diglyme; thus, not the whole product can be recovered in the precipitate, but the mother liquor may be recycled *via* a subsequent synthesis to further increase the yield.

Expanding on these findings, we next sought to a simple solvothermal synthesis method for $Li_2B_{12}H_{12}$, which is very interesting as a precursor in the synthesis of solid-state electrolytes but challenging to be synthesized by solvothermal methods due to its strong coordinating ability with ethers. **In Chapter 4**, we firstly compared the reactions in autoclaves and Schlenk setup, identifying optimal conditions for synthesis of solvated $Li_2B_{12}H_{12}$ at 120 °C in an autoclave for 48 h, resulting in a 96% yield. Lower reaction temperatures resulted in incomplete conversion of BH_4^- to $B_{12}H_{12}^{2-}$, due to the slow reaction kinetics between $B_3H_8^-$ and $B_9H_{14}^-$ and $B_{11}H_{14}^-$. Higher temperatures led to the direct formation of dehydrogenated $B_{12}H_{12-x}^{2-}$. The enclosed system of the autoclave, enabling a higher (autogenous) pressure of DMS, prevented decomposition of BH_3 into higher boranes and facilitated the reaction and increased the overall yield. In turn, the use of high boiling solvent in a Schlenk flask favored the formation of $B_{11}H_{14}^-$. The use of diglyme under reflux allowed for the syntheses of $Na_2B_{12}H_{12}$ and $K_2B_{12}H_{12}$ in high yields using a Schlenk setup, making the synthesis

much more accessible to typical synthetic chemist.

However, use of glymes as solvents presented a challenge for Li-based salts, as it resulted in the formation of glyme-solvated $Li_2B_{12}H_{12}$ with a strong coordination of solvents to Li^+. We found that simple thermal treatment under vacuum was ineffective to remove the coordinated diglyme from the product. In that case, we came up with an exchange of diglyme by higher boiling point but less coordinating polar solvents such as DMSO or *N*,*N*-diethylformamide followed by heating under vacuum. We demonstrated this procedure being successful for obtaining unsolvated $Li_2B_{12}H_{12}$. In addition, starting the reaction with monoglyme as solvent in an autoclave also led to pure DME-solvated $Li_2B_{12}H_{12}$. In contrast to the diglyme solvate, the coordinated monoglyme can be removed from $Li_2B_{12}H_{12}$ by a simple heat treatment, leaving only a small amount of the residual solvent. Interestingly, the substitution of DME by H_2O allows for the preparation of chemically pure $Li_2B_{12}H_{12}$·n H_2O. We also tried to perform the reaction in non-coordinating solvents such as toluene, and we obtained diffraction pure $Li_2B_{12}H_{12}$ directly, containing amorphous impurities according to NMR, thus further purification or extraction steps are required. Finally, a stepwise buildup mechanism of $B_{12}H_{12}^{2-}$ under the developed reaction conditions was elucidated through ex situ follow-up of reaction intermediates using solution ^{11}B NMR. This evidenced a stepwise buildup mechanism of $B_{12}H_{12}^{2-}$ from BH_4^- through $B_2H_7^-$, $B_3H_8^-$, $B_9H_{14}^-$, and $B_{11}H_{14}^-$ intermediates. Furthermore, $B_{11}H_{13}^{2-}$ was proposed as the final intermediate based on experiments starting from the isolated $B_{11}H_{14}^-$. The developed synthetic method represents a significant improvement compared to previous strategies in terms of yield, purity, and cost-effectiveness for lithium and other alkali metal dodecaborates both in their solvated and desolvated forms.

To broaden the scope of the work to divalent cation borohydrides, further work was conducted to obtain alkali earth metal dodecaborates ($MB_{12}H_{12}$). **In Chapter 5**, high-purity $CaB_{12}H_{12}$ was obtained using a combination of THF and DME as solvents. This method successfully tackled the problem of preventing the formation of unwanted borane clusters while also ensuring the solubility of smaller borane clusters during the interaction between calcium hydride and the $DMS{\cdot}BH_3$ complex. In addition, the presence of dimethoxyethane (DME) in the reaction mixture aimed for the stronger bidentate coordination of metal ions, lowering the risk of $B_{12}H_{12-x}^{2-}$ anion formation. As a result of this improved combination, $CaB_{12}H_{12}$ samples are both X-ray and ^{11}B NMR pure. The established solvothermal approach for $CaB_{12}H_{12}$ not only solves earlier hurdles but also lays the groundwork for future research into other divalent cation borohydrides.

We also attempted to synthesize $MgB_{12}H_{12}$. However, difficulties arose because of the strong coordination between Mg^{2+} ions and oxygen donor atoms, limiting the use of ethers as solvents. While using toluene as a solvent, the insolubility of borohydrides spurred the self-condensation of $DMS{\cdot}BH_3$ in an alternate manner, culminating in the synthesis of $B_{12}H_{11}S(CH_3)_2^-$, as evidenced by the isolation and characterization of $(CH_3)_3S{\cdot}B_{12}H_{11}S(CH_3)_2$ single crystal.

Despite the high oxophilicity of magnesium cation makes the synthesis of $MgB_{12}H_{12}$ challenging in ethers, it has enabled us to explore its potential in CO_2 capture and conversion. **In Chapter 6**, we investigated reaction between porous magnesium borohydride (γ-$Mg(BH_4)_2$) and CO_2 at near ambient conditions. We attempted the reaction by a direct contact with gas and mechanical activation and both methods revealed the spontaneous character of the reaction already at room temperature. Formylhydroborates, $Mg[H_xB(OCHO)_{4-x}]$ (x = 1-3), were identified as main intermediates by solid state ^{11}B NMR, and transformations lead to the generation of hydrogen, diborane, as well as $B(OCH_3)_3$ and methanol. Localization of CO_2 in

the porous structure in the initial stages of the interaction was characterized by neutron and synchrotron X-ray powder diffraction.

Further on, we developed a simple synthesis for tetraalkylammonium $B_{12}H_{12}$ and B_3H_8 salts using a combination of autoclave synthesis and metathesis, as described in **In Chapter 7**. Since tetraalkylammonium is known as non-coordinating cations, there was no coordinated solvent in our final product. We started this work by detailing two distinct methods for synthesizing $(Me_4N)_2B_{12}H_{12}$. Notably, this compound exhibits intriguing, isolated pores within its crystal structure. Although these pores lack interconnection, they demonstrate high potential for gas adsorption, particularly for CO_2.

In summary, this project proposed a simple and efficient solvothermal method for preparing a series of anhydrous $B_{12}H_{12}^{2-}$ salts with metal (Li^+, Na^+, K^+, Ca^{2+}) or organic cations ($(CH_3)_4N^+$, $(C_3H_7)_4N^+$, $(C_4H_9)_4N^+$). These findings not only provide an alternative to existing methods but also lay a foundation for future research in practical applications like electrolytes and gas adsorption. It is interesting to note that relatively simple reaction setups used in this work allowed to find completely new and excellent conditions for high-purity and high-yield synthesis of these important families of compounds. This was not achieved by a simple optimization of the reaction conditions, as this might appear on the first sight, but thanks to a buildup of the understanding based on careful analysis of the reaction products. This included clarifying the role of temperature in the stepwise formation of the $B_{12}H_{12}^{2-}$ anions, numerous attempts to get around the highly stable intermediates, such as solvates with heavy ethers etc. The *in situ* studies of the reaction pathways using NMR spectroscopy has allowed to practically “visualize” chemistry, while the X-ray crystallography gave a feeling of stability of the various

solvates, serving as a guide to changing the synthetic approaches. It is important also to make sometimes a larger step, passing from convenient well studied systems (like Na- and Li-based salts) to quite different ones, such as alkali earth metals and organic cations. This requires not only a courage to address very different systems, but also the experience accumulated in the first steps. Without the experience accumulated in the first half of this work, the real advances with more complex systems seem to be less likely. This evolution inspired us to take further large steps, taking bigger challenges and extending these approaches beyond obtaining dodecaborates. Some of the ideas will be described in the next section, called Perspectives.

Perspectives

During this thesis we produced several fascinating, phase-pure, porous, and well-characterized $B_{12}H_{12}^{2-}$ phases. These novel compounds show potential for a variety of applications as solid-state electrolytes and in gas sorption, both in their current form or after modifications. The success of the developed synthetic methods highlights the potential of using borohydrides and borane complexes for the synthesis of corresponding dodecaborate salts. Future perspectives of this work can focus on optimizing the process for greater efficiency, particularly by using larger enclosed reactors. This, however, requires a thorough understanding of the solubility of dodecaborates in the reaction solution (diglyme for instance), which can lead to higher yields and larger-scale production. Furthermore, it would be interesting to develop a large-scale convenient route to obtain these materials without using an autoclave. This would simplify the synthesis process and potentially broaden the applicability of the method. We see the following directions for further progress:

1. A cheaper and larger scale synthesis
2. A simpler and efficient desolvation process
3. Isolation of other intermediates and synthesis of alternative borate anions
4. Applications

Further efforts should initially focus on scaling up the synthesis to tens of grams by utilizing a larger volume autoclave. We recommend using more economical borohydrides, such as $NaBH_4$ and KBH_4, as precursors. However, it is crucial to understand the solubility of $Na_2B_{12}H_{12}$ and $K_2B_{12}H_{12}$ in solvents, especially diglyme, since these compounds exhibit some solubility in it. Additionally, exploring the use of less expensive Lewis acids, such as halogenated alkanes, to react with $NaBH_4$ and generate BH_3 in situ for the synthesis of $Na_2B_{12}H_{12}$ could further reduce overall costs.

After synthesis, it is important to efficiently remove coordinated solvents. In the thesis work, we used excess solvents for solvent exchange, but some of these solvents are quite heavy, making the synthesis less efficient. Further optimization of the solvent exchange process, particularly in terms of the proportions between coordinated solvents and the solvent used for exchange, may improve overall process effectiveness. Using lighter solvents, especially less bulky ethers such as THF, might enable easier removal by heat treatment.

In this thesis, we only report the way to isolate $B_{11}H_{14}^-$ with Li ion (diglyme solvated) and $NaB_{11}H_{14}$ (H_2O solvated). It would be interesting to try isolating $B_{11}H_{14}^-$ with other alkali metal cations, including Na^+ and K^+, as these nido-B_{11} unit salts are known important intermediates to for conducting *closo* borates, such as $CB_{11}H_{12}^-$. Efforts can also be directed toward exploring reaction conditions and

isolating intermediates using weaker donating solvents, such as N- or S-based solvents, which might help obtain other intermediates, such as $B_9H_{14}^-$.

Transforming some materials from this thesis work, like $CaB_{12}H_{12}$, into solid-state electrolytes containing other neutral molecules (e.g., amines and H_2O) should be conducted to demonstrate an integrated solution for the synthesis of Ca-ion electrolytes. Moreover, It is also possible to obtain $Ca(CB_{11}H_{12})_2$ by using a mixture of THF and DME as solvents, *via* the reaction of $CaB_{11}H_{13}$ and a carbene. Notably, $Ca(CB_{11}H_{12})_2$ is highly soluble in the THF and DME mixture whereas $CaB_{12}H_{12}$ not, making it promising to synthesize both $CaB_{12}H_{12}$ and $Ca(CB_{11}H_{12})_2$ from one synthesis using these combined solvents.[1] To access $MgB_{12}H_{12}$, substitution reactions using organometallic precursors like di-butyl magnesium ($Mg(nBu)_2$) and $[(CH_3)_3NH]_2B_{12}H_{12}$ in non-coordinating solvents can be explored, similar work can be done to access $Mg(CB_{11}H_{12})_2$. The preparation and applications of these alkali-earth metal dodecaborates represent a relatively new area of study.

Future work on CO_2 reduction can focus on finding specific reaction conditions that lead to a single product from the reaction of CO_2 with γ-$Mg(BH_4)_2$. This could help reduce carbon dioxide under mild conditions, potentially making the cycle closed by the easy recycling of borohydrides, as recently discovered via ball-milling with MgH_2.[2]

CO_2 adsorption and other gas adsorption and separation studies should be conducted with $[(CH_3)_4N]_2B_{12}H_{12}$. Besides volumetric studies of gas adsorption, focusing on both equilibrium adsorption/desorption curves and kinetic barriers of adsorption/gas diffusion, future work should involve characterizing gas-loaded

structures with different gases to provide valuable mechanistic insights into the interaction of guests with hydridic pores. Additionally, exploring the synthesis of $(CH_3)_4N^+$ salts with other *closo* borate anions holds promise. Changing the cations could enable control over pore size and, to some extent, the nature of its surface. We hope hydrogen adsorption in these porous materials will prove the concept of dense hydrogen loading in porous hydrides, exemplified by the example of γ-$Mg(BH_4)_2$.[3]

Taken together, this thesis, as well as the follow-up work described in the perspectives contributes significantly to the field of hydride-based solid-state electrolytes (dodecaborates, carborates), CO_2 transformation using γ-$Mg(BH_4)_2$, gas storage and separation in small-pore hydridic materials, such as $[(CH_3)_4N]_2B_{12}H_{12}$, as well as understanding of the stepwise formation of $B_{12}H_{12}^{2-}$ and of the related anions.

References

(1) Kisu, K.; Kim, S.; Shinohara, T.; Zhao, K.; Züttel, A.; Orimo, S. Monocarborane Cluster as a Stable Fluorine-Free Calcium Battery Electrolyte. *Sci. Rep.* **2021**, *11*, 7563.

(2) Chen, K.; Liu, M.; Peng, Z.; Zhing, H. ; Gan, L.; Huang, J.; Zhao, J.; Wang, H.; Liu, J.; Shao H.; Ouyang, L. Enabling one-step regeneration of $LiBH_4$ with self-sustaining hydrogen in its spent fuel−One pathway to storing renewable hydrogen. *J. Alloys Comp.*, **2024**, *987*, 174209.

(3) Oh, H.; Tumanov, N.; Ban, V.; Li, X.; Richter, B.; Hudson, M. R.; Brown, C. M.; Iles, G. N.; Wallacher, D.; Jorgensen, S. W.; Daemen, L.; Balderas-Xicohténcatl, R.; Cheng, Y.; Ramirez-Cuesta, A. J.; Heere, M.; Posada-Pérez, S.; Hautier, G.; Hirscher, M.; Jensen, T. R.; Filinchuk, Y. Small-Pore Hydridic Frameworks Store Densely Packed Hydrogen. *Nat. Chem.* **2024**, *16*, 809−816.

Appendix I: Supporting Information of Chapter 3

The supporting info of this Chapter has been published online (Inorg. Chem. 2023, 62, 5, 2153–2160) and is accessible through the following doi: https://doi.org/10.1021/acs.inorgchem.2c03810

Appendix

Appendix II: Supporting Information of Chapter 4

Table S1. Reported solubilities of alkali borohydrides in the solvents used in this work (at 25 °C).

Description	$LiBH_4$	$NaBH_4$	KBH_4
Diglyme	9.64 g/100 g (4.25 M)	5.5 g/100 g	Insoluble
Monoglyme	9.81 g/100 g (4.7 M)	0.8 g/100 g	n.d.
Toluene	Insoluble	Insoluble	Insoluble
DMSO	soluble	soluble	7.6 g/100 g

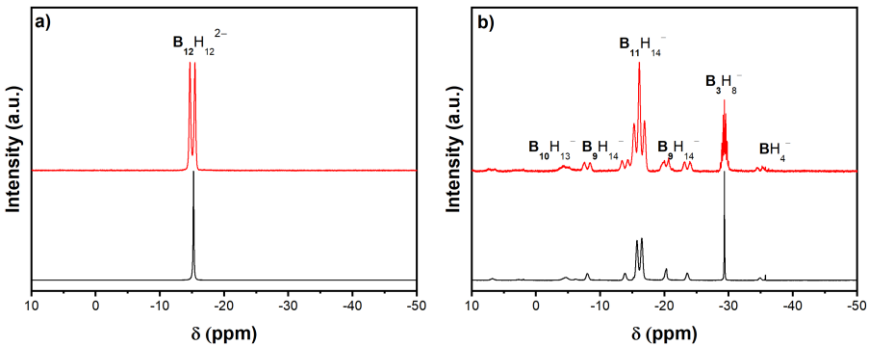

Figure S1. Proton decoupled (black) and coupled (red) ^{11}B NMR spectra of a) solid precipitate and b) filtrate of after reaction of $LiBH_4$ with 5 equiv (10% excess) of $DMS{\cdot}BH_3$ for 24 h at 120 °C in a Schlenk flask.

Appendix

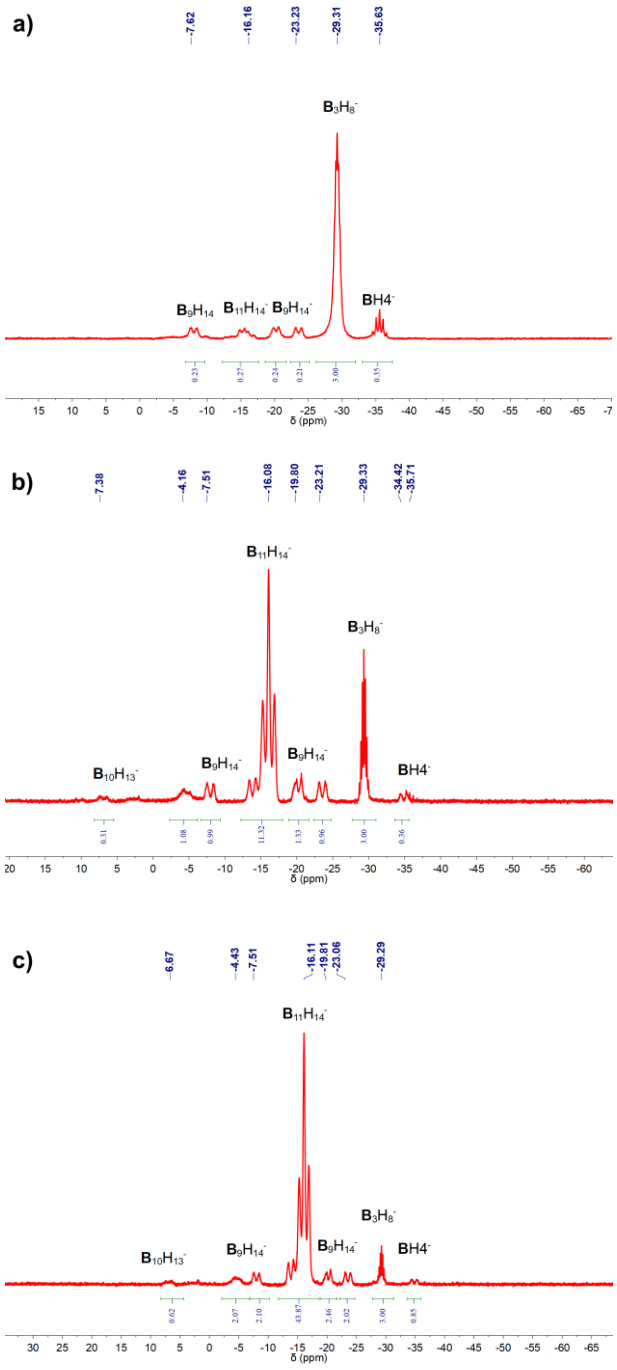
a)
-7.62
-16.16
-23.23
-29.31
-35.63
B3H8-
B9H14-
B11H14-
B9H14-
BH4-
δ (ppm)
b)
-7.38
-4.16
-7.51
-16.08
-19.80
-23.21
-29.33
-34.42
-35.71
B11H14-
B3H8-
B10H13-
B9H14-
B9H14-
BH4-
δ (ppm)
c)
-6.67
-4.43
-7.51
-16.11
-19.81
-23.06
-29.29
B11H14-
B3H8-
B10H13-
B9H14-
B9H14-
BH4-
δ (ppm)

Figure S2. Integrated proton-coupled ^{11}B NMR spectra of filtrates obtained from Schlenk flask syntheses of $Li_2B_{12}H_{12}$ using different $LiBH_4/DMS{\cdot}BH_3$ ratios: (a) $LiBH_4 : DMS{\cdot}BH_3 = 1:2$ (using 5 mmol $LiBH_4$ and 10 mmol $DMS{\cdot}BH_3$), (b) $LiBH_4 : DMS{\cdot}BH_3 = 1:5.5$ (using 27.5 mmol $DMS{\cdot}BH_3$) and (c) $LiBH_4 : DMS{\cdot}BH_3 = 1:10$ (using 50 mmol $DMS{\cdot}BH_3$).

Table S2. Composition of filtrates obtained from experiments using different $LiBH_4$: BMS ratios, as determined from the NMR spectra in Figure S4.

Description	**$LiBH_4$: BMS ratio**	**Composition (molar ratio relative to $B_3H_8^-$)**				
		BH_4^-	**$B_3H_8^-$**	**$B_9H_{14}^-$**	**$B_{10}H_{13}^-$**	**$B_{11}H_{14}^-$**
a	1: 2	0.35	1	0.23	n.d.	0.07
b*	1: 5	n.d.	1	0.36	0.175	1.03
c	1: 10	n.d.	1	0.73	0.355	3.98

*Note: for the filtrate b, the signals originating from small clusters were overlapped, as observed in the $^{11}B\{^1H\}$ spectrum (Figure S4b). This suggests that BH_4^- and $B_2H_7^-$ coexist in the filtrate, with a slight residual amount of $B_{12}H_{12}^{2-}$, leading to a potentially substantial error in the integration of the signal of $B_{11}H_{14}^-$

Appendix

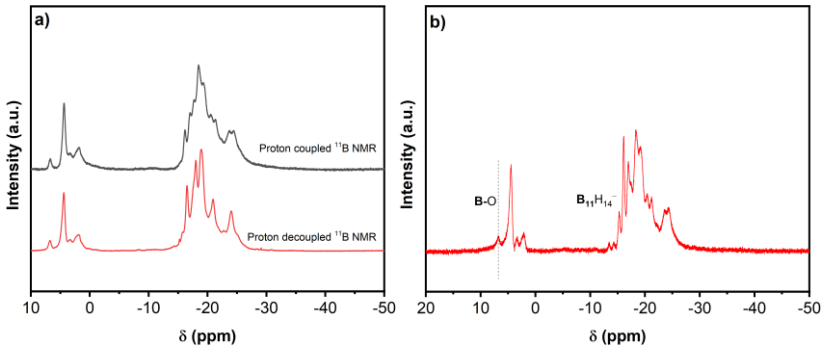

Figure S3. a) Proton-coupled and decoupled ^{11}B NMR spectra of yellow oily residue obtained upon reaction of $LiBH_4$ with 5 equiv (10% excess) of $DMS{\cdot}BH_3$ for 24 h at 160 °C in a Schlenk flask without condenser and b) ^{11}B NMR spectrum of the filtrate diluted in DMSO-d_6. The reaction at 160 °C leads to partial dehydrogenation of $Li_2B_{12}H_{12}{\cdot}n$ diglyme (diglyme = $C_6H_{14}O_3$), forming $Li_2B_{12}H_{12-x}{\cdot}n\ C_6H_{14-x}O_3$.

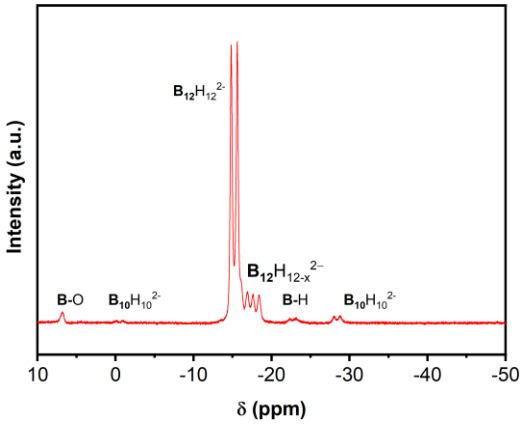

Figure S4. Proton-coupled ^{11}B NMR spectrum of the solid precipitate obtained upon reacting $LiBH_4$ with 5 equiv (10% excess) of $DMS{\cdot}BH_3$ for 24 h at 160 °C in a Schlenk flask equipped with a condenser. The reaction at 160 °C leads to dehydrogenation of $Li_2B_{12}H_{12}{\cdot}n$ diglyme (diglyme = $C_6H_{14}O_3$), forming $Li_2B_{12}H_{12-x}{\cdot}n\ C_6H_{14-x}O_3$.

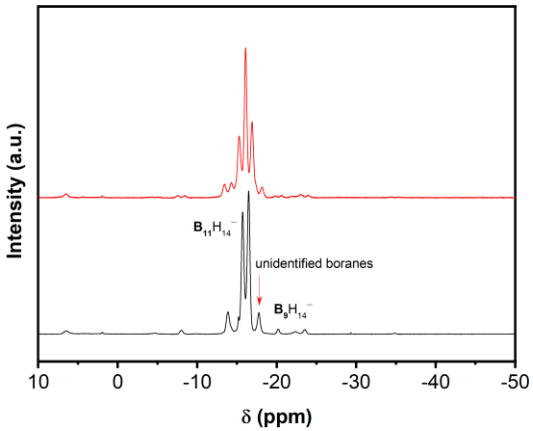

Figure S5. Proton decoupled (black) and coupled (red) ^{11}B NMR spectra of a filtration obtained upon reacting $LiBH_4$ with 5 equiv. (10% excess) of $DMS{\cdot}BH_3$ for 24 h at 120 °C in a Schlenk flask equipped with a condenser.

note: Conducting the synthesis in a setup equipped with a condenser facilitated the dehydrocondensation reaction of lower borane clusters, resulting in the formation of $B_{11}H_{14}^-$. Additionally, the presence of partially dehydrogenated $Li_2B_{12}H_{12-x}\cdot$ n $C_6H_{14-x}O_3$ anions can also be attributed to the presence of traces of H_2O in the solvents used in the process.

Appendix

Table S3. Yields of $Li_2B_{12}H_{12}$ isolated from the reaction of $LiBH_4$ and BMS in a Schlenk flask under various conditions.

Entry (*)	Reagents			Reaction conditions		Crude sample weight after drying	Composition of precipitates based on ^{1}H NMR	Yield of $Li_2B_{12}H_{12}$
	$LiBH_4$ (mmol)	DMS·BH_3 (mmol)	Diglyme (ml)	Temp (°C)	Time (h)	(g)		(%)
S1	5	27.5	20	85	24/48	Uncollectible	/	< 5
S2	5	10	20	120	24	0.19	$Li_2B_{12}H_{12}$ + 4.07 diglyme	11
S3	5	50	20	120	24	0.32	$Li_2B_{12}H_{12}$ + 2.8 diglyme	25
S4	5	27.5	20	120	12	0.47	$Li_2B_{12}H_{12}$ + 3.73 diglyme	30
S5	5	27.5	20	120	24	0.68	$Li_2B_{12}H_{12}$ + 3.57 diglyme	45
S6	10	55	20	120	24	0.88	$Li_2B_{12}H_{12}$ + 2.28 diglyme	40
S7	5	27.5	20	120 (Refluxing)	24	0.52	$Li_2B_{12}H_{12}$ + 2.24 diglyme	48
S8	5	27.5	20	120	48	0.92	$Li_2B_{12}H_{12}$ + 4.18 diglyme	54
S9	5	27.5	20	160	24	Yellow oily compound	unidentified boranes; $B_{11}H_{14}^-$; $B_{12}H_{12-x}^{2-}$	
S10	5	27.5	20	160 (Refluxing)	24	1.46	$B_{12}H_{12}^{2-}$; $B_{10}H_{10}^{2-}$; $B_{12}H_{12-x}^{2-}$	

Table S4. Isolated yields from the reactions between $NaBH_4$ (KBH_4) and DMS·BH_3 in refluxing diglyme.

Entry (*)	Reagents			Reaction conditions		Crude sample weight after drying	Composition of precipitate based on ^{1}H NMR	Yield of $M_2B_{12}H_{12}$ (M = Na or K) (%)
	BH_4^- (mmol)	DMS·BH_3 (mmol)	Diglyme (ml)	Temp (°C)	Time (h)			
$NaBH_4$	5	27.5	20	160	24	0.98 g	$Na_2B_{12}H_{12}$ + 1.76 diglyme	92
KBH_4*	5	27.5	20	160	24	0.5 g	$K_2B_{12}H_{12}$	88

* The sample contains ~5% $K_2B_{12}H_{12-x}$· n $C_6H_{14-x}O_3$ impurities after purification, based on integration of the ^{11}B NMR spectrum.

Table S5. Yields of $Li_2B_{12}H_{12}$ isolated from the reaction of $LiBH_4$ and BMS in an autoclave under various conditions.

Entry (*)	Reagents			Reaction conditions		Crude sample weight after drying	Composition of precipitates based on ^1H NMR	Yield of $Li_2B_{12}H_{12}$
	$LiBH_4$ (mmol)	DMS·BH_3 (mmol)	Diglyme (ml)	Temp (°C)	Time (h)	(g)		(%)
A1	5	27.5	20	120	12	0.94	$Li_2B_{12}H_{12}$ + 3.31 diglyme	66
A2	5	27.5	20	120	24	1.13	$Li_2B_{12}H_{12}$ + 2.75 diglyme	91
A3	5	27.5	20	120	48	1.44	$Li_2B_{12}H_{12}$ + 3.54 diglyme	96
A4	10	55	20	120	24	2.81	$Li_2B_{12}H_{12}$ + 3.99 diglyme	86
A5	5	55	20	160	24	Colorless oily compound	unknown boranes	

Table S6. Yields of $Li_2B_{12}H_{12}$ isolated from the reaction of $LiBH_4$ and BMS in monoglyme in an autoclave.

Entry (*)	Reagents			Reaction conditions		Crude sample weight after drying	Composition of precipitates based on ^1H NMR	Yield of $Li_2B_{12}H_{12}$
	$LiBH_4$ (mmol)	DMS·BH_3 (mmol)	monoglyme (ml)	Temp (°C)	Time (h)	(g)		(%)
A6*	10	55	20	120	24	1.38	$Li_2B_{12}H_{12}$ + 5.92 monoglyme	42
A7	10	55	20	120	24	1.42	$Li_2B_{12}H_{12}$ + 1.99 monoglyme	89

* Particle size with A6is too small to allow filtration (below 16 μm), solid

precipitates remain in the filtrate

The calculation of yields is based on the equation (1) below:

$$2\ MBH_4 + 10\ (CH_3)_2S{\cdot}BH_3 \rightarrow M_2B_{12}H_{12} + 10\ (CH_3)_2S + 13\ H_2 \quad (M = Li, Na, K) \qquad (1)$$

The theoretical yields of $M_2B_{12}H_{12}$ from 5 mmol MBH_4 (M = Li, Na, K), which is the typical amount used in the experiments, are listed in Table S7 below:

Table S7. Theoretical yields of $M_2B_{12}H_{12}$ from 5 mmol MBH_4 (M = Li, Na, K).

MBH_4	**Weight (g)**	**Purity (%)**	**Theoretical yields of $M_2B_{12}H_{12}$ (g)**
$LiBH_4$	0.11	95	0.37
$NaBH_4$	0.19	95	0.45
KBH_4	0.27	98	0.54

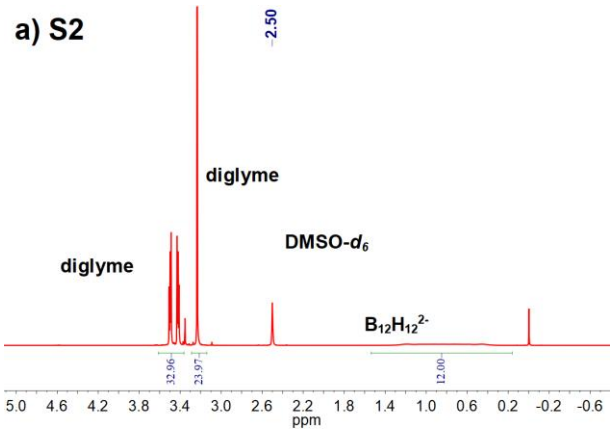

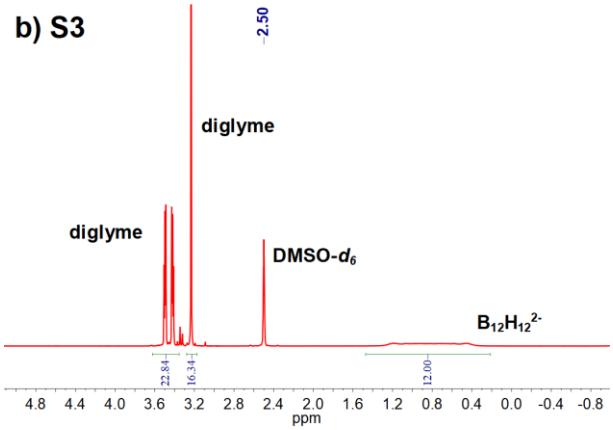
b) S3
2.50
diglyme
diglyme
DMSO-d_6
$B_{12}H_{12}^{2-}$
22.84
16.34
12.00
4.8 4.4 4.0 3.6 3.2 2.8 2.4 2.0 1.6 1.2 0.8 0.4 0.0 -0.4 -0.8
ppm

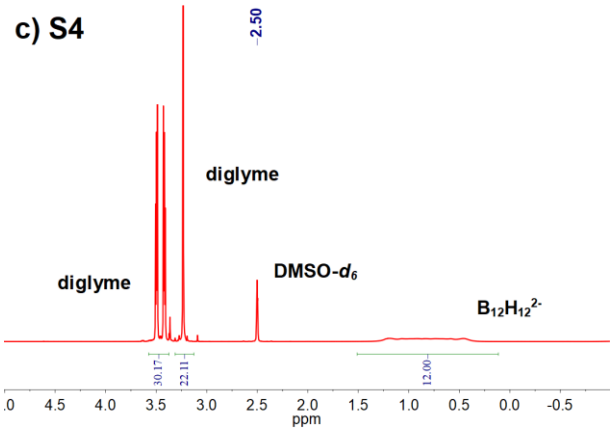
c) S4
2.50
diglyme
diglyme
DMSO-d_6
$B_{12}H_{12}^{2-}$
30.17
22.11
12.00
.0 4.5 4.0 3.5 3.0 2.5 2.0 1.5 1.0 0.5 0.0 -0.5
ppm

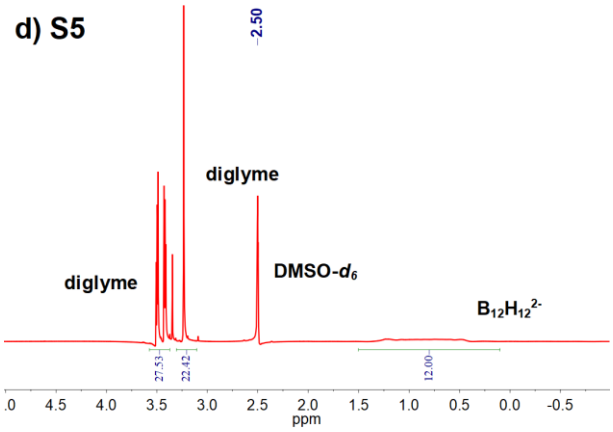
d) S5
2.50
diglyme
diglyme
DMSO-d_6
$B_{12}H_{12}^{2-}$
27.53
22.42
12.00
.0 4.5 4.0 3.5 3.0 2.5 2.0 1.5 1.0 0.5 0.0 -0.5
ppm

Appendix

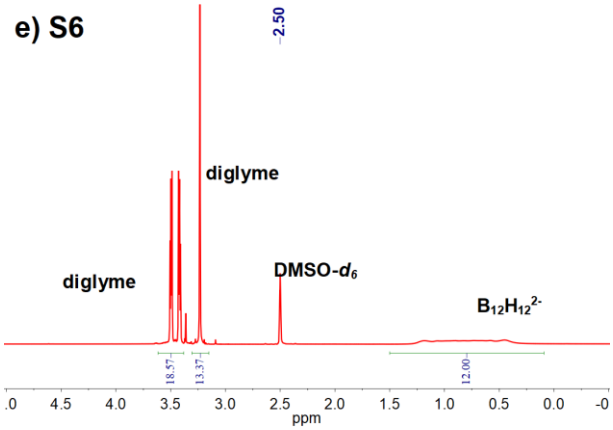
e) S6
2.50
diglyme
diglyme
DMSO-d_6
$B_{12}H_{12}^{2-}$
18.57
13.37
12.00
ppm

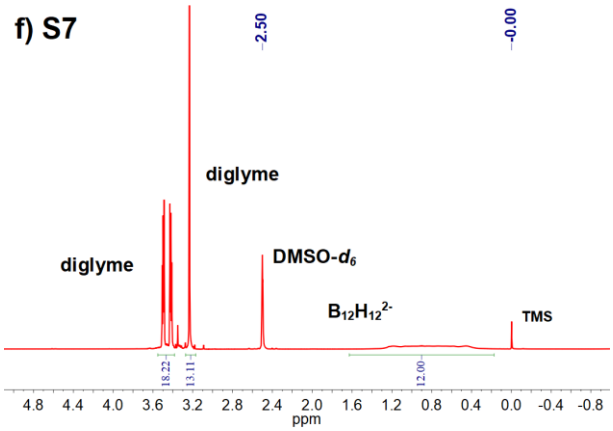
f) S7
2.50
0.00
diglyme
diglyme
DMSO-d_6
$B_{12}H_{12}^{2-}$
TMS
18.22
13.11
12.00
ppm

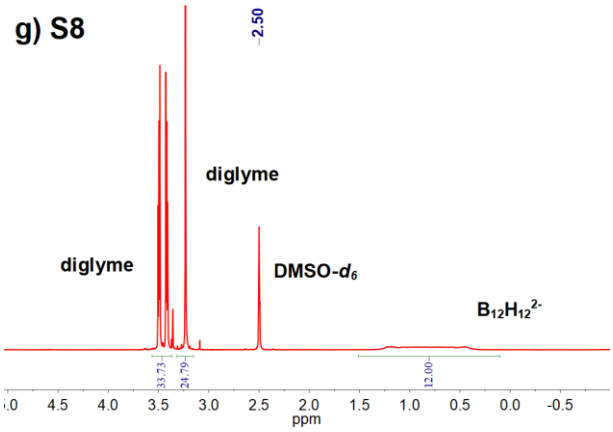
g) S8
2.50
diglyme
diglyme
DMSO-d_6
$B_{12}H_{12}^{2-}$
33.73
24.79
12.00
ppm

Figure S6. Integrated ^{1}H NMR spectra of isolated $Li_2B_{12}H_{12}$ samples obtained in a Schlenk setup, according to the conditions described in Table S3. Values indicated in blue correspond to the integration of the signals. The singlets at 3.31 ppm are due to residual water in the DMSO-d_6 used for dissolving the samples.

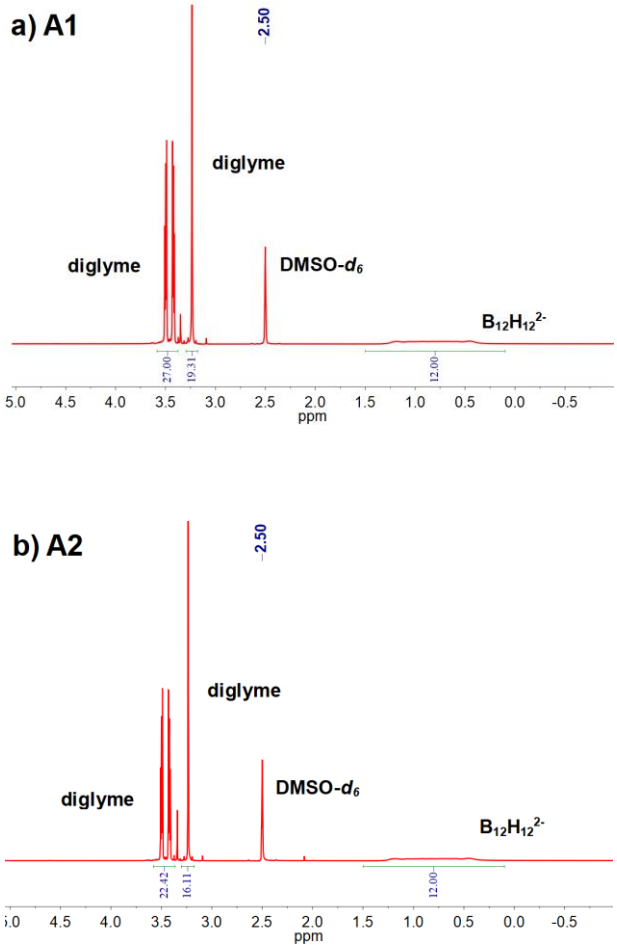

Appendix

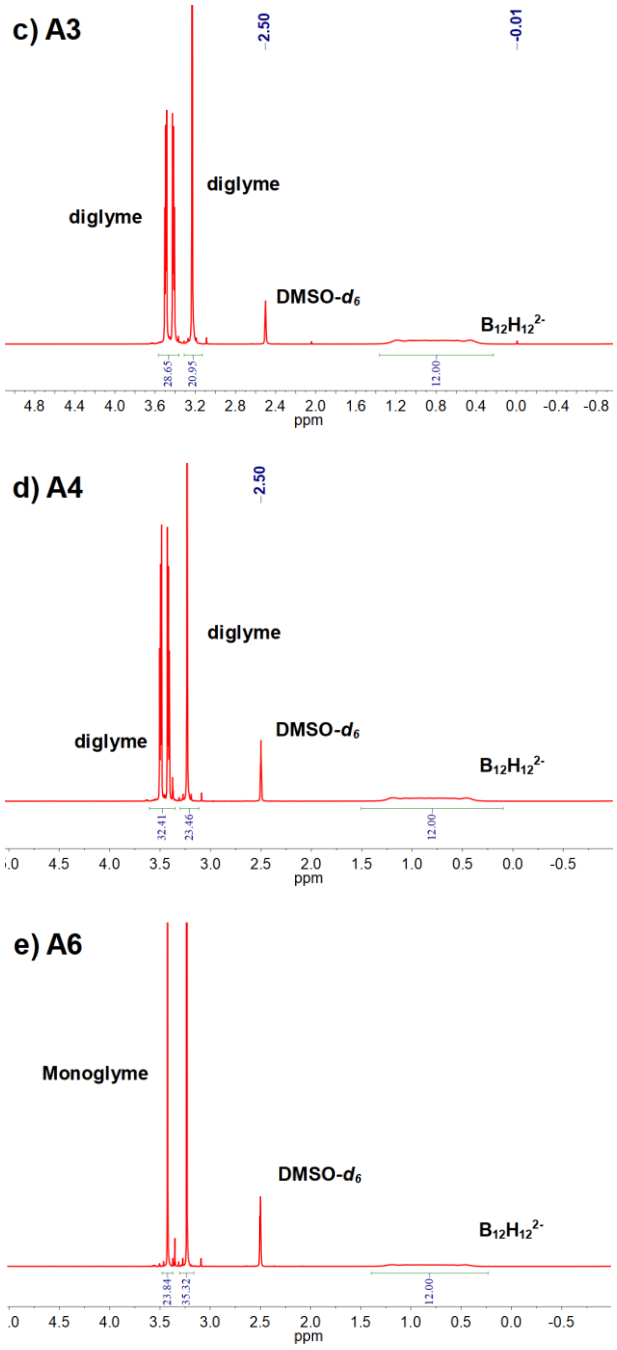
c) A3
2.50
0.01
diglyme
diglyme
DMSO-d_6
$B_{12}H_{12}^{2-}$
28.65
20.95
12.00
4.8 4.4 4.0 3.6 3.2 2.8 2.4 2.0 1.6 1.2 0.8 0.4 0.0 -0.4 -0.8
ppm
d) A4
2.50
diglyme
diglyme
DMSO-d_6
$B_{12}H_{12}^{2-}$
32.41
23.46
12.00
4.5 4.0 3.5 3.0 2.5 2.0 1.5 1.0 0.5 0.0 -0.5
ppm
e) A6
Monoglyme
DMSO-d_6
$B_{12}H_{12}^{2-}$
23.84
35.32
12.00
4.5 4.0 3.5 3.0 2.5 2.0 1.5 1.0 0.5 0.0 -0.5
ppm

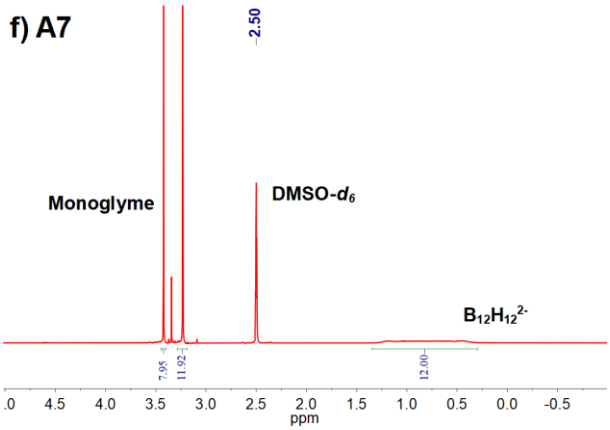

Figure S7. Integrated ^{1}H NMR spectra of isolated $Li_2B_{12}H_{12}$ samples obtained in an autoclave, according to the conditions described in Table S4. The singlets at 3.31 ppm are due to residual water in the DMSO-d_6 used for dissolving the samples.

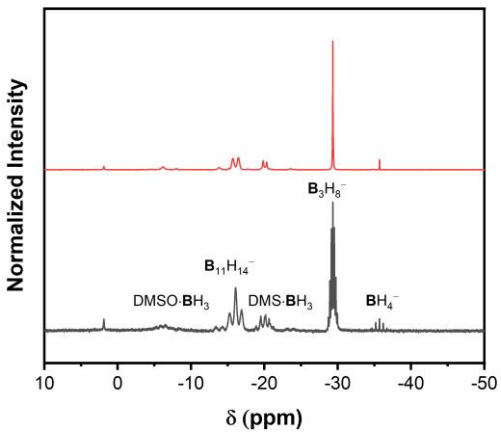

Figure S8. Proton-coupled and decoupled ^{11}B NMR spectra of filtrates obtained upon reaction of 5 mmol $LiBH_4$ with 5 equiv (10% excess) of DMS·BH_3 for 24 h at 120 °C in autoclave in diglyme.

Appendix

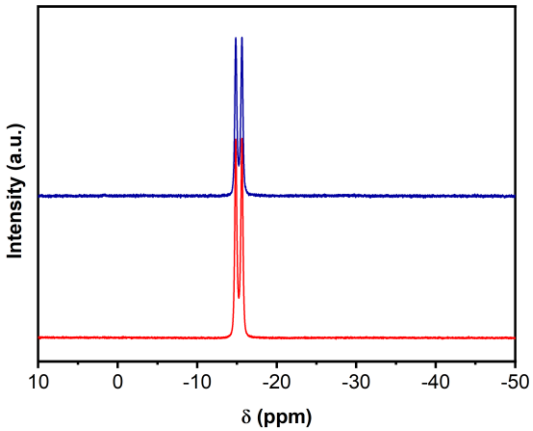

Figure S9. Proton-coupled ^{11}B NMR spectra of two batches of solid precipitates obtained by reaction of 10 mmol $LiBH_4$ with 55 mmol (10% excess) of $DMS{\cdot}BH_3$ for 24 h at 120 °C in an autoclave (red = first batch, same spectrum as the one represented in Figure 2; blue = second batch).

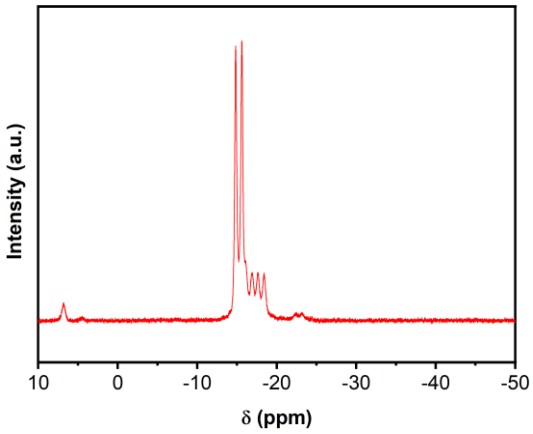

Figure S10. Proton-coupled ^{11}B NMR spectrum of $Li_2B_{12}H_{12}{\cdot}n$ diglyme upon heating at 180 °C under air for 5 minutes.

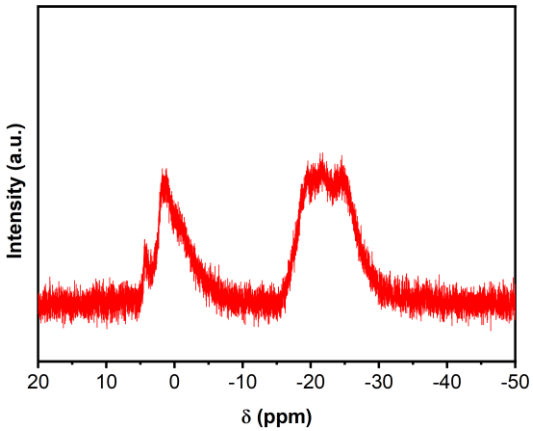

Figure S11. Proton-coupled ^{11}B NMR spectrum of $Li_2B_{12}H_{12}$·n diglyme upon heating at 180 °C under air for 12 h.

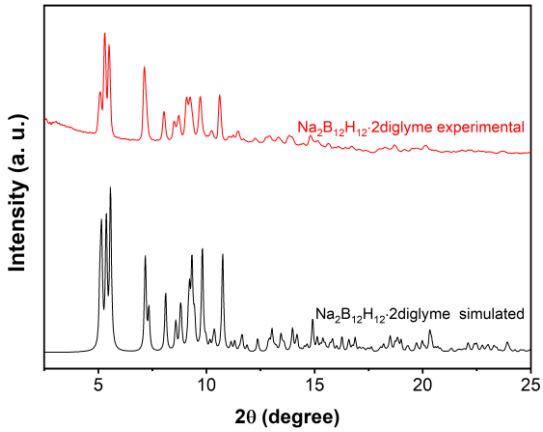

Figure S12. Experimental PXRD pattern of as synthesized diglyme solvated $Na_2B_{12}H_{12}$ sample upon initial drying at 80 °C under vaccum, and simulated pattern from the structure solved from a single crystal of $Na_2B_{12}H_{12}$·2 diglyme (λ = 0.71073 Å).

Appendix

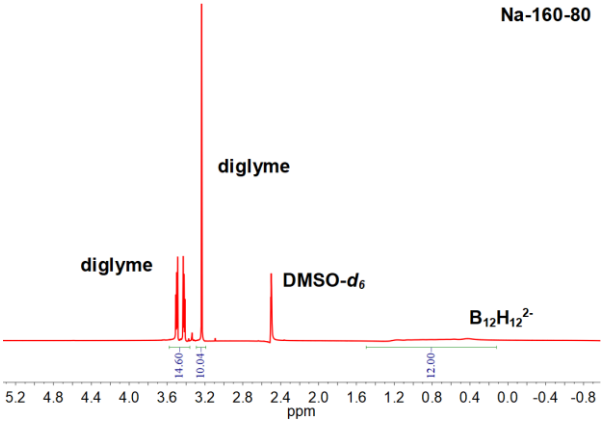

Figure S13. Integrated ^{1}H NMR spectrum of diglyme solvated $Na_2B_{12}H_{12}$ upon initial drying at 80 °C under vacuum. The composition of the sample was determined as $Na_2B_{12}H_{12}$·1.76 diglyme.

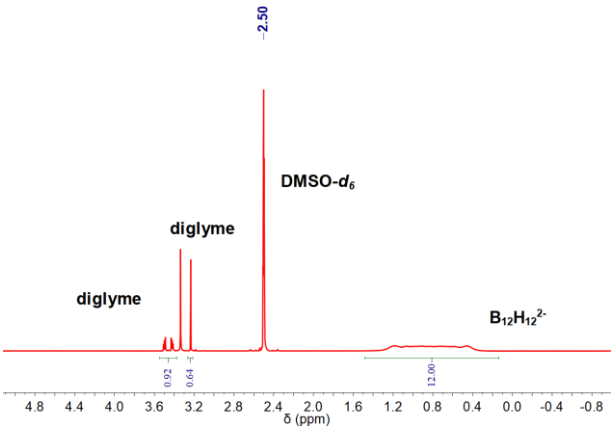

Figure S14. Integrated ^{1}H NMR spectrum of diglyme solvated $Na_2B_{12}H_{12}$ upon drying at 200 °C for 2 h under vacuum.

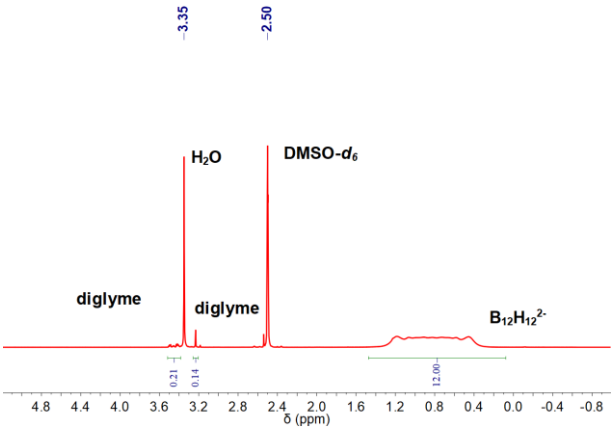

Figure S15. Integrated ^{1}H NMR spectrum of diglyme solvated $Na_2B_{12}H_{12}$ upon addition of H_2O (10 ml for 1 g of sample) and drying at 200 °C for 2 h under vacuum.

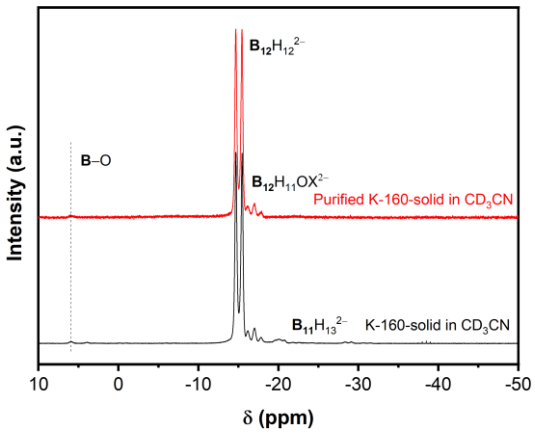

Figure S16. Proton-coupled ^{11}B NMR spectra of product obtained by reaction between KBH_4 and 5 equiv (10% excess) of $DMS{\cdot}BH_3$ before (black) and after (red) purification with H_2O.

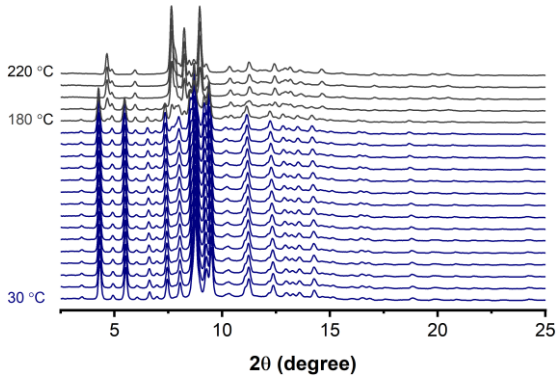

Figure S17. Vacuum in-situ PXRD patterns of the DMSO-rich solvate of $Li_2B_{12}H_{12}$ obtained upon preliminary drying at 100 °C under vacuum (λ = 0.71073 Å).

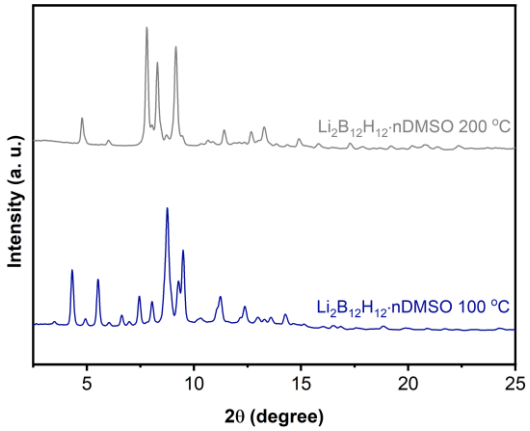

Figure S18. PXRD patterns of the DMSO-rich (dried at 100 °C under vacuum) and DMSO-poor (dried at 200 °C under argon flow) solvates of $Li_2B_{12}H_{12}$ (λ = 0.71073 Å).

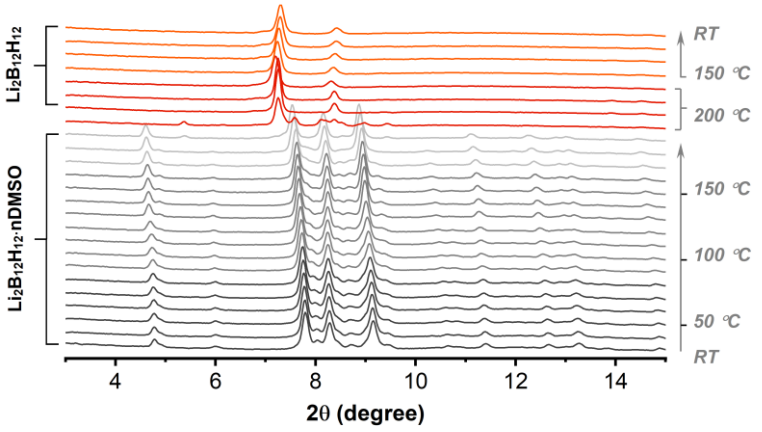

Figure S19. Vacuum in-situ PXRD patterns of the DMSO-poor solvate of $Li_2B_{12}H_{12}$ obtained upon preliminary drying at 200 °C under argon flow (λ = 0.71073 Å).

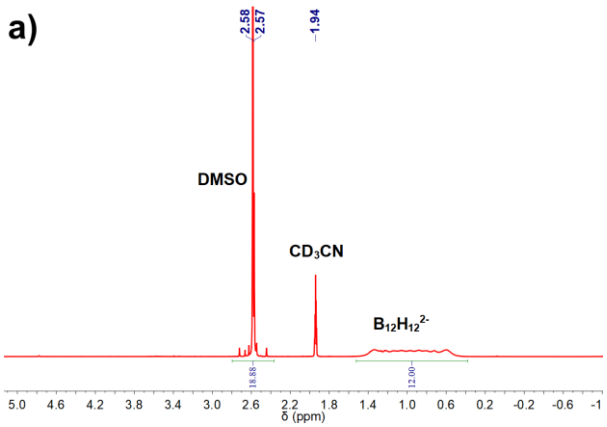

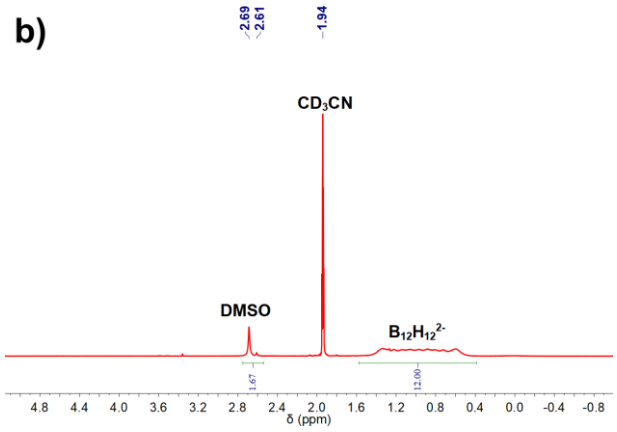

Figure S20. ^{1}H NMR spectra of DMSO solvated $Li_2B_{12}H_{12}$ a) before and b) after heat treatment at 200 °C under vacuum for 12 h.

Samples were dissolved in CD_3CN-d_3.

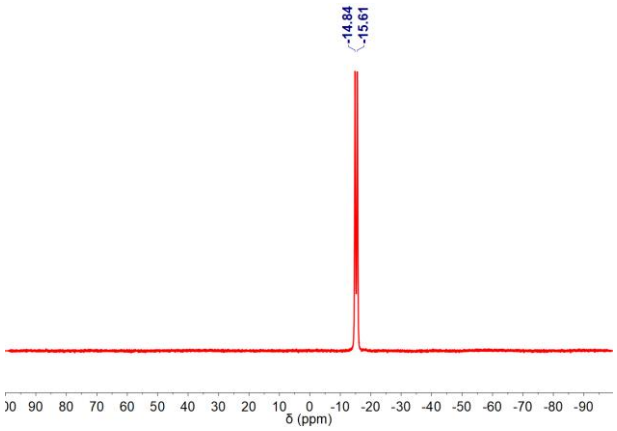

Figure S21. ^{11}B NMR spectrum of $Li_2B_{12}H_{12}$·n DMSO after heat treatment at 200 °C under vacuum for 12 h.

Note: The in situ PXRD experiments on $Li_2B_{12}H_{12}$·n DMSO were first performed with the solvated form of $Li_2B_{12}H_{12}$·n DMSO obtained after preliminary treatment at 100 °C under vacuum. However, the

high boiling point of DMSO caused it to condense in the colder parts of the capillary, resulting in a DMSO-rich atmosphere that could affect the measurements. To address this issue, some sample was preliminary dried at 200 °C under argon to obtain a DMSO-poor phase. An in situ PXRD measurement was then performed on this phase, enabling to observe the desolvation into anhydrous $Li_2B_{12}H_{12}$.

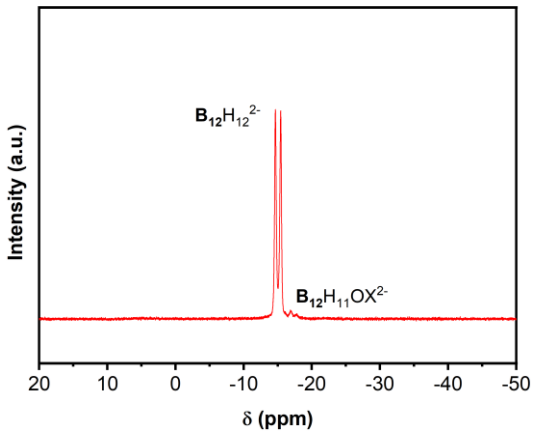

Figure S22. Proton-coupled ^{11}B NMR spectrum of DME solvated $Li_2B_{12}H_{12}$ after drying at 180 °C for 12 h under vacuum. The sample was dissolved in CD_3CN-d_3 for the measurement.

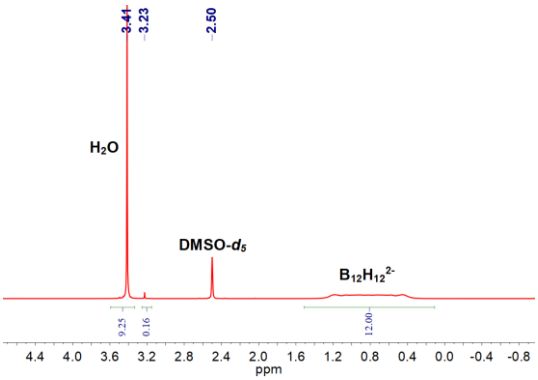

Figure S23. ^1H NMR spectrum of H_2O substituted DME solvated $Li_2B_{12}H_{12}$ after addition of H_2O (10 ml for 1 g of sample) and heat treatment at 40 °C under vacuum.

Appendix

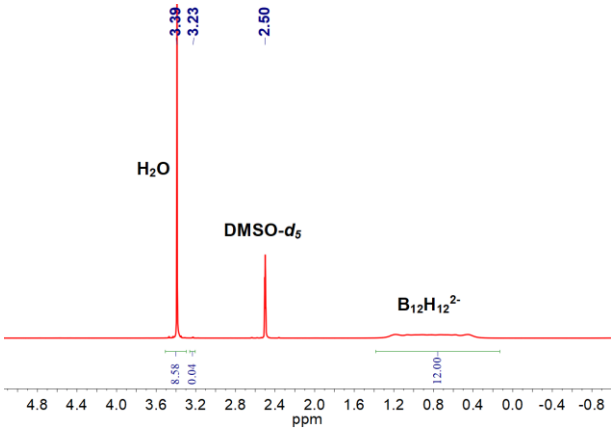

Figure S24. ^{1}H NMR spectrum of H_2O substituted DME solvated $Li_2B_{12}H_{12}$ after 3 subsequent treatments with H_2O (10 ml each time, for 1 gram of sample) and heat treatment at 40 °C under vacuum until dry.

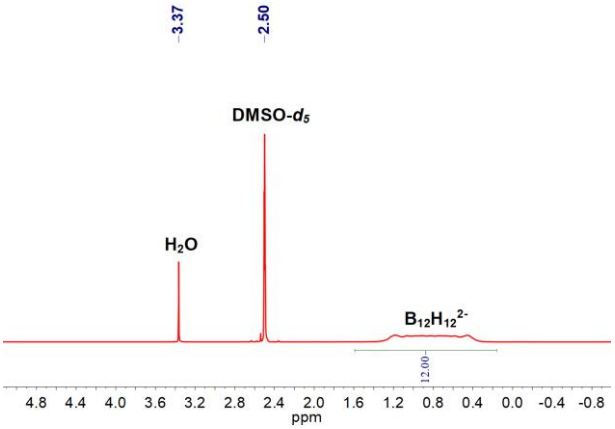

Figure S25. ^{1}H NMR spectrum of desolvated $Li_2B_{12}H_{12}{\cdot}n\ H_2O$ after heat treatment at 200 °C under vacuum for 12 h. The observed signal of H_2O (HDO) results from traces of moisture in the used DMSO-d_6.

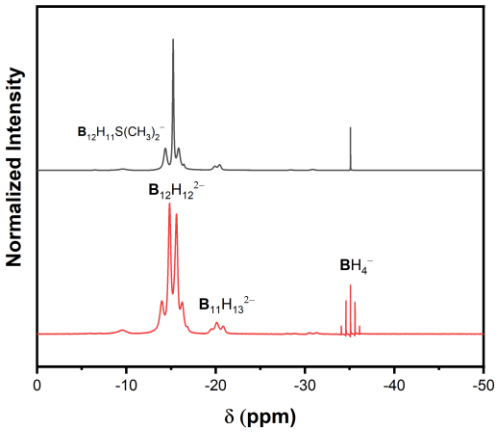

Figure S26. (a) Proton coupled and (b) proton decoupled ^{11}B NMR spectra of solid samples obtained by reaction of 5 mmol $LiBH_4$ with 27.5 mmol (10% excess) of $DMS{\cdot}BH_3$ in 20 ml toluene for 24 h at 120 °C. The sample was washed with 3 x 5 ml diglyme. The absence of $B_{11}H_{13}^{2-}$ signals after the diglyme washing is explained by the solubility of this species in glymes.

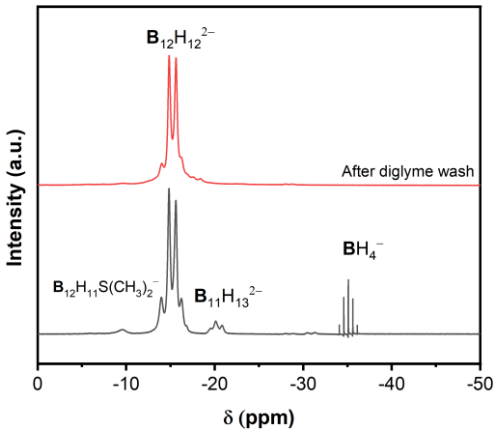

Figure S27. Proton-coupled ^{11}B NMR spectra of solid samples obtained by reaction of 5 mmol $LiBH_4$ with 27.5 mmol (10% excess) of $DMS{\cdot}BH_3$ in 20 ml toluene for 24 h at 120 °C (a) before and (b) after diglyme washing.

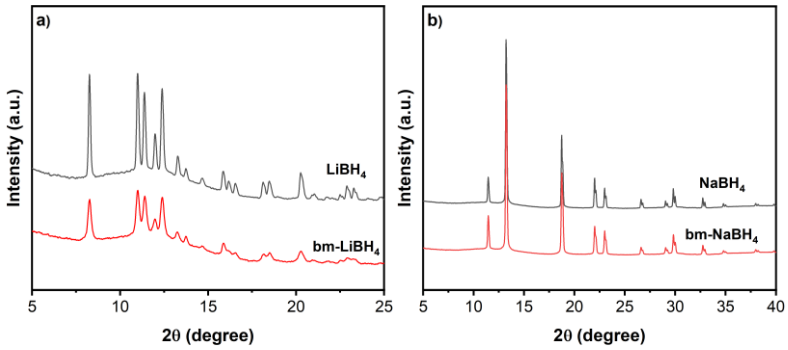

Figure S28. PXRD patterns of commercial and ball milled a) $LiBH_4$ and b) $NaBH_4$.

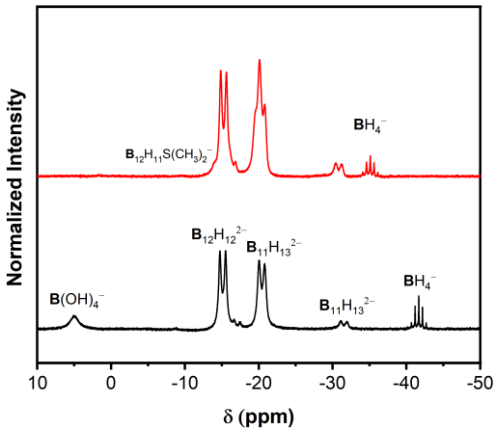

Figure S29. Proton-coupled ^{11}B NMR spectra in D_2O (black) and DMSO-d_6 (red) of solid samples obtained by reaction of 5 mmol ball milled $LiBH_4$ with 5 equiv (10 % excess) of $DMS{\cdot}BH_3$ for 24 hours at 120 °C in toluene in a Schlenk setup.

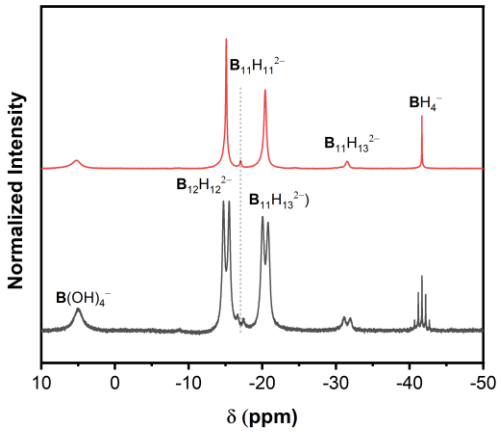

Figure S30. Proton-coupled (black) and decoupled (red) ^{11}B NMR spectra of solid samples obtained by reaction of 5 mmol ball milled $LiBH_4$ with 5 equiv (10% excess) of $DMS{\cdot}BH_3$ for 24 h at 120 °C in toluene in a Schlenk setup. Samples were dissolved in D_2O.

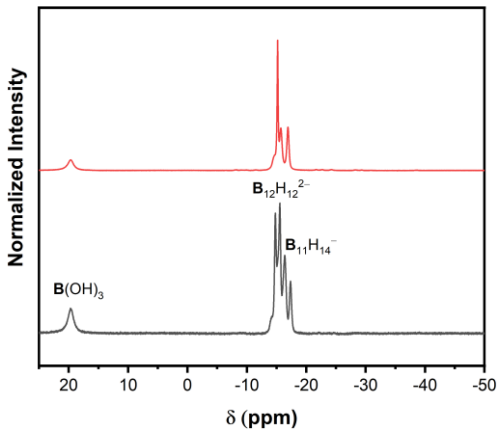

Figure S31. Proton-coupled (black) and decoupled (red) ^{11}B NMR spectra of sample obtained by reaction of 5 mmol ball milled $LiBH_4$ with 5 equiv (10% excess) of $DMS{\cdot}BH_3$ for 24 h at 120 °C in toluene in a Schlenk setup. Prior to the measurement, 3 M HCl was added dropwise to the solution until no further formation of bubbles was observed, to completely convert the $B_{11}H_{13}^{2-}$ anion into $B_{11}H_{14}^-$.

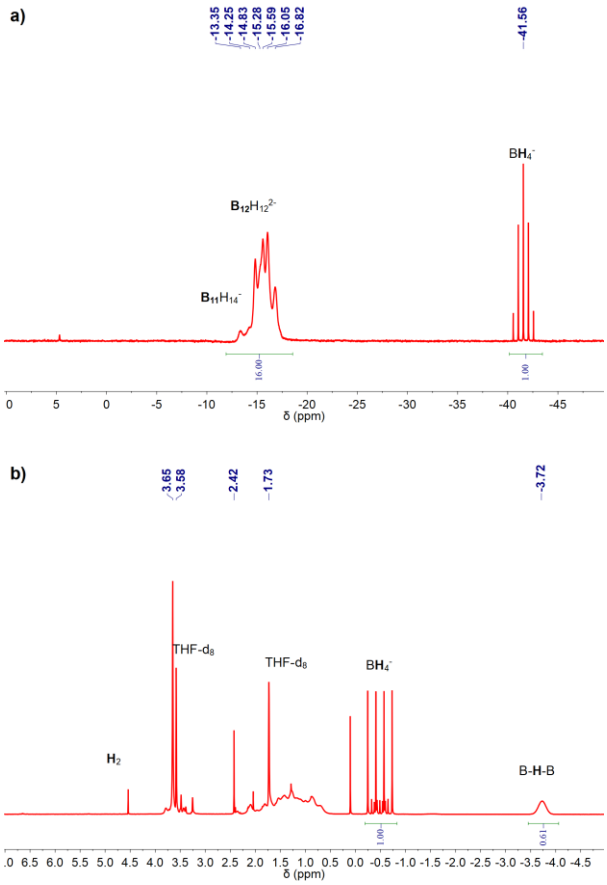

Figure S32. (a) Proton coupled ^{11}B NMR and (b) ^{1}H NMR spectra of solid samples obtained by reaction of 5 mmol ball milled $LiBH_4$ with 5 equiv (10% excess) of $DMS{\cdot}BH_3$ for 24 h at 120 °C in toluene in a Schlenk setup. Samples were dissolved in THF-d_8.

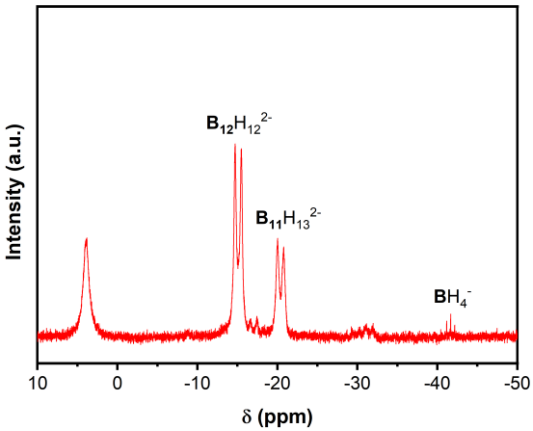

Figure S33. Proton-coupled ^{11}B NMR spectra of solid samples obtained by reaction of 5 mmol ball milled $LiBH_4$ with 5 equiv (10 % excess) of $DMS{\cdot}BH_3$ for 60 h at 120 °C in toluene in a Schlenk setup, upon washing with an excess of THF.

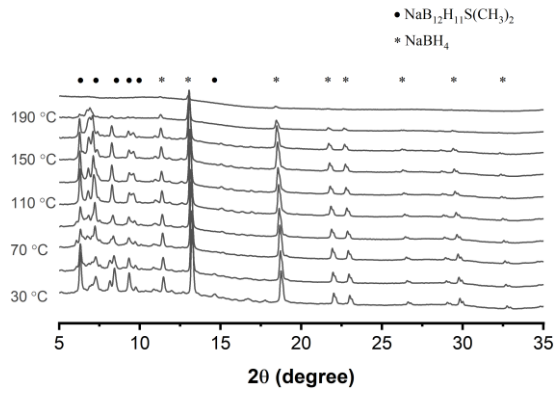

Figure 34. In situ variable temperature powder X-ray diffraction data of solid samples obtained by reaction of 5 mmol ball milled $NaBH_4$ with 27.5 mmol (10% excess) of $DMS{\cdot}BH_3$ in 20 ml toluene for 24 h at 120 °C in a Schlenk flask (λ = 0.71073 Å).

Appendix

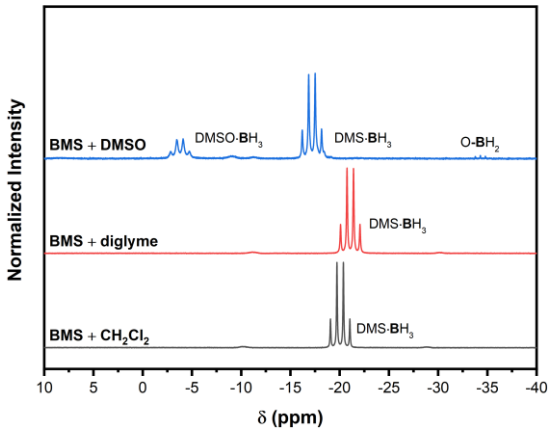

Figure S35. Proton-coupled ^{11}B NMR spectra of borane dimethyl sulfide complex (BMS) diluted in different solvents. Prior to measurements, the BMS solutions were diluted in CD_2Cl_2 at room temperature.

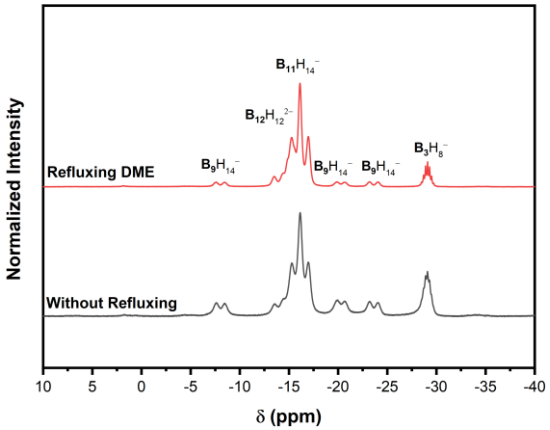

Figure S36. Proton-coupled ^{11}B NMR spectra of mixtures obtained by reacting $LiBH_4$ and 10 equiv. $DMS{\cdot}BH_3$ in 20 ml monoglyme in a Schlenk flask without (black curve) or equipped with (red curve) a condenser.

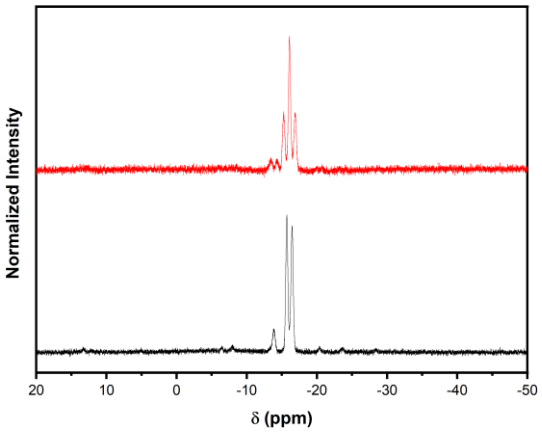

Figure S37. Proton decoupled (black) and coupled (red) ^{11}B NMR spectra of the diethyl ether layer obtained after liquid-liquid extraction of an aqueous solution of diglyme solvated $Li_2B_{12}H_{12}$ at pH = 4.

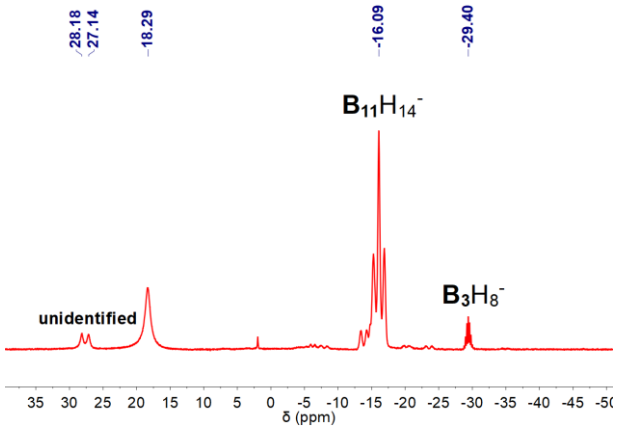

Figure S38. Proton-coupled ^{11}B NMR spectrum of the mixture obtained upon reacting $LiBH_4$ with 10 equiv. of $THF{\cdot}BH_3$ in an autoclave at 85 °C for 24 h.

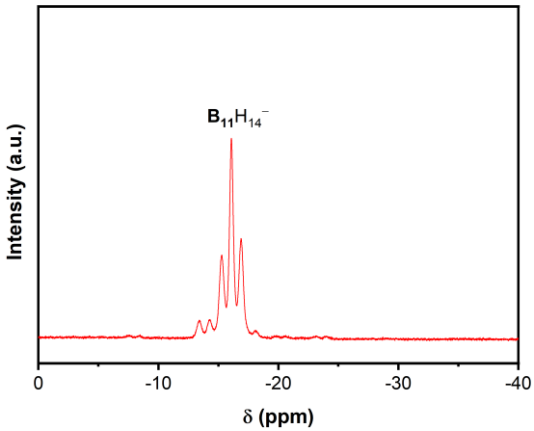

Figure S39. Proton-coupled ^{11}B NMR spectrum of solution obtained by reacting $LiBH_4$ with 10 equiv $DMS{\cdot}BH_3$ in diglyme at 85 °C for 24 h, followed by heating at 160 °C for 4 h.

Crystallographic information

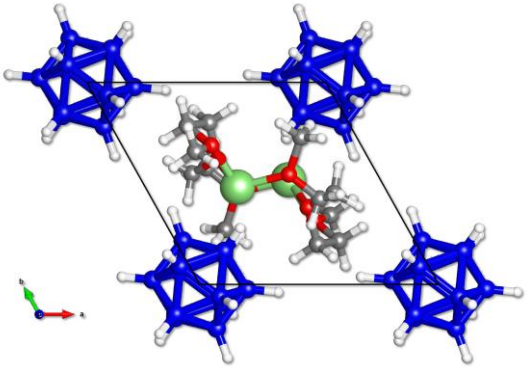

Table S8. Crystal data and structure refinement for $Li_2B_{12}H_{12}$·2 diglyme.

Identification code	$Li_2B_{12}H_{12}$·2 diglyme
Empirical formula	$C_6H_{20}B_6LiO_3$
Formula weight	212.02
Temperature (K)	150(2)
Wavelength (Å)	0.71073
Crystal system	Triclinic
Space group	*P*-1
Unit cell dimensions (Å,°)	a = 8.5691(12) b = 9.3870(9) c = 9.7731(10) α = 118.061(10) β = 90.881(12) γ = 115.069(14)
Volume ($Å^3$)	605.28(15)
Z	2
Density (calculated) (g/cm^3)	1.163
Absorption coefficient (mm^{-1})	0.073
F(000)	226
Crystal size (mm^3)	0.15 x 0.15 x 0.09
Theta range for data collection (°)	3.138 to 26.174
Reflections collected	10377
Independent reflections	2409 [$R_{(int)}$ = 0.0400]
Completeness to q = 25.242° (%)	99.6
Absorption correction	Semi-empirical from equivalents
Max. and min. transmission	1.00000 and 0.89753
Refinement method	Full-matrix least-squares on F^2
Data / restraints / parameters	2409 / 0 / 165
Goodness-of-fit on F^2	1.062
Final R indices [I>2s(I)]	R_1 = 0.0359, wR_2 = 0.0861
R indices (all data)	R_1 = 0.0456, wR_2 = 0.0904
(max,min)($e.Å^{-3}$)	0.220, -0.182

Appendix

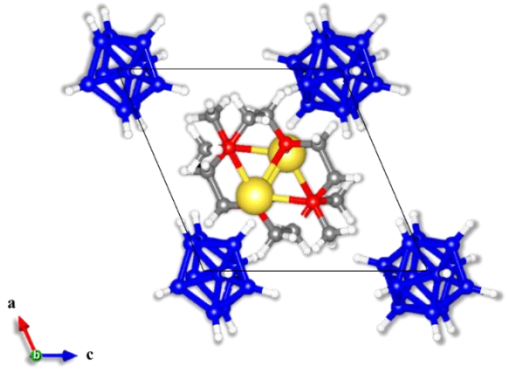

Table S9. Crystal data and structure refinement for $Li_2B_{12}H_{12}\cdot {}^{3}/_{2}$ monoglyme.

Identification code	$Li_2B_{12}H_{12}$.3/2 monoglyme
Empirical formula	$C_6H_{21}B_6LiO_3$
Formula weight	213.03
Temperature (K)	150(2)
Wavelength (Å)	0.71073
Crystal system	Monoclinic
Space group	I2/a
Unit cell dimensions (Å,°)	a = 16.480(5) b = 10.115(2) c = 17.144(5)
Volume ($Å^3$)	2624.0(13)
Z	8
Density (calculated) (g/cm^3)	1.078
Absorption coefficient (mm^{-1})	0.068
F(000)	912
Crystal size (mm^3)	0.18 x 0.10 x 0.05
Theta range for data collection (°)	3.131 to 21.257
Reflections collected	5062
Independent reflections	1458 [R(int) = 0.0936]
Completeness to q = 21.257° (%)	99.6
Absorption correction	Semi-empirical from equivalents
Max. and min. transmission	1.00000 and 0.64350
Refinement method	Full-matrix least-squares on F^2
Data / restraints / parameters	1458 / 0 / 148
Goodness-of-fit on F^2	1.088
Final R indices [I>2s(I)]	R1 = 0.0602, wR2 = 0.0908
R indices (all data)	R1 = 0.0994, wR2 = 0.1005
Dr (max,min)($e.Å^{-3}$)	0.164, -0.153

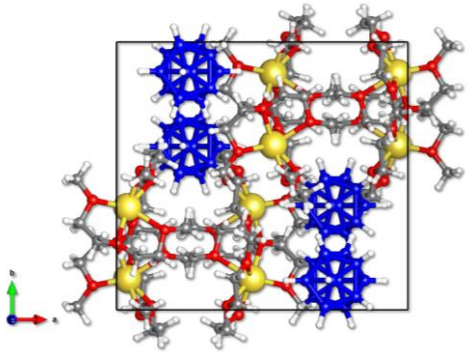

Table S10. Crystal data and structure refinement for $Na_2B_{12}H_{12}$·4 diglyme.

Identification code	$Na_2B_{12}H_{12}$·4 diglyme
Empirical formula	$C_{12}H_{34}B_6NaO_6$
Formula weight	362.24
Temperature (K)	150(2)
Wavelength (Å)	0.71073
Crystal system	Monoclinic
Space group	*I*2/*a*
Unit cell dimensions (Å,°)	a = 17.4862(17) b = 14.6333(9) c = 17.7938(19)
Volume ($Å^3$)	4147.7(8)
Z	8
Density (calculated) (g/cm^3)	1.160
Absorption coefficient (mm^{-1})	0.098
F(000)	1560
Crystal size (mm^3)	0.480 x 0.350 x 0.300
Theta range for data collection (°)	3.506 to 26.507
Reflections collected	4138
Independent reflections	4138 [$R_{(int)}$ = /]†
Completeness to q = 25.242° (%)	98.8
Absorption correction	Semi-empirical from equivalents
Max. and min. transmission	1.00000 and 0.50355
Refinement method	Full-matrix least-squares on F^2
Data / restraints / parameters	4138 / 0 / 249
Goodness-of-fit on F^2	1.081
R indices (all data)	R_1 = 0.0824, wR_2 = 0.1833
(max,min)($e.Å^{-3}$)	0.331, -0.360

† The crystal was twinned and refined against HKLF5 formatted data, imposing MERGE 0

Appendix

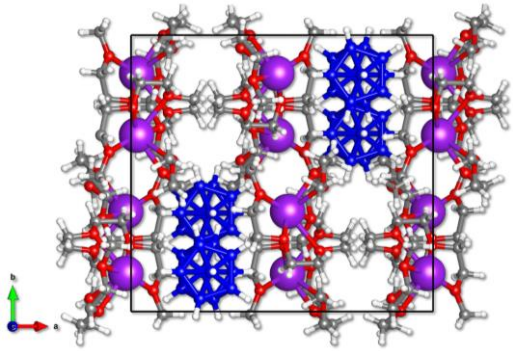

Table S11. Crystal data and structure refinement for $K_2B_{12}H_{12}$·4 diglyme.

Identification code	$K_2B_{12}H_{12}$·4 diglyme
Empirical formula	$C_{24}H_{68}B_{12}K_2O_{12}$
Formula weight	756.70
Temperature (K)	150(2)
Wavelength (Å)	0.71073
Crystal system	Monoclinic
Space group	*I*2/*a*
Unit cell dimensions (Å,°)	a = 18.627(2) b = 14.8544(10) c = 17.877(2)
Volume ($Å^3$)	4306.2(10)
Z	4
Density (calculated) (g/cm^3)	1.167
Absorption coefficient (mm^{-1})	0.268
F(000)	1624
Crystal size (mm^3)	0.28x 0.11 x 0.02
Theta range for data collection (°)	2.582 to 26.395
Reflections collected	5525
Independent reflections	5525 [$R_{(int)}$ = ?] †
Completeness to q = 25.242° (%)	97.5
Absorption correction	Semi-empirical from equivalents
Max. and min. transmission	1.00000 and 0.69426
Refinement method	Full-matrix least-squares on F^2
Data / restraints / parameters	5525 / 0 / 231
Goodness-of-fit on F^2	0.994
R indices (all data)	R_1 = 0.0831, wR_2 = 0.1314
(max,min)($e.Å^{-3}$)	0.429, -0.274

† The crystal was twinned and refined against HKLF5 formatted data, imposing MERGE 0

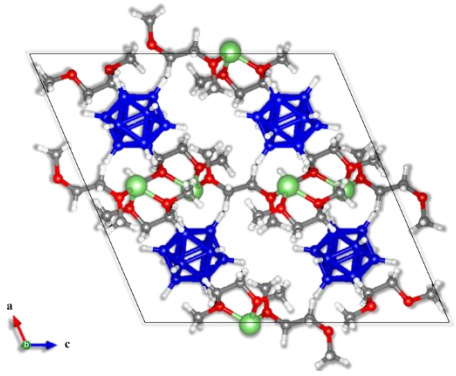

Table S12. Crystal data and structure refinement for $Na_2B_{12}H_{12}$·2 diglyme.

Identification code	$Na_2B_{12}H_{12}$·2 diglyme
Empirical formula	$C_{12}H_{40}B_{12}Na_2O_6$
Formula weight	456.14
Temperature (K)	150(2)
Wavelength (Å)	0.71073
Crystal system	Triclinic
Space group	P-1
Unit cell dimensions (Å,°)	a = 9.098(2) b = 9.165(3) c = 9.536(2)
Volume ($Å^3$)	637.3(4)
Z	1
Density (calculated) (g/cm^3)	1.189
Absorption coefficient (mm^{-1})	0.105
F(000)	242
Crystal size (mm^3)	0.30x 0.09 x 0.04
Theta range for data collection (°)	3.669 to 20.837
Reflections collected	1191
Independent reflections	1191 [R(int) = ?]
Completeness to q = 20.837° (%)	88.8
Absorption correction	Semi-empirical from equivalents
Max. and min. transmission	1.00000 and 0.14822
Refinement method	Full-matrix least-squares on F^2
Data / restraints / parameters	1191 / 51 / 148
Goodness-of-fit on F^2	1.081
Final R indices [I>2s(I)]	R1 = 0.1091, wR2 = 0.2672
R indices (all data)	R1 = 0.1347, wR2 = 0.2834
Dr (max,min)($e.Å^{-3}$)	0.692, -0.548

Appendix

Appendix III: Supporting Information of Chapter 5

Table S1. *List of solvents used and their properties.*[1]

Solvent	Formula	ε	AN	DN	Boiling point /°C
Toluene	C_7H_8	2.33		0.1	110.6
Diethyl ether	$C_4H_{10}O$	4.19	3.9	19.2	35
Diglyme	$C_6H_{14}O_3$	7.23	9.9	18	162
THF	C_4H_8O	7.36	8.0	20	66
Monoglyme	$C_4H_{10}O_2$	7.55	10.2	24	84.5
DMSO	C_2H_6OS	47.13	19.3	29.8	189
Water	H_2O	78.4	54.8	18	100

ε = dielectric constant; **AN**: acceptor number; **DN**: donor number.

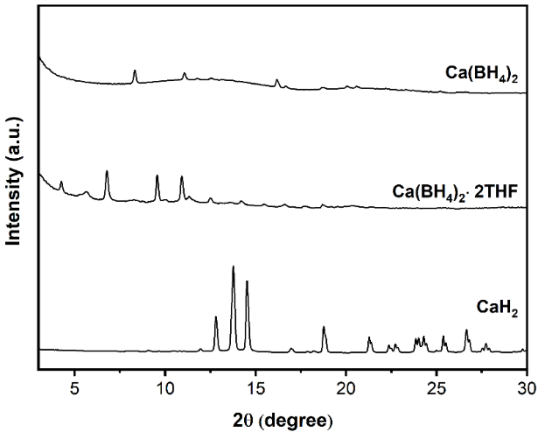

Figure S1. PXRD patterns of solid reactants employed for the synthesis of $CaB_{12}H_{12}$.

Appendix

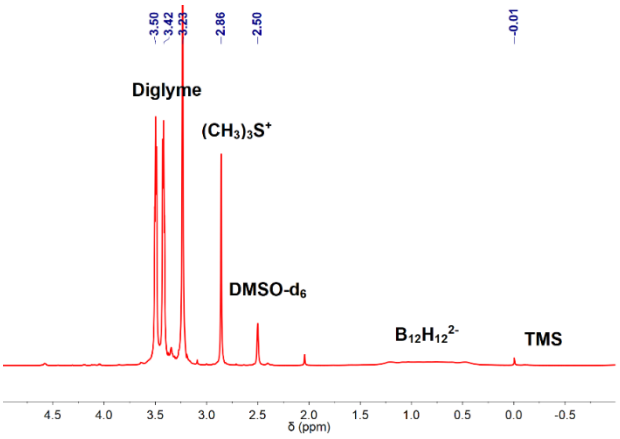

Figure S2. ^{1}H NMR spectrum of solid substance obtained by reacting $Ca(BH_4)_2$ with 10 equiv. $DMS{\cdot}BH_3$ at 120 °C in diglyme in a Schlenk flask. Samples were dissolved in DMSO-d_6.

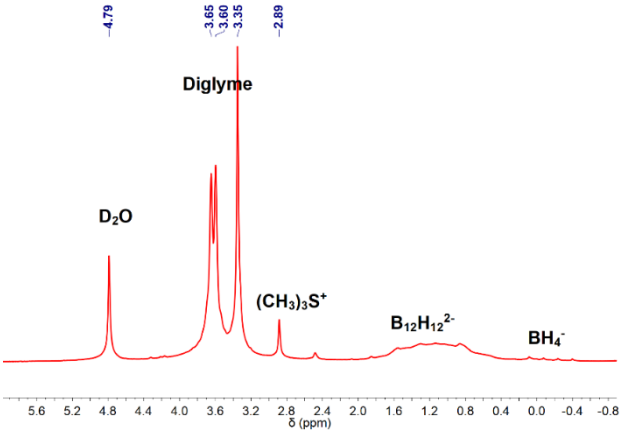

Figure S3. ^{1}H NMR spectrum of solid substance obtained by reacting $Ca(BH_4)_2$ with 10 equiv. $DMS{\cdot}BH_3$ at 120 °C in diglyme in a Schlenk flask. Samples were dissolved in D_2O.

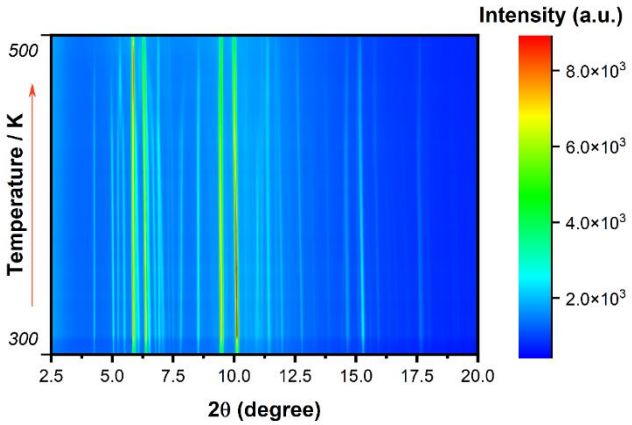

Figure S4. In-situ synchrotron radiation powder X-ray diffraction (SR-PXRD) data of $CaB_{12}H_{12}$·n diglyme. Heating rate = 10 °C/min (λ = 0.77509 Å).

Note: The main phase are diglyme solvated $CaB_{12}H_{12}$, which is thermal stable until 230 °C(500 K)

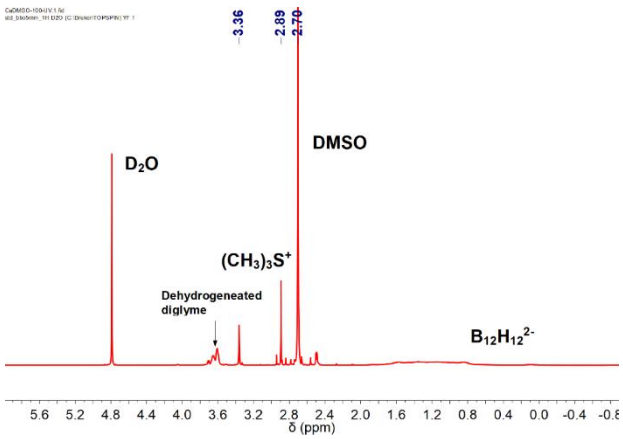

Figure S5. ^{1}H NMR spectrum of $CaB_{12}H_{12}$·n diglyme upon substitution with DMSO. The solvent exchange was performed at 100 °C under vacuum. Samples were measured by dissolved in D_2O.

Appendix

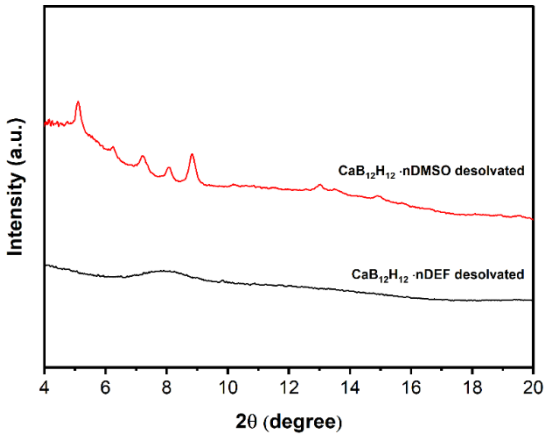

Figure S6. PXRD patterns of $CaB_{12}H_{12}$ thermally desolvated after DMSO and N,N-diethylamine exchange of the crude product obtained in diglyme.

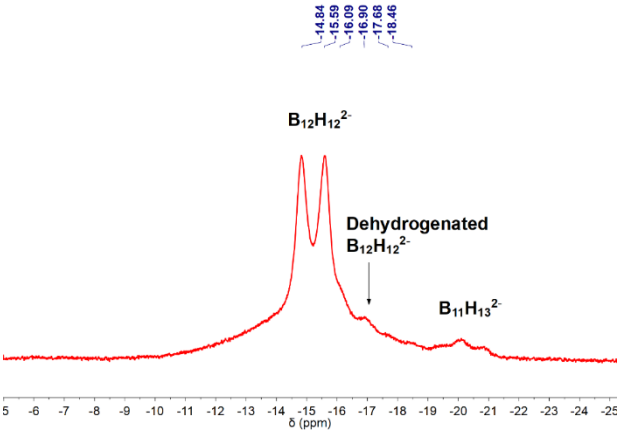

Figure S7. ^{1}H-coupled ^{11}B NMR spectrum of the product obtained by reacting 5 mmol CaH_2 with 12 equiv. $DMS{\cdot}BH_3$ in 16 ml of THF in an autoclave. Sample dissolved in DMSO-d_6.

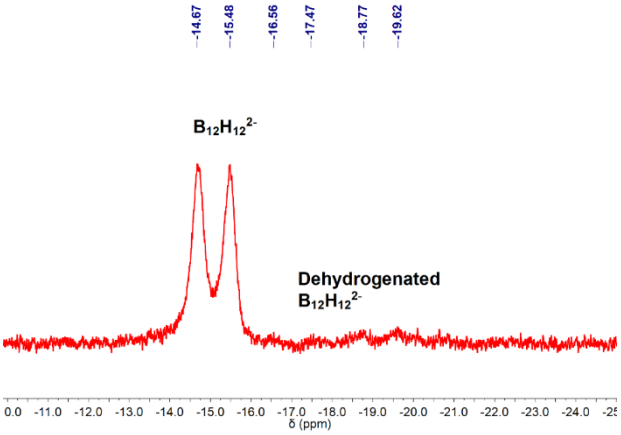

Figure S8. ^{1}H-coupled ^{11}B NMR spectrum of the product obtained by reacting 5 mmol $Ca(BH_4)_2$ with 10 equiv. $DMS{\cdot}BH_3$ in 16 ml of THF in an autoclave (sample dissolved in D_2O).

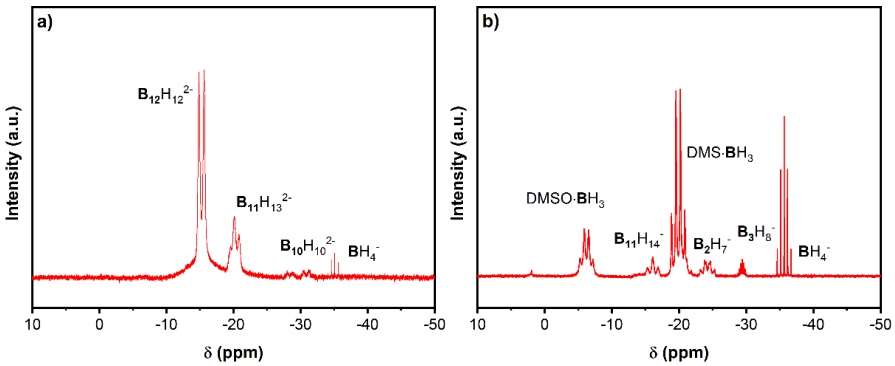

Figure S9. ^{1}H-coupled ^{11}B NMR spectra of a) solid substance and b) filtrate obtained by reacting CaH_2 with 12 equiv. $DMS{\cdot}BH_3$ in a mixture of THF and DME in 1:1 (v/v) ratio in an autoclave. Samples dissolved in DMSO-d_6.

Appendix

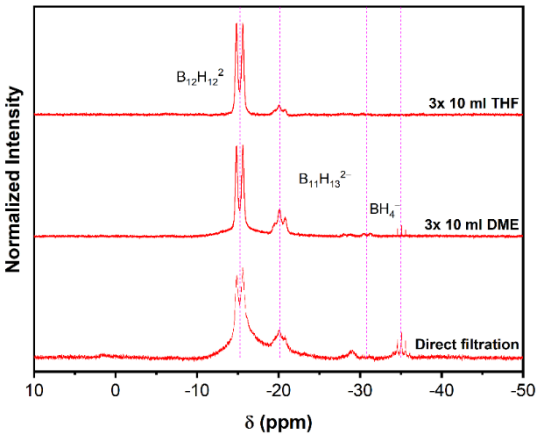

Figure S10. ^{1}H-coupled ^{11}B NMR spectra of the solid after each individual washing of the product obtained from the reaction of CaH_2 with 12 equiv. DMS·BH_3 in a mixture of DME and THF in 1:1 (v/v) ratio in an autoclave. Using 3 x 10 ml THF allows for effective removal of the residual BH_4^-. Samples dissolved in DMSO-d_6.

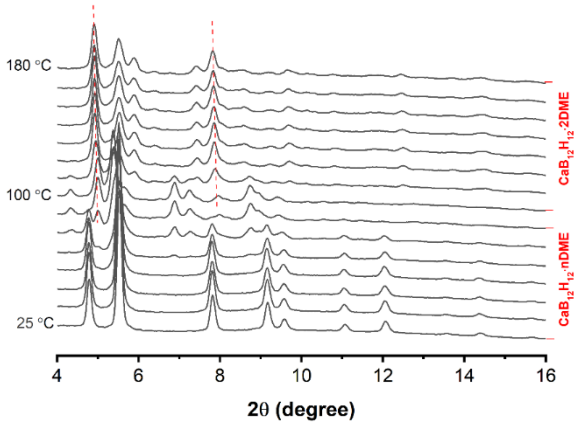

Figure S11. In situ PXRD measurement of solid substance obtained by reacting CaH_2 with 12 equiv. DMS·BH_3 in a mixture of THF and DME in 1: 1 (v/v) ratio at 120 °C for 24 h in an autoclave, while heating up the sample.

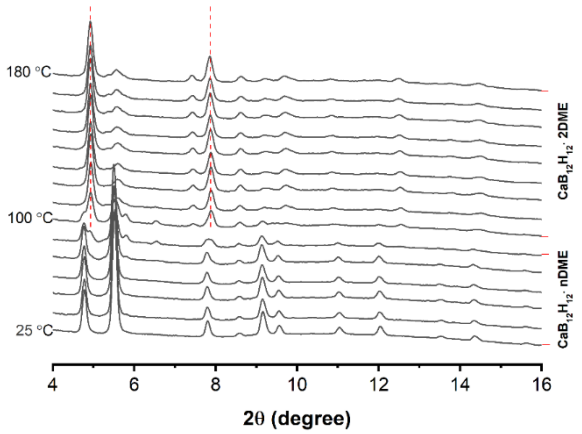

Figure S12. In situ PXRD measurement of solid substance obtained by reacting $Ca(BH_4)_2 \cdot 2THF$ with 10 equiv. $DMS \cdot BH_3$ in 16 ml DME at 120 °C for 24 h in an autoclave, while heating up the sample. The found $CaB_{12}H_{12} \cdot 2DME$ phase indicates that ligand substitution occurred during synthesis.

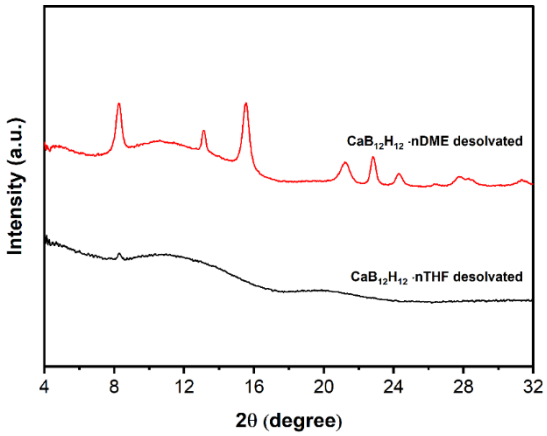

Figure S13. PXRD patterns of products obtained upon thermal desolvation at 200 °C of DME-solvated and THF-solvated $CaB_{12}H_{12}$.

Appendix

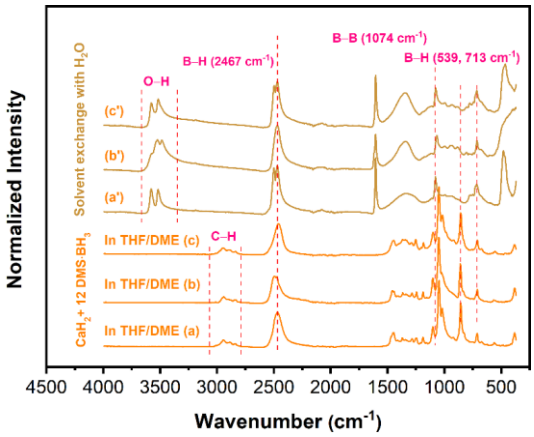

Figure S14. FTIR spectra of the as-synthesized samples and after H_2O substituted obtained from the reaction with 5 mmol $Mg(BH_4)_2$ + 10 equiv. $DMS{\cdot}BH_3$ in THF/DME (1:1 (v/v) ratio) at 120 °C in an autoclave.

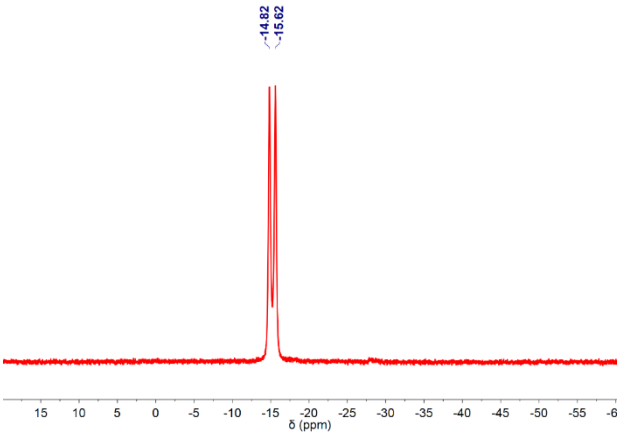

Figure S15. ^{1}H-coupled ^{11}B NMR spectrum of $CaB_{12}H_{12}$ obtained in a mixture of THF and DME in 1:1 (v/v) ratio +15 ml H_2O dried at 40 °C under vacuum. Samples dissolved in DMSO-d_6.

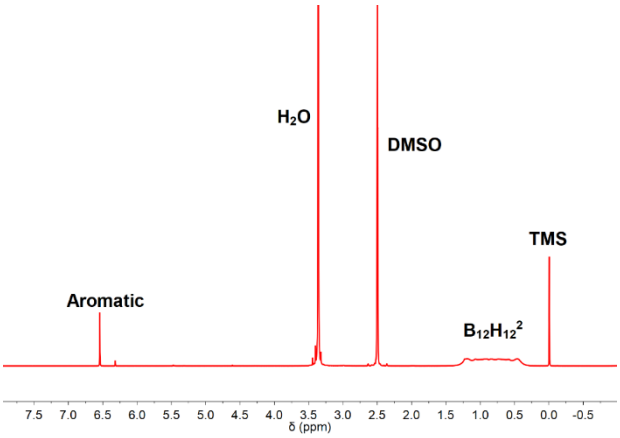

Figure S16. ^{1}H NMR spectrum of $CaB_{12}H_{12}$ obtained in a mixture of THF and DME in 1:1 (v/v) ratio +15 ml H_2O dried at 40 °C under vacuum. Samples dissolved in DMSO-d_6.

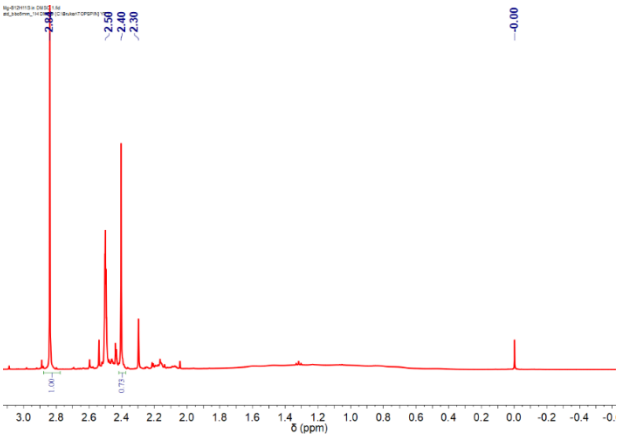

Figure S17. ^{1}H NMR spectrum of sample obtained from the reaction with 5 mmol $Mg(BH_4)_2$ + 10 equiv. $DMS{\cdot}BH_3$ in toluene at 120 °C for 24 h. Samples dissolved in DMSO-d_6.

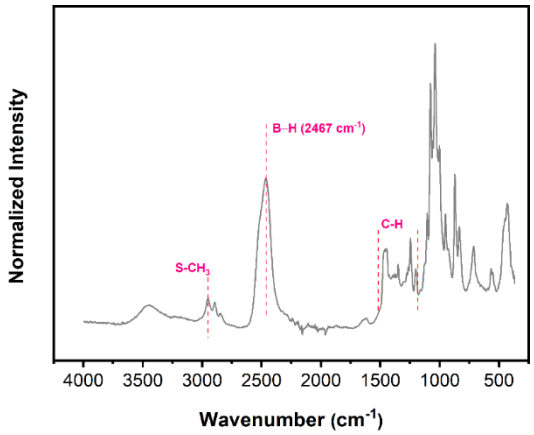

Figure S18. FTIR spectrum of the as-synthesized sample obtained from reaction of 5 mmol $Mg(BH_4)_2$ +10 equiv. $DMS{\cdot}BH_3$ in diglyme at 120 °C for 24 h in a Schlenk flask.

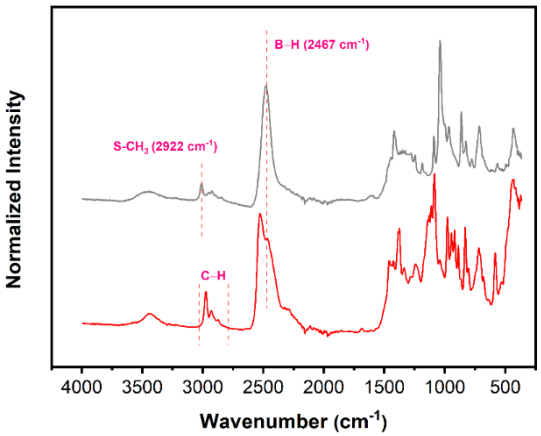

Figure S19. FTIR spectra of the as-synthesized sample obtained from reaction of 5 mmol $Mg(BH_4)_2$ +10 equiv. $DMS{\cdot}BH_3$ in toluene at 120 °C for 24 h (red: obtained in a Schlenk flask; grey: obtained in an autoclave).

Table S2. Crystal data and structure refinement for $(CH_3)_3SB_{12}H_{11}S(CH_3)_2$.

Identification code	$(CH_3)_3SB_{12}H_{11}S(CH_3)_2$
Empirical formula	C5 H26 B12 S2
Formula weight	280.10
Temperature (K)	297(2)
Wavelength (Å)	0.71073
Crystal system	Orthorhombic
Space group	$P2_12_12$
Unit cell dimensions (Å,°)	a = 15.0171(17) b = 13.3854(14) c = 8.7993(8)
Volume ($Å^3$)	1768.7(3)
Z	4
Density (calculated) (g/cm^3)	1.052
Absorption coefficient (mm^{-1})	0.275
F(000)	592
Crystal size (mm^3)	0.26x 0.02 x 0.02
Theta range for data collection (°)	2.315 to 19.979
Reflections collected	8982
Independent reflections	1656 [R(int) = 0.0746]
Completeness to q = 19.979° (%)	99.8
Absorption correction	Semi-empirical from equivalents
Max. and min. transmission	1.00000 and 0.40791
Refinement method	Full-matrix least-squares on F^2
Data / restraints / parameters	1656 / 61 / 214
Goodness-of-fit on F^2	1.068
R indices (all data)	R1 = 0.1093, wR2 = 0.2166
Absolute structure parameter	0.52(8)
Dr (max,min)($e.Å^{-3}$)	0.447, -0.196

Appendix

Table S3. Crystal data and structure refinement for

UCL2532_yf_jw_$B_{12}H_{12}$_$S(CH_3)_2$_combined.

Identification code	yf_jw_B12H12_S(CH3)2_combined
Empirical formula	C4 H20 B12 S2
Formula weight	262.04
Temperature (K)	100(2)
Wavelength (Å)	0.7529
Crystal system	Monoclinic
Space group	P21
Unit cell dimensions (Å,°)	a = 8.6246(8) b = 14.743(2) c = 13.1027(14)
Volume (Å3)	1665.2(3)
Z	4
Density (calculated) (g/cm3)	1.045
Absorption coefficient (mm-1)	0.334
F(000)	544
Crystal size (mm3)	0.2x 0.015 x 0.015
Theta range for data collection (°)	1.647 to 27.326
Reflections collected	18933
Completeness to q = 26.855° (%)	98.4
Absorption correction	Semi-empirical from equivalents
Max. and min. transmission	1.00000 and 0.75321
Refinement method	Full-matrix least-squares on F2
Data / restraints / parameters	18933 / 127 / 410
Goodness-of-fit on F2	1.067
R indices (all data)	R1 = 0.1302, wR2 = 0.2134
Absolute structure parameter	0.44(12)
Dr (max,min)(e.Å-3)	0.742, -0.297

The single crystal of was isolated from $Ca(BH_4)_2$.THF + 10 $DMS{\cdot}BH_3$ in 16 ml THF, whereas autoclave contain very small amount diglyme from last experiment, and the sample is not diffracting.

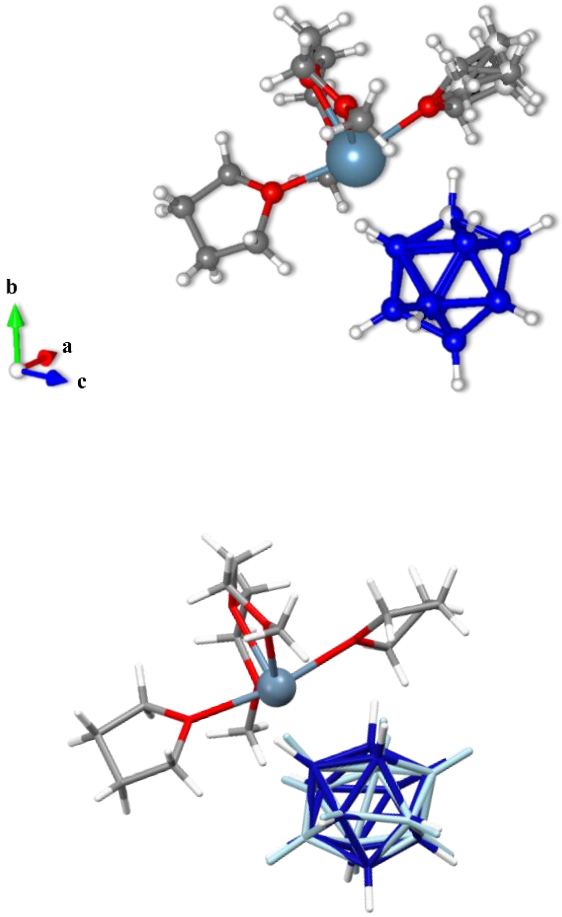

Structure of $CaB_{12}H_{12}$: B_{16} is refined at 50% occupancy giving a mixture of $B_{12}H_{12}^{2-}$ and $B_{11}H_{11}^{2-}$

Table S4. Crystal data and structure refinement for UCL2534_yf_jw_CaB12H12_thf.

Identification code	yf_jw_CaB12H12_thf
Empirical formula	C28 H83 B23 Ca2 O10
Formula weight	908.73
Temperature (K)	150(2)
Wavelength (Å)	0.71073
Crystal system	Monoclinic
Space group	$P2_1/c$
Unit cell dimensions (Å,°)	a = 14.7066(17) b = 9.7744(9) c = 18.0106(19)
Volume ($Å^3$)	2554.9(5)
Z	2
Density (calculated) (g/cm^3)	1.181
Absorption coefficient (mm^{-1})	0.269
F(000)	972
Crystal size (mm^3)	0.05 x 0.04 x 0.01
Theta range for data collection (°)	2.486 to 20.815
Reflections collected	10642
Independent reflections	2671 [R(int) = 0.1191]
Completeness to q = 20.815° (%)	99.8
Absorption correction	Semi-empirical from equivalents
Max. and min. transmission	1.00000 and 0.94641
Refinement method	Full-matrix least-squares on F^2
Data / restraints / parameters	2671 / 78 / 320
Goodness-of-fit on F^2	1.028
R indices (all data)	R1 = 0.1018, wR2 = 0.1081
Dr (max,min)($e.Å^{-3}$)	0.249, -0.228

Reference

(1) Gutmann, V. Solvent Effects on the Reactivities of Organometallic Compounds. *Coord. Chem. Rev.* **1976**, *18* (2), 225–255.

Appendix IV: Supporting Information of Chapter 6

1. Experimental Section

1.1. Mechanochemical solid-gas reaction of γ-$Mg(BH_4)_2$ with CO_2

The mechanochemical synthesis by ball milling at 600 rpm was performed in a 80 mL stainless steel EASY GTM grinding bowl, equipped with a gas pressure and temperature measuring system for controlling the milling process, using a FRITSCH PULVERISETTE 7 premium line Planetary Ball Mill. γ-$Mg(BH_4)_2$ (0,108 g; 2 mmol) and solid CO_2 (0.350 g; 8 mmol) were loaded into the bowl with stainless steel balls (2 × 4 g, ø = 10 mm). The mixture was ball milled for 6 milling cycles, with a cycle duration of 5 min and a pause of 1 min, leading to the formation of a grey product.

1.2. Thermal-induced solid gas reaction of γ-$Mg(BH_4)_2$ with CO_2

TGA-MS analysis of the solid-gas reaction of γ-$Mg(BH_4)_2$ with CO_2 was performed using a Mettler Toledo AG – TGA/SDTA 851e instrument coupled with ThermoStar GSD 301T spectrometer. Temperature was increased from room temperature to 500 °C with a heating rate of 2 °C/min, followed by an isothermal stabilization for 1 h at 500 °C. γ-$Mg(BH_4)_2$ (8.2 mg) was loaded into a Al_2O_3 crucible and exposed to a dynamic CO_2 flow (25 mL/min) through the sample.

1.3. TG-DTA measurements

TG-DTA analysis of the solid-gas reaction of γ-$Mg(BH_4)_2$ with CO_2 was performed using a SDT 2960 Simultaneous DTA-TGA instrument. Temperature was increased from room temperature to

500 °C with a heating rate of 2 °C/min, followed by an isothermal stabilization for 1 h at 500 °C. γ-$Mg(BH_4)_2$ (2.1 mg) was loaded into a Al_2O_3 crucible and exposed to a dynamic CO_2 flow (100 mL/min) through the sample.

1.4. NMR spectroscopy

NMR spectra in DMSO-d6 were collected on a Bruker Avance DRX500 spectrometer operating at 500.133 MHz for 1H, 125.770 MHz for ^{13}C and 160.462 MHz for ^{11}B nuclei. Chemical shifts are reported with reference to SiMe4 for ^{1}H and ^{13}C and $BF_3{\cdot}OEt_2$ for ^{11}B.

1.5. Solid state NMR spectroscopy

^{1}H and ^{11}B NMR spectra were performed on a Bruker Ascend 600 spectrometer (14.1 T) operating at ^{1}H and ^{11}B Larmor frequencies of 600.130 MHz and 192.546 MHz, respectively, and were recorded with a 3.2 mm probe with 16 kHz magic angle spinning (MAS). Chemical shifts are reported with reference to $SiMe_4$ for ^{1}H and $BF_3{\cdot}OEt_2$ for ^{11}B. (To be confirmed)

1.6. ATR-FTIR

The attenuated total reflectance Fourier transform infrared (ATR-FTIR) spectra were measured on a Bruker Alpha II spectrometer set in an argon-filled glovebox. For the measurements, the spectrometer was equipped with a Platinum ATR module (Bruker, diamond crystal, single bounce).

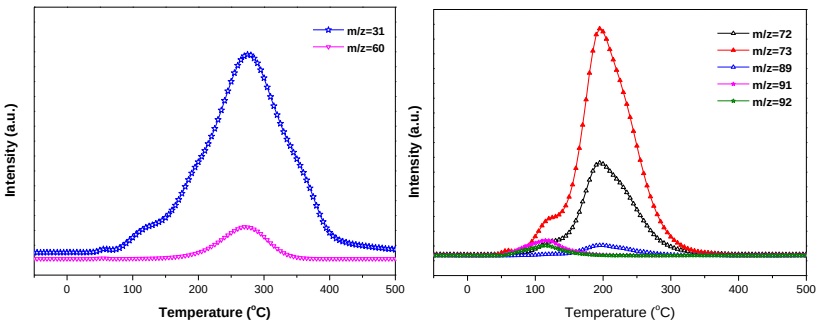

Figure S1. MS spectra of the solid gas reaction of

γ-$Mg(BH_4)_2$ with CO_2.

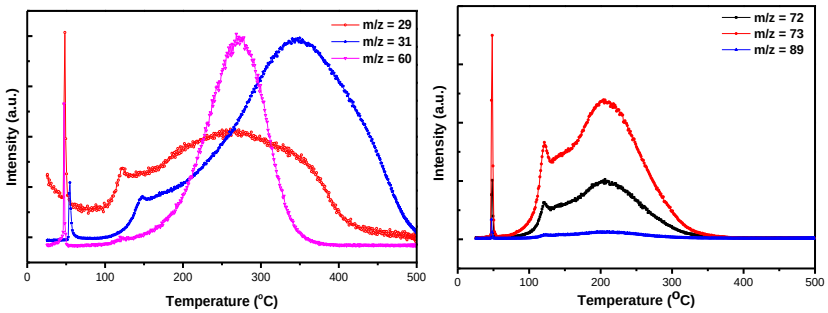

Figure S2. MS spectra of the solid gas reaction of

am-$Mg(BH_4)_2$ with CO_2.

Appendix

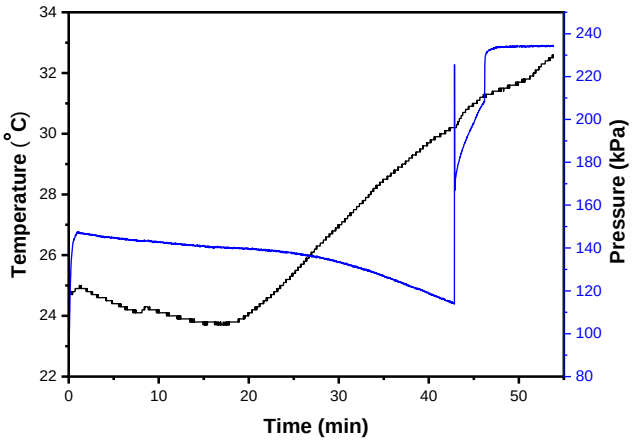

Figure S3. Temperature and pressure monitored during mechanochemical induced solid gas reaction of γ-$Mg(BH_4)_2$ with CO_2.

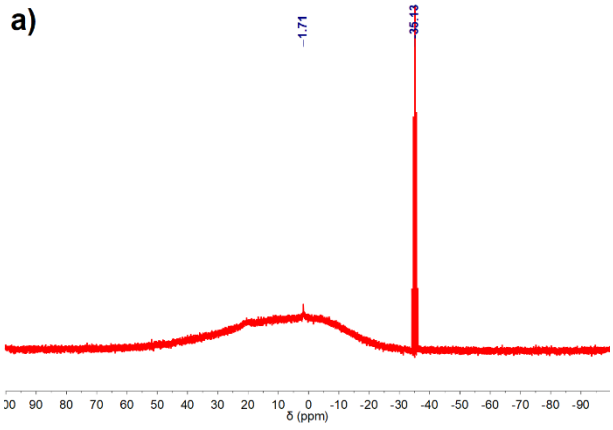

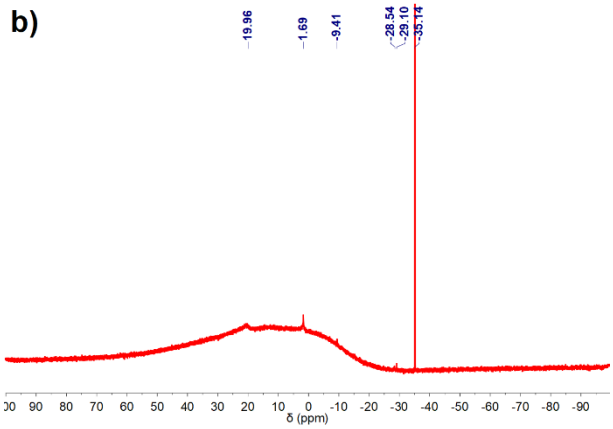
b)
19.96
1.69
-9.41
28.54
29.10
35.14
90 80 70 60 50 40 30 20 10 0 -10 -20 -30 -40 -50 -60 -70 -80 -90
δ (ppm)

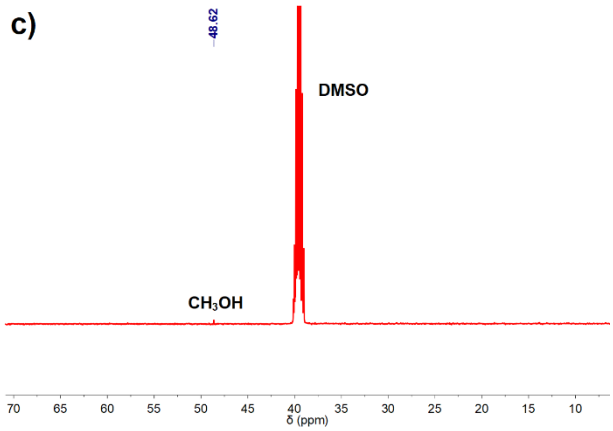
c)
48.62
DMSO
CH3OH
70 65 60 55 50 45 40 35 30 25 20 15 10
δ (ppm)

Appendix

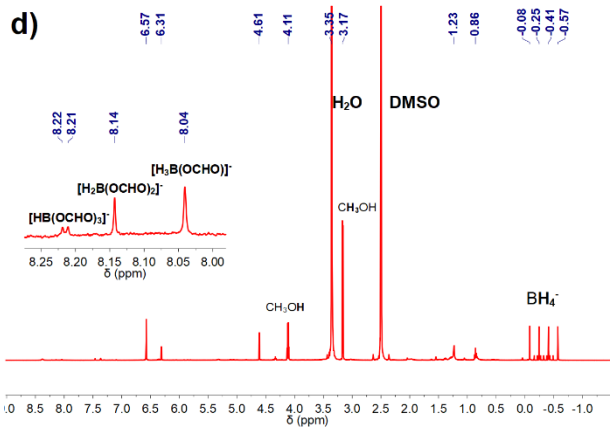

Figure S4. (a) ^{11}B NMR, (b) $^{11}B\{^{1}H\}$ NMR, (c) ^{13}C NMR and (d) ^{1}H NMR of the solid product obtained from mechanochemical induced solid gas reaction of γ-$Mg(BH_4)_2$ with CO_2.

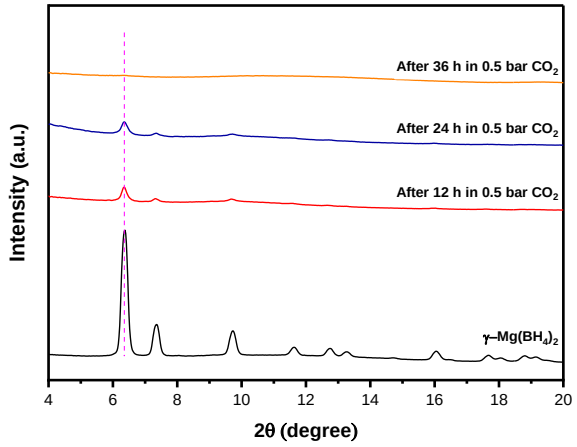

Figure S5. PXRD patterns of γ-$Mg(BH_4)_2$ before and after various reaction times CO_2 interaction at RT and 0.5 bar.